5-7-2011

Rate-Dependent Behavior of Clay

Harry F. Martindale IV
University of Connecticut - Storrs, harry.f.martindale@gmail.com

Rate-Dependent Behavior of Clay

Harry Fredrick Martindale IV

B.S., University of Connecticut, 2009

A Thesis

Submitted in Partial Fulfillment of the

Requirements for the Degree of

Masters of Science

at the

University of Connecticut

2011

APPROVAL PAGE

Masters of Science Thesis

Rate-Dependent Behavior of Clay

Presented by

Harry Fredrick Martindale IV, B.S.

Major Advisor 

Dipanjan Basu

Associate Advisor 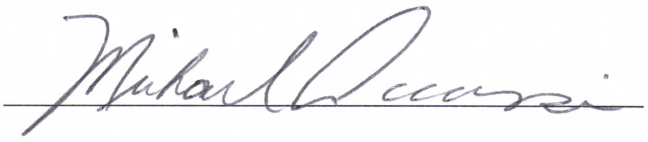

Michael Accorsi

Associate Advisor 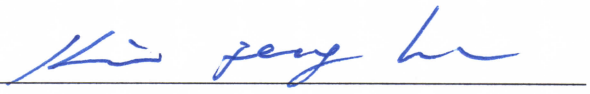

Jeong-Ho Kim

University of Connecticut

2011

To my Grandfather:

Harry Fredrick Martindale II

Acknowledgement

Throughout life we face many challenges. Without the support and encouragement of dedicated individuals the progress you see here would not be possible.

I'd like to thank my advisor, Dr. Dipanjan Basu for his constant patience, care, and undeviating dedication to me as his student.

I owe a special thank you to Dr. Tanusree Chakraborty for her supreme guidance, and foresight. Without her immense support this study would not be possible.

The technical support and guidance of them both is gratefully acknowledged.

I would also like to thank the members of my thesis committee, Dr. Michael Accorsi, and Dr. Jeong-Ho Kim, for their supporting comments and guidance on this research.

I would like to thank Michelle Levenduski for her caring, everlasting support and encouragement.

Table of Contents

Rate-Dependent Behavior of Clay

Harry Fredrick Martindale IV, B.S.

University of Connecticut, 2011

This thesis presents a strain-rate dependent two-surface plasticity constitutive model for clays based on the critical-state soil mechanics. The model reproduces the mechanical response of clays under multi-axial loading conditions and predicts both drained and undrained behaviors at small and large strains. Model parameter values are determined for Boston Blue Clay, London Clay and Kaolin Clay. The performance of the model in simulating the mechanical response of clays is demonstrated for a variety of strain rates. Sensitivity of each model parameter is checked for ±5, ±10 and ±20% of the deterministic values. Probabilistic analysis using Monte Carlo simulations were done to study the model performance. The probability distributions of undrained shear strength were obtained through random selection of model parameters that follow normal and uniform probability distribution functions.

Chapter 1: Rate-Dependent Behavior of Clay

1.1 Introduction

The effect of strain-rate on the clay stress-strain behavior is well-recognized in the literature. Clay shows strain-rate dependence from a very small rate of strain (10^{-5}/sec). The effect of strain-rate becomes an important factor when we deal with either deformation problems involving constant loading applied over a very long time (e.g., secondary compression - creep) or problems involving slow to medium rate of loading (loading on foundation, and slow landslides) or involving rapid loading (e.g. fast landslides, and pile installation). Nonetheless, analysis and design of geotechnical problems often rely on rate-independent experimental data and soil constitutive models, which is rather inaccurate. In order to achieve realistic simulations of geotechnical problems involving clays, we need to characterize the response of clay under both rate-independent and strain-rate dependent loading. Hence, both experimental data and a constitutive model that takes into account the dependence of clay behavior on strain-rate are necessary.

Among the experimental studies on the characterization of clay response under rate-dependent loading, Casagrande and Shannon (1948) pioneered the investigation of the rate-dependent strength characteristics of clays through triaxial tests in which strain-rates were varied from about 2×10^{-4}/sec to 5/sec. They observed that the strength and stiffness of the clay increased by 10% for each log-cycle

increase in strain-rate. The rate effects on clays have subsequently been investigated by several researchers (Whitman 1960, Richardson and Whitman 1963, Ladd et al. 1972, Berre and Bjerrum 1973, Kavazanjian and Mitchell 1980, Hight et al. 1983, Biscontin 2001, Katti et al. 2003, Zhou et al. 2005, Sorensen et al. 2007, Sheahan 2005, Jung 2005, Hinchberger and Rowe 2005, Jung and Biscontin 2006, Díaz-Rodríguez et al. 2009, Matesic and Vucetic 2003). The maximum strain-rate attained in these experiments was 0.02/sec under triaxial conditions (Lefebvre and LeBoeuf 1987). It was observed that the undrained shear strength increased at a rate of about 5-20% per log-cycle increase in strain-rate. The initial shear modulus increased at a rate of about 10% per log-cycle increase in strain-rate. Tatsuoka and Kohata (1995), and Tatsuoka et al. (1995) examined cyclic tests on Toyoura sand and Pisa clay and found that at strains less than 0.001% the behavior is strain-rate independent. The residual shear strength and critical state were shown to be functions of the material; with the response depending on the dominate clay particle shape and internal friction (Ramiah et al. 1970, Vaid and Campanella 1977, Lupini 1980, Lupini et al. 1981, Skempton 1985, Sheahan et al. 1996, Tika et al. 1996, Fearon et al. 2004, Sorensen et al. 2007, Díaz-Rodríguez et al. 2009). The effect of strain-rate on the critical-state friction angle ϕ_c remains unclear due to experimental difficulties and contradictory data (Richardson and Whitman 1963, Ladd et al. 1972, Vaid and Campanella 1977, Hight et al. 1983, Lefebvre and LeBoeuf 1987, O'Reilly et al. 1989, Sheahan et a. 1996). Positive, neutral and negative rate effects have been observed on the critical-state and residual strength behavior of clays (Lupini 1980, Ramiah et al. 1970, Vaid and Campanella 1977, Lupini et al. 1981, Skempton 1985, Sheahan et al. 1996, Tika et al.

1996, Fearon et al. 2004, Sorensen et al. 2007, Díaz-Rodríguez et al. 2009). Several researchers (Bjerrum et al. 1958, Crawford 1959, Alberro and Santoyo 1973, Hight et al. 1983, O'Reilly et al. 1989) showed an increase in peak friction angle, ϕ_p, with an increase in strain-rate. Richardson and Whitman (1963), Ladd et al. (1972), and Lefebvre and Leboeuf (1987), however show little or no dependence of peak friction angle with strain-rate.

In examining the response of pore pressure to strain-rate, researchers found that with an increase in strain-rate a decrease in pore pressure (Δu) occurred in clays (Bjerrum et al. 1958, Crawford 1959, Richardson and Whitman 1963, Murayama and Shibata 1964, Ladd et al. 1972, Lacerda and Houston 1973, Akai et al. 1975, Hight et al. 1983, Lefebvre and LeBoeuf 1987, Hicher 1988, Sheahan et al. 1994). The response of clay has been shown by several researchers to be highly influenced by the rate of loading, the development of a constitutive model capable of simulating these rate effects is highly desirable.

1.2 Constitutive Modeling

A constitutive model is a mathematical model used to describe the relationship observed for a material under certain conditions. Constitutive models are relations which describe how stress and strain are related for a certain material. Typically a model can be classified as an elastic or inelastic model, a linear or non-linear model, and a rate-dependent or rate-independent model. Constitutive models are used for many materials including metal, asphalt, soil, and clay. However no current constitutive model available can completely describe the complexity of soil

under real loading conditions. Both sand and clay behave drastically different in drained and undrained cases – thus, the development of a model that can simulate both drained and undrained responses of soil under various loading rates is highly advantageous.

Since soil is a very complex material, not many constitutive models exist which can fully capture all of the responses of soil to the vast variety of strain-rates. Several rate-dependent models which capture low strain-rate creep and stress relaxation behaviors of soil can be found in the literature (Bjerrum 1967, Singh and Mitchell 1968, Mesri 1973, Lacerda and Houston 1973, Mesri and Godlewski 1977, Kavazanjian and Mitchell 1977, Tavenas et al. 1978, Ting 1983, Yin and Graham 1989a, b, 1994, Bardet 1986, Yin et al. 1994 and Yin and Graham 1996). Primarily, clay rate-dependent constitutive models can be divided into three main categories: empirical relations, rheological models, and plastic constitutive laws. Empirical relations only apply to problems with specific boundary conditions; however, these can supply the basis for more complex models to be developed. Empirical relations can be classified as both primary and secondary, with primary models being those directly derived from curve fitting data, and secondary models being those derived from a series of combinations of primary models.

Rheological models are typically composed of a group of elastic springs, plastic sliders, and viscous dashpots (Feda 1992). Three well known models are the Maxwell model, Kelvin-Voigt model, and Bingham model. These models are discussed in detail in Feda (1992). The last group is those models which fall under the category of plastic constitutive laws.

Several rhelogical and empirical models are presented in the literature by Murayama and Shibata (1958), Christensen and Wu (1964), Abdel-Hady and Herrin (1966). However more sophisticated models are required in order to simulate the time-dependent behavior exhibited during creep and relaxation (Borja and Kavazanjian 1985, Hsieh et al. 1990, Borja et al. 1990, Cristescu 1991, Borja 1992, Tatsuoka et al. 2000 and 2002, Di Bendetto et al. 2002, Boukpeti et al. 2002, 2004).

Plastic constitutive law models can be divided into three groups, those that are based on the overstress theory of Perzyna, those that are based on the concept of nonstationary flow surface theory (NSFS), and those that do not fit these two categories. A review of key empirical, rheological and constitutive models can be found in Liingaard et al. (2004).

1.3 Overstress Theory

The concept of overstress theory was developed by Ludwick (1922), Prandtl (1928), Hohenemser and Prager (1932), Sokolvsky (1948), and Malvern (1951). The model that Perzyna proposed is a three dimensional extension of Malvern's (1951) model. The key papers describing the development of Perzyna's overstress model are Perzyna (1963, 1966), Olszak and Perzyna (1966a, 1970), and Sekiguchi (1985).

Many rate-dependent soil constitutive models are based on Perzyna's (1966) overstress theory. The overstress model assumes that the inelastic strain is entirely time-dependent. The rate of inelastic strain is caused by the difference between the current stress state and the stress state defined by the hardening parameters. The derivation of the overstress model is different from that of elasto-plasticity in that the

inelastic strains are not related to the stress history, but to the current stress point. The stress state is allowed to be on, within, or even outside the yield surface.

The models which use Perzyna's overstress theory to incorporate viscoplasticity (time-dependent plasticity) can be found widely throughout the literature (Oka and Adachi 1985, Desai and Zhang 1987, Adachi et al. 1987, 1990, 1996, 1997, Oka et al. 1994, 2002 and 2004, di Prisco and Imposimato 1996, 2003, di Prisco et al. 2000, 2002, Zienkiewicz and Cormeau 1974, Adachi and Okano 1974, Zienkiewicz et al. 1975, Adachi and Oka 1982a, b, Dafalias 1982, Oka et al. 1988, Kaliakin 1985, Kaliakin and Dafalias 1990a, 1990b,1991, Kutter and Sathialingam 1992, Tong and Tuan 2007). Yue (2001) incorporated Perzyna's bounding surface model with modifications for clay anisotropy. Despite the wide spread popularity of Perzyna's model, the model lacks the capability to model tertiary creep (Katona 1984, Oka 1985, Mimura and Sekiguchi 1985).

In order to improve Perzyna's model several other models where proposed. A short review of the common models which lead up to the development of the bounding surface concept are presented.

Strain-rate dependent clay constitutive models in the literature are often focused on creep and stress-relaxation behavior of clays. Researchers have incorporated strain-rate effects into clay constitutive models through viscoplasticity, following the classical overstress approach proposed by Perzyna (1963, 1966) (e.g., Zienkiewicz and Cormeau 1974, Kaliakin and Dafalias 1990a, Kutter and Sathialingam 1992, Oka et al. 2002 and 2004). The notion of combining viscoplasticity with bounding surface plasticity was first proposed by Dafalias (1982).

Later, Kaliakin and Dafalias (1990a and 1990b) used this concept to develop a bounding-surface constitutive model for normally and overconsolidated clays, which predicts creep, stress relaxation and secondary compression. Explicit strain-rate dependent constitutive model equations have also been considered in the literature by many researchers (e.g. Kulhawy and Maine 1990, Biscontin and Pestana 2001, Jung and Biscontin 2006, Zhou and Randolph 2007 and Chakraborty 2009). Rate-dependent shear strength relationships, typically considering 5-20% increase of the peak undrained shear strength $s_{u,peak}$ of clay per log cycle increase in shearing rate (without considering any viscous effect) have been considered by Biscontin and Pestana (2001), Jung and Biscontin (2006), Zhou and Randolph (2007). Chakraborty (2009) modified the critical state line equation in the e-ln(p') space to capture the increase in $s_{u,peak}$ of clay per log cycle increase in shearing rate.

1.4 Conclusions From Literature Review

Clay has been shown to exhibit strain-rate dependent response. Strain-rate affects the strength and stiffness of clay, affecting the critical, peak and residual state. These rate effects occur at strain-rates as little as strains greater than 0.001% (Tatsuoka and Kohata 1995, Tatsuoka et al. 1995). The development of a constitutive model capable of simulating the rate dependent response is highly desirable.

In the following sections, first, we present the rate-independent model proposed by Chakraborty (2009) in brief along with the new modifications that we have proposed in the current thesis. Additional model equations required to incorporate the rate-dependence of clay is presented in the next section. Model

parameter determination, sensitivity study of model parameters and Monte Carlo simulation results are arranged in the subsequent sections.

Chapter 2: Rate-Dependent Constitutive Modeling of Clay

2.1 Proposed Model

This thesis generalizes the two-surface clay constitutive model proposed by Chakraborty (2009) to closely simulate clay stress-strain behavior under low to medium loading rates (up to 50%/hr ≈ 1×10^{-4}/sec). Apart from rate-dependent clay behavior, the model also captures other details of clay behavior with reasonable accuracy (e.g., clay mechanical response at both small and large strain levels, multi-axial behavior, and stress induced anisotropy). The model is based on the critical state soil mechanics (CSSM) framework. The model was originally developed for sands by Manzari and Dafalias (1997). It includes a number of features from subsequent work by Li and Dafalias (2000), Papadimitriou and Bouckovalas (2002), Dafalias and Manzari (2004), Dafalias et al. (2004), Loukidis (2006), Loukidis and Salgado (2009) and Chakraborty (2009). The generalized model can successfully simulate the behavior of clays under low to medium strain-rates, under various loading conditions in multi-axial stress space.

Determination of model parameters is an indivisible part of constitutive modeling. For the current model, the majority of the rate-independent constitutive model parameters for Boston Blue Clay (BBC) and London Clay (LC) are obtained from Chakraborty (2009). Only few model parameters for these two clays have been re-calibrated because we made some modifications to some of the rate-independent

model equations. We determined the rate-independent parameters for Kaolin Clay (KC) from one-dimensional and isotropic consolidation tests, resonant column tests, triaxial compression/extension tests, and simple shear tests following the hierarchical process of model parameter determination described by Chakraborty (2009). Rate-dependent model parameters for BBC, LC and KC are determined by comparing the model simulation results with the strain-rate dependent triaxial compression test data taken from the literature.

Determination of constitutive model parameters requires extensive use of experimental data. Therefore, one question that naturally arises is whether there could be any uncertainty present in the model parameters which could affect the performance of the model. It is true that the experimental data used for model parameter determination may contain human and machine related errors which can have direct or indirect influence on the model parameters. As a result, model parameters may vary depending on the experimental data used for parameter determination. In order to understand the relative influence of constitutive model parameters on the model predictions, we perform sensitivity analysis of the constitutive model parameters by varying one parameter at a time. In order to understand the effect of combined uncertainty of the model parameters, Monte Carlo simulation is performed using randomly selected model parameter values (following normal and uniform probability density functions) as inputs. From the Monte Carlo simulations, the distribution of undrained shear strength at peak and critical states are obtained for random selection of model parameters.

2.2 The State Parameter

The model proposed is based on that of a CSSM, critical state soil mechanics model (Schofield and Wroth 1968). A soil can be classified as being at critical state when its void ratio is in equilibrium with the applied stresses. Been and Jefferies (1985) proposed a state parameter defined by the following relationship,

$$\xi = e - e_{cr} \tag{2.2.1}$$

where the state parameter, ξ, is a function of the difference between the current void ratio (e), and the void ratio at critical state (e_{cr}). The critical state line can be defined in e vs ln(p') space by the following equation

$$e_{cr} = \Gamma - \lambda \ln\left(\frac{p'}{p_a}\right) \tag{2.2.2}$$

where p_a is a reference stress equal to 100 kPa, p' is the current stress, λ is the slope of the critical state line, and Γ is the void ratio at the reference stress for the critical state line. Plugging in Been and Jefferies (1985) state parameter into the critical state line equation.

$$\xi = e - \Gamma + \lambda \ln\left(\frac{p'}{p_a}\right) \tag{2.2.3}$$

Further defining the spacing ratio ρ as the ratio of the mean stress at normal consolidation (p'_c) to the mean stress at critical state along some overconsolidation line with slope κ (p'_x).

$$\rho = \frac{p'_c}{p'_x} \tag{2.2.4}$$

The void ratio along the normal consolidation line, $e_{x,}$ can be defined by the following equation.

$$e_x = N - \lambda \ln\left(\frac{p'_x}{p'_c}\right) \tag{2.2.5}$$

where the parameter N, is the void ratio of the normal consolidation line at the reference pressure. The void ratio along the normal consolidation line can be further related to the void ratio along the critical state line, based on the overconsolidation line. Where p'_c corresponds to a void ratio e_c and a p'_x corresponds to a void ratio e_x.

$$e_c = e_x - \kappa \ln \frac{p'_c}{p'_x} \tag{2.2.6}$$

Thus the void ratio along the normal consolidation line, e_n

$$e_n = N - \lambda \ln \frac{p'_c}{p'_a} \tag{2.2.7}$$

Defining e_n in terms of critical state line

$$e_n = \Gamma - \lambda \ln \frac{p'_x}{p'_a} - \kappa \ln \frac{p'_c}{p'_x} \tag{2.2.8}$$

Thus solving for Γ

$$\Gamma = \mathrm{N} - (\lambda - \kappa)\ln(\rho) \tag{2.2.9}$$

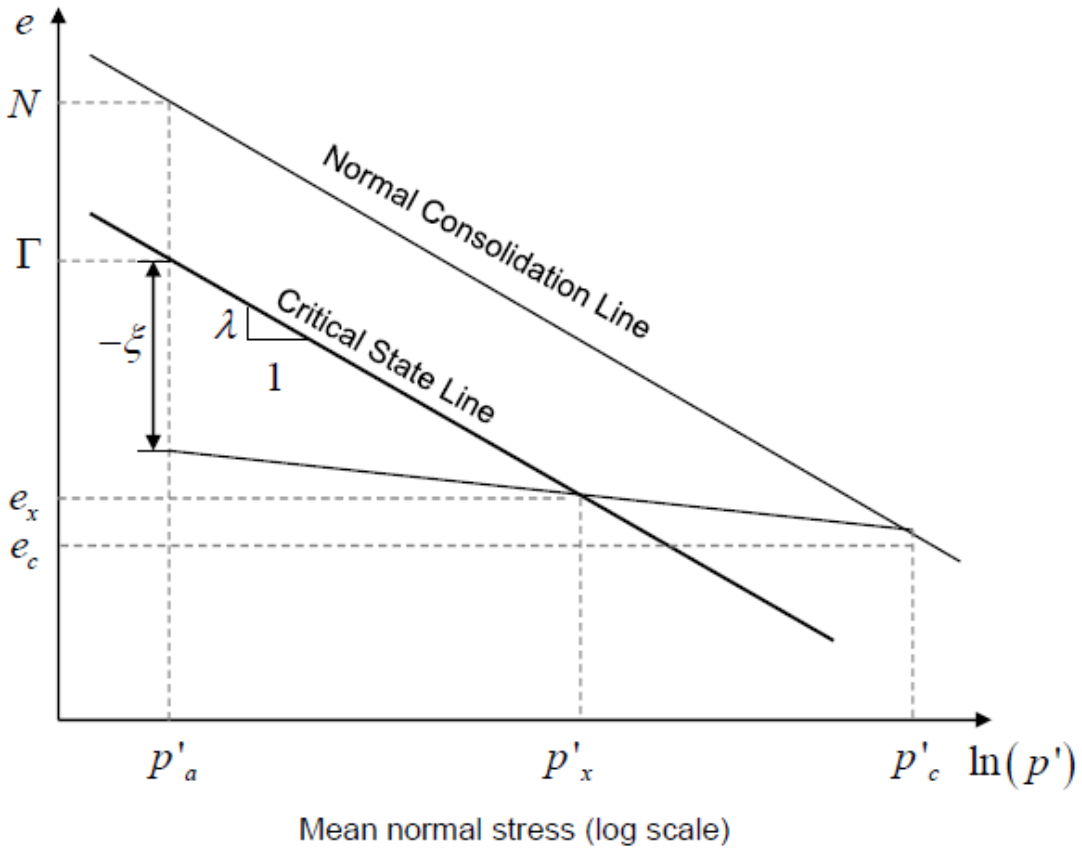

(Figure 2.2.1) Normal consolidation line and Critical state line in e ln(p') space (After Chakraborty 2009)

2.3 Model Surfaces in Stress Space

The model contains three surfaces: the yield surface, the dilatancy surface, and the bounding surface, which, in this model, is made up of two distinct geometrical surfaces: the critical state surface, and the bounding flat cap. The yield, dilatancy, and critical state surfaces are "conical" surfaces with straight surface meridians and apex at the origin. Figure 2.3.1 shows the model surfaces in the stress space, while Figure 2.3.2(a) shows the surface cross-sections in the normalized

deviatoric plane, i.e., in the s_1-s_2-s_3 plane normalized with respect to p'; the tensor **r** in this figure is the normalized deviatoric stress tensor [$r_{ij} = \frac{s_{ij}}{p'}$]. Figure 2.3.2(b) shows the cross-section of the surfaces along the hydrostatic axis.

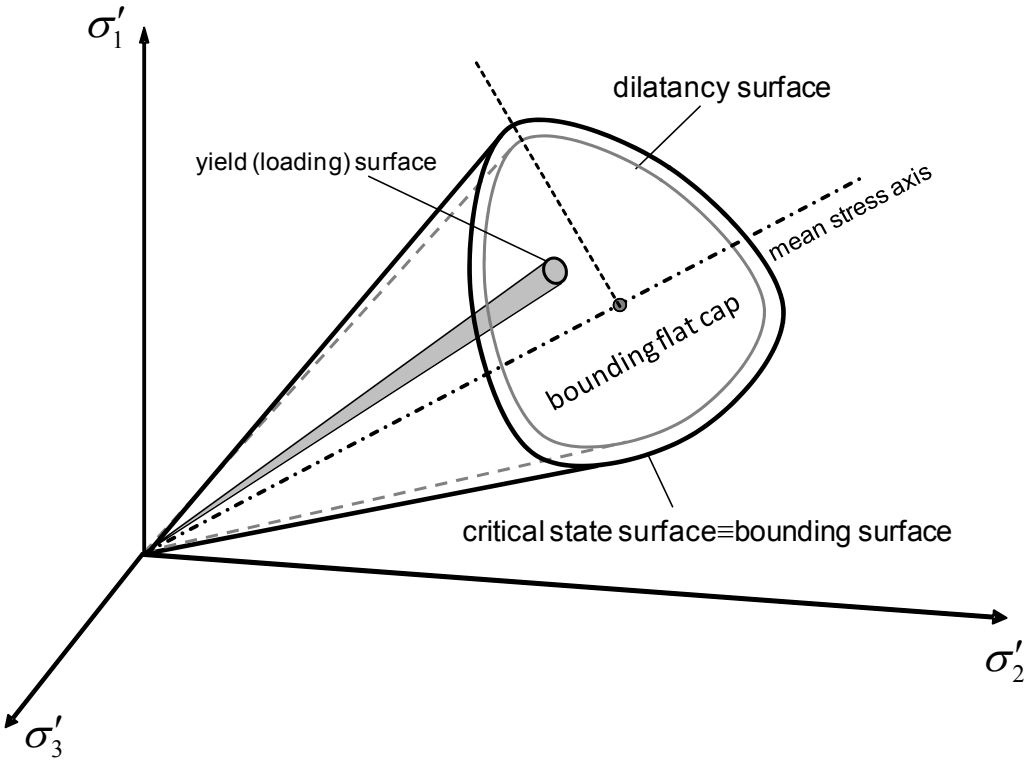

(Figure 2.3.1) Schematic representation of the model surfaces in general stress-space**.** (After Chakraborty 2009)

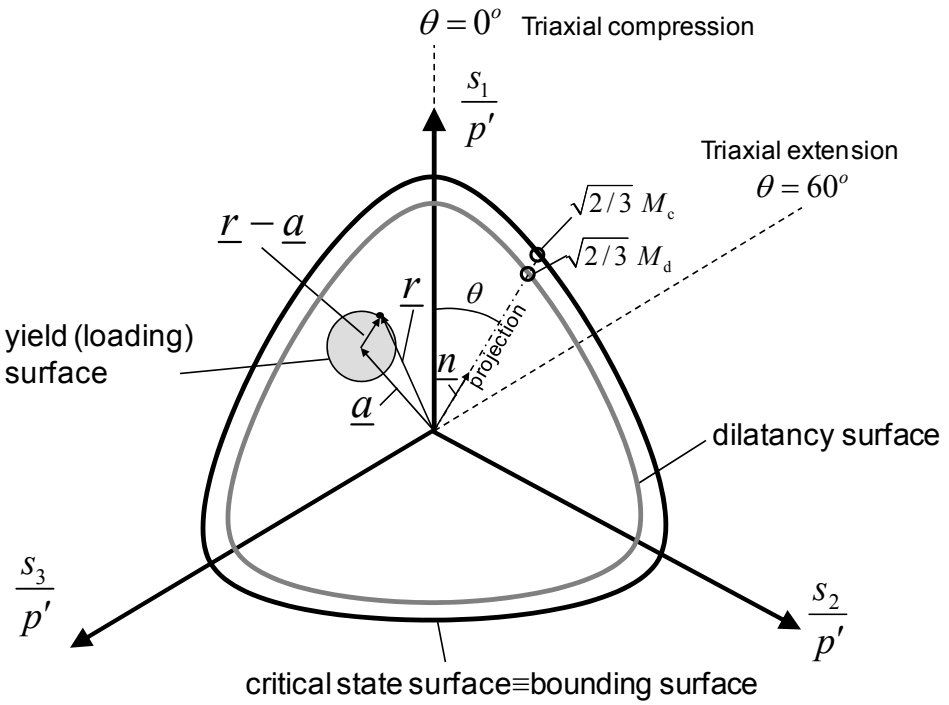

(a)

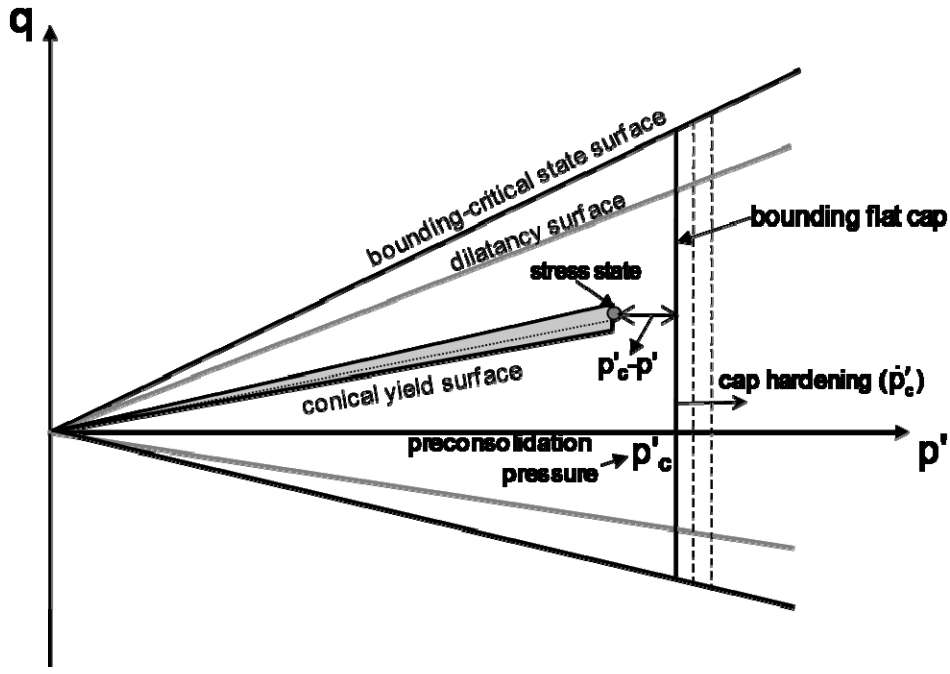

(b)

(Figure 2.3.2) Yield surface cross-section in (a) the deviatoric plane and (b) the meridional plane. (After Chakraborty 2009)

The yield surface of the model is given by

$$f = \sqrt{\rho_{ij}\rho_{ij}} - \sqrt{2/3}\, m = 0 \tag{2.3.1}$$

where m is the radius of the yield surface and ρ_{ij} is the stress ratio given by

$$\rho_{ij} = r_{ij} - \alpha_{ij} \tag{2.3.2}$$

in which r_{ij} is the normalized deviatoric stress tensor ($r_{ij} = s_{ij}/p'$; s_{ij} is the deviatoric stress tensor and p' is the effective mean stress) and α_{ij} is a kinematic hardening tensor. The radius m is constant, i.e there is no isotropic hardening or softening of the yield surface.

The yield surface can harden only kinematically through the use of the kinematic hardening tensor α_{ij}. The dilatancy surface can harden or soften isotropically through the dependence of the corresponding stress ratio M_d on the state parameter ξ.

$$M_d = g(\theta)\left(2M_{cc} + \frac{M_{cc}k_d\xi\ OCR}{1-\exp(k_d\xi\ OCR)}\right) \tag{2.3.3}$$

where OCR is the overconsolidation ratio of clay and the function $g(\theta)$ determines the shape of the dilatancy and the critical state surfaces in the deviatoric plane. Parameter θ is the Lode's angle. The parameter k_d is defined as:

$$k_d = \frac{M_{cc}}{(\lambda-\kappa)\ln\rho} \tag{2.3.4}$$

From Loukidis and Salgado (2009), the following function for *g(θ)* is implemented.

$$g(\theta)=\frac{\left(1-\frac{1-c_1^{1/n_s}}{1+c_1^{1/n_s}}\right)^{n_s}}{\left[1-\left(\frac{1-c_1^{1/n_s}}{1+c_1^{1/n_s}}\right)\cos(3\theta)\right]^{n_s}} \tag{2.3.5}$$

where

$$c_1=\frac{3}{M_{cc}+3} \tag{2.3.6}$$

where n_s is a model parameter.

Loukidis and Salgado (2009), define Lode's angle, θ, through the following relation.

$$\theta=\tan^{-1}\left(\frac{1}{\sqrt{3}}\left(2\frac{n_2-n_3}{n_1-n_3}-1\right)\right)+\frac{\pi}{6} \tag{2.3.7}$$

In terms of effective stress (Manzari 1994 and Manzari and Dafalias 1997), Lode's angle can be expressed as

$$\cos(3\theta)=\frac{3\sqrt{3}}{2}\left(\frac{\bar{S}}{\bar{J}}\right)^3 \tag{2.3.8}$$

where

$$\bar{S}=\left[\frac{1}{3}s\cdot s:s\right]^{\frac{1}{3}} \tag{2.3.9}$$

$$\bar{J}=\left[\frac{1}{2}s:s\right]^{\frac{1}{2}} \tag{2.3.10}$$

$$s=\sigma-pI \tag{2.3.11}$$

where s is the deviatoric stress tensor.

The parameters λ and κ are the slopes the linear normal and overconsolidation lines in the e-ln(p') space. Parameter ρ is the ratio of preconsolidation pressure and the critical state pressure along the same overconsolidation line. In the present

model, the bounding surface is the same as the critical state surface. The critical state surface is given by:

$$M_c = g(\theta)M_{cc} \tag{2.3.12}$$

where M_{cc} is the critical-state stress ratio in triaxial compression [$M_{cc} = 3(\sigma'_{1,CS} - \sigma'_3)/(\sigma'_{1,CS} + 2\sigma'_3)$].

The flat cap to the bounding surface helps to capture yielding and development of plastic strains at shallow stress paths (paths with an inclination that is smaller than the critical stress ratio). This primarily occurs for low OCR clays and NC clays, in which the evolution of *p* varies significantly over the simulation. The bounding flat cap is perpendicular to the mean stress (hydrostatic) axis (Figure 2.3.2b) and is represented mathematically by $F_c = 0$:

$$F_c = p' - p'_c = 0 \tag{2.3.13}$$

The flat cap is part of the bounding surface, intersecting the hydrostatic axis at p' equal to the cap hardening variable p'_c. The variable p'_c has the physical meaning of the preconsolidation pressure. As in the case of the bounding – critical state surface that controls shearing behavior of the clay, the consistency condition is not applied to the cap and, thus, stress states marginally outside the cap are possible.

2.4 Elastic Shear and Bulk Moduli

The stress-strain relation for the present model is shown as:

$$\dot{\sigma}'_{ij} = 2G\left(\dot{\varepsilon}_{ij} - \dot{\varepsilon}^p_{ij}\right) + \left(K - \frac{2}{3}G\right)\left(\dot{\varepsilon}_{kk} - \dot{\varepsilon}^p_{kk}\right)\delta_{ij} \tag{2.4.1}$$

The total strain rate ($\dot{\varepsilon}_{ij}$) has an elastic ($\dot{\varepsilon}_{ij}^{e}$) and a plastic ($\dot{\varepsilon}_{ij}^{p}$) component [$\dot{\varepsilon}_{ij} = \dot{\varepsilon}_{ij}^{e} + \dot{\varepsilon}_{ij}^{p}$]. When the stress state is entirely within the yield surface, there is no plastic strain and a unique relation between stress and strain exists there. Since, in the present model, the yield surface is very small, a plastic process is operative during almost the entire loading process. The shear modulus G and bulk modulus K are used as the elastic pair in model equations.

The small-strain shear modulus G_0 is calculated using Hardin (1978),

$$G_0 = C_g \frac{(e_g - e)^2}{1+e} \left(\frac{p'}{p_a} \right)^{n_g} OCR^{m_g} \tag{2.4.2}$$

where c_g is a material parameter, and e_g, n_g, and m_g are defined at 2.97, 0.5, and 0.2 respectively. Thus the equation becomes

$$G_0 = c_g \frac{(2.97 - e)^2}{1+e} \sqrt{p' p_a} OCR^{0.2} \tag{2.4.3}$$

The initial bulk modulus K_i is related to the small-strain shear modulus G_0 through a constant Poisson's ratio ν:

$$K_i = G_0 \frac{2(1+\nu)}{3(1-2\nu)} \tag{2.4.4}$$

The inclination κ of the unloading or reloading overconsolidation lines observed in one-dimensional compression tests is directly related to the bulk modulus:

$$K_{min} = \frac{p'(1+e)}{\kappa} \tag{2.4.5}$$

$$G_{min} = \frac{3(1-2\nu)}{2(1+\nu)} K_{min} \tag{2.4.6}$$

However, this bulk modulus value is much smaller than the true small-strain bulk modulus K_i (i.e. the value corresponding to G_0, as measured in resonant column or bender element tests, and a realistic value of the Poisson's ratio). In this model, G and K are assumed to decrease exponentially with increasing shear and/or mean stresses from the initial values G_0 and K_i until the limiting values G_{min} and K_{min} are reached:

$$G = G_{min} + (G_{max} - G_{min}) \exp\left[-\zeta \left(\frac{|p' - p'_{ini}|}{p_c} + \frac{\sqrt{3/2}\sqrt{(r_{ij} - a_{ij,ini})(r_{ij} - a_{ij,ini})}}{M_{cc}} \right) \right] \tag{2.4.7}$$

$$K = K_{min} + (K_{max} - K_{min}) \exp\left[-\zeta \left(\frac{|p' - p'_{ini}|}{p_c} + \frac{\sqrt{3/2}\sqrt{(r_{ij} - a_{ij,ini})(r_{ij} - a_{ij,ini})}}{M_{cc}} \right) \right] \tag{2.4.8}$$

p'_{ini} is the initial mean stress and $a_{ij,ini}$ is the initial stress ratio. Upon change in loading direction, the values of the elastic moduli take again the G_0 and K_i values by setting the p'_{ini} and $a_{ij,ini}$ equal to the current p' and a_{ij} values. This formulation is capable of predicting the hysteresis in unloading-reloading loops even when the loops lie entirely inside the yield surface. Hence, the simulated material behavior inside the yield surface is not elastic but non-linear elastic, as in the paraelastic approach of Hueckel and Nova (1979).

2.5 Flow Rule

The plastic strain tensor ε_{ij}^p has two components: $\varepsilon_{ij,shear}^p$ and $\varepsilon_{ij,cap}^p$. The first component is related to the conical yield, bounding and dilatancy surfaces and is determined using:

$$\dot{\varepsilon}_{ij,shear}^p = \dot{\lambda}_{shear} \left(R'_{ij} + \frac{1}{3} D \delta_{ij} \right) \tag{2.5.1}$$

where $\dot{\lambda}_{shear}$ is the shearing-related plastic multiplier, D is shear related dilatancy and R'_{ij} is the deviatoric part of the plastic potential gradient.

The second component is related to the cap and is calculated based on:

$$\dot{\varepsilon}^{p}_{ij,cap} = \frac{\dot{\lambda}_{cap}}{D^{*}}\left(R'_{ij} + \frac{1}{3}\delta_{ij}D^{*} \right) \tag{2.5.2}$$

where $\dot{\lambda}_{cap}$ is the cap related plastic multiplier and D* is the cap related dilatancy (Chakraborty 2009). The cap related dilatancy is derived in Appendix AII.2.3.

Satisfaction of the consistency condition for the conical yield surface provides the expression for the plastic multiplier $\dot{\lambda}_{shear}$ for yielding in shearing mode

$$\dot{\lambda}_{shear} = \frac{1}{H_s}\frac{\partial f}{\partial \sigma'_{ij}}\dot{\sigma}'_{ij} = \frac{1}{H_s}\left(n_{ij} - \frac{1}{3}(n_{kl}r_{kl})\delta_{ij} \right)\dot{\sigma}'_{ij} \tag{2.5.3}$$

As indicated earlier, the tensor **n** represents the direction of the projection of the current stress on the critical-state and dilatancy surfaces (i.e., the mapping rule). The gradient of the plastic potential R_{ij} in stress space is divided in a deviatoric component R'_{ij} expressing the direction of deviatoric plastic strain rate $\dot{e}^{p}_{ij,shear}$ (Chakraborty 2009), and a mean component related directly to the dilatancy D that controls the shear-induced plastic volumetric strain rate $\dot{\varepsilon}^{p}_{kk,shear}$:

$$D = \frac{D_0}{M_{cc}OCR}\left(\sqrt{\frac{2}{3}}\left(M_d - m \right) - a_{ij}n_{ij} \right)e^{\left(d_1(1-OCR) \right)} \tag{2.5.4}$$

The dilatancy D depends on the distance between the current stress state and the projected stress state on the dilatancy surface (Manzari and Dafalias 1997) [$\sqrt{2/3}\left(M_d - m \right) - \alpha_{ij}n_{ij}$]. D_0 in the same equation is an input parameter controlling the inclination of the stress ratio-dilatancy curve. The expression for the dilatancy D

contrasts with that used for the clay model by Chakraborty (2009). In Chakraborty (2009), the exponential, OCR dependent part of the equation was not present. With this addition, the model better predicts the dilatancy behavior of clay for higher OCR values.

The plastic modulus H_s in equation (2.5.3), controlling the development of $\varepsilon^{p}_{ij,shear}$ is determined using:

$$H_s = h_0 \frac{G\ OCR}{\left[\sqrt{\frac{3}{2}}\sqrt{(r_{ij}-a_{ij,ini})(r_{ij}-a_{ij,ini})}\right]}\sqrt{\frac{2}{3}}\left(\sqrt{\frac{2}{3}}(M_c-m)-a_{ij}n_{ij}\right) \tag{2.5.5}$$

H_s depends on the distance between the current stress state and the image stress state on the bounding surface pointed to by the loading tensor n_{ij} (Figure 2.3.2a).

The evolution of the kinematic hardening variable α_{ij} is given by:

$$\dot{\alpha}_{ij} = \dot{\lambda}_{shear}\frac{H_s}{p'}\left(\sqrt{\frac{2}{3}}(M_c-m)n_{ij}-\alpha_{ij}\right)\Big/\left(\sqrt{\frac{2}{3}}(M_c-m)-\alpha_{ij}n_{ij}\right)$$

(2.5.6)

α_{ij} is based form the work of Loukidis and Salgado (2009) and Dafalias et al. (2004). It follows the kinematic hardening rule by which the yield surface moves in the direction of $\sqrt{2/3}(M_c\text{-}m)n_{ij}\text{-}\alpha_{ij}$ within the deviatoric plane; n_{ij} is defined as $\left[n_{ij} = \left(s_{ij}-p'\alpha_{ij}\right)/\sqrt{\left(s_{kl}-p'\alpha_{kl}\right)\left(s_{kl}-p'\alpha_{kl}\right)}\right]$ and is parallel to the vector connecting the center of the yield surface in the deviatoric plane (i.e., the axis of the yield surface) to the current stress point on the yield surface in the same deviatoric plane (Figure 2.3.2a). It also represents the direction of projection of the current stress on the critical-state surface and the dilatancy surface.

2.6 Influence of Strain-Rate on Mechanical Response

To take into account the effect of strain rate on the mechanical response of clays, a number of modification and additions are made to the model formulation proposed by Chakraborty (2009). Data from numerous experimental studies show that the peak strength and the stiffness increases substantially for normally consolidated and lightly overconsolidated clays (OCR=2) with increasing rate of strain, while the increase in critical-state strength is small. This is captured by the model in a simple but practical way by assuming that the critical state and normal consolidation lines (CSL and NCL) move upward in the e-ln(p') space with increasing strain rate . This is achieved by using Γ (intercept of the critical state line in the e-ln(p') space on the void ratio axis at reference stress = 100 kPa) with Γ^*, which is given by:

$$\Gamma^* = \Gamma\left(1 + c_0 \ln\left(\frac{c_0}{10}\dot{\varepsilon}_{eq} + 1\right)\ln\left(d_c + 1\right)\right)$$

(2.6.1)

where c_0 is a model parameter. The rate-dependent CSL intercept Γ^* is a function of $\dot{\varepsilon}_{eq}\left(=\sqrt{\dot{\varepsilon}_{ij}\dot{\varepsilon}_{ij}}\right)$ (in %/hr), which is used as a general measure of strain rate, and the distance d_c between the current soil state and the critical state. Γ^* is equal to Γ when $\dot{\varepsilon}_{eq}$ is zero. The distance d_c is defined by:

$$d_c = \sqrt{c_0\left[\xi_i^{\,2} + \left(\bar{d}\right)^2\right]} \tag{2.6.2}$$

$$\bar{d} = \frac{\left\langle M_c - \sqrt{\frac{3}{2}}\sqrt{r_{ij}r_{ij}}\right\rangle}{M_c} \tag{2.6.3}$$

where ξ_i is the state parameter (difference of the current void ratio from the critical-state void ratio) for zero strain-rate; and $\bar{d}$ is a normalized distance of the current stress state from the critical-state surface along the direction of the stress ratio tensor r_{ij} in the deviatoric plane. As Γ increases, the mean stress at critical state ($p_{critical}$), increases and so does the peak undrained shear strength. With further shearing, clay softens towards the critical and residual states, d_c tends to zero, Γ tends to Γ_0, and the deviatoric stress q decreases towards $s_{u,critical}$.

Equation (2.6.1) is a slightly modified form of the one proposed in Chakraborty (2009) in a way that the present equation has reduced number of model parameters. One major change brought in equation (2.6.1) is the OCR-dependence of the parameter c_0 which will be discussed in detail in the model parameter determination section of this thesis.

To better capture the strain rate effects at higher OCR values, we modify the rate-independent dilatancy equation and incorporate strain rate-dependence of dilatancy through the following equation:

$$D = \frac{D_0}{M_{cc} OCR}\left(\sqrt{\frac{2}{3}}\left(M_d - m\right) - \alpha_{ij} n_{ij}\right)\left(1 + \log\left(\dot{\varepsilon}_{eq} + 1\right)\right) e^{\left(d_i (1 - OCR)\right)} \tag{2.6.4}$$

Strain rate-dependence of dilatancy parameter causes expansion of dilatancy surface and as a result lesser dilatancy with increasing rate of strain. Figure 2.6.1 illustrates the evolution of D with ξ and OCR for Boston Blue Clay and triaxial compression conditions. For OCR=1, the exponential OCR dependent part of dilatancy equation remains inactive. The curved loop in D for OCR= 2 helps capturing the phase transformation behavior. The current expression better captures the OCR dependent

dilatancy of clays and strain-rate dependent behavior of clays with higher OCR values (above OCR=2). It was observed that, should the OCR is not introduced in eq. (2.6.4), adequate simulation of strongly overconsolidated specimens require larger k_d values than simulations of normally consolidated (NC) specimens. In other words, the curvature of the D vs. ξ function needs to larger for large OCR values and higher strain rates than for small OCR values and rate-independence.

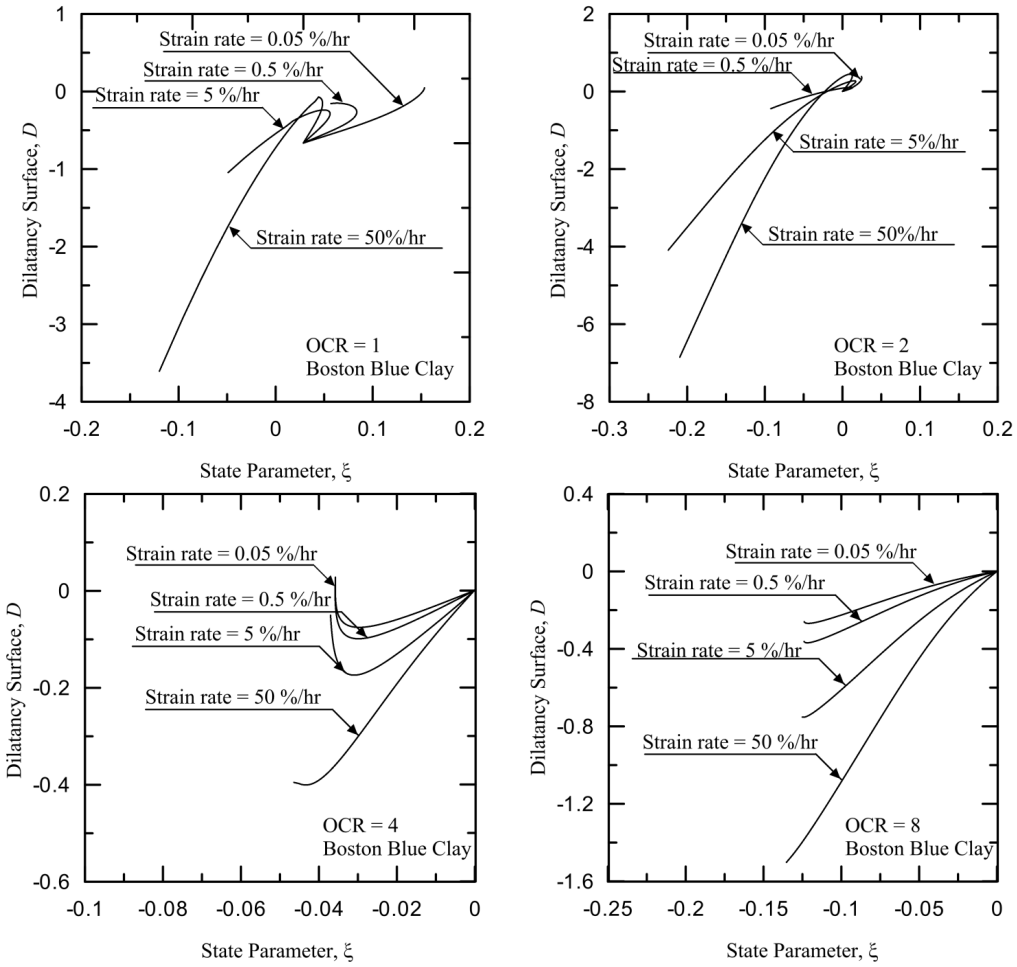

Figure 2.6.1 Variation of D with state parameter ξ for BBC at different *OCR* values under triaxial compression condition predicted by eq. (2.6.4) for different strain-rates

As opposed to the model proposed by Chakraborty (2009), the distance between the CSL and the NCL in e-ln(p′) space is not constant in e-ln(p′) space in the current model. This is because in the Chakraborty (2009) model, the increase in preconsolidation pressure was proportional to the rightward movement of the CSL in the e-ln(p') which was hypothetical. The shift of the normal consolidation line with increasing strain rate has been observed by many researchers (Bjerrum 1967, Leroueil et al. 1985, Sheahan 2005, etc.). In the present model, we collected a database of increasing preconsolidation pressure with strain rate and fitted a trend line through the data (Figure 2.6.2) given by:

$$P_c = P_1\left(1.3\dot{\varepsilon}_{eq}^{\ 0.05}\right) \tag{2.6.5}$$

Here P_1 is the initial value of the preconsolidation pressure. Please note that for rate-independent simulations, we need to put $P_c = P_1$. The strain rate values are in %/hr. It was observed that this equation works best for NC clays whereas it does not play any role for the overconsolidated (OC) clays.

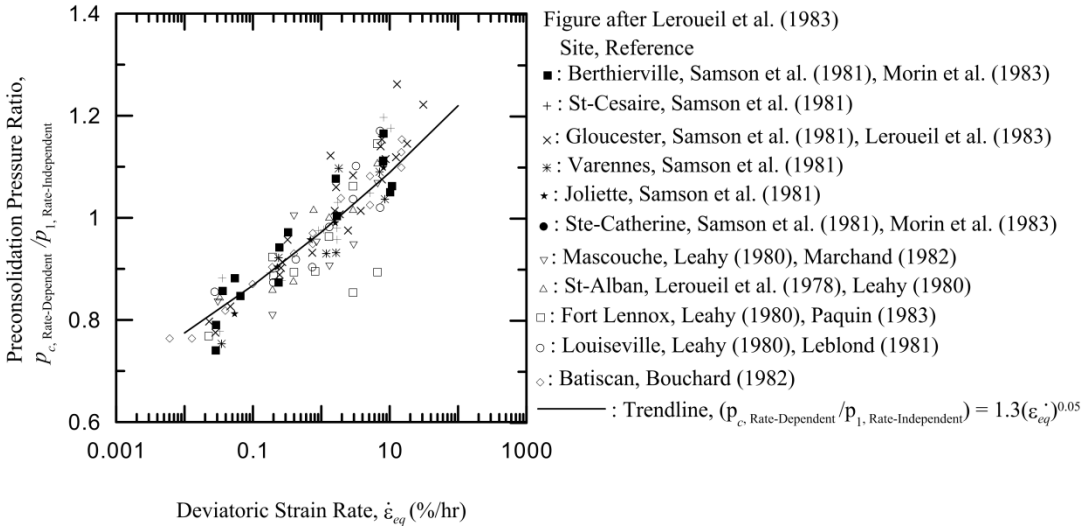

(Figure 2.6.2) Effect of Strain-Rate on Preconsolidation Pressure Ratio

2.7 Determination of model parameters

The present model formulation has fifteen parameters altogether – fourteen rate-independent and one rate-dependent parameters. Determination of these parameters relies on data from one-dimensional consolidation, triaxial compression and extension (at various strain rates), simple shear, and small-strain tests (like bender element or resonant column tests). The constitutive model is formulated in such a way that the model can be calibrated in a hierarchical manner by curve fitting over given sets of experimental data points; only a few model parameters require trial-and-error simulations of element tests. The hierarchical process of model parameter determination is described in details in Chakraborty (2009).

We determine the model parameter c_0, controlling the strain-rate dependent behavior of the model, by comparing the simulation results with the experimental data for three different clays: Boston Blue Clay (BBC), Kaolin Clay (KC), and London Clay (LC). BBC is a low-plasticity marine clay, composed of illite and quartz (Terzaghi et al. 1996). LC contains illite, kaolinite, smectite and quartz (Al-Tabbaa and Stegemann 2005, Gasparre et al. 2007a and 2007b). KC mainly contains Kaolinite (Prashant 2004). Table 2.7.1 shows the index properties of BBC, LC and KC. Strain rate dependent experimental data for BBC are taken Sheahan (1991) and (1996). KC data are obtained from Ling et al. (2002) and Mukabi and Tatsuoka (1999) for rate-independent and strain-rate dependent triaxial compression tests respectively. Strain-rate independent data for LC are collected from Hight et al. (2003), Gasparre (2005) and Atkinson and Richardson (1987). Strain-rate dependent experimental data for LC comes from Sorensen et al. (2007). The model parameters

and their values for the four clays are summarized in Table 2.7.2. Determination of the strain-rate dependent model parameter is discussed next.

Index properties of clays					
Clays	LL (%)	PL (%)	PI (%)	Classification	References
Boston Blue Clay	32.6	19.5	13.1	Inorganic clay or Silt of Low to Medium Plasticity (CL) (USCS)	Ladd and Varallyay (1965)
London Clay	69.6	26.2	43.4	High Plasticity Stiff Clay	Nishimura (2005)
Kaolin Clay	62	30	32	Low compressibility (CL/ML) (USCS)	Prashant (2004)

(Table 2.7.1) Index properties of Boston Blue Clay, London Clay and Kaolin Clay

Constitutive Model Parameters				
Model Relationships		BBC	LC	Kaolin
Small-strain (elastic) Poisson's ratio	υ	0.25	0.2	0.25
G_0 correlation parameter	C_g	250	100	120
Elastic moduli with degradation	ζ	5	10	5
	κ	0.036	0.064	0.033
Normal consolidation line	N	1.138	1.07	0.984
	λ	0.187	0.168	0.18
Critical state surface	M_{c0}	1.305	0.827	1.18
	ρ	2.2	2.5	2.7
Dilatancy surface	d_1	0.2	0.2	0.2
	d_0	1	0.24	0.8
Flow rule	c_2	0.95	0.95	0.95
	n_s	0.2	0.2	0.2
Hardening	h_0	1.1	1.1	1.1

(Table 2.7.2) Constitutive Model Parameters for Boston Blue Clay, London Clay and Kaolin Clay

2.8 Parameters Describing Strain-Rate Dependence

The present model has only two parameters c_0 and d_1 controlling the strain-rate dependent behavior of clays. c_0 plays a major role for normally consolidated clays whereas d_1 is important for OC clays. It was observed that maintaining a constant c_0 value for all OCR values results in not so good comparison with test data. On the other hand d_1 did not play any role for normally consolidated clays. It has been observed by researchers that the constitutive models that capture normally consolidated clay behavior well, do not capture the overconsolidated clay behavior well and vice versa (Dafalias et al. 2006, Chakraborty 2009, Hajek et al. 2009). From the simulations in Chakraborty (2009), it was observed that their model worked best for OCR values 1 and 2, i.e., for the soils which are on the wet side of the critical state line to start with. However, for higher OCR values, i.e., for the soils on the dry side of the critical state line, their equation showed phase transformation behavior at higher strain-rates which is not observed in the experimental data. Therefore, in the present model, we follow an OCR dependent modeling calibration approach for parameter c_0 under strain-rate dependent loading. In order to determine parameter c_0, we compare the predicted increase in peak normalized deviatoric stress q_{peak} obtained from undrained triaxial compression simulations with strain rate with the test data [Dafalias et al. 2006, Chakraborty 2009, Hajek et al. 2009 for KC] . The values of q_{peak} are normalized with respect to maximum axial stress. In order to decrease the subjectivity of the model calibration, a scalar measure of the ‘‘peak stress difference error” between the model predictions and the experimental data has been introduced. The c_0 value that predicted the minimum error was considered for model simulation.

$$\text{error} = \frac{q_{peak}^{simulation} - q_{peak}^{experimental}}{q_{peak}^{experimental}} \times 100\% \qquad (2.8.1)$$

Appendix I presents stress-strain and stress-path plots examining error values for different c_0 values at different OCR. Table 3.3.1 presents the c_0 values for different strain rates and OCRs. The effect of c_0 is shown in Figure 2.8.1 and Figure 2.8.2. The equation (2.6.1) worked best for normally consolidated and lightly overconsolidated clays (OCR=2). For OCR values higher than 2, we deactivated the equation (2.6.1) using a very small value of c_0 and, for all practical purposes, Γ^* remained equal to Γ even for higher strain rates.

The model parameter d_1 was determined by comparing the stress-strain results obtained from the simulations with the experimental data. A constant value of d_1 worked well for all strain rate values and OCRs and for all clays.

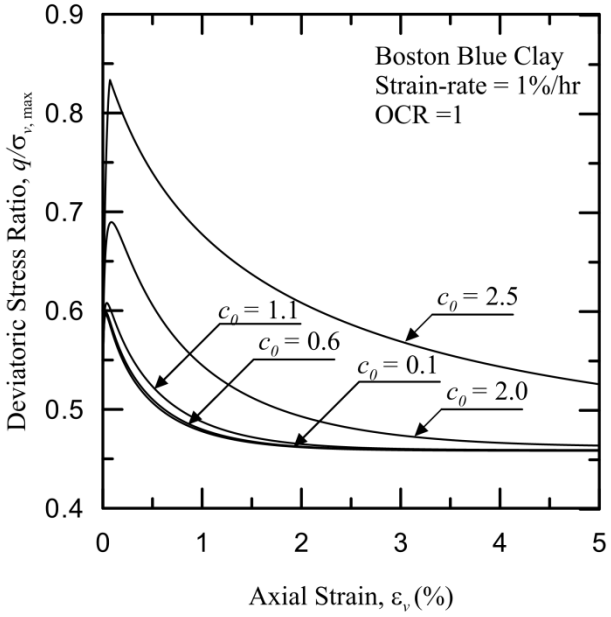

(Figure 2.8.1) Effect of parameter c_0 stress-strain plot

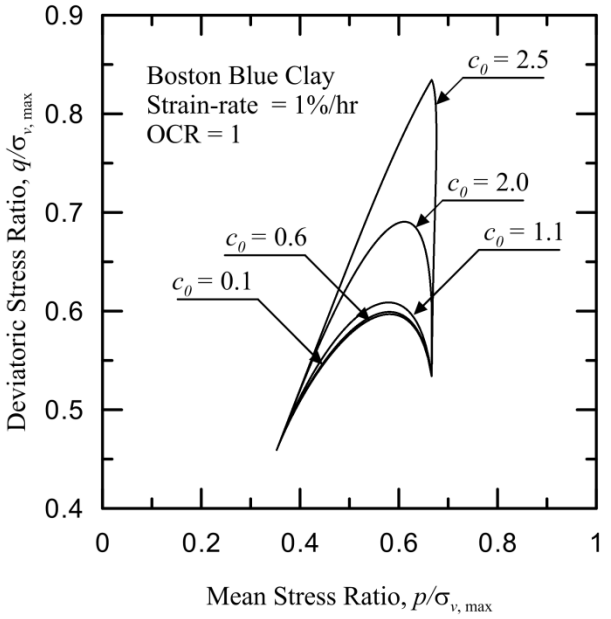

(Figure 2.8.2) Effect of parameter c_0 stress-path plot

Rate-Dependent Constitutive Model Parameters						
Model Relationships		OCR	Strain-rate %/hr	BBC	LC	KC
Rate Dependence	c_0	1	50	0.6	-	-
			30	-	-	0.5
			6	-	-	0.5
			5	1.1	-	-
			0.9	-	2.0	-
			0.6	-	-	0.5
			0.5	2.0	-	-
			0.05	2.0	2.0	-
		2	50	0.5	-	-
			5	1.1	-	-
			0.5	2.0	-	-
			0.05	2.0	-	-
		4	50	0.1	-	-
			5	0.1	-	-
			0.5	0.1	-	-
			0.05	0.1	-	-
		5	0.5	-	2.0	-
			0.05	-	2.0	-
			0.00714	-	2.0	-
		8	50	0.1	-	-
			5	0.1	-	-
			0.5	0.1	-	-
			0.05	0.1	-	-

(Table 2.8.1) c_0 Constitutive Model Parameter for Boston Blue Clay, London Clay and Kaolin Clay

2.9 Rate-Independent Undrained Shearing

K_0-Condition:

Figure 2.9.1 to Figure 2.9.12 compare the model predictions with strain rate independent experimental data for undrained triaxial compression of K_0-consolidated specimens of BBC, LC and KC . In the proposed model, we use the same M_{cc} value for isotropic and K_0 consolidation cases. This causes slight under prediction of stresses for BBC at OCR values 4 and 8.

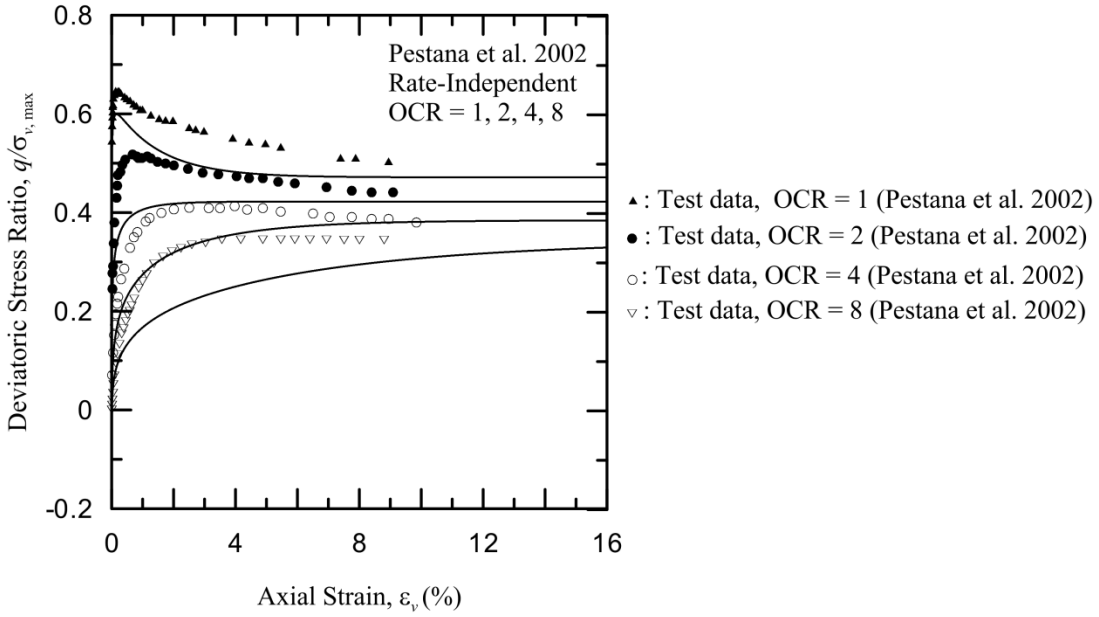

(Figure 2.9.1) Simulation of Pestana et al. (2002), Boston Blue Clay, Rate-independent, K_0, stress-strain plot

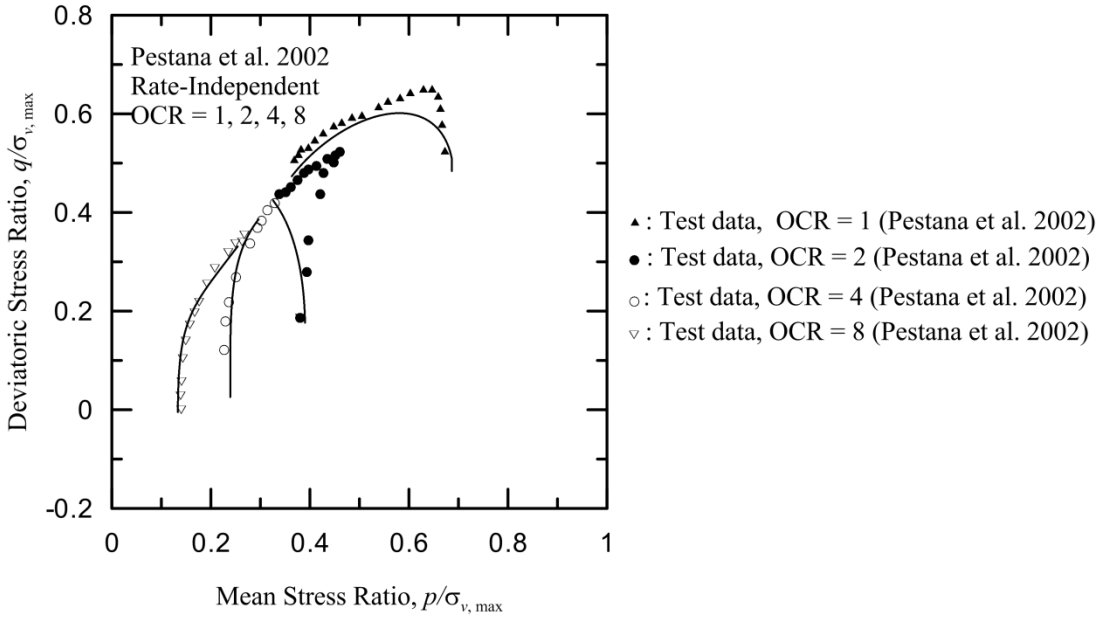

(Figure 2.9.2) Simulation of Pestana et al. (2002), Boston Blue Clay, Rate-independent, K_0, stress-path plot

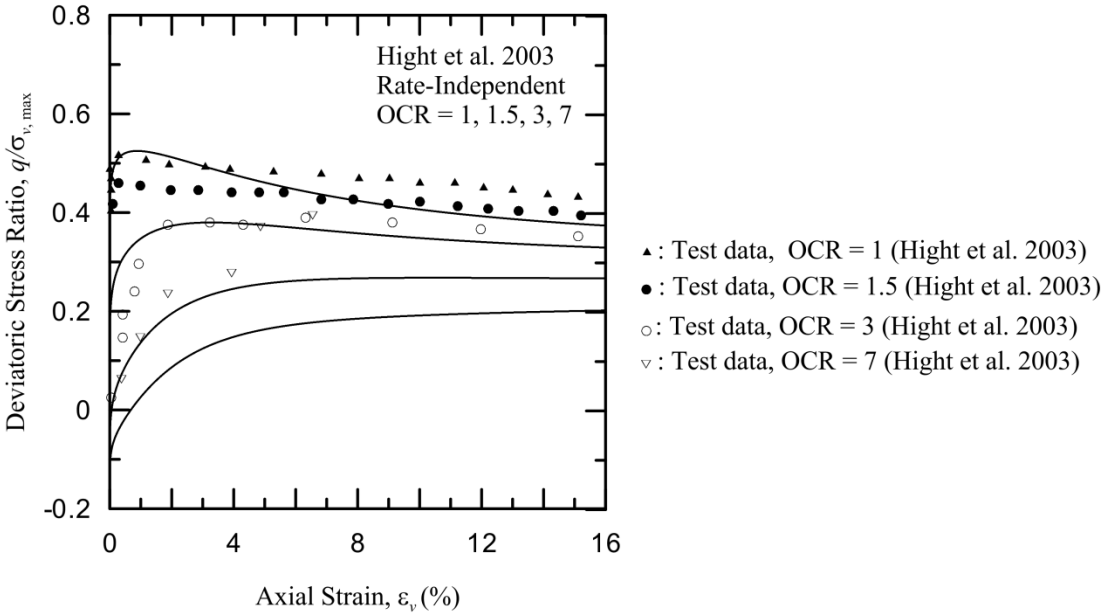

(Figure 2.9.3) Simulation of Hight et al. (2003), London Clay, Rate-independent, stress-strain plot

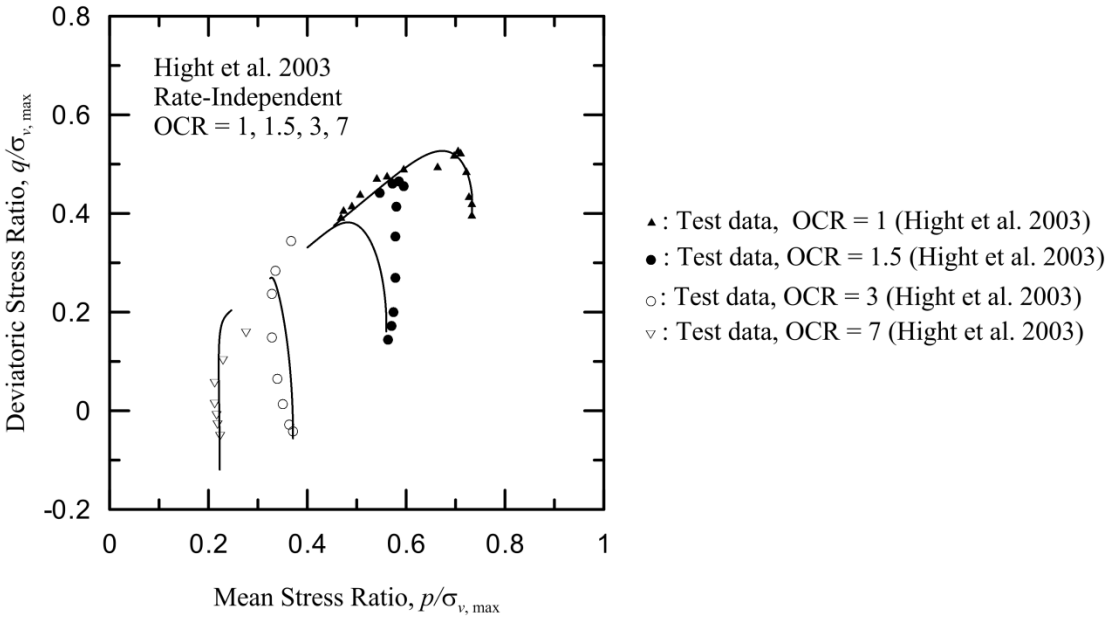

(Figure 2.9.4) Simulation of Hight et al. (2003), London Clay, Rate-independent, stress-path plot

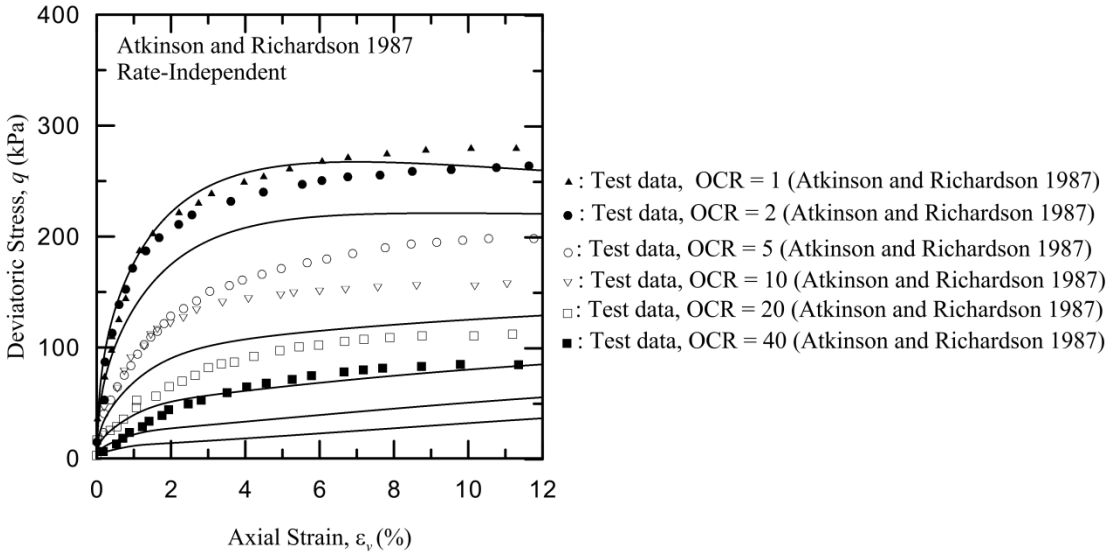

(Figure 2.9.5) Simulation of Atkinson and Richardson (1987), London Clay, Rate-independent, stress-strain plot

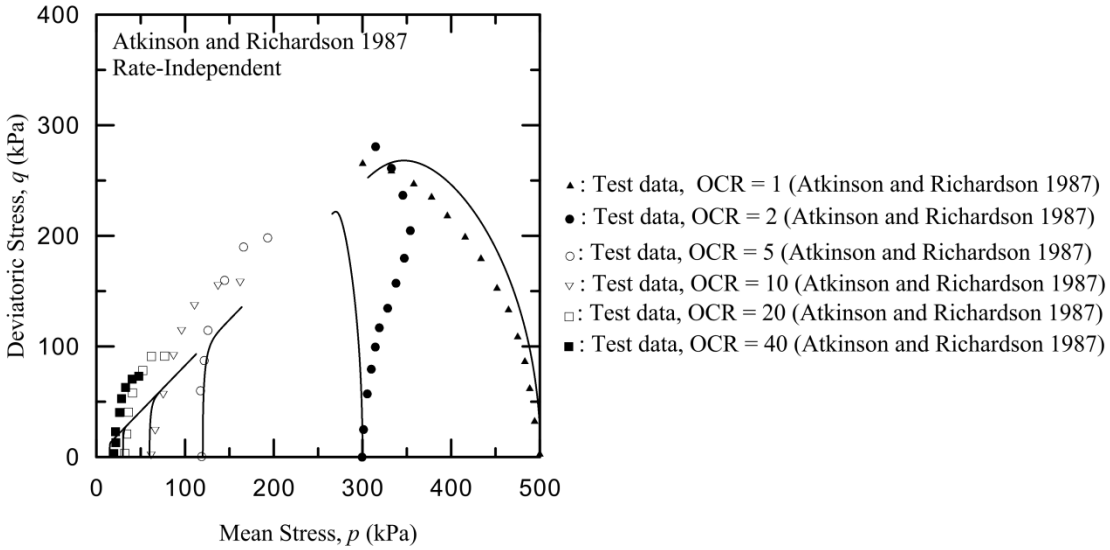

(Figure 2.9.6) Simulation of Atkinson and Richardson (1987), London Clay, Rate-independent, stress-path plot

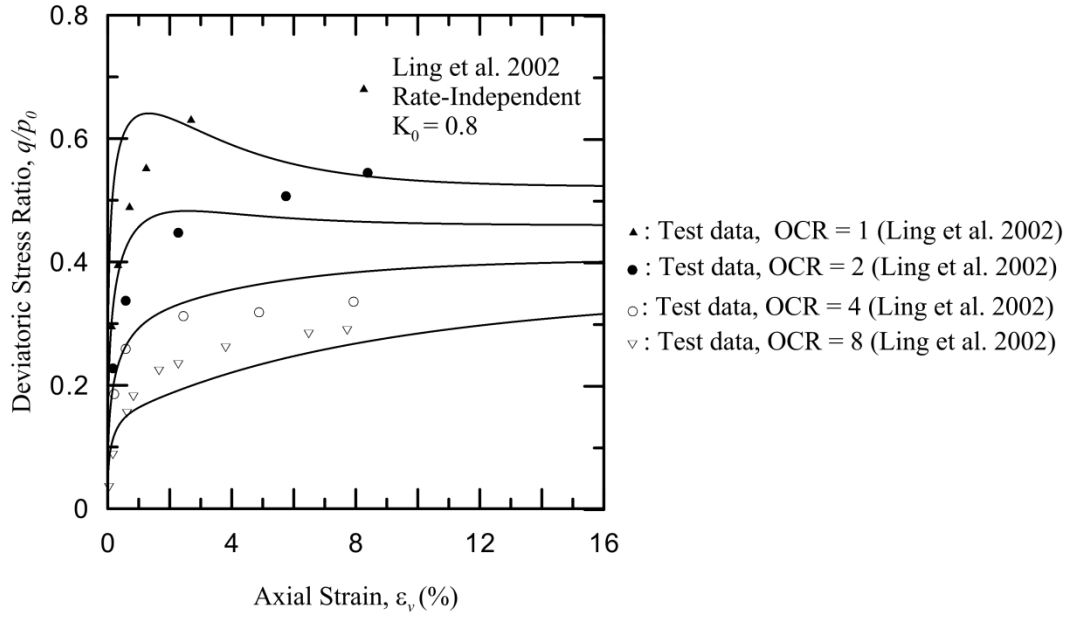

(Figure 2.9.7) Simulation of Ling et al. (2002), Kaolin Clay, Rate-independent, stress-strain plot

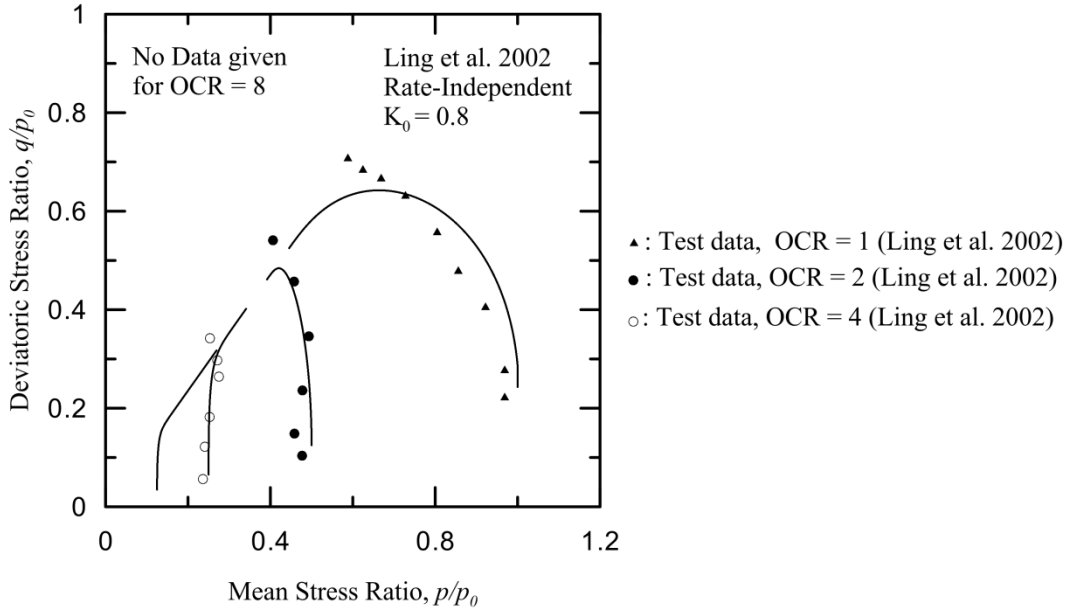

(Figure 2.9.8) Simulation of Ling et al. (2002), Kaolin Clay, Rate-independent, stress-path plot

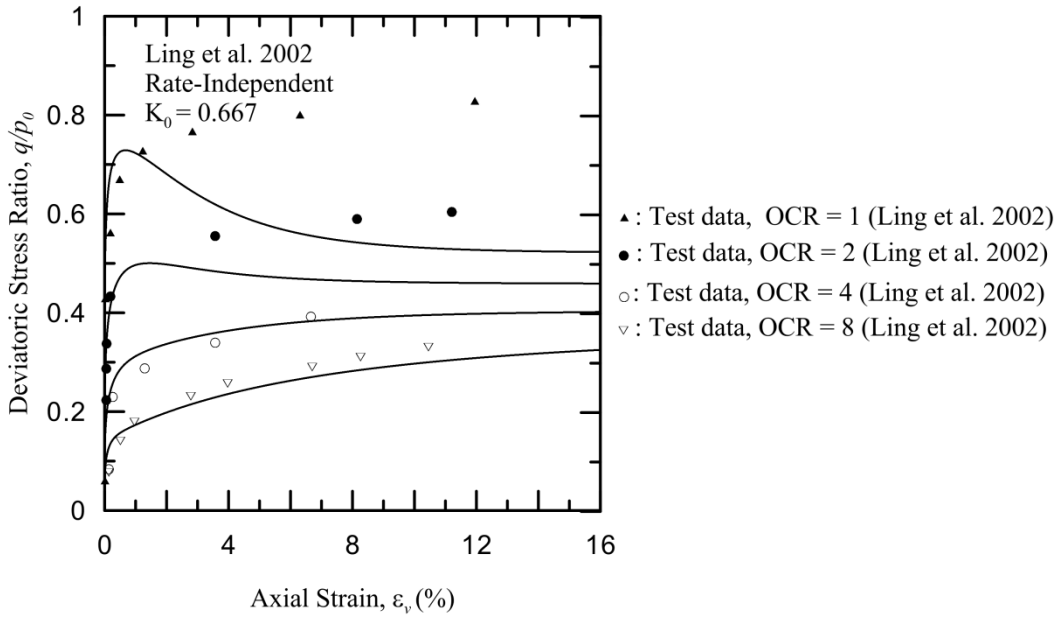

(Figure 2.9.9) Simulation of Ling et al. (2002), Kaolin Clay, Rate-independent, stress-strain plot

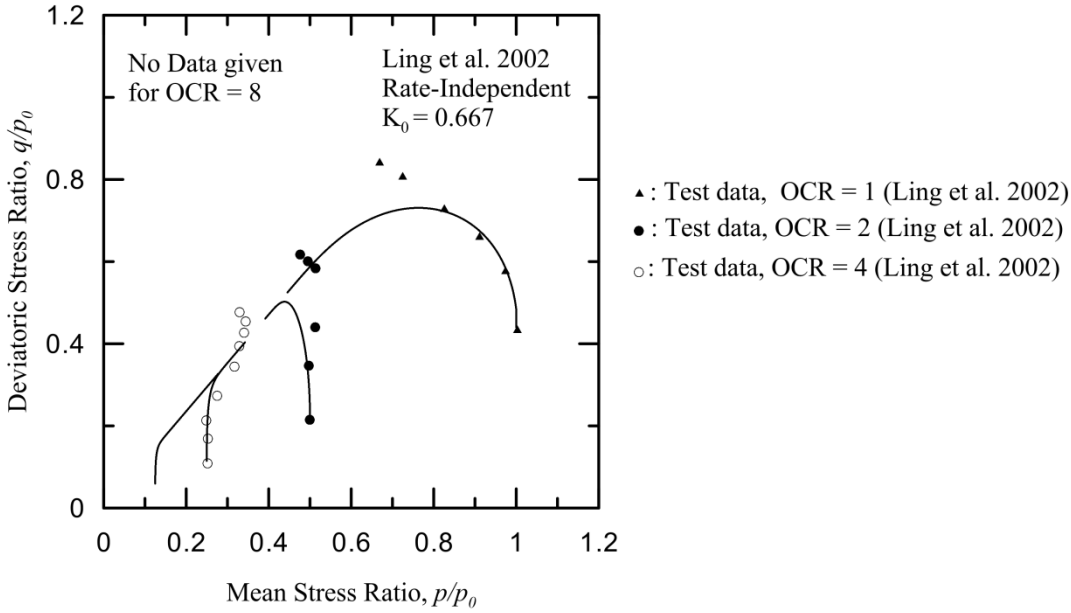

(Figure 2.9.10) Simulation of Ling et al. (2002), Kaolin Clay, Rate-independent, stress-path plot

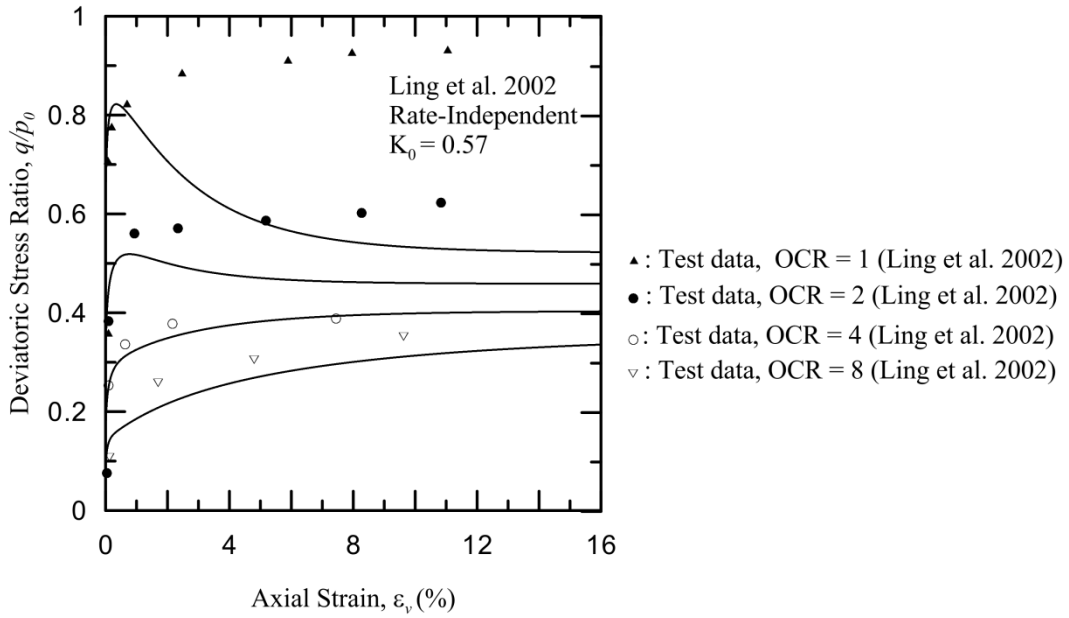

(Figure 2.9.11) Simulation of Ling et al. (2002), Kaolin Clay, Rate-independent, stress-strain plot

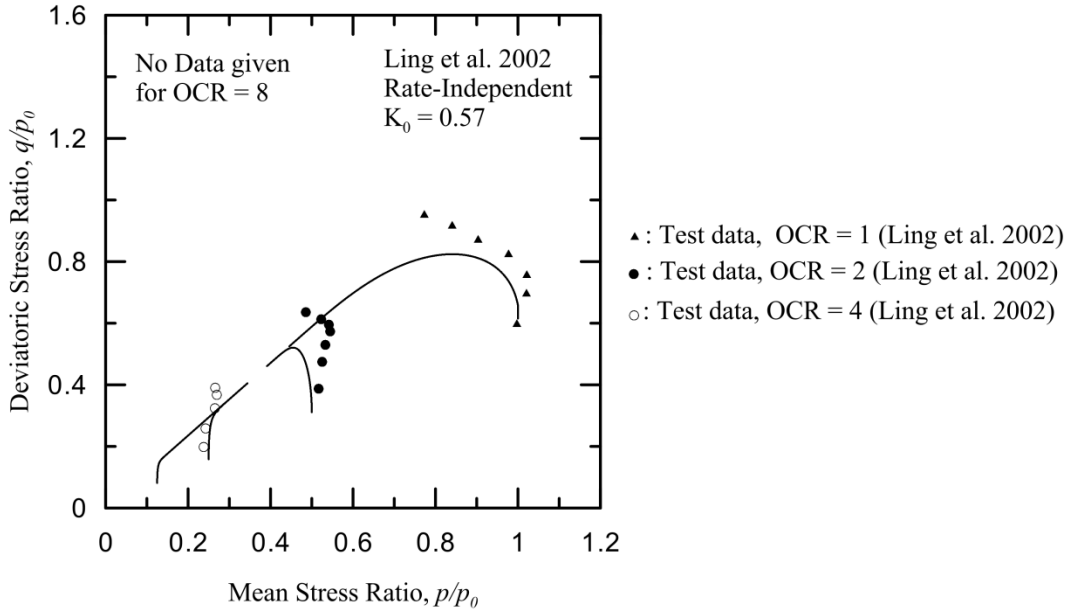

(Figure 2.9.12) Simulation of Ling et al. (2002), Kaolin Clay, Rate-independent, stress-path plot

Isotropic condition:

Figure 2.9.13 to Figure 2.9.18 compare model predictions with strain rate-independent experimental data for undrained triaxial compression of isotropically consolidated specimens. The isotropic consolidation comparisons for BBC have been sacrificed in this model to obtain better comparison for K_0 consolidation by decreasing the value of ρ than the same in Chakraborty (2009). The plots for LC and KC compare well with the experimental data.

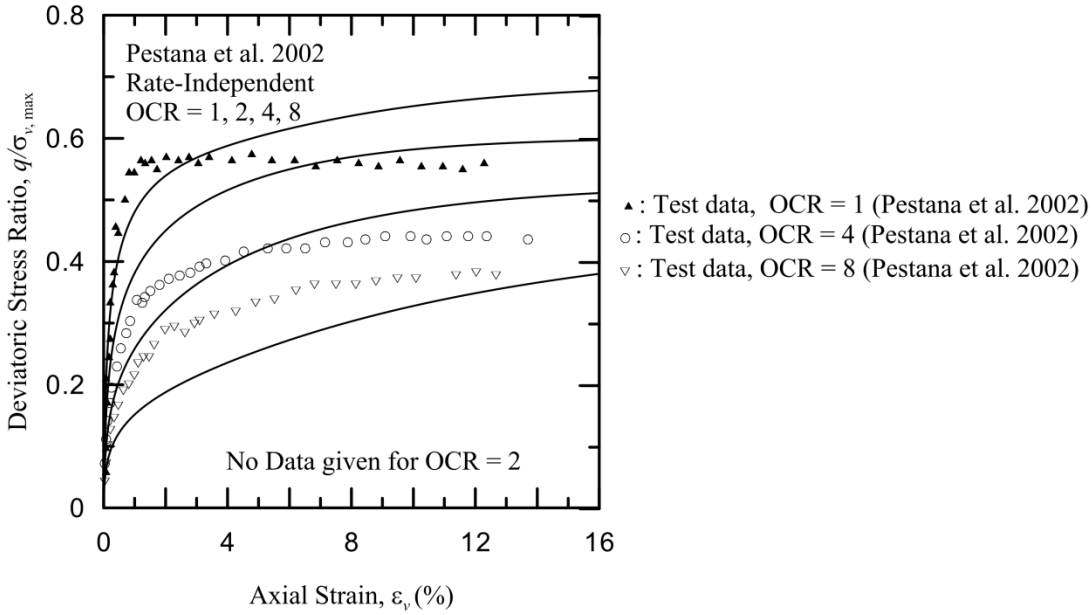

(Figure 2.9.13) Simulation of Pestana et al. (2002), Boston Blue Clay, Rate-independent, Isotropic, stress-strain plot

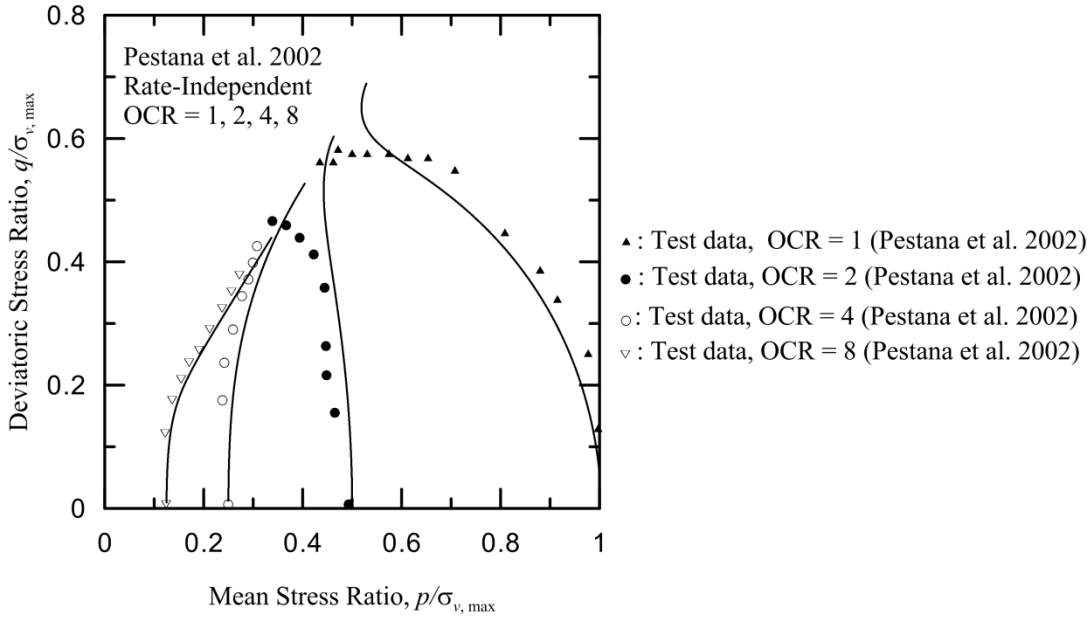

(Figure 2.9.14) Simulation of Pestana et al. (2002), Boston Blue Clay, Rate-independent, Isotropic, stress-path plot

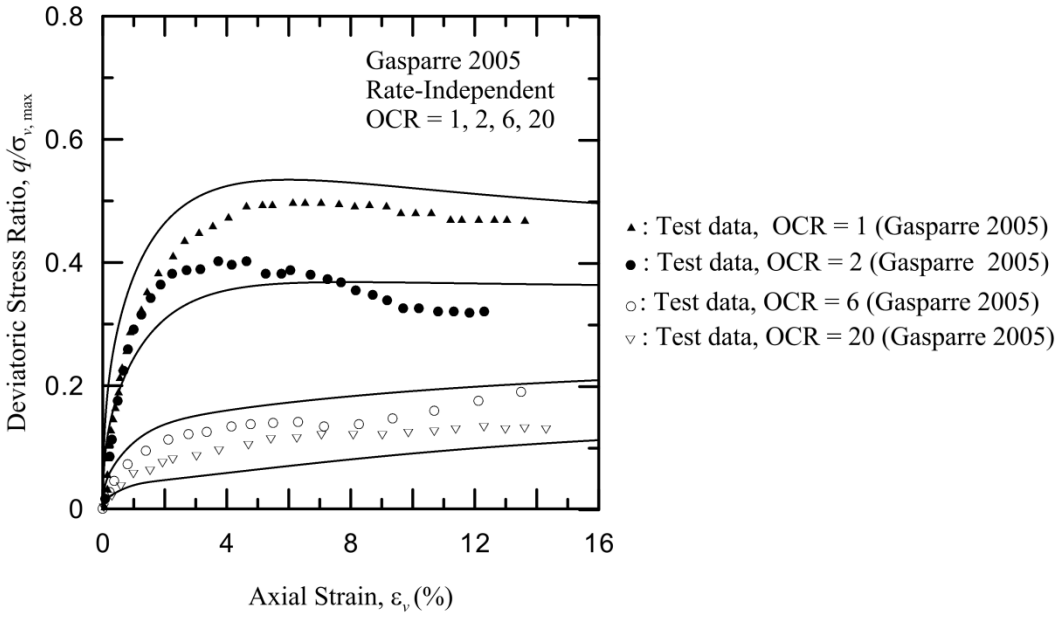

(Figure 2.9.15) Simulation of Gasparre (2005), London Clay, Rate-independent, stress-strain plot

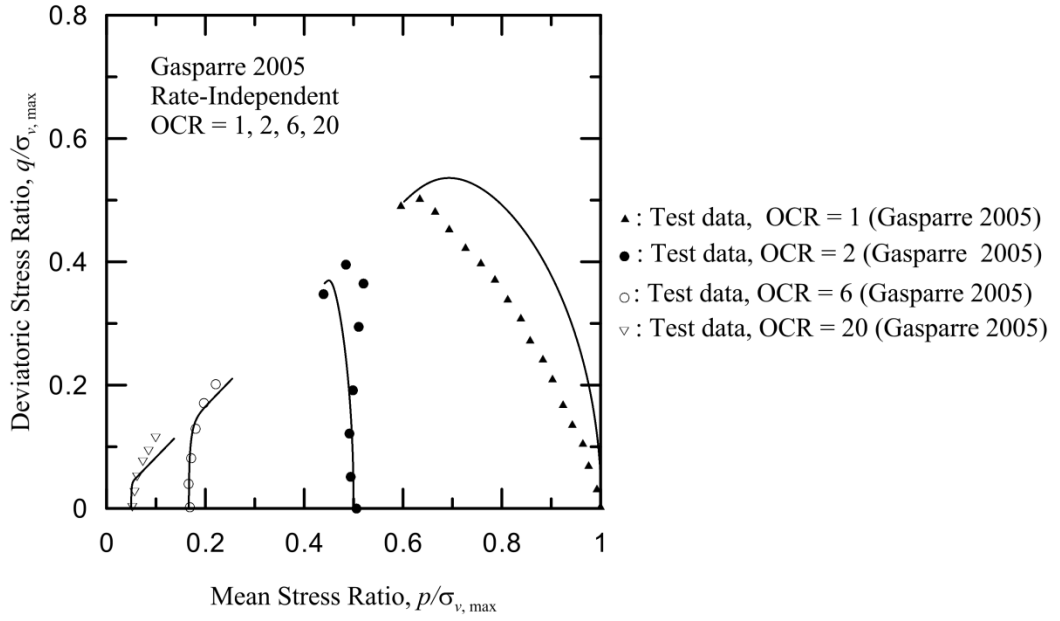

(Figure 2.9.16) Simulation of Gasparre (2005), London Clay, Rate-independent, stress-path plot

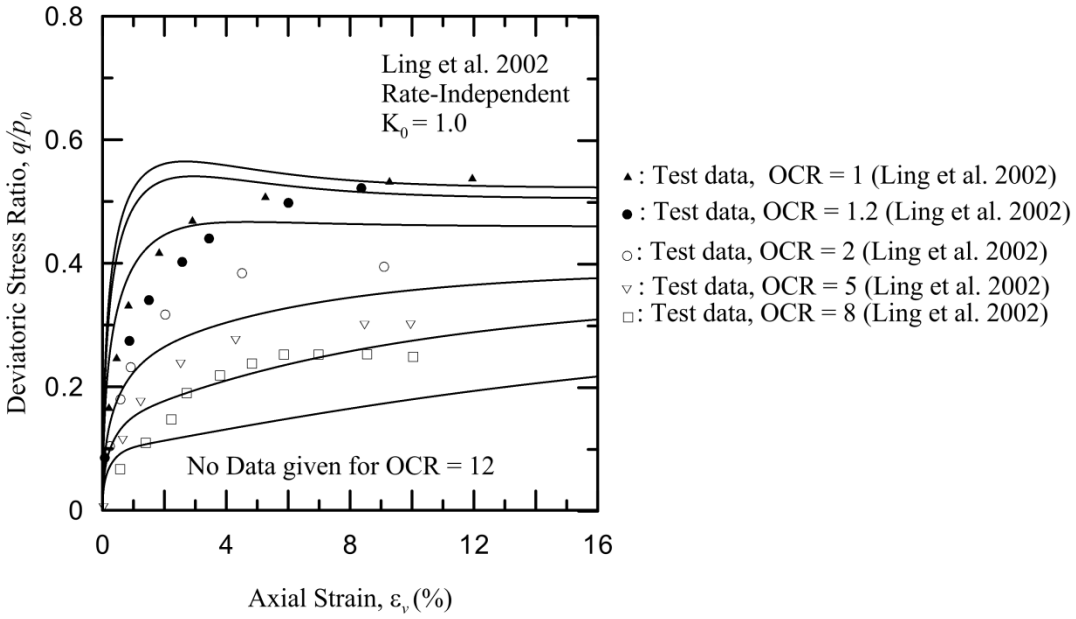

(Figure 2.9.17) Simulation of Ling et al. (2002), Kaolin Clay, Rate-independent, stress-strain plot

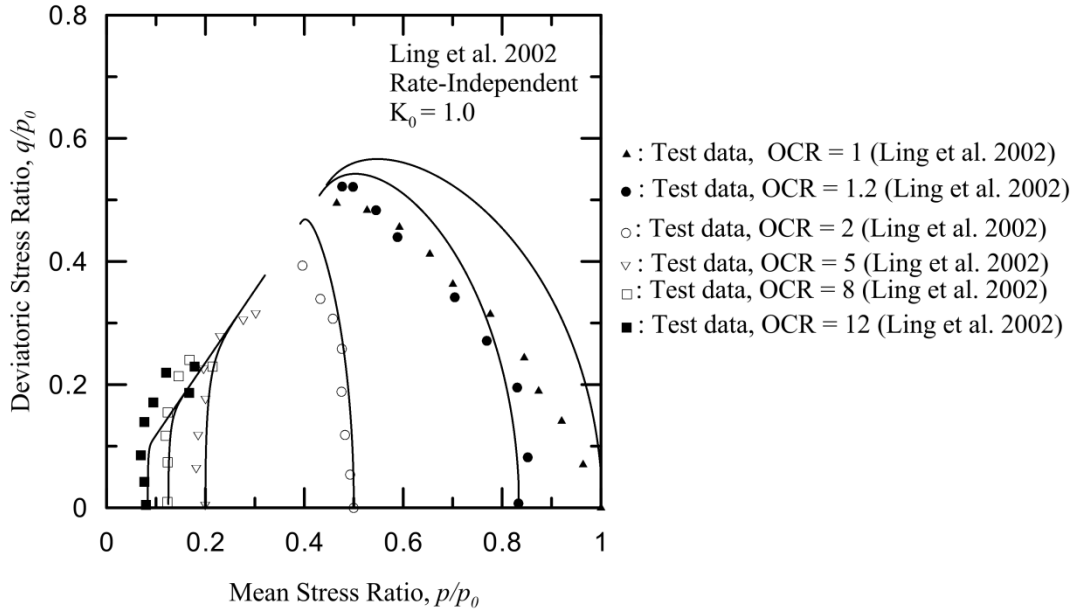

(Figure 2.9.18) Simulation of Ling et al. (2002), Kaolin Clay, Rate-independent, stress-path plot

2.10 Undrained Rate-Dependent Behavior

Figure 2.10.1 to Figure 2.10.10 reproduce the normalized shear stress vs. normalized normal stress plot for undrained, K_0 consolidated triaxial compression tests on BBC for OCR values 1, 2, 4 and 8. The normalizations are performed with respect to the vertical preconsolidation pressure $\sigma'_{a,max.}$ This figure demonstrates the ability of the model to capture the mechanical response of clays in strain-rate-dependent loading. From Chakraborty (2009), it was clearly observed that the strain-rate dependent equations predicted the stress-strain curves for OCR=1 quite well, however, the model failed to predict the stress paths for higher OCR values with reasonable accuracy. Therefore, the parameter c_0 is calibrated for different OCRs and strain rates separately. The model captures the peak strength with increasing strain rate reasonably well for all OCR values. In the post-peak region we under-predict the stress-strain plots. However, we capture the stress paths with reasonable accuracy. For LC and Kaolin clay, the OCR dependence of the model parameters was not necessary.

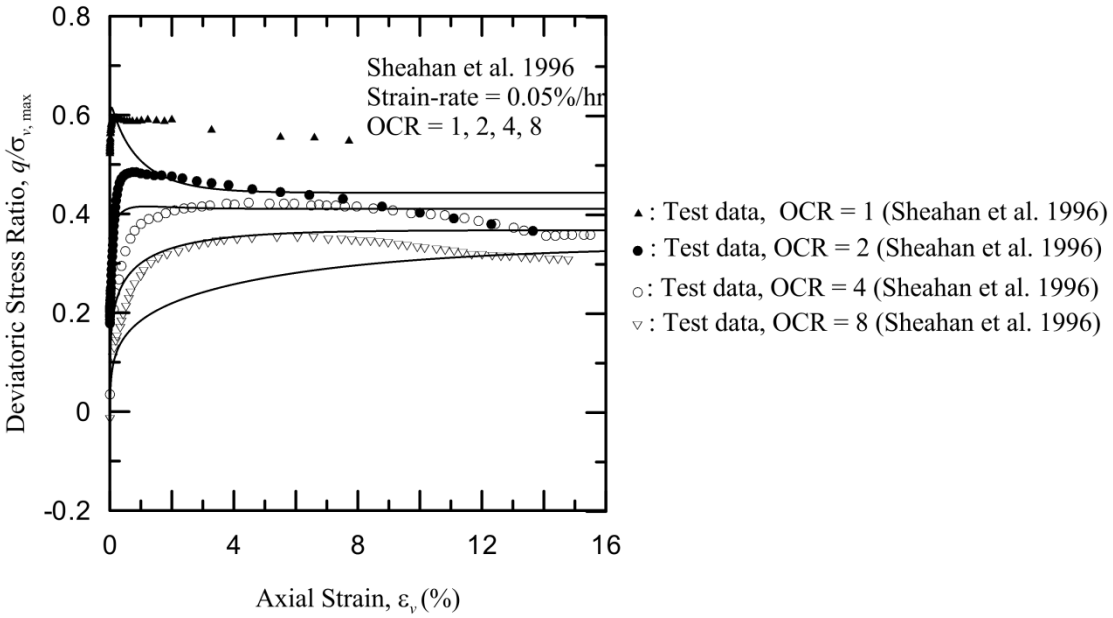

(Figure 2.10.1) Simulation of Sheahan et al. (1996), Strain-rate = 0.05%/hr, Boston Blue Clay, stress-strain plot

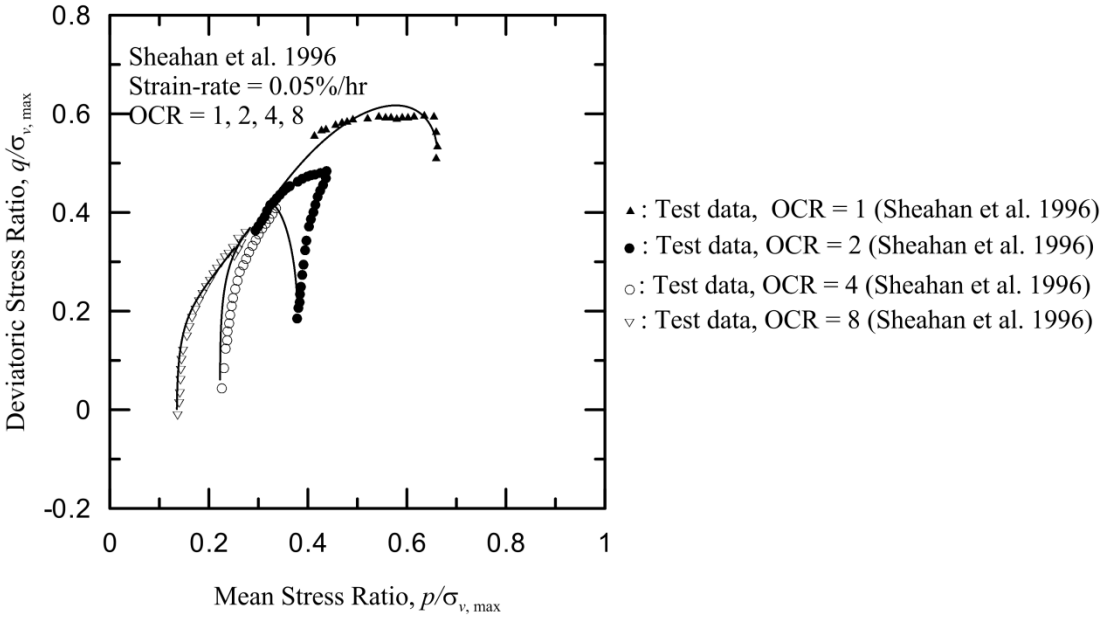

(Figure 2.10.2) Simulation of Sheahan et al. (1996), Strain-rate = 0.05%/hr, Boston Blue Clay, stress-path plot

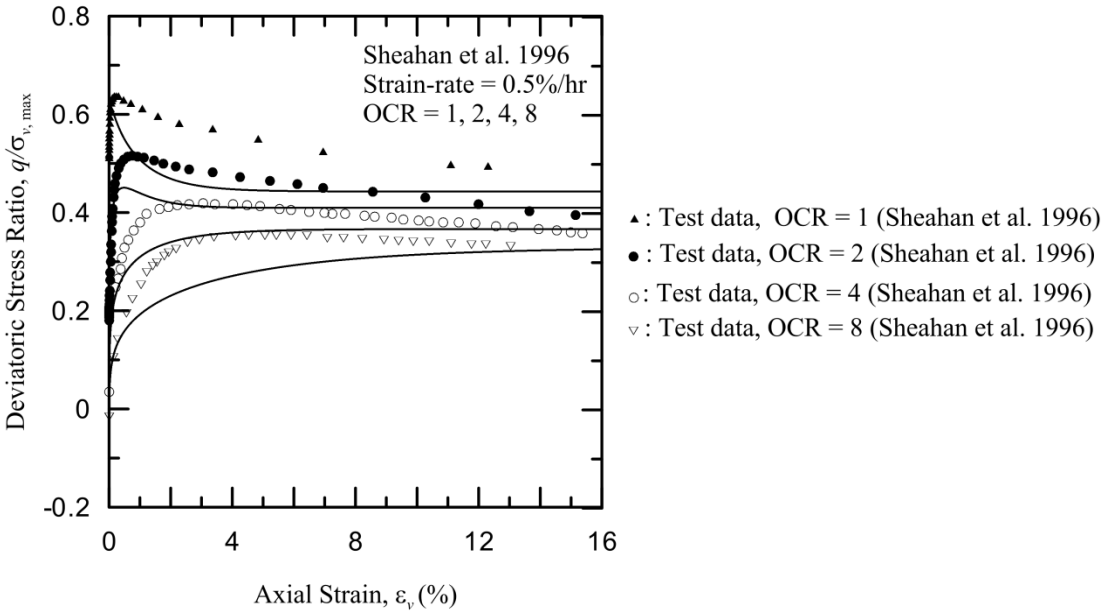

(Figure 2.10.3) Simulation of Sheahan et al. (1996), Strain-rate = 0.5%/hr, Boston Blue Clay, stress-strain plot

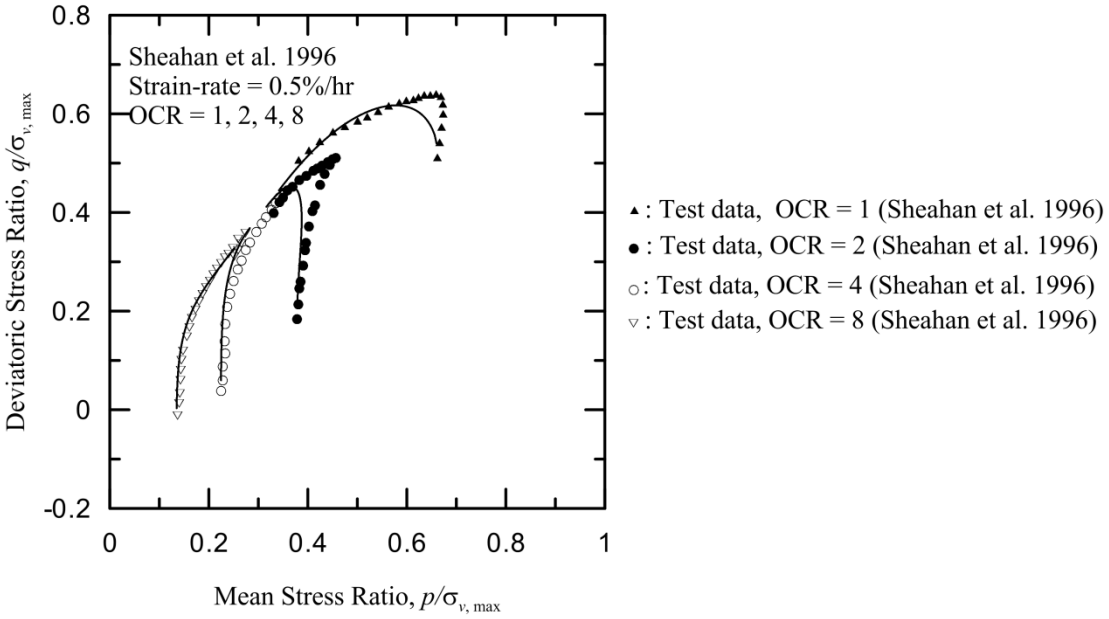

(Figure 2.10.4) Simulation of Sheahan et al. (1996), Strain-rate = 0.5%/hr, Boston Blue Clay, stress-path plot

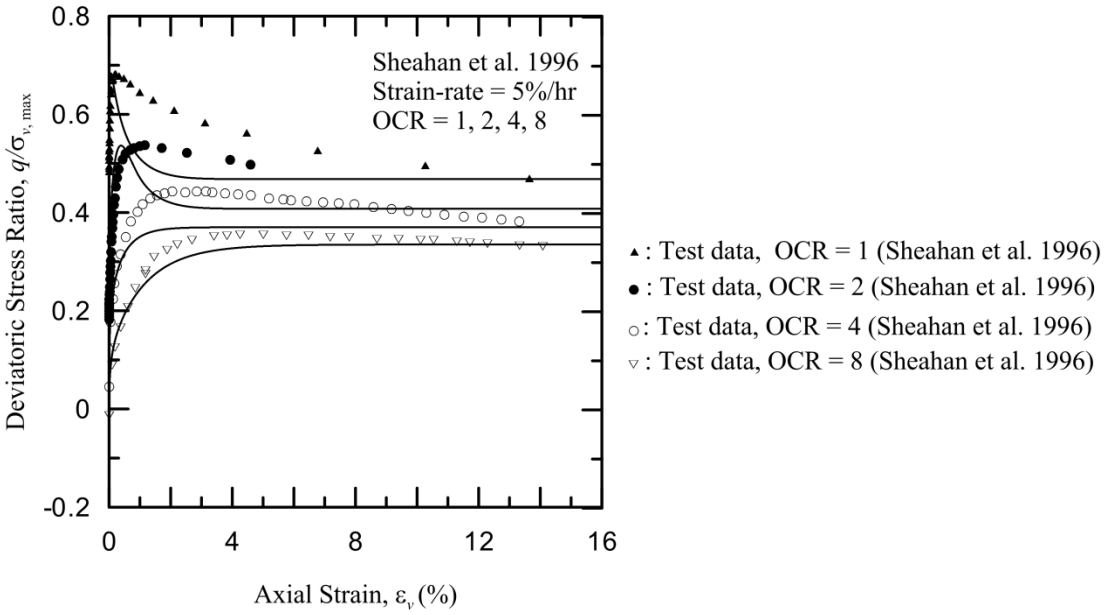

(Figure 2.10.5) Simulation of Sheahan et al. (1996), Strain-rate = 5%/hr, Boston Blue Clay, stress-strain plot

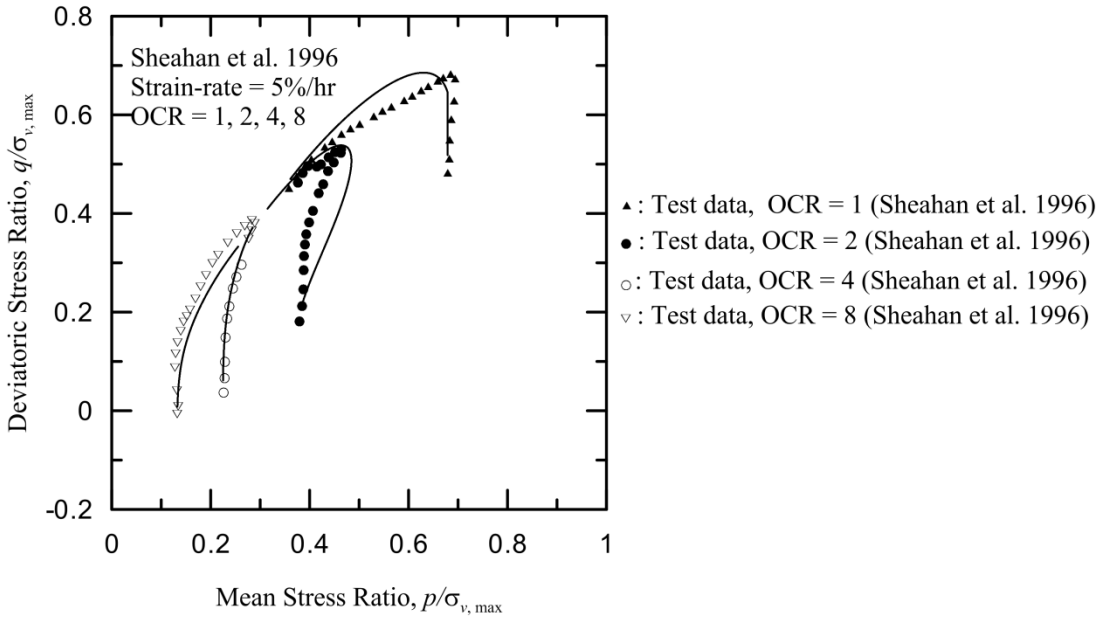

(Figure 2.10.6) Simulation of Sheahan et al. (1996), Strain-rate = 5%/hr, Boston Blue Clay, stress-path plot

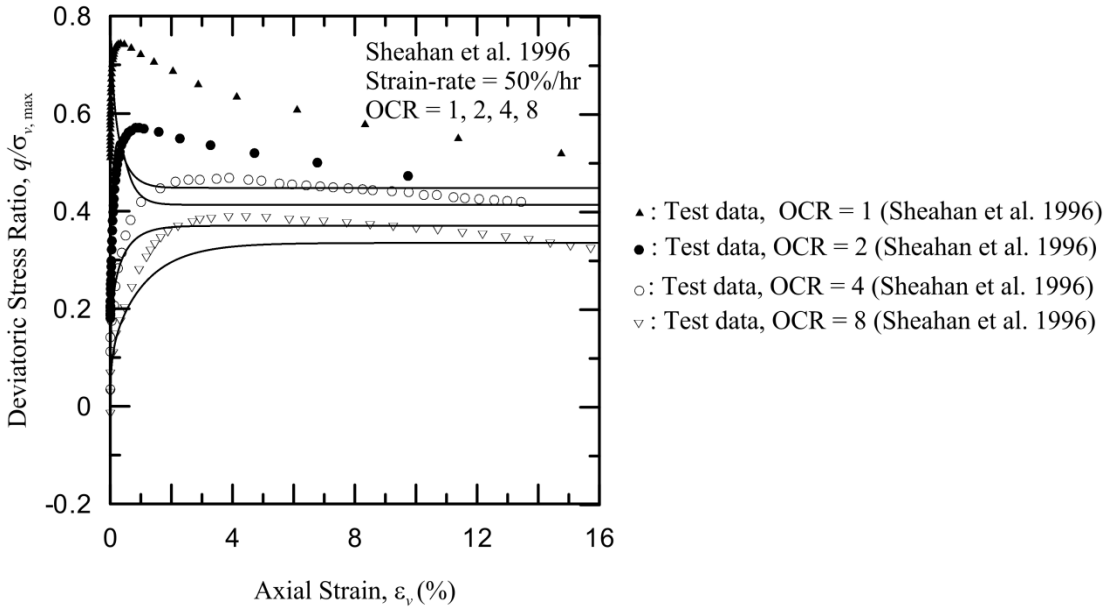

(Figure 2.10.7) Simulation of Sheahan et al. (1996), Strain-rate = 50%/hr, Boston Blue Clay, stress-strain plot

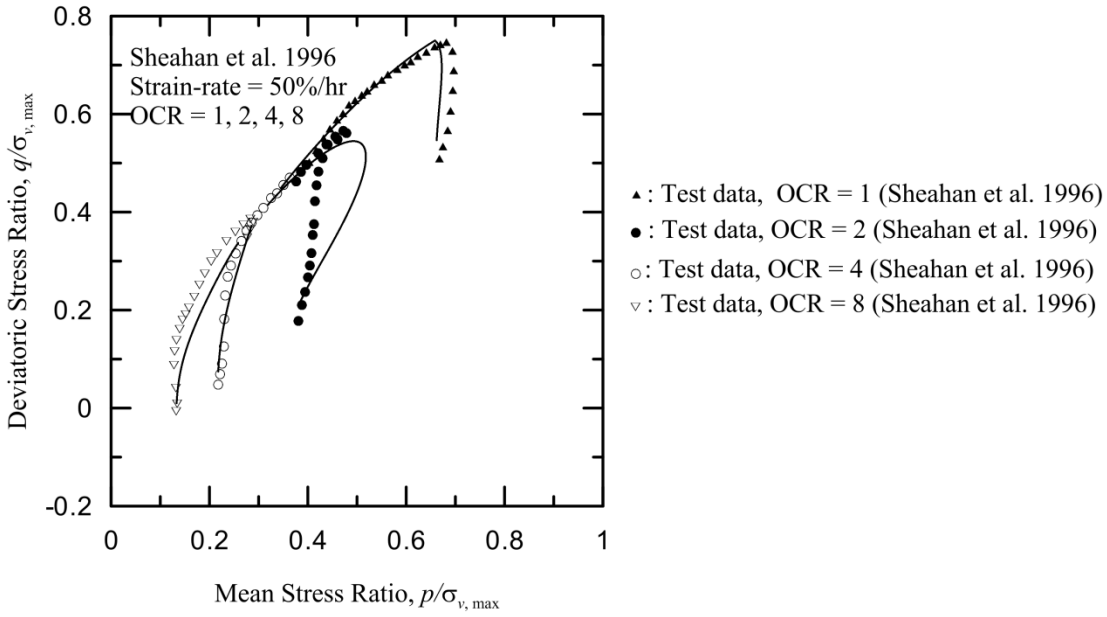

(Figure 2.10.8) Simulation of Sheahan et al. (1996), Strain-rate = 50%/hr, Boston Blue Clay, stress-path plot

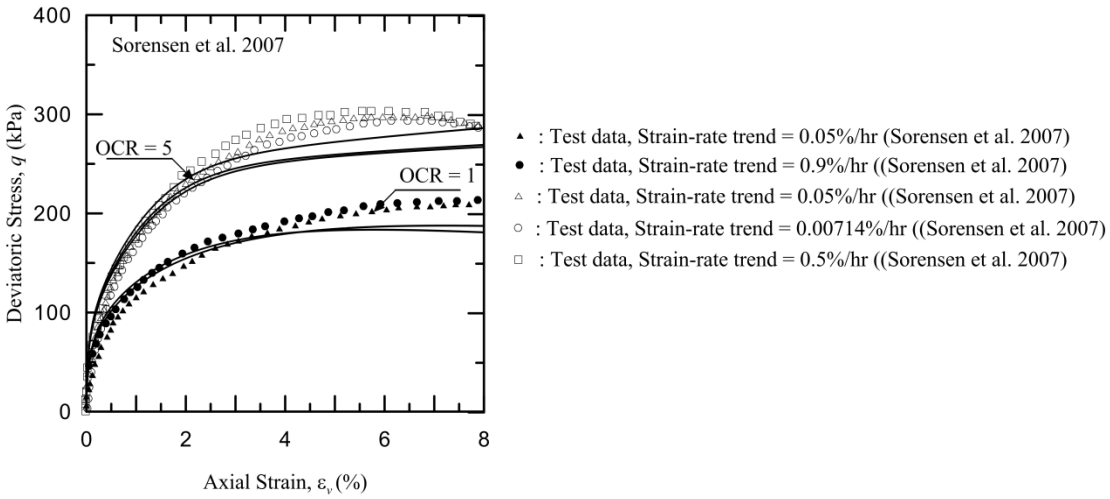

(Figure 2.10.9) Simulation of Sorensen et al. (2007), London Clay, stress-strain plot

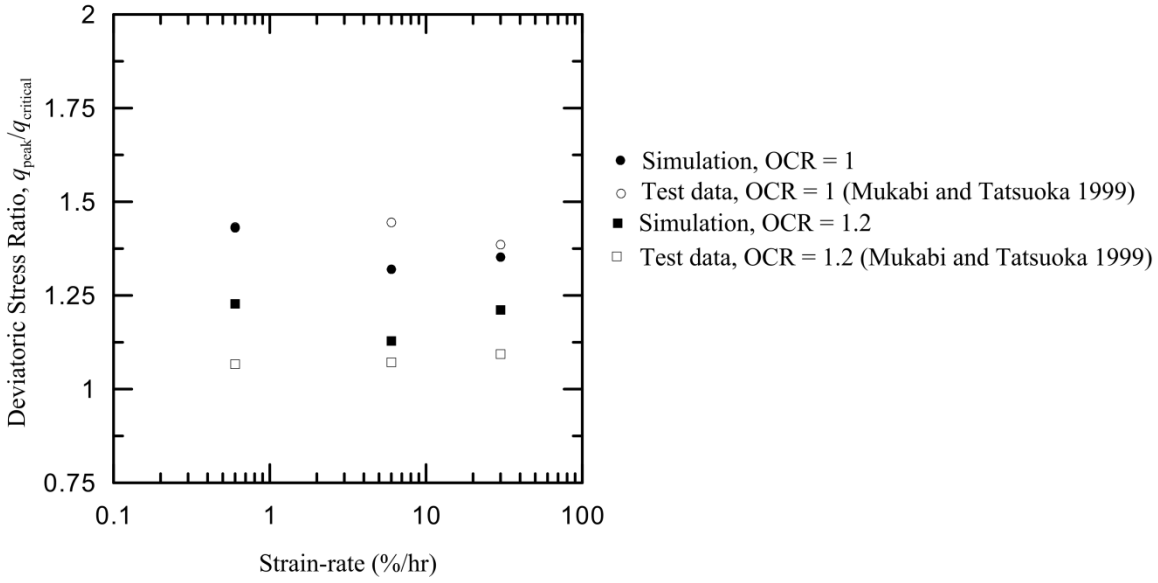

(Figure 2.10.10) Simulation of Mukabi and Tatsuoka (1999), Kaolin Clay, Deviatoric Stress Ratio vs. Strain-rate

2.11 Parametric Sensitivity Study

Sensitivity of each model parameter is checked for six other values aside from a particular parameter's deterministic value – ±5, ±10 and ±20% of the deterministic value. The study has been performed for BBC for OCR values 1, 2, 4 and 8. For the sensitivity study, we changed one parameter at a time and maintained all other parameters at their deterministic values. Appendix I, presents the sensitivity study for BBC, LC and KC for all input parameters. We calculate the average cumulative error in percentage for each parameter change as:

$$\text{Average Cumulative Error} = \left[\frac{\sum \left(q_{simulation\_base} - q_{simulation\_with\_variation} \right)}{q_{simulation\_base}} \right] \times 100\% \qquad (2.11.1)$$

Figure 2.11.1 to Figure 2.11.16 show bar diagrams of cumulative error values. Individual error values are also presented in Table 2.11.1. It was observed that the critical state stress ratio makes the maximum difference in the model prediction followed by spacing ratio. We also studied parametric sensitivity of inherent parameters like OCR and K_0. It was observed that slight variations in OCR and K_0 affect the results significantly. Among the model parameters, variation of κ and λ affects the results quite significantly because change in κ and λ causes change in slope for NC, OC and CS lines and affects the state parameter. The other parameters do not have significant effect for OCR 1. However, for higher OCR values, i.e. 4 and 8, the effect of dilatancy parameter becomes most significant. Therefore, a specific parameter may have significant influence on a specific behavior.

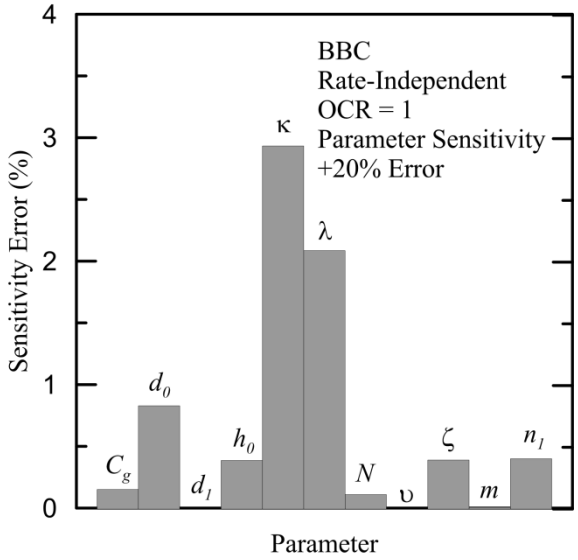

(Figure 2.11.1) Parameter Sensitivity Error for BBC at OCR = 1 with +20% variation

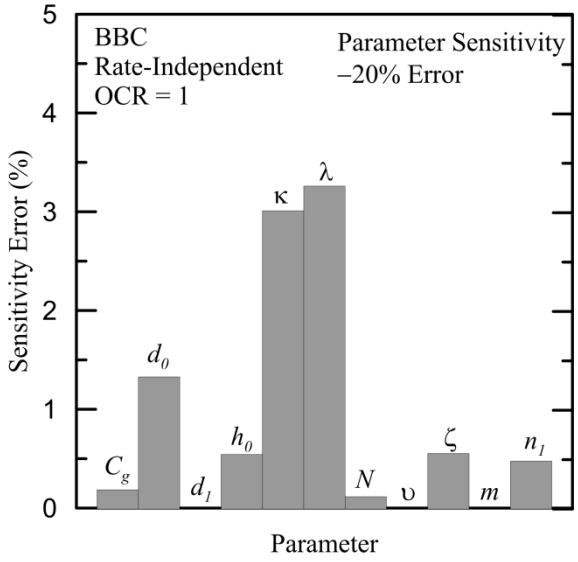

(Figure 2.11.2) Parameter Sensitivity Error for BBC at OCR = 1 with –20% variation

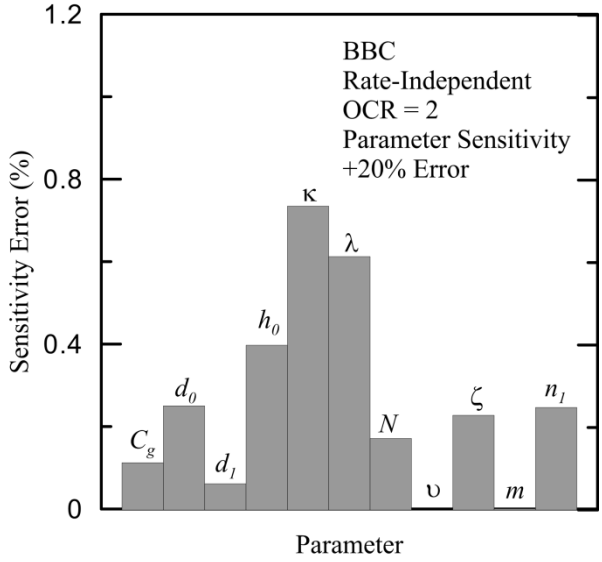

(Figure 2.11.3) Parameter Sensitivity Error for BBC at OCR = 2 with +20% variation

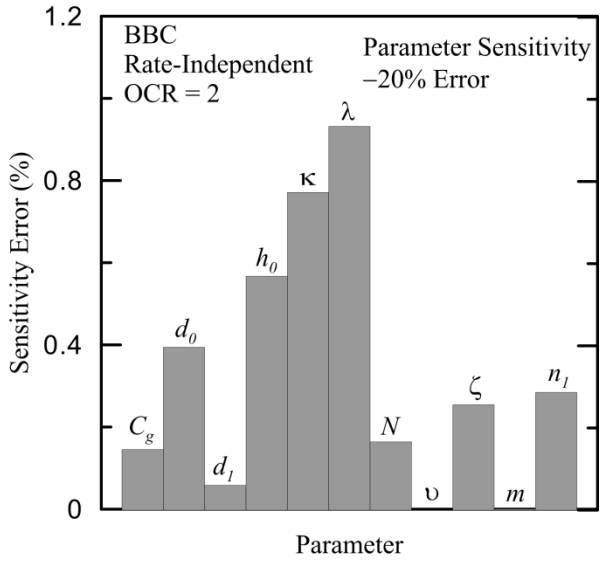

(Figure 2.11.4) Parameter Sensitivity Error for BBC at OCR = 2 with –20% variation

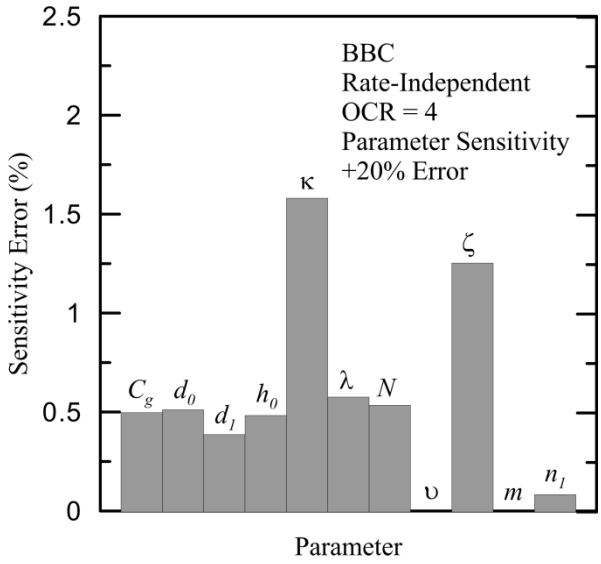

(Figure 2.11.5) Parameter Sensitivity Error for BBC at OCR = 4 with +20% variation

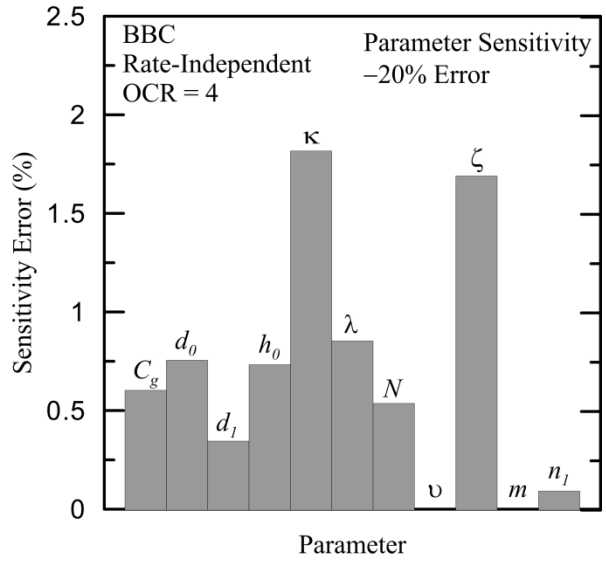

(Figure 2.11.6) Parameter Sensitivity Error for BBC at OCR = 4 with –20% variation

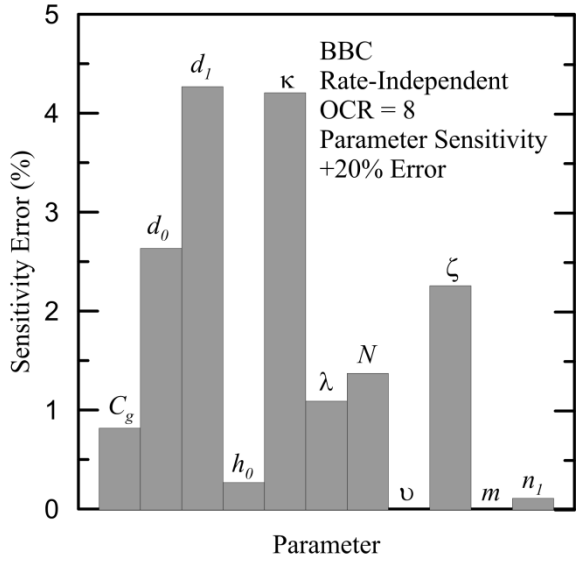

(Figure 2.11.7) Parameter Sensitivity Error for BBC at OCR = 8 with +20% variation

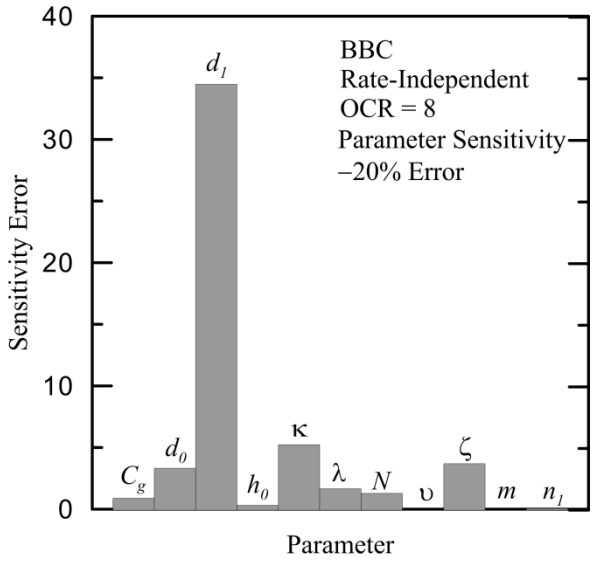

(Figure 2.11.8) Parameter Sensitivity Error for BBC at OCR = 8 with –20% variation

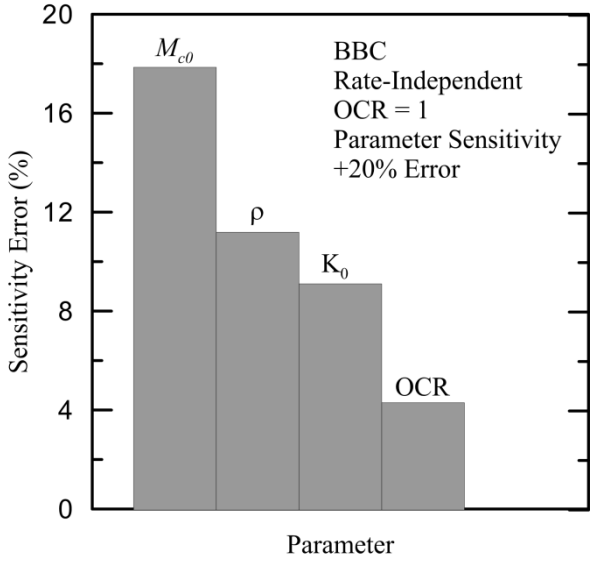

(Figure 2.11.9) Parameter Sensitivity Error for BBC at OCR = 1 with +20% variation

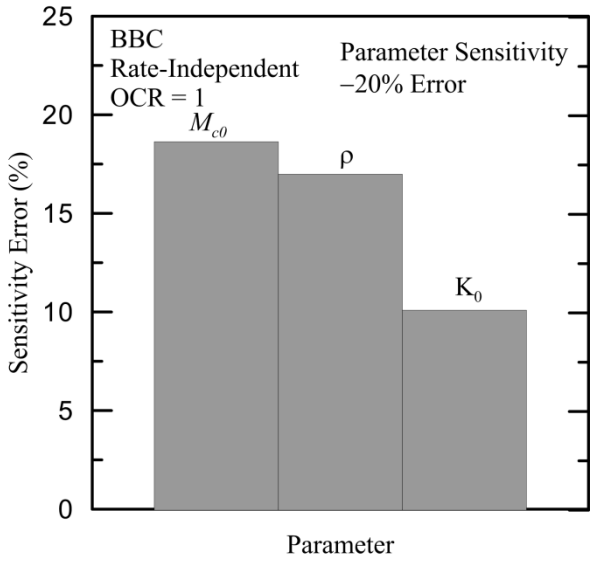

(Figure 2.11.10) Parameter Sensitivity Error for BBC at OCR = 1 with –20% variation

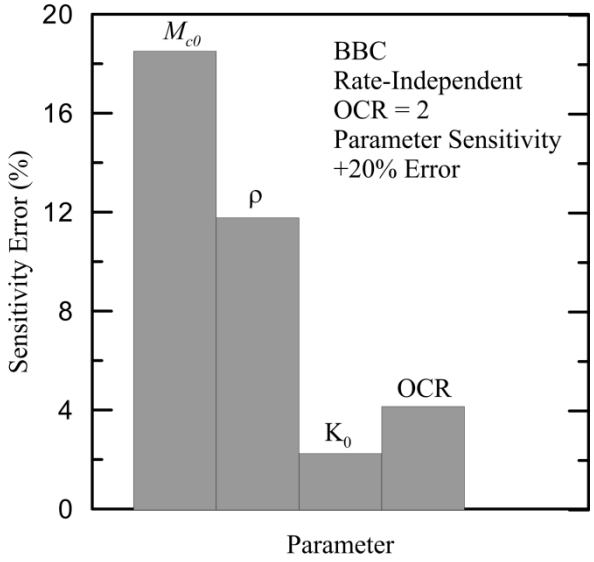

(Figure 2.11.11) Parameter Sensitivity Error for BBC at OCR = 2 with +20% variation

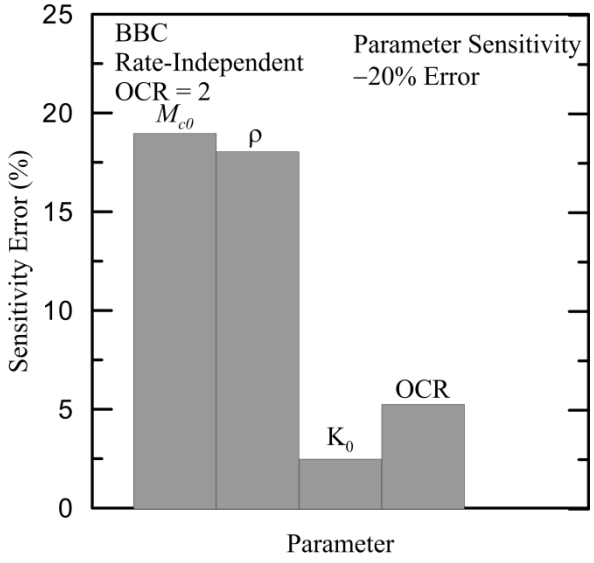

(Figure 2.11.12) Parameter Sensitivity Error for BBC at OCR = 2 with –20% variation

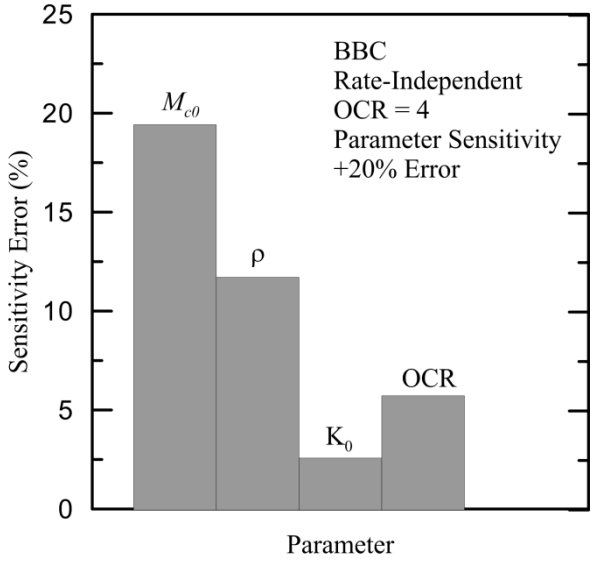

(Figure 2.11.13) Parameter Sensitivity Error for BBC at OCR = 4 with +20% variation

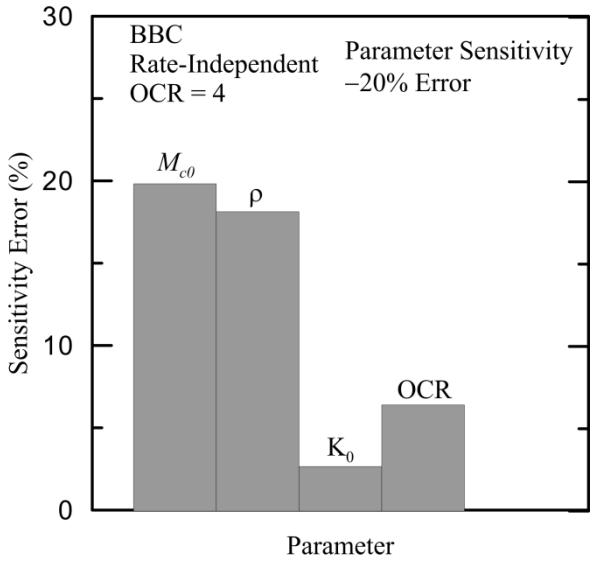

(Figure 2.11.14) Parameter Sensitivity Error for BBC at OCR = 4 with –20% variation

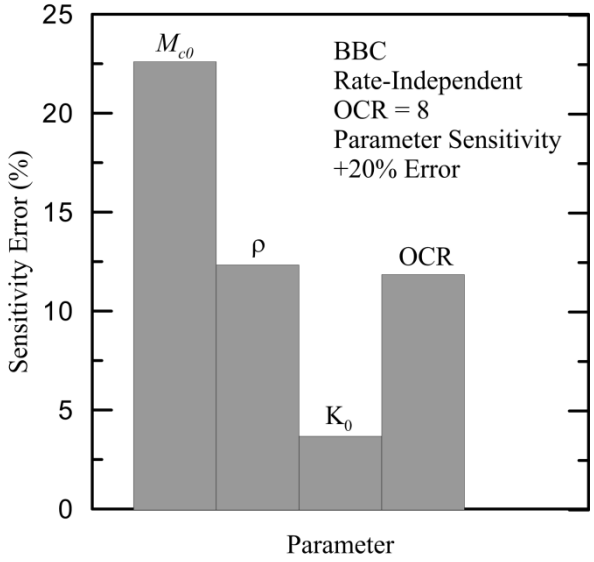

(Figure 2.11.15) Parameter Sensitivity Error for BBC at OCR = 8 with +20% variation

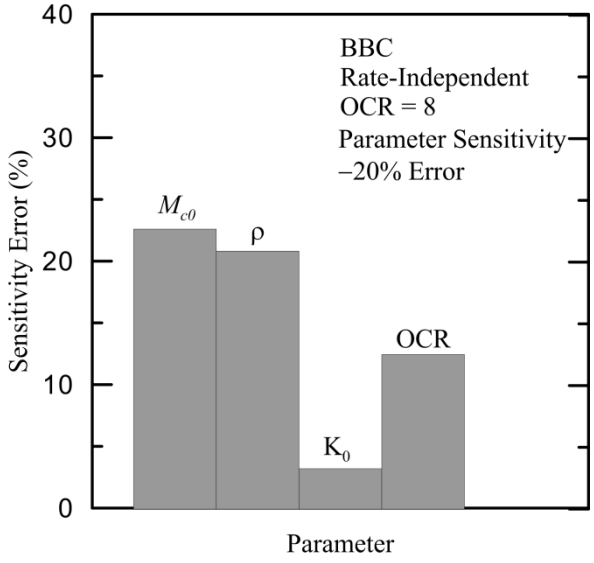

(Figure 2.11.16) Parameter Sensitivity Error for BBC at OCR = 8 with –20% variation

Cumulative Parameter Sensitivity Error (%)								
	+20% Variation				-20% Variation			
Parameter	OCR = 1	OCR = 2	OCR = 4	OCR = 8	OCR = 1	OCR = 2	OCR = 4	OCR = 8
C_g	0.15	0.11	0.50	0.82	0.19	0.14	0.60	0.96
d_0	0.83	0.25	0.51	2.64	1.33	0.39	0.75	3.39
d_1	0	0.06	0.39	4.27	0	0.06	0.35	34.55
M_{c0}	17.89	18.54	19.46	22.64	18.68	19.01	19.87	22.67
h_0	0.39	0.39	0.48	0.27	0.55	0.56	0.73	0.39
κ	2.94	0.73	1.58	4.21	3.01	0.77	1.82	5.30
λ	2.09	0.61	0.58	1.09	3.26	0.93	0.85	1.73
N	0.11	0.17	0.53	1.38	0.12	0.16	0.54	1.36
ρ	11.22	11.802	11.75	12.38	17.03	18.08	18.18	20.89
υ	0	0	0	0	0	0	0	0
ζ	0.39	0.22	1.25	2.26	0.56	0.25	1.69	3.76
K_0	9.14	2.27	2.62	3.72	10.14	2.52	2.70	3.26
OCR	4.33	4.18	5.77	11.89	NA	5.29	6.44	12.51
m_r	0.01	0	0	0	0	0	0	0
n_1	0.40	0.24	0.08	0.11	0.48	0.28	0.09	0.12

(Table 2.11.1) Average Cumulative Parameter Sensitivity Error

2.12 Uncertainties in Model Parameters:

In order to consider the combined uncertainty of all the model parameters, we perform Monte Carlo analysis considering each of the model parameters as a random variable. In order to define the random distribution of the model parameters, two most common, continuous probability distribution function are considered in the present paper: (1) normal distribution and (2) uniform distribution. The mean and the coefficient of variation (COV) (COV= Standard deviation/ mean) are considered to be the same for both the probability distribution functions. The mean values of the parameters for both the probability distribution function are taken same as the deterministic model parameter values. In order to calculate COV for normal distribution, we consider that a maximum of ±20% deviation may happen in model parameter determination. The 3σ limit becomes equal to the value of model parameter with 20% deviation – the base value of that parameter. This results in a COV value of 0.0667. For the uniform distribution, we consider the same mean and the COV values for the model parameters. This sets the upper and the lower limits of the uniform distribution as ±12%.

We determine the distribution of $s_{u,peak}$ and $s_{u,critical}$ from the Monte Carlo simulations. Figure 2.12.1 to Figure 2.12.12 present the histograms of $s_{u,peak}$ and $s_{u,critical}$ obtained from normal and Figure 2.12.13 to Figure 2.12.24 present the histograms of $s_{u,peak}$ and $s_{u,critical}$ obtained from uniform probability distributions. The descriptive parameters of each of the distributions (coefficient of variation, mean, standard deviation) are examined in Figure 2.12.25 to Figure 2.12.27.

Both the normal and uniform distributions produced peak like histograms with the peak located at the mean. The shape of the normal distribution histogram was found to have a curvier shape than the uniform distribution, which had a more triangular shape.

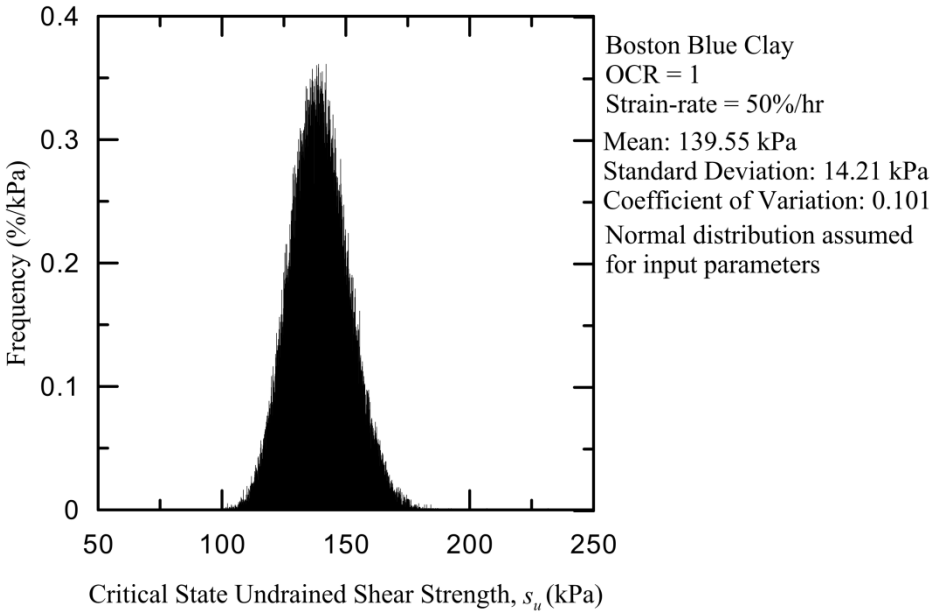

(Figure 2.12.1) Histogram for OCR = 1 for BBC at Critical State Undrained Shear Strength, Rate-Dependent Model

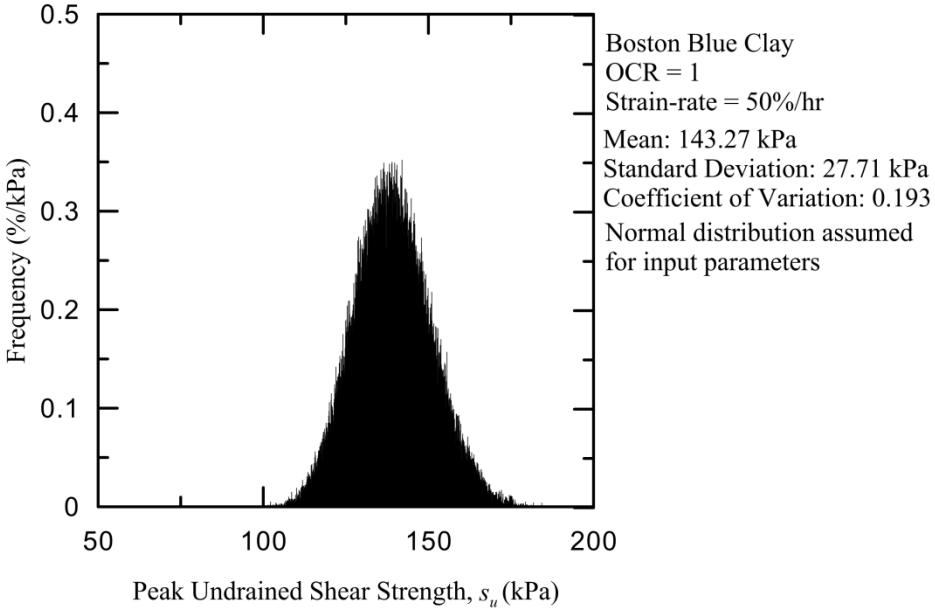

(Figure 2.12.2) Histogram for OCR = 1 for BBC at Peak Undrained Shear Strength, Rate-Dependent Model

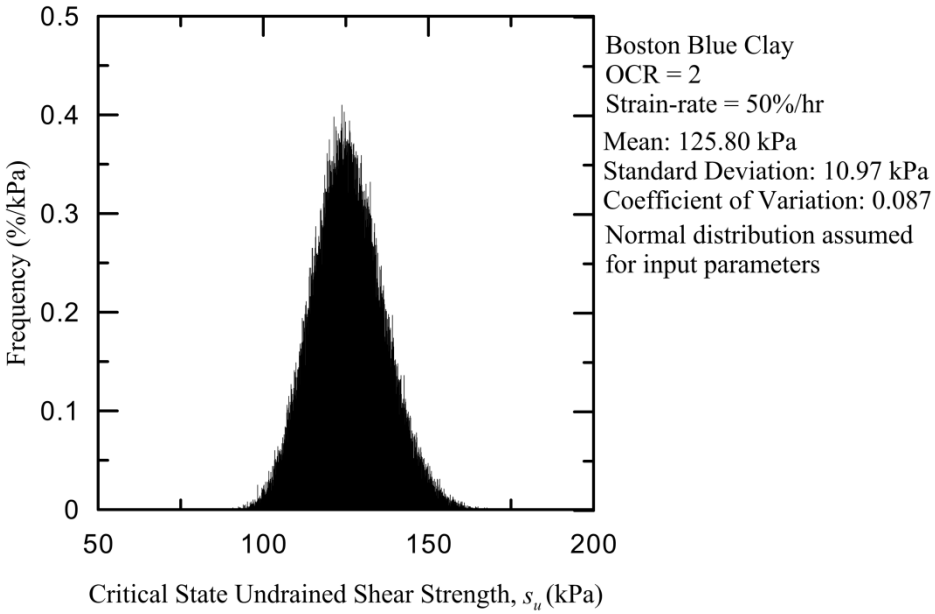

(Figure 2.12.3) Histogram for OCR = 2 for BBC at Critical State Undrained Shear Strength, Rate-Dependent Model

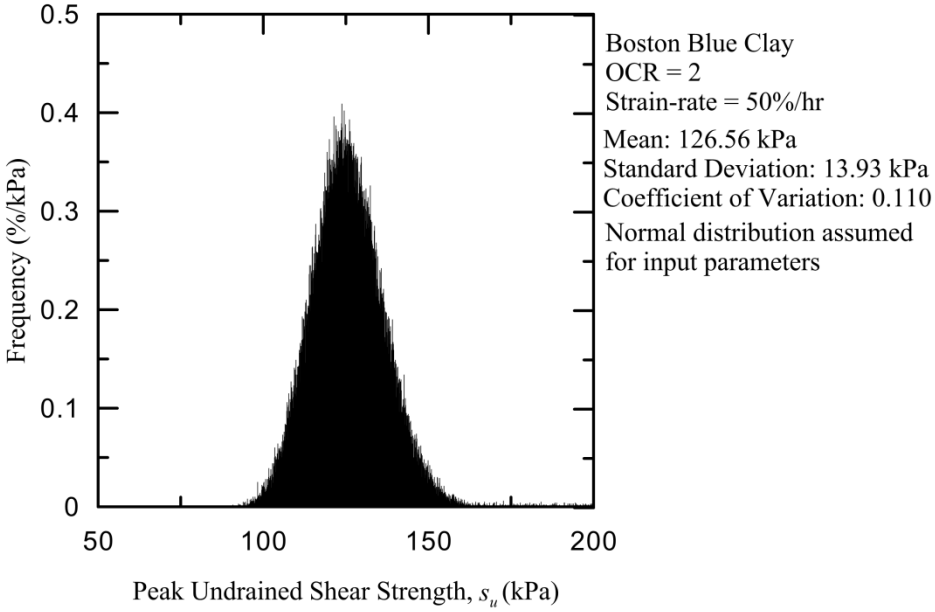

(Figure 2.1**2**.4) Histogram for OCR = 2 for BBC at Peak Undrained Shear Strength, Rate-Dependent Model

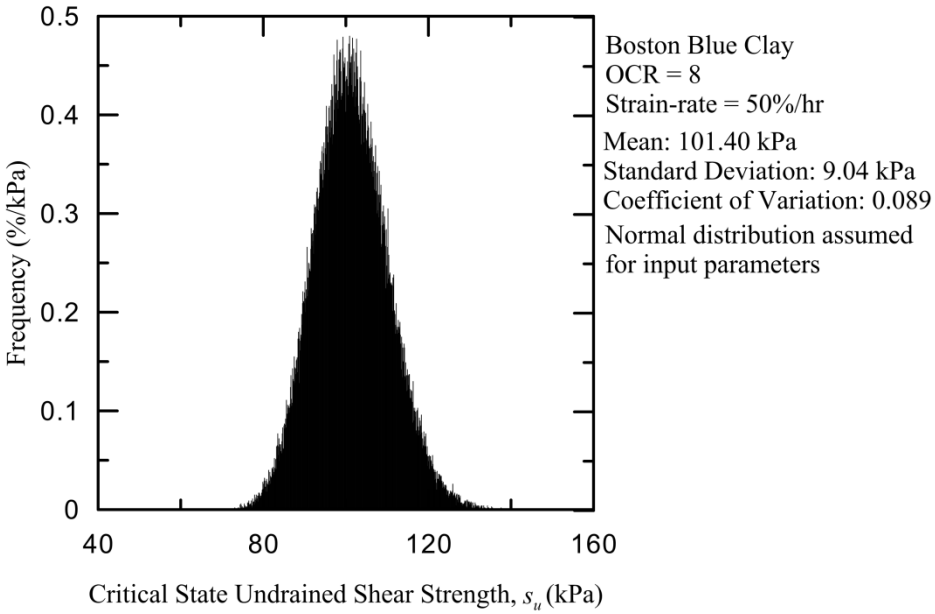

(Figure 2.12.5) Histogram for OCR = 8 for BBC at Critical State Undrained Shear Strength, Rate-Dependent Model

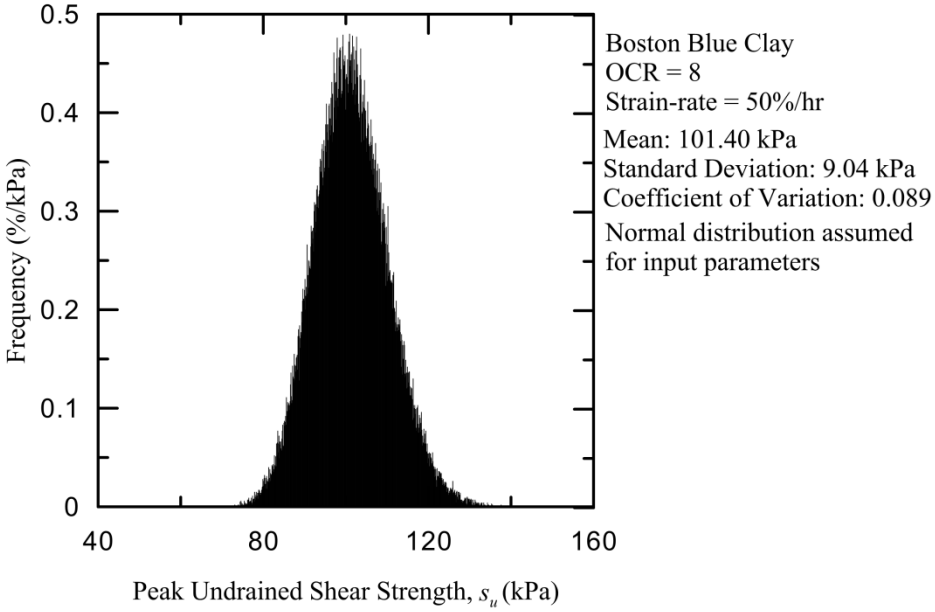

(Figure 2.12.6) Histogram for OCR = 8 for BBC at Peak Undrained Shear Strength, Rate-Dependent Model

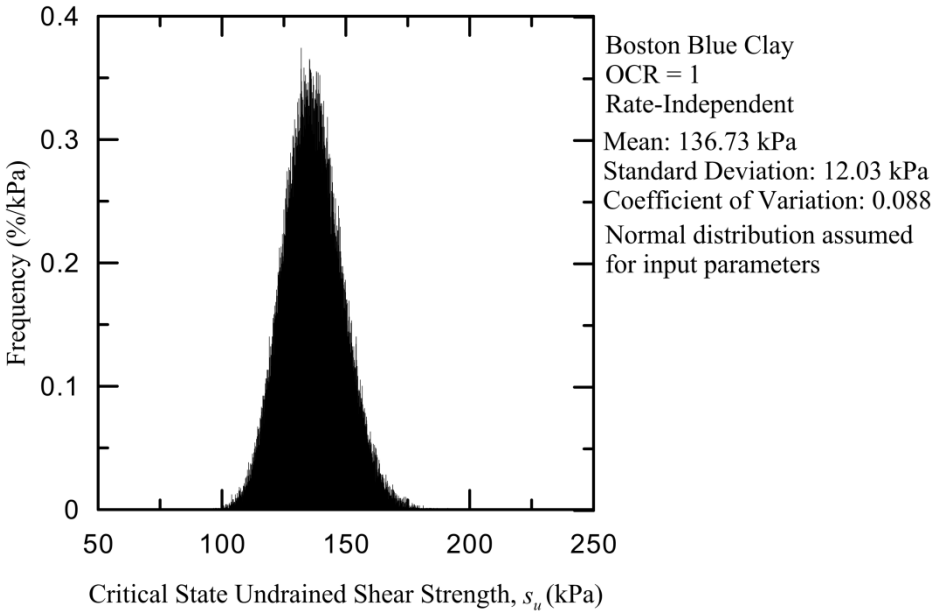

(Figure 2.1**2**.7) Histogram for OCR = 1 for BBC at Critical State Undrained Shear Strength, Rate-Independent Model

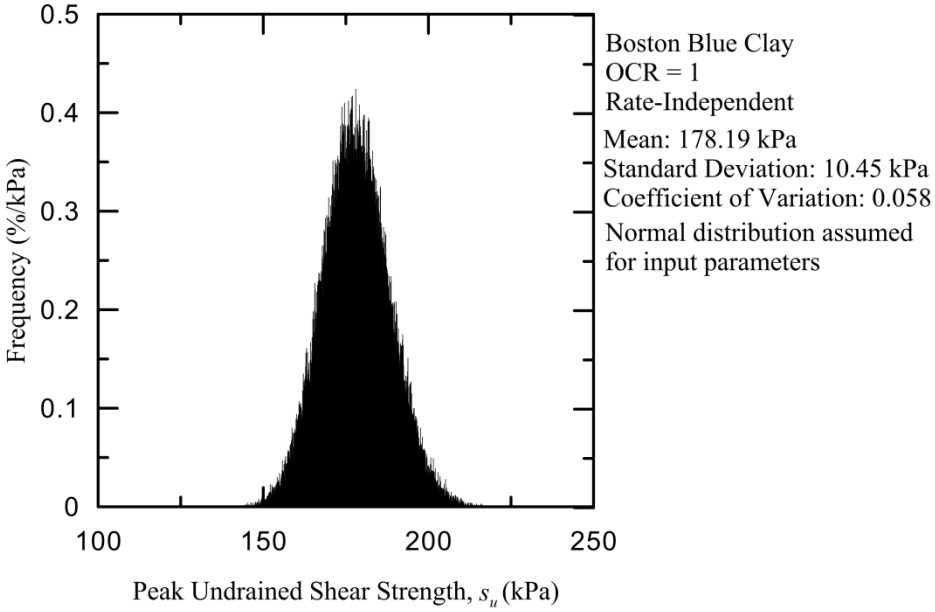

(Figure 2.12.8) Histogram for OCR = 1 for BBC at Peak Undrained Shear Strength, Rate-Independent Model

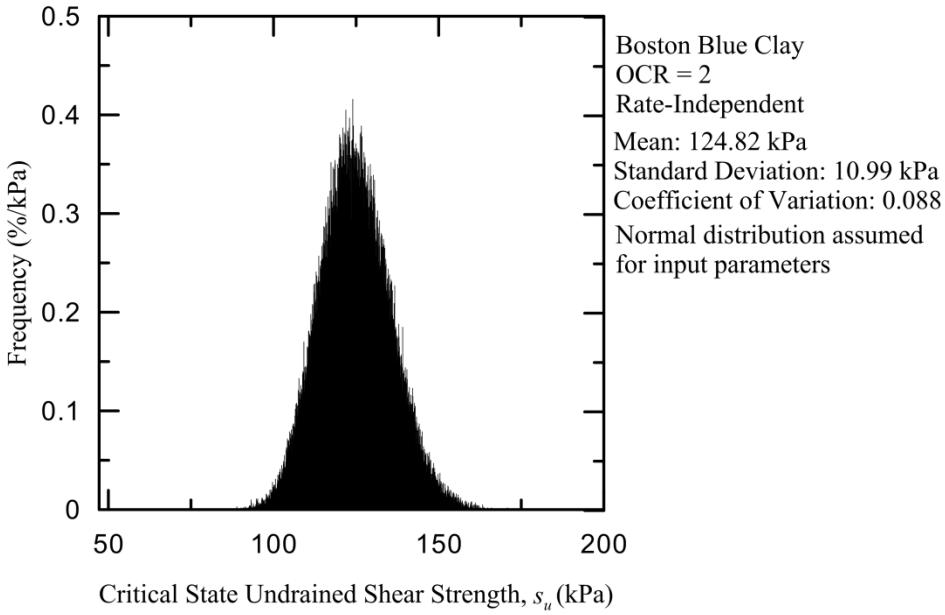

(Figure 2.12.9) Histogram for OCR = 2 for BBC at Critical State Undrained Shear Strength, Rate-Independent Model

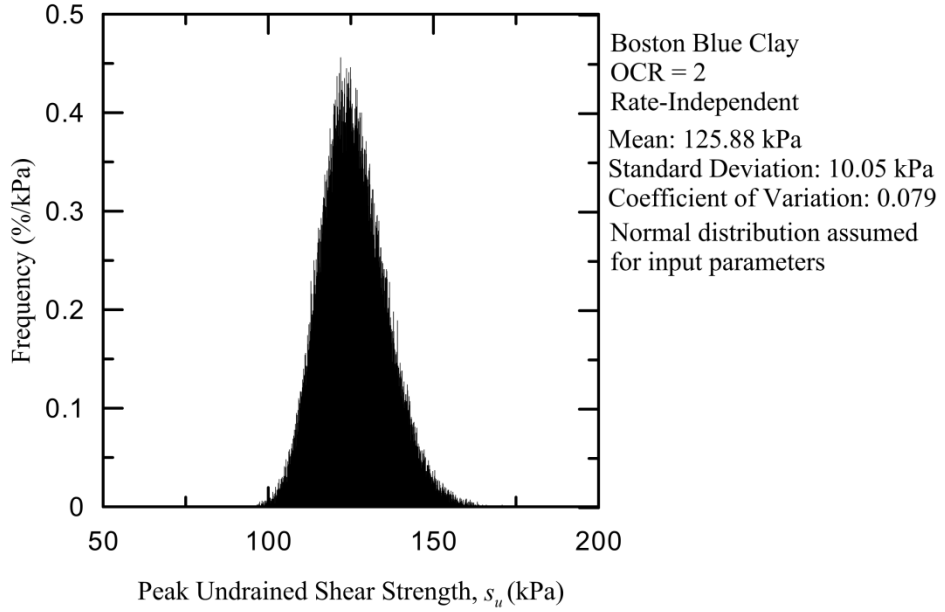

(Figure 2.12.10) Histogram for OCR = 2 for BBC at Peak Undrained Shear Strength, Rate-Independent Model

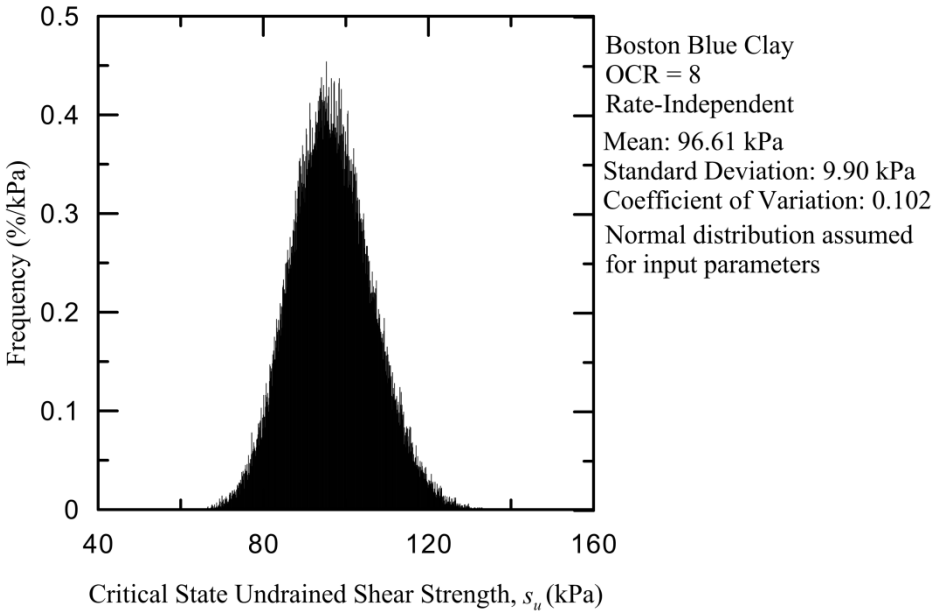

(Figure 2.12.11) Histogram for OCR = 8 for BBC at Critical State Undrained Shear Strength, Rate-Independent Model

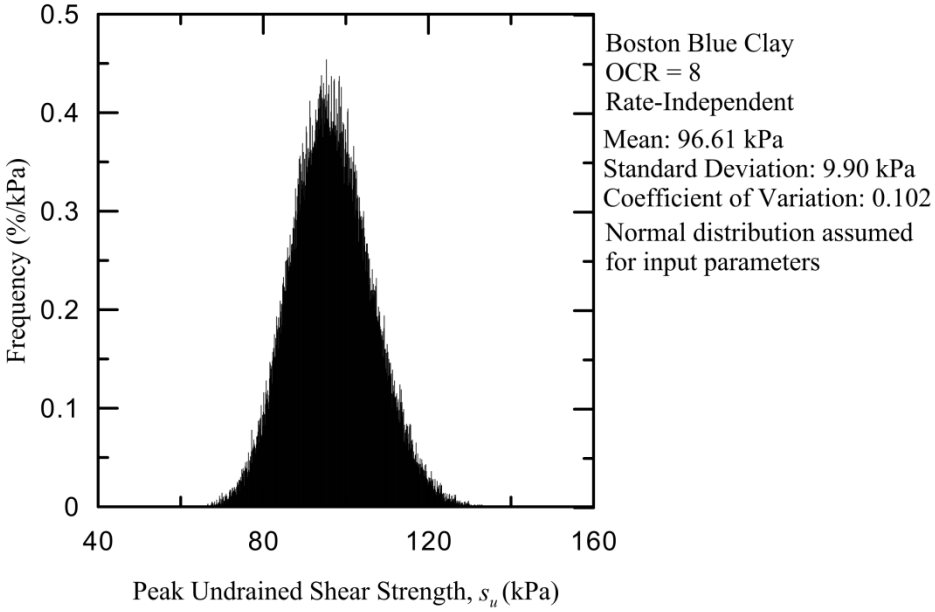

(Figure 2.12.12) Histogram for OCR = 8 for BBC at Peak Undrained Shear Strength, Rate-Independent Model

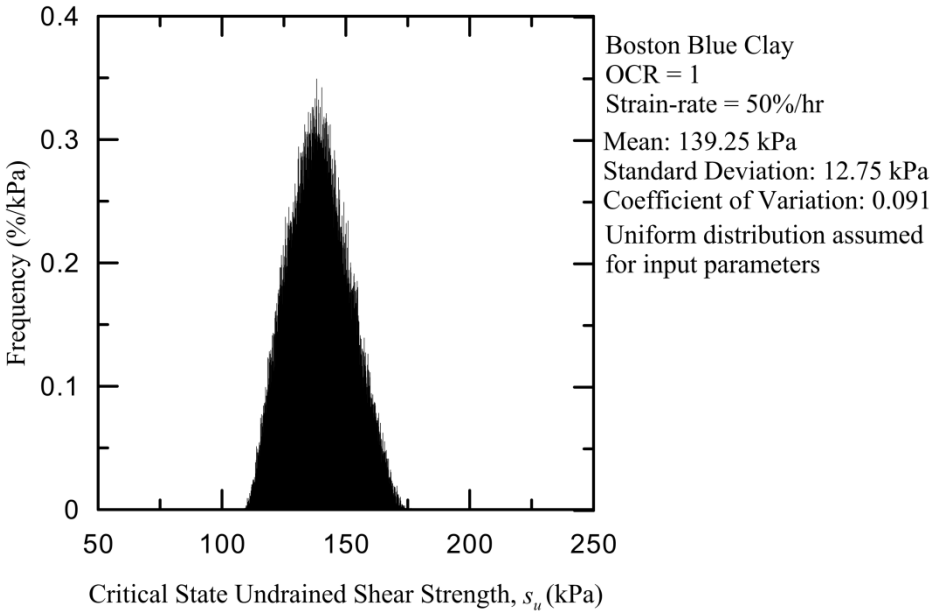

(Figure 2.12.13) Histogram for OCR = 1 for BBC at Critical State Undrained Shear Strength, Rate-Dependent Model

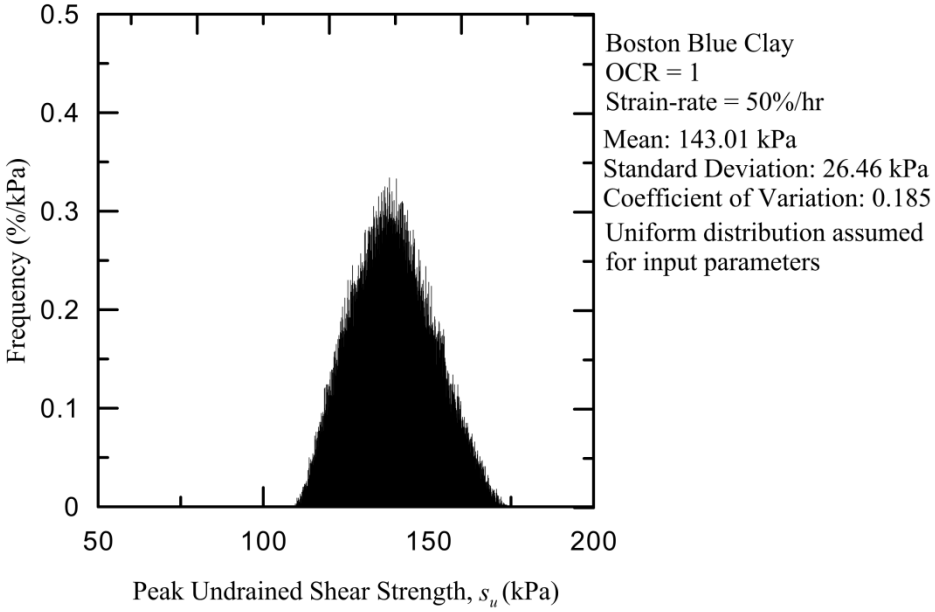

(Figure 2.12.14) Histogram for OCR = 1 for BBC at Peak Undrained Shear Strength, Rate-Dependent Model

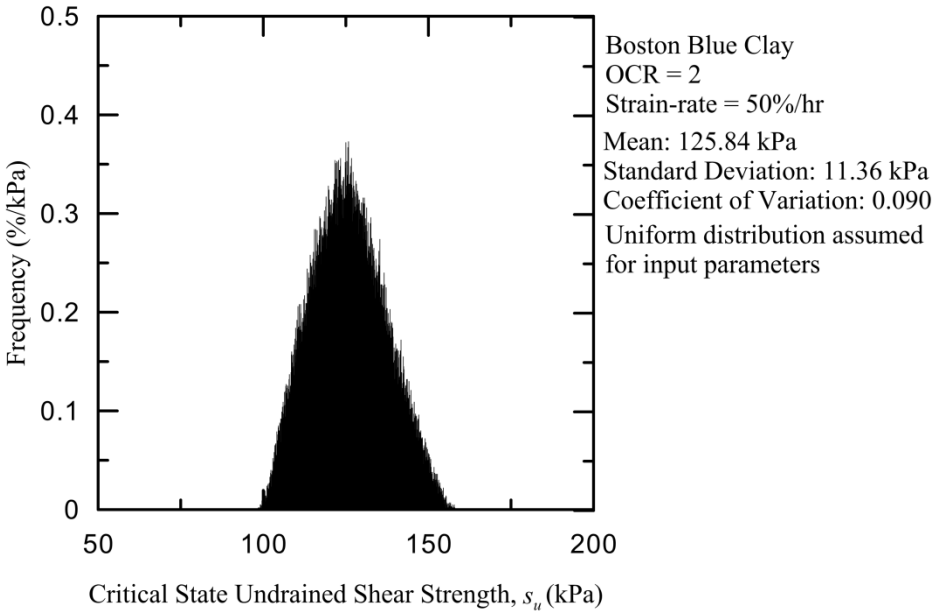

(Figure 2.12.15) Histogram for OCR = 2 for BBC at Critical State Undrained Shear Strength, Rate-Dependent Model

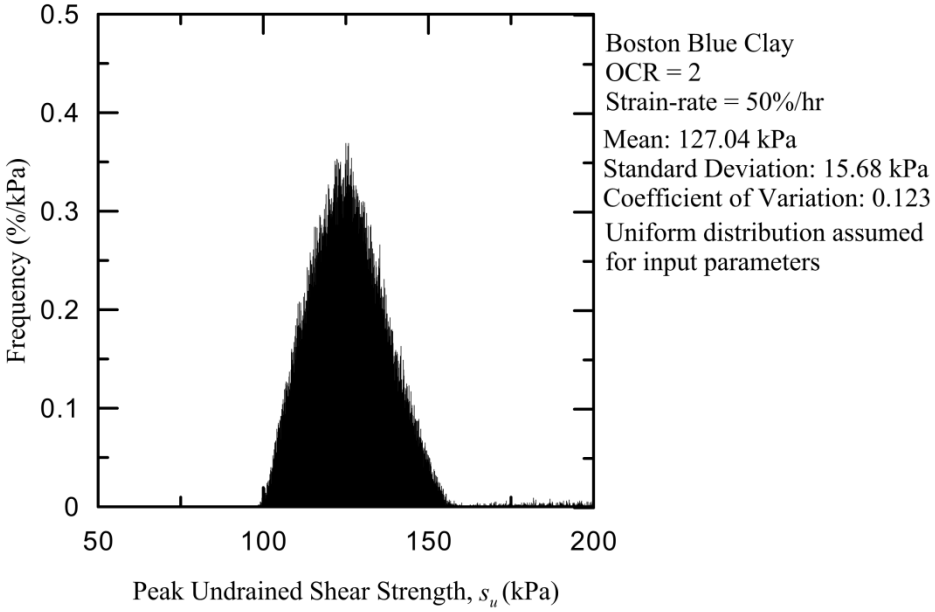

(Figure 2.12.16) Histogram for OCR = 2 for BBC at Peak Undrained Shear Strength, Rate-Dependent Model

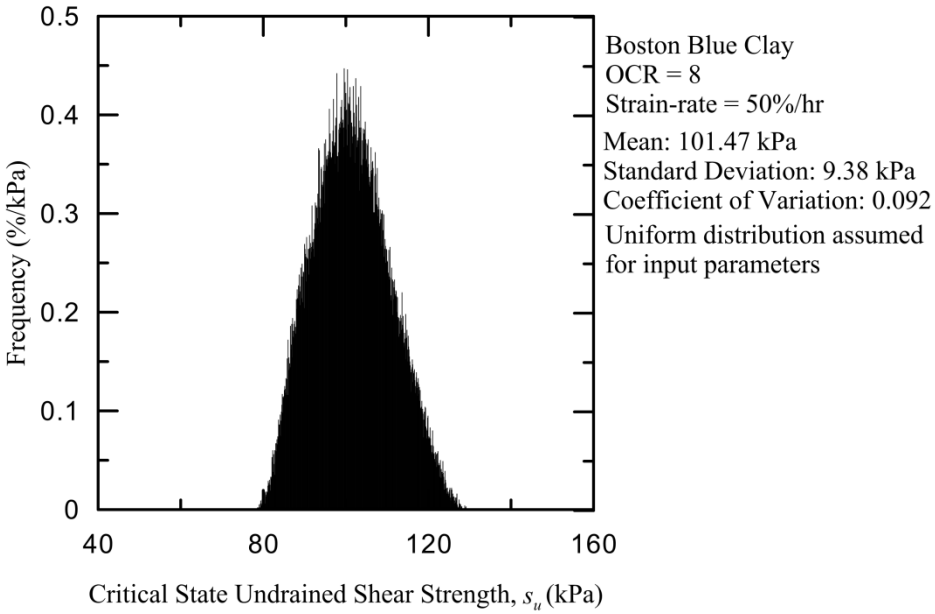

(Figure 2.12.17) Histogram for OCR = 8 for BBC at Critical State Undrained Shear Strength, Rate-Dependent Model

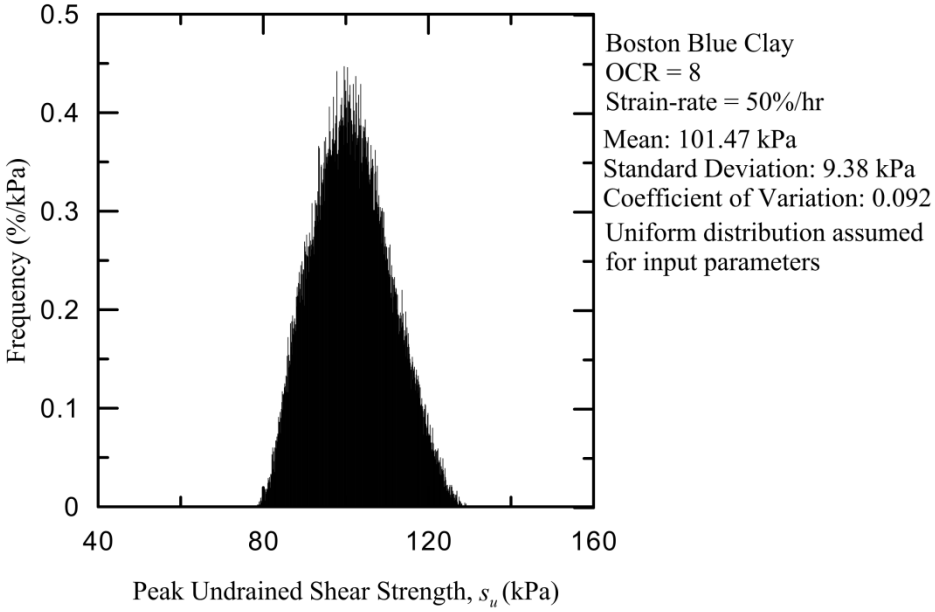

(Figure 2.12.18) Histogram for OCR = 8 for BBC at Peak Undrained Shear Strength, Rate-Dependent Model

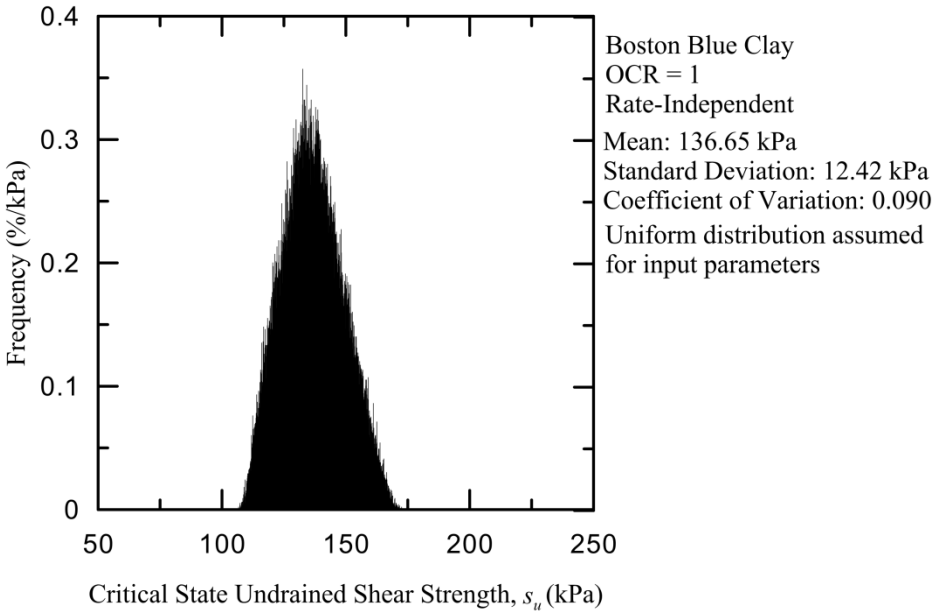

(Figure 2.12.19) Histogram for OCR = 1 for BBC at Critical State Undrained Shear Strength, Rate-Independent Model

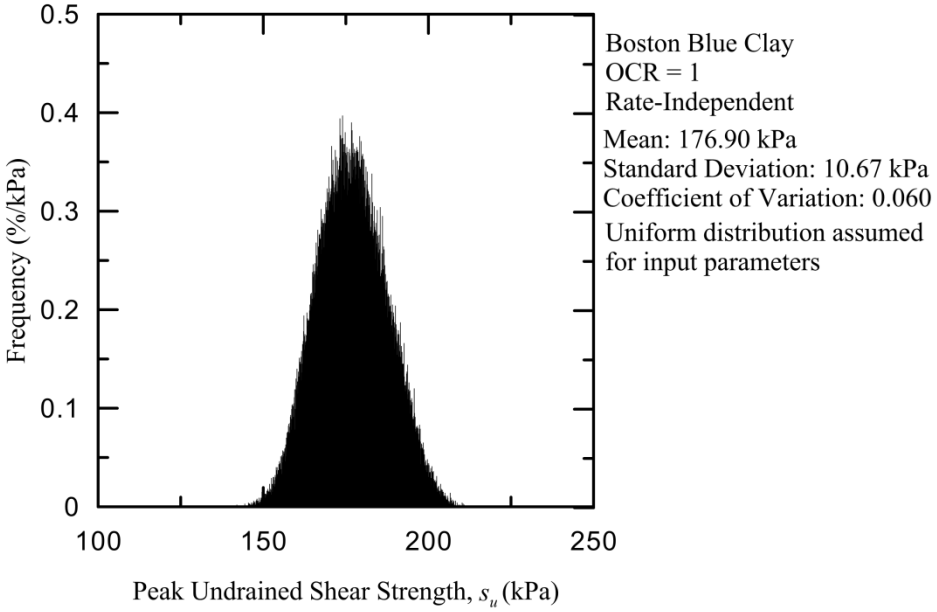

(Figure 2.12.20) Histogram for OCR = 1 for BBC at Peak Undrained Shear Strength, Rate-Independent Model

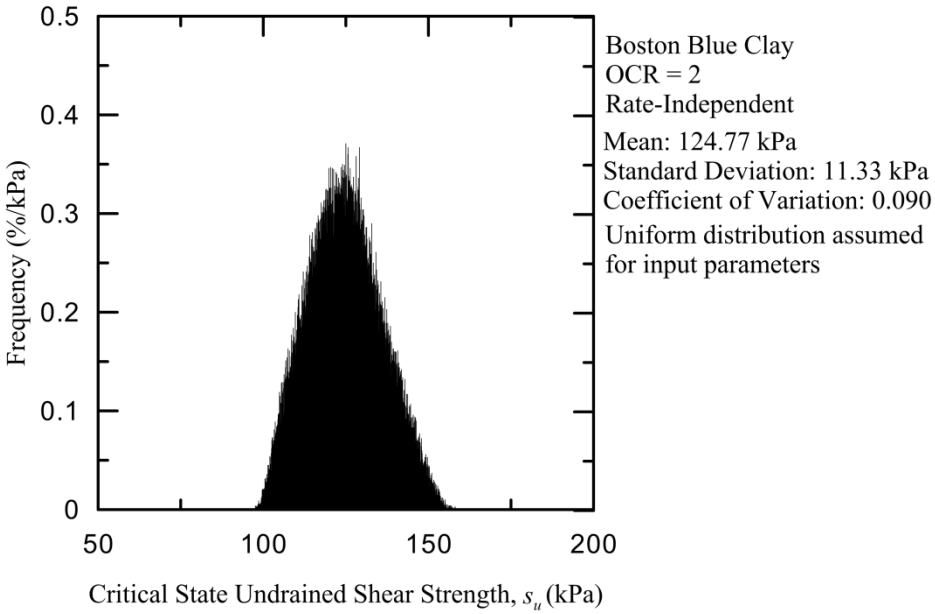

(Figure 2.12.21) Histogram for OCR = 2 for BBC at Critical State Undrained Shear Strength, Rate-Independent Model

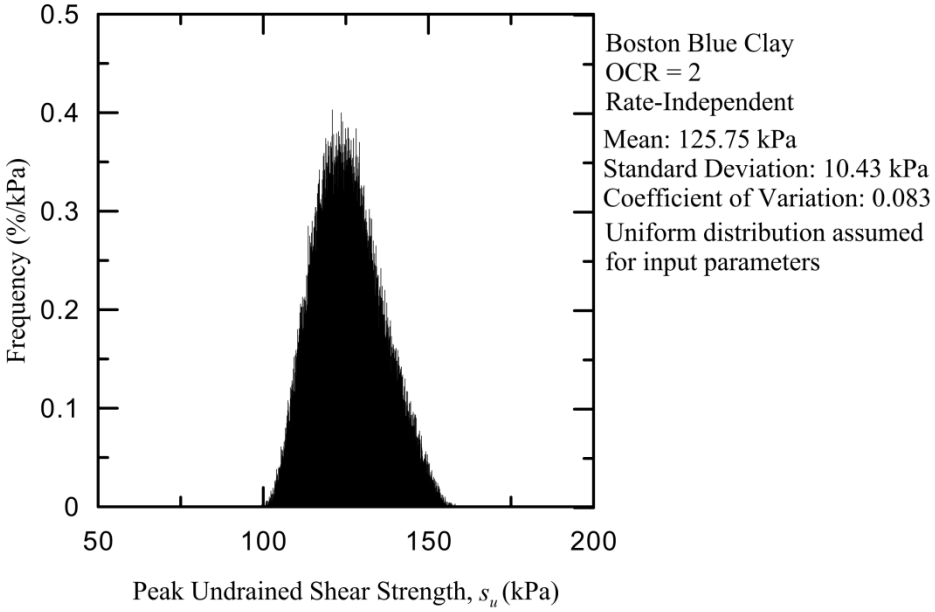

(Figure 2.12.22) Histogram for OCR = 2 for BBC at Peak Undrained Shear Strength, Rate-Independent Model

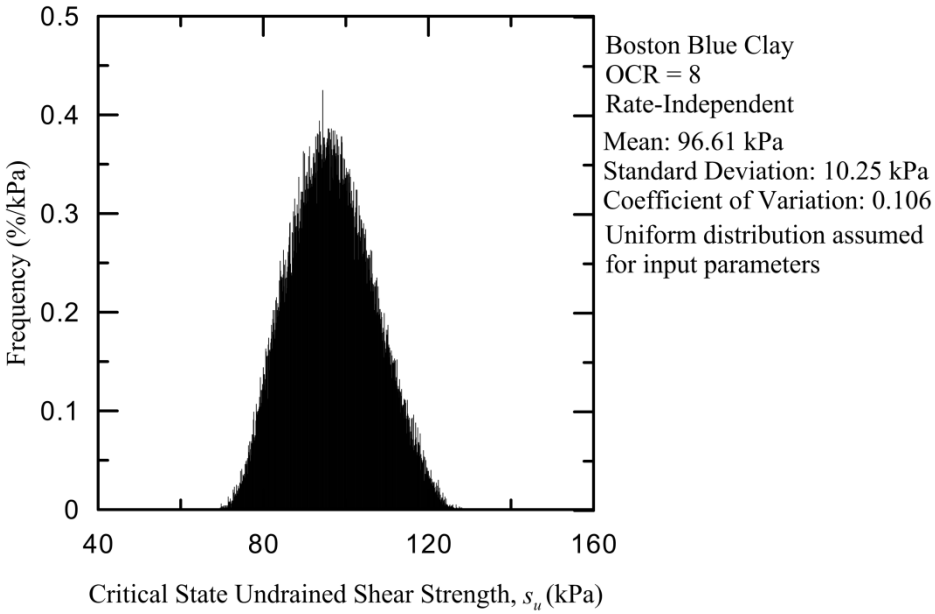

(Figure 2.12.23) Histogram for OCR = 8 for BBC at Critical State Undrained Shear Strength, Rate-Independent Model

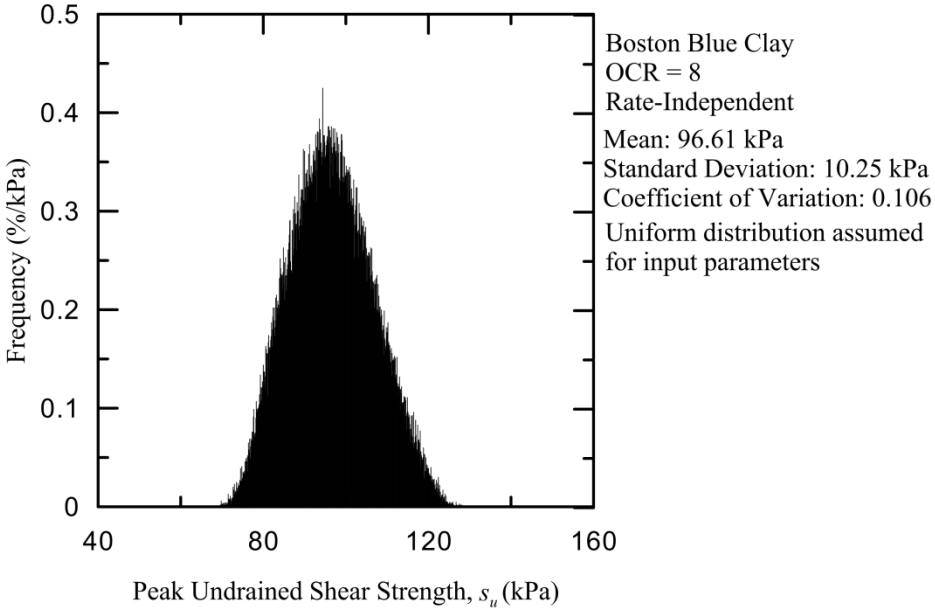

(Figure 2.12.24) Histogram for OCR = 8 for BBC at Peak Undrained Shear Strength, Rate-Independent Model

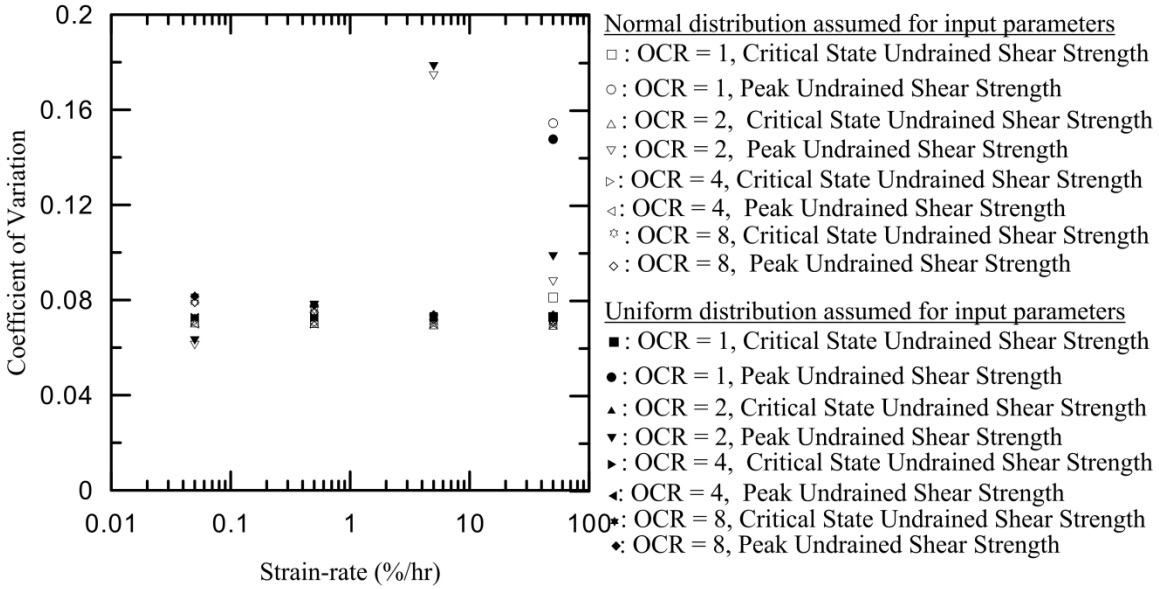

(Figure 2.12.25) Coefficient of variation with respect to strain-rate for normal and uniform distributions assumed for input parameters

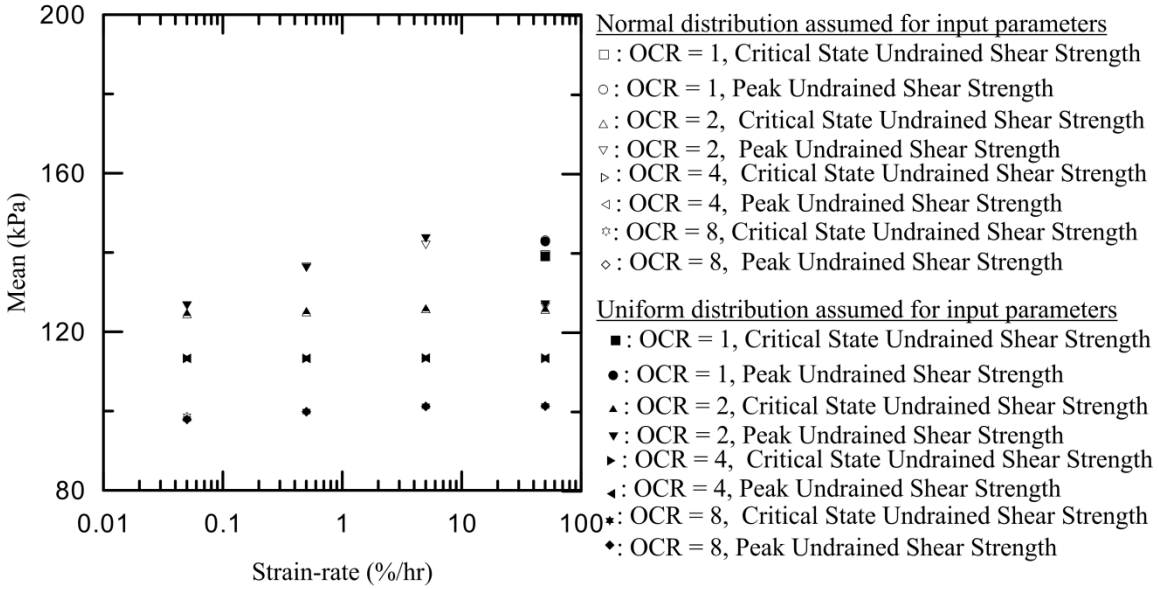

(Figure 2.12.26) Mean with respect to strain-rate for normal and uniform distributions assumed for input parameters

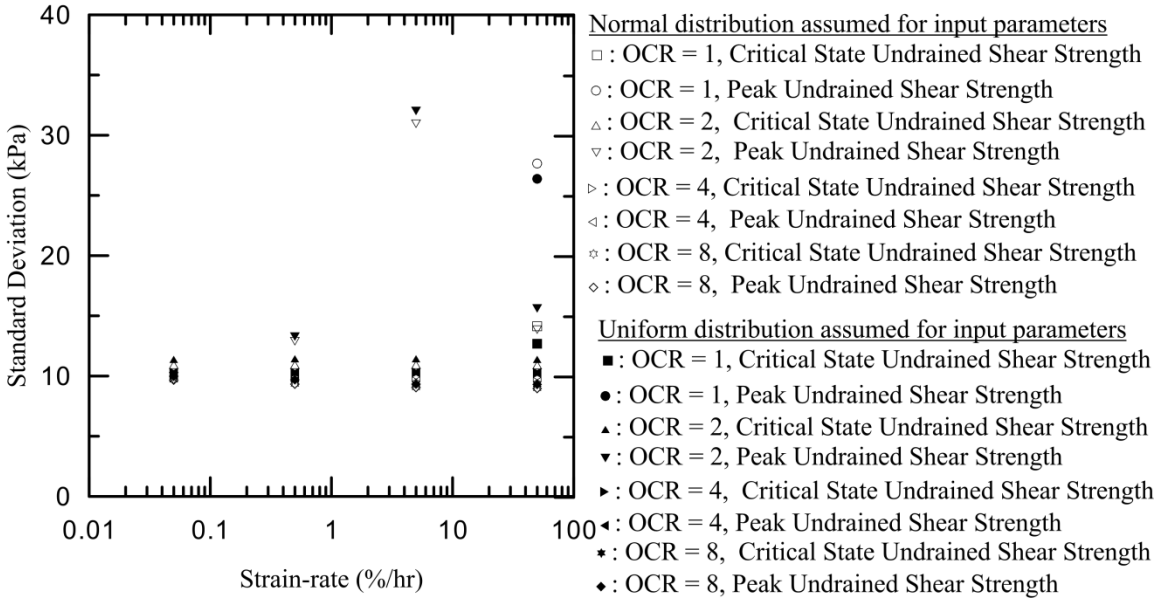

(Figure 2.12.27) Standard deviation with respect to strain-rate for normal and uniform distributions assumed for input parameters

2.13 Summary and Conclusions

This thesis presents a rate-dependent two-surface plasticity constitutive model for clay based on critical-state soil mechanics concepts. The model is based on the rate-independent model developed by Chakraborty (2009). The proposed model is capable of simulating clay behavior for both isotropic and anisotropic initial stress states and for loading paths that are more general than triaxial compression/extension.

The proposed rate-independent model has 15 parameters. The rate-dependent model contains only 1 additional parameter from the rate-independent model. Most of these parameters can be directly determined either through inspection of the experimental data or by fitting simple model equations through data obtained from laboratory tests, like isotropic and 1-D consolidation, isotropic and anisotropic triaxial compression and extension, simple shear, and ring shear tests, without resorting to

trial-and-error simulations of these tests. Both rate-independent and rate-dependent parameters are proposed for Boston Blue Clay, London Clay and Kaolin Clay.

Since constitutive models are heavily based on experimental calibration data. The effect of uncertainty in the calibration parameters on the response of the proposed model is investigated. A sensitivity analysis was performed, examining a single parameter at a time at ±5, ±10, and ±20% variation from the deterministic value. Additionally, to consider the conglomerate effect of parameter uncertainty, Monte-Carlo analyses were performed considering random selection of all model parameters following both normal and uniform probability distribution functions. This paper is the first to consider constitutive modeling uncertainty through Monte-Carlo analyses.

2.14 Future Research Paths

From fully examining the rate-dependent response of clay three primary problems according to the author remain to be examined by future researchers in utilizing the model developed. The first challenge is examining further how the mean, standard deviation and coefficient of variation for the proposed model vary with respect to strain rate for different soil types. The second is the incorporation the proposed model in to a full probabilistic design constitutive model in finite elements. The Third is performing similar sensitivity studies simulating experimental tests other than undrained triaxial compression. By examining how the mean, standard deviation and coefficient of variation changes, the development of design equations using safety factors based on these distributions can be proposed for calibrated soil types.

The development of constitutive model design equations based on probabilistic design will aid geotechnical engineers in determining the response of soil quickly. The expansion of the model into finite elements allows for the simulation of complex interactions through which design insight and design equations can be further developed. Simulation of pile driving, loading on foundations or construction loads with the developed work will lead to prediction of the complex response of clay. The utilization of the proposed model to determine factors safety, based on input parameter variability or quality of design data is highly desirable. Finally performing a sensitivity analysis on tests other than undrained triaxial compression to determine if similar trends in sensitivity are observed throughout will lead to a more complete classification of the model sensitivity.

The developed model represents a base model from which high strain-rate constitutive models can be developed. A high strain-rate model ideally would be capable of simulating Split Hopkinson Pressure Bar (SHPB) data. The scarcity of data at very high strain rates limits the further development of this model toward high strain-rate. Constitutive models in the past have typically covered the low strain rate to medium strain rate range; the development of a model which simulates high strain-rate is desirable. The proposed model can serve as a basis from which a high strain rate model can be developed.

This thesis is the first to examine probability with constitutive modeling. The author believes that future research involving constitutive modeling and probability analysis will lead to the development of precise, highly efficient, yet safe design and simulation methods.

Appendix I: Results of the Sensitivity Analysis

This section presents the results of the rate-independent and rate-dependent sensitivity analysis. Input parameters were varied at ±5%, ±10%, and ±20%. During each simulation only one parameter was varied at a time. Results are presented for Boston Blue Clay, Kaolin Clay and London Clay.

Rate-independent sensitivity analysis for Boston Blue Clay at 5% variation:

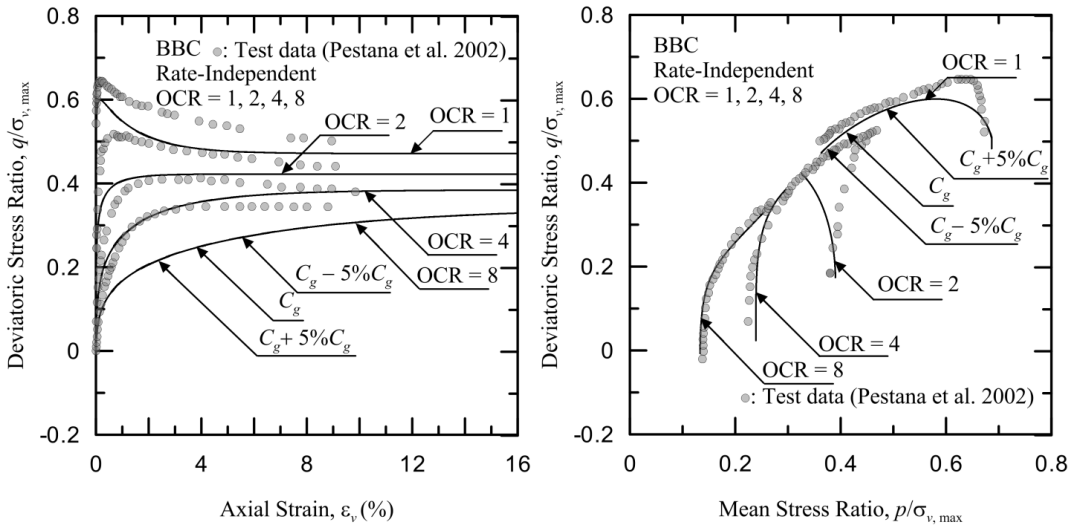

(Figure AI.1.1) Sensitivity of C_g at 5% variation for Boston Blue Clay, test data taken from Pestana et al. (2002)

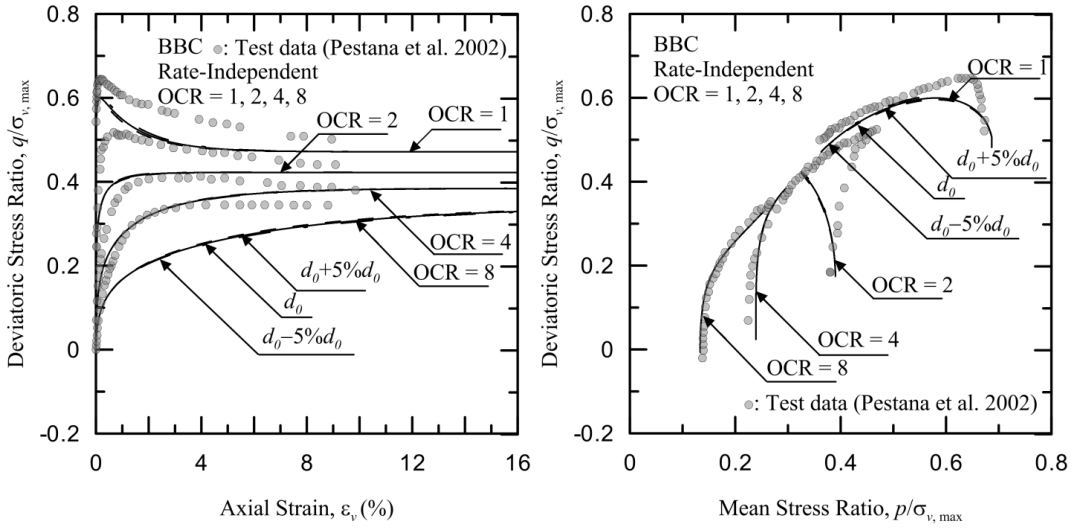

(Figure AI.1.2) Sensitivity of d_0 at 5% variation for Boston Blue Clay, test data taken from Pestana et al. (2002)

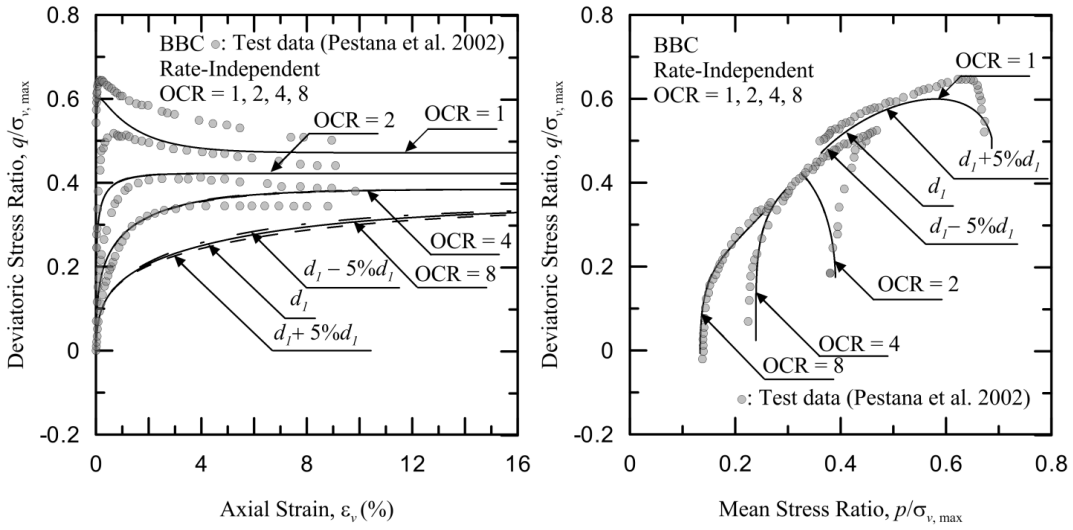

(Figure AI.1.3) Sensitivity of d_1 at 5% variation for Boston Blue Clay, test data taken from Pestana et al. (2002)

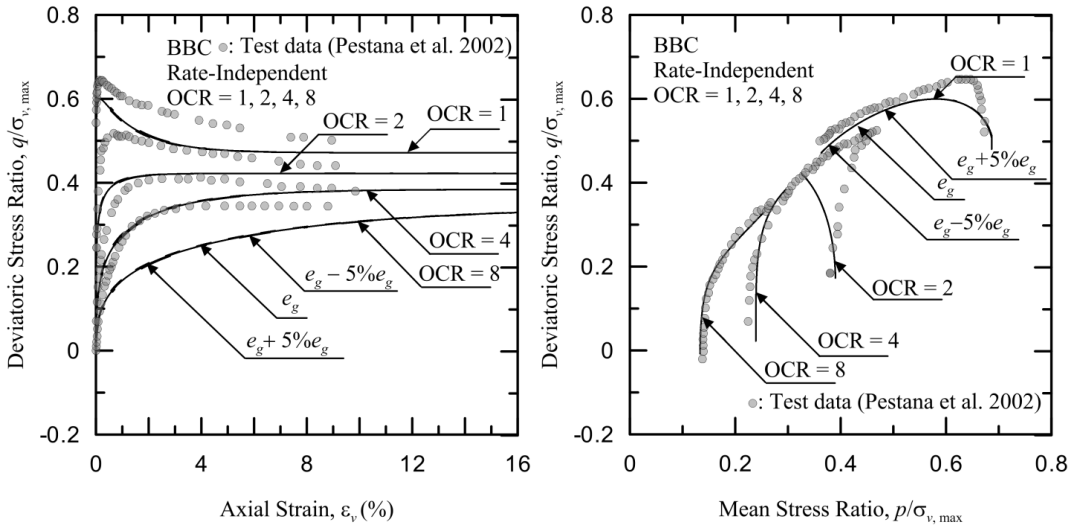

(Figure AI.1.4) Sensitivity of e_g at 5% variation for Boston Blue Clay, test data taken from Pestana et al. (2002)

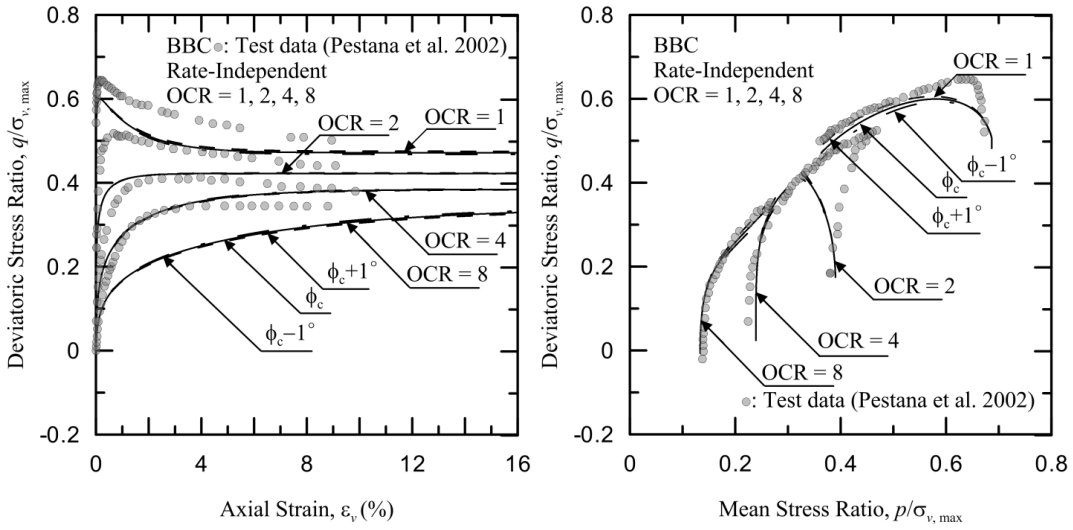

(Figure AI.1.5) Sensitivity of ϕ_c at 1° variation for Boston Blue Clay, test data taken from Pestana et al. (2002)

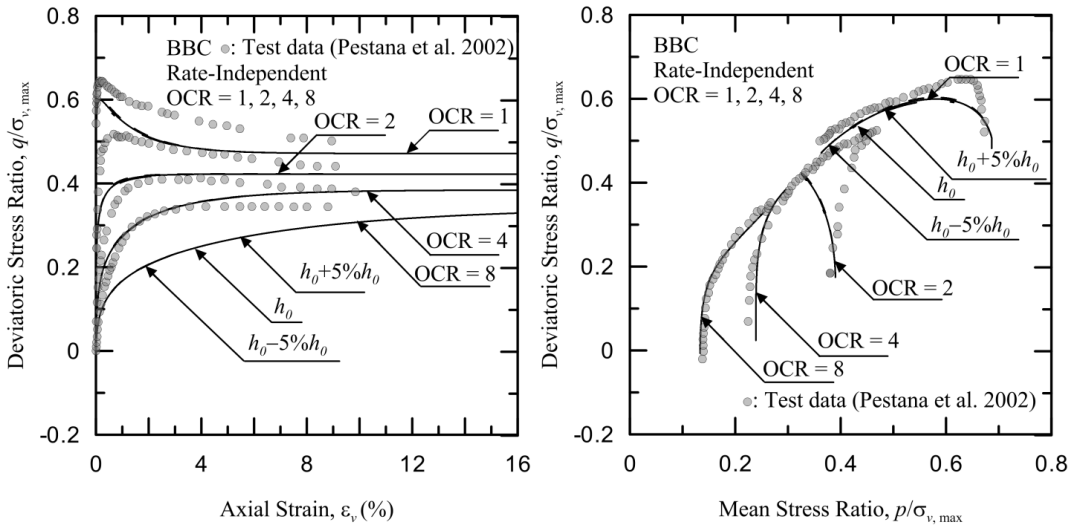

(Figure AI.1.6) Sensitivity of h_0 at 5% variation for Boston Blue Clay, test data taken from Pestana et al. (2002)

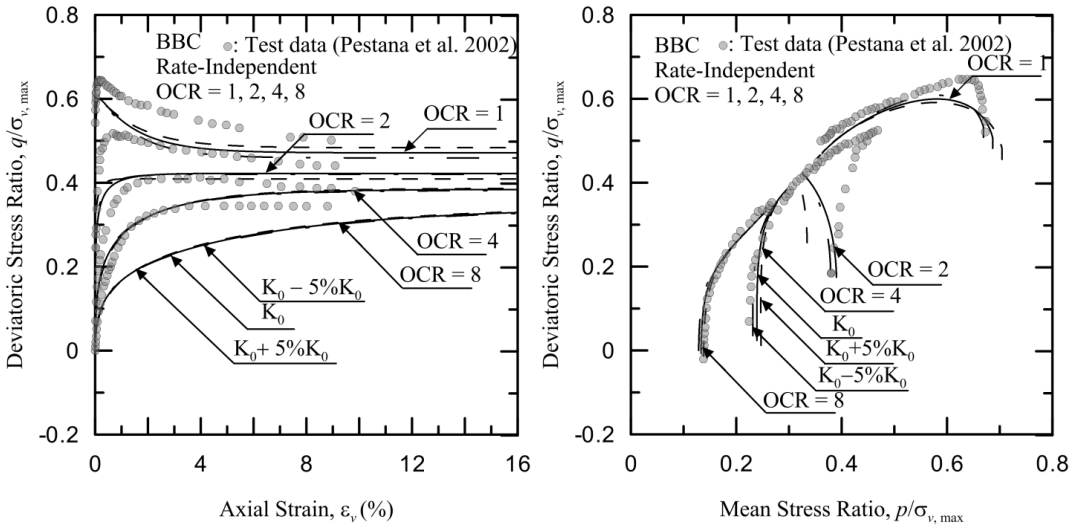

(Figure AI.1.7) Sensitivity of K_0 at 5% variation for Boston Blue Clay, test data taken from Pestana et al. (2002)

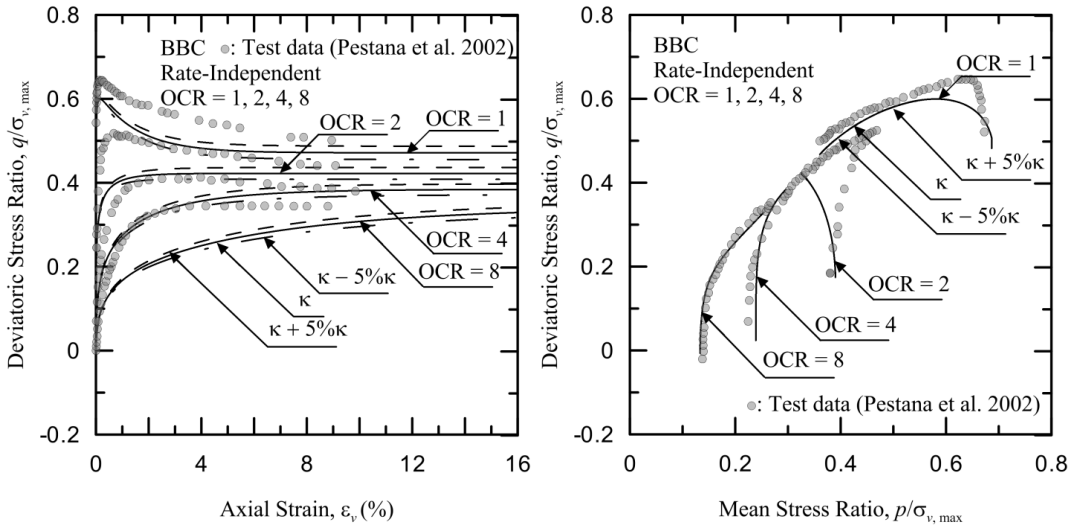

(Figure AI.1.8) Sensitivity of κ at 5% variation for Boston Blue Clay, test data taken from Pestana et al. (2002)

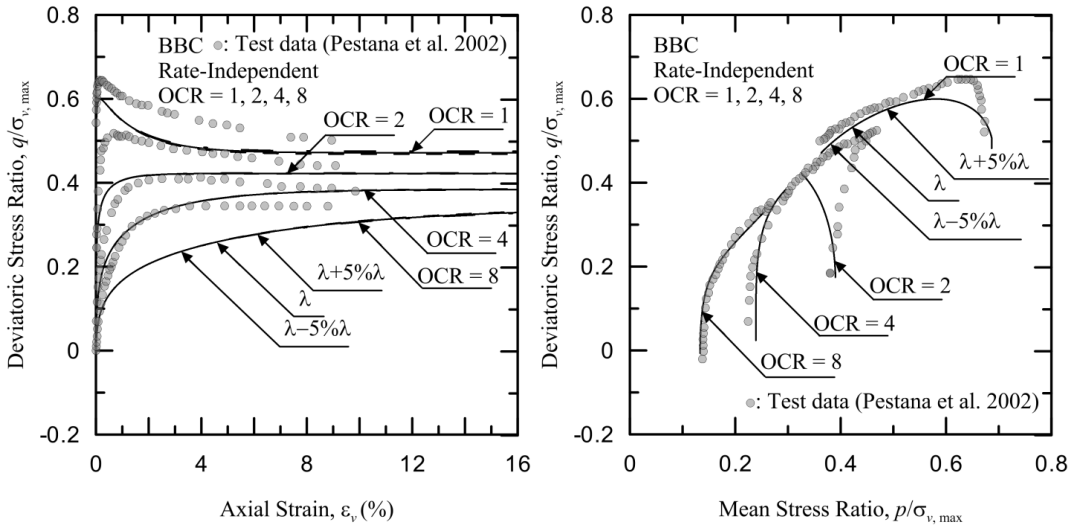

(Figure AI.1.9) Sensitivity of λ at 5% variation for Boston Blue Clay, test data taken from Pestana et al. (2002)

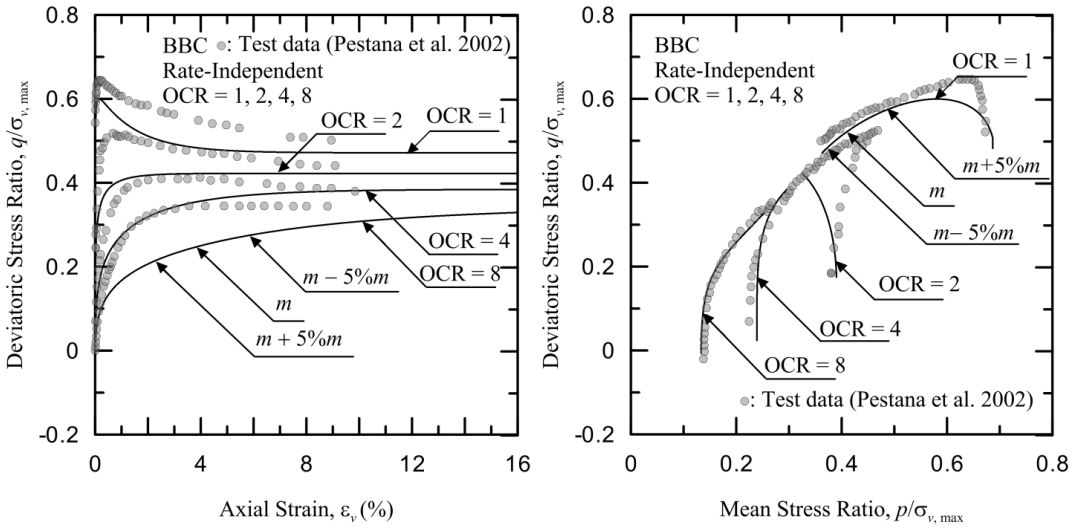

(Figure AI.1.10) Sensitivity of *m* at 5% variation for Boston Blue Clay, test data taken from Pestana et al. (2002)

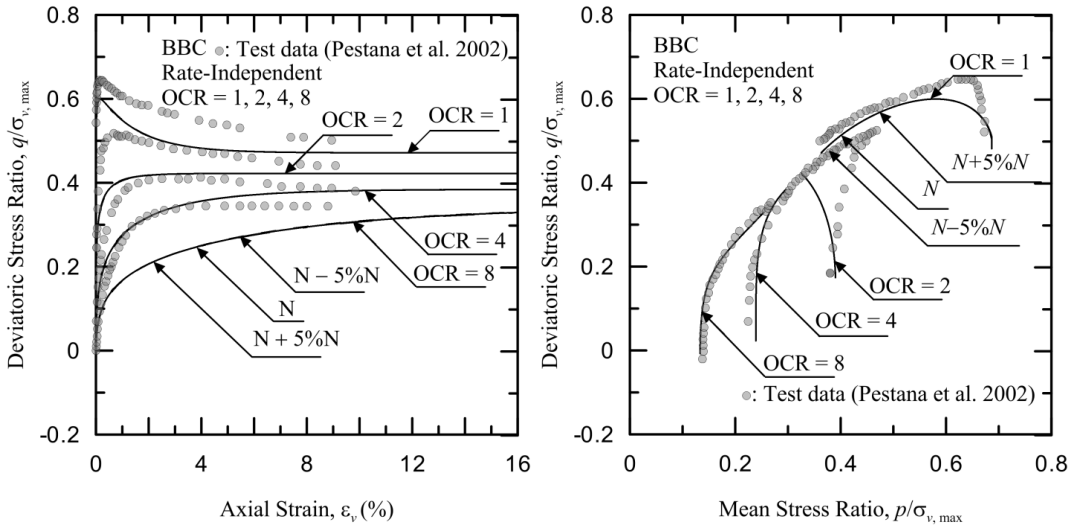

(Figure AI.1.11) Sensitivity of N at 5% variation for Boston Blue Clay, test data taken from Pestana et al. (2002)

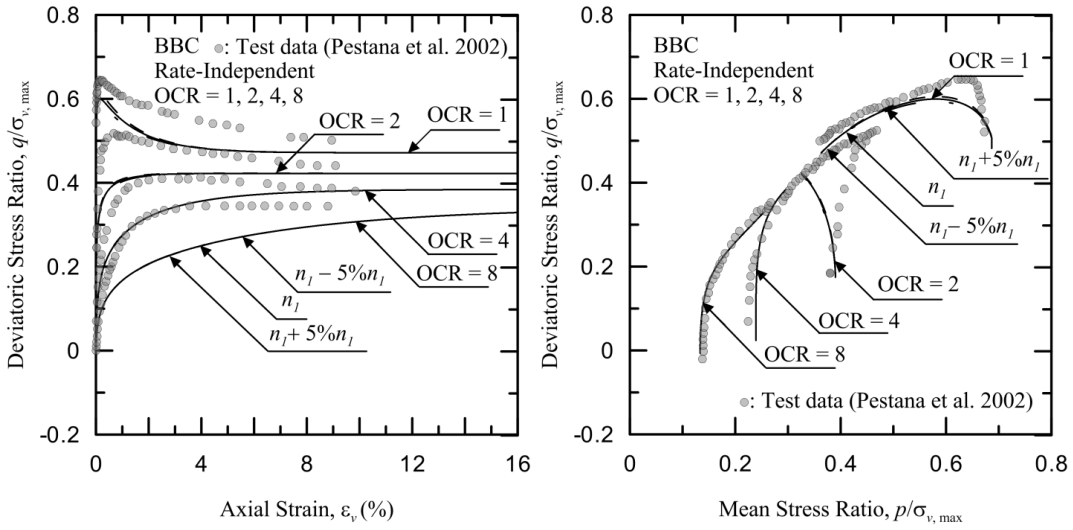

(Figure AI.1.12) Sensitivity of n_1 at 5% variation for Boston Blue Clay, test data taken from Pestana et al. (2002)

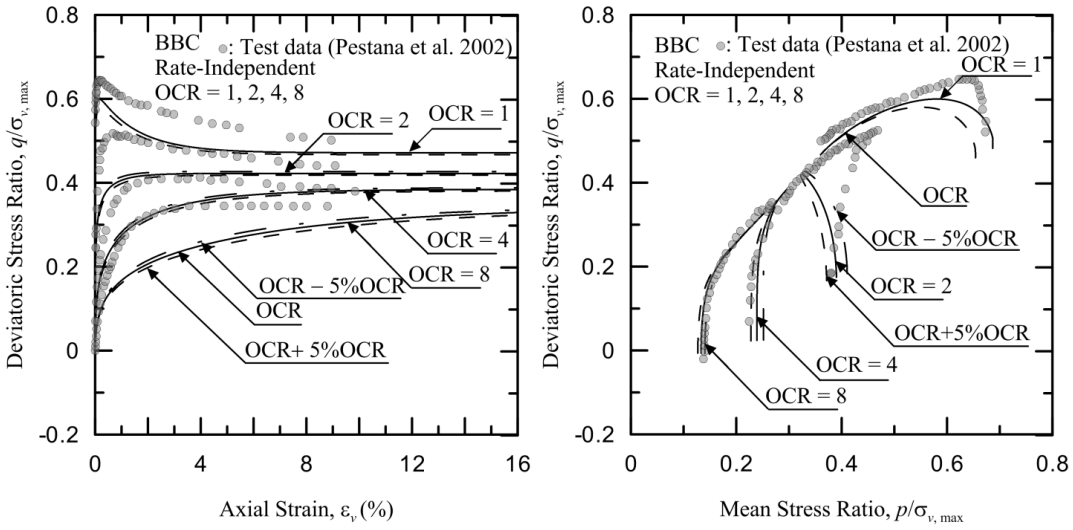

(Figure AI.1.13) Sensitivity of OCR at 5% variation for Boston Blue Clay, test data taken from Pestana et al. (2002)

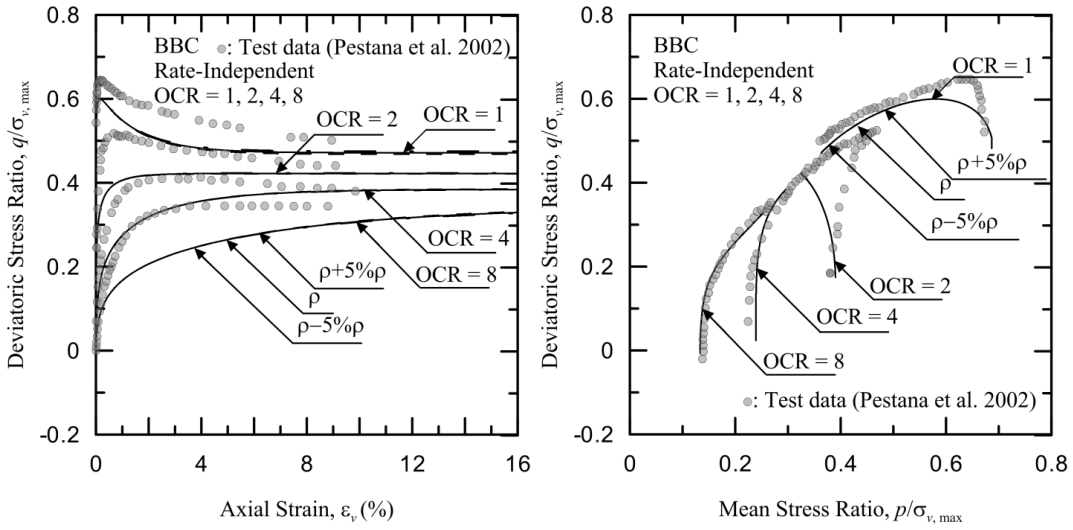

(Figure AI.1.14) Sensitivity of ρ at 5% variation for Boston Blue Clay, test data taken from Pestana et al. (2002)

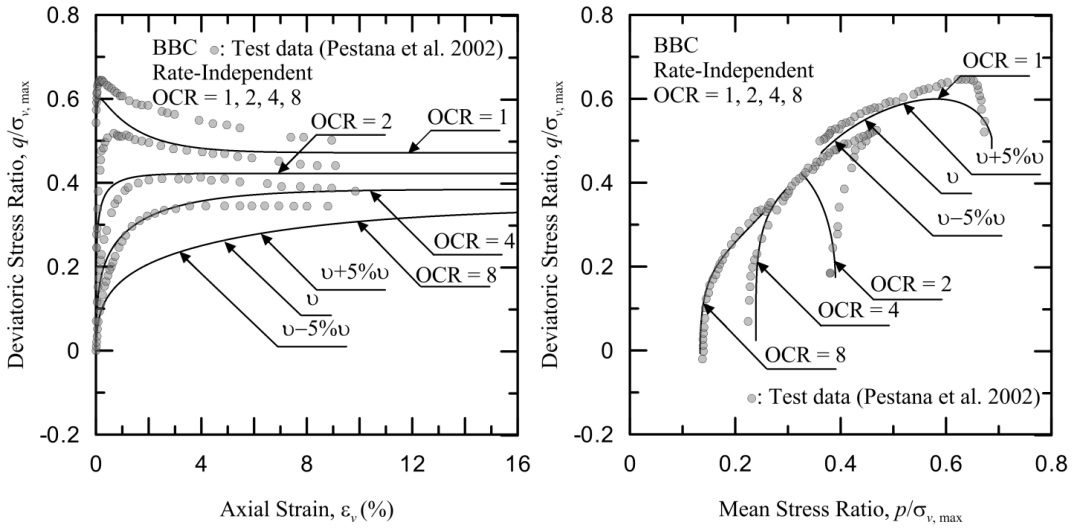

(Figure AI.1.15) Sensitivity of υ at 5% variation for Boston Blue Clay, test data taken from Pestana et al. (2002)

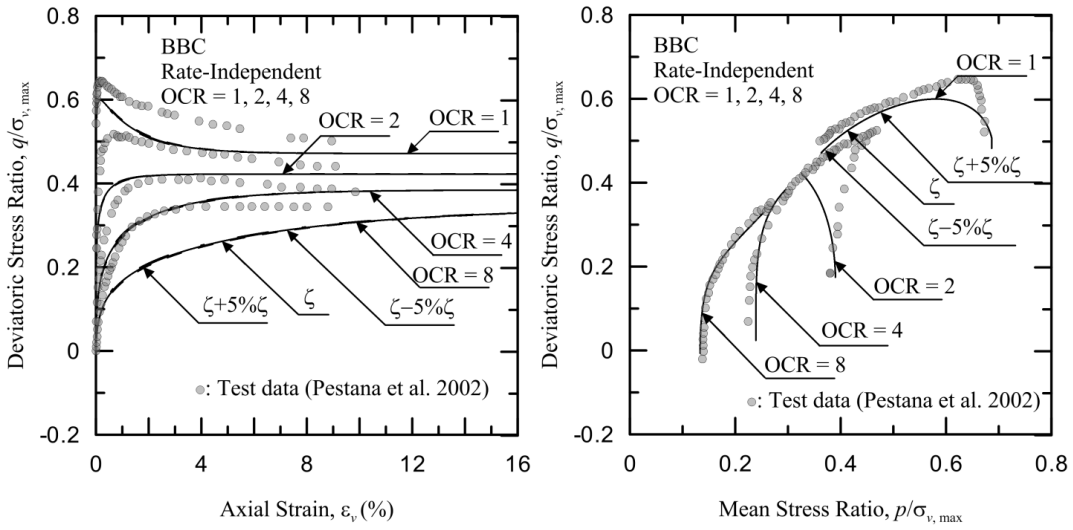

(Figure AI.1.16) Sensitivity of ζ at 5% variation for Boston Blue Clay, test data taken from Pestana et al. (2002)

Rate-independent sensitivity analysis for Boston Blue Clay at 10% variation:

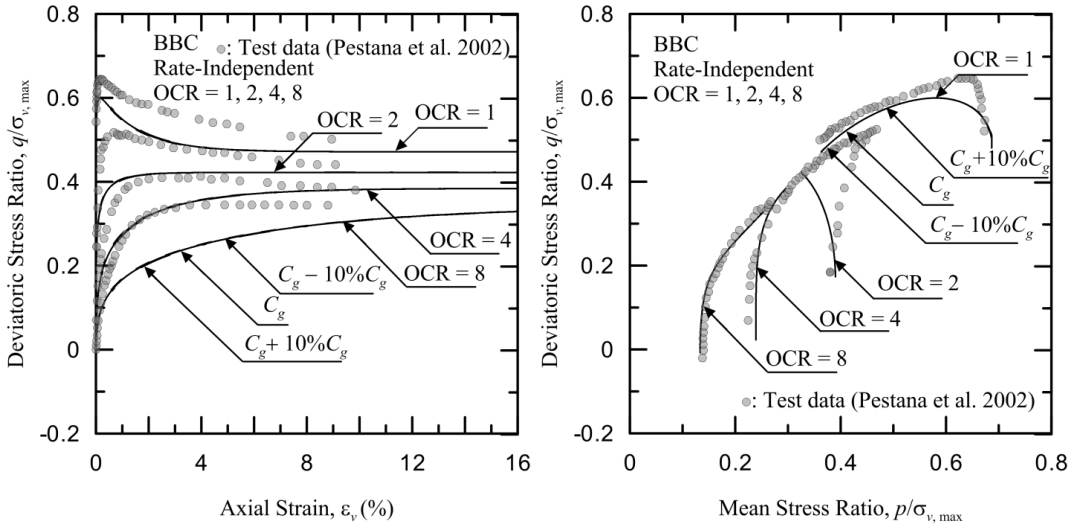

(Figure AI.1.17) Sensitivity of C_g at 10% variation for Boston Blue Clay, test data taken from Pestana et al. (2002)

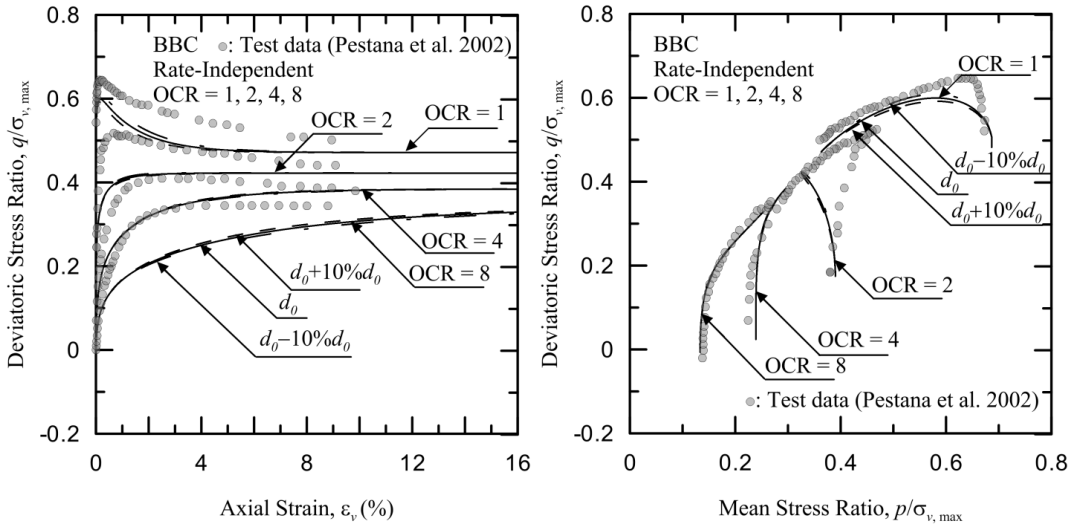

(Figure AI.1.18) Sensitivity of d_0 at 10% variation for Boston Blue Clay, test data taken from Pestana et al. (2002)

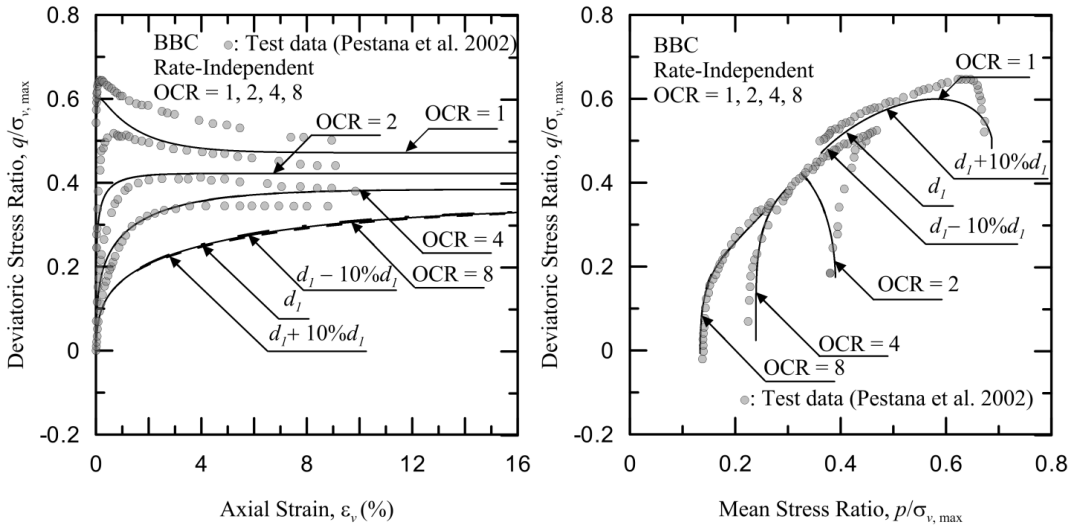

(Figure AI.1.19) Sensitivity of d_1 at 10% variation for Boston Blue Clay, test data taken from Pestana et al. (2002)

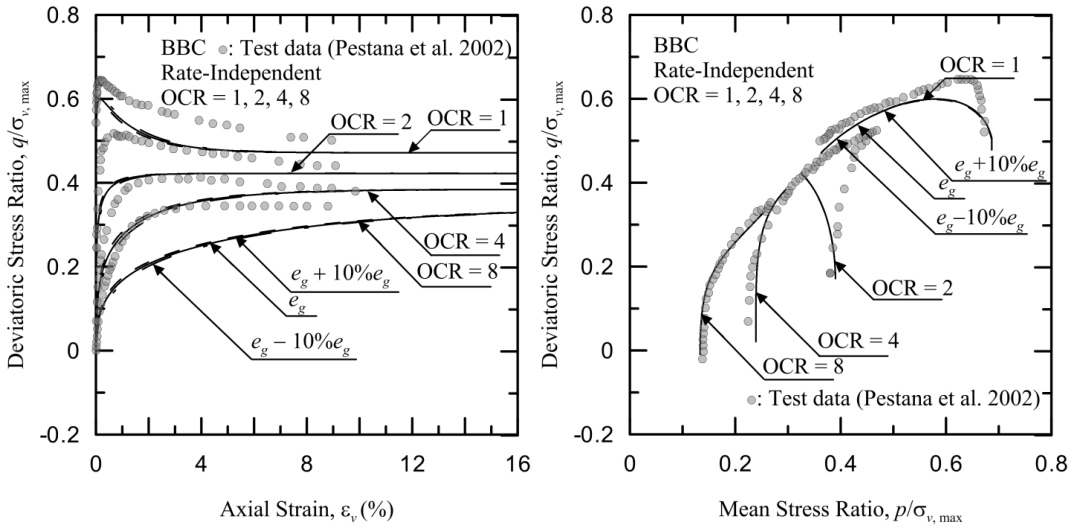

(Figure AI.1.20) Sensitivity of e_g at 10% variation for Boston Blue Clay, test data taken from Pestana et al. (2002), stress-strain plot

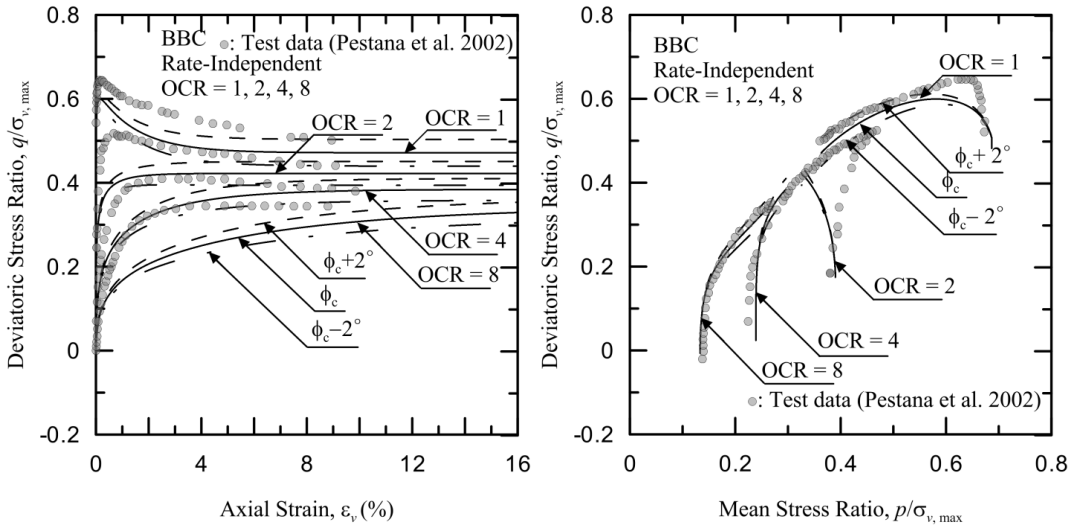

(Figure AI.1.21) Sensitivity of ϕ_c at 2° variation for Boston Blue Clay, test data taken from Pestana et al. (2002)

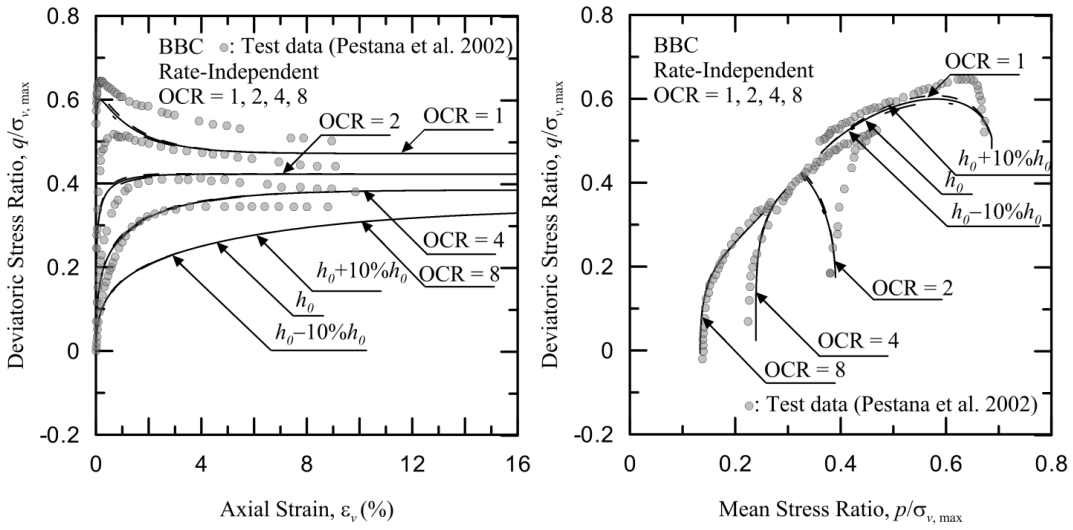

(Figure AI.1.22) Sensitivity of h_0 at 10% variation for Boston Blue Clay, test data taken from Pestana et al. (2002)

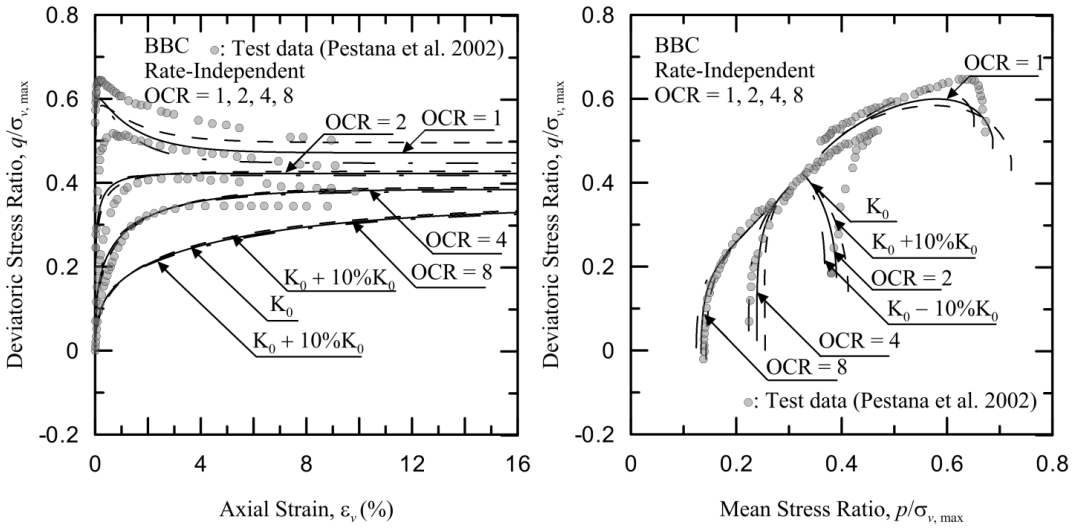

(Figure AI.1.23) Sensitivity of K_0 at 10% variation for Boston Blue Clay, test data taken from Pestana et al. (2002)

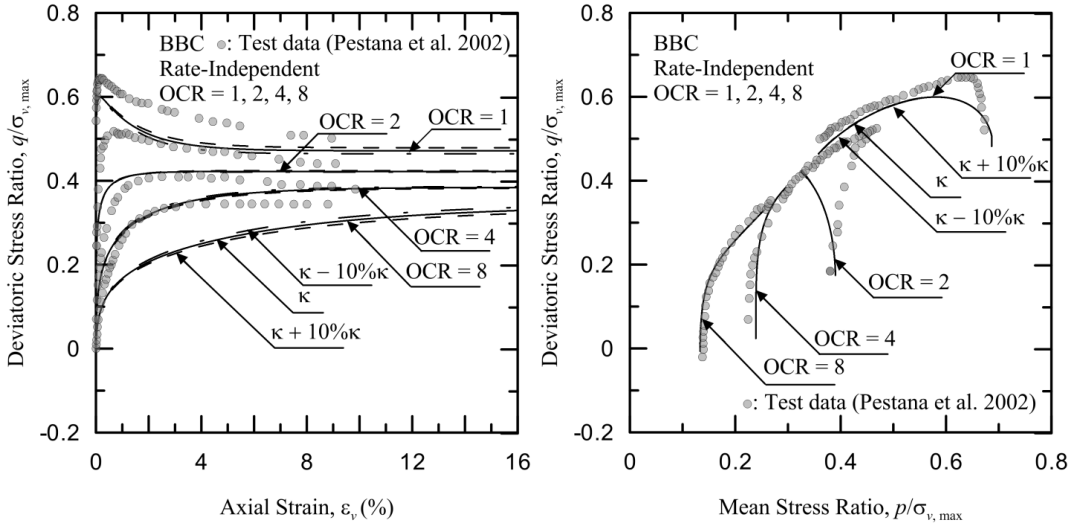

(Figure AI.1.24) Sensitivity of κ at 10% variation for Boston Blue Clay, test data taken from Pestana et al. (2002)

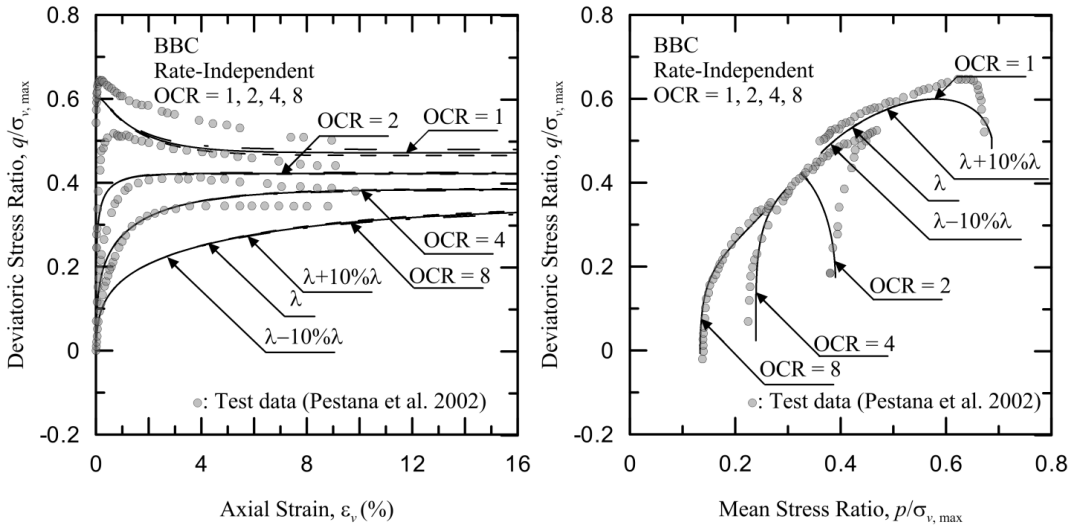

(Figure AI.1.25) Sensitivity of λ at 10% variation for Boston Blue Clay, test data taken from Pestana et al. (2002)

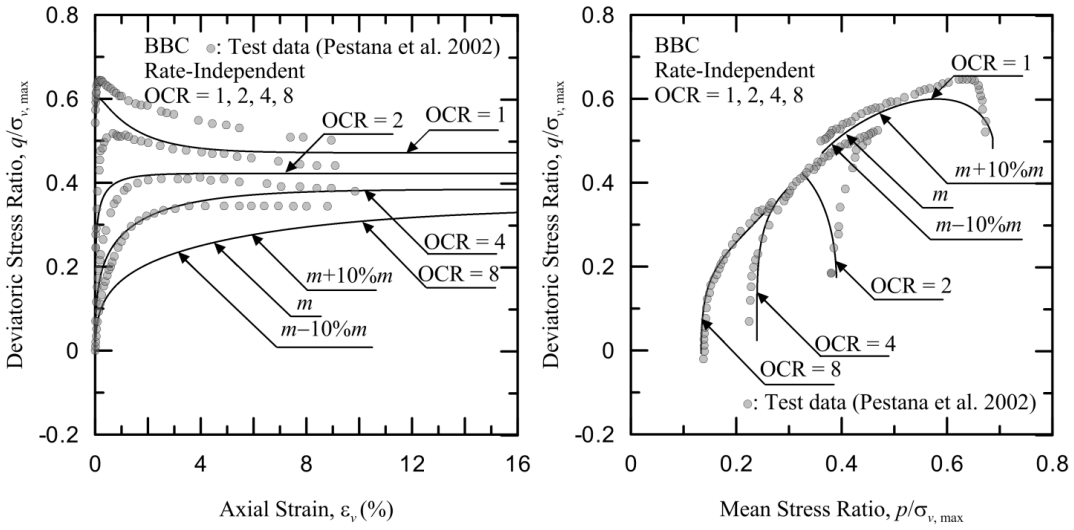

(Figure AI.1.26) Sensitivity of *m* at 10% variation for Boston Blue Clay, test data taken from Pestana et al. (2002)

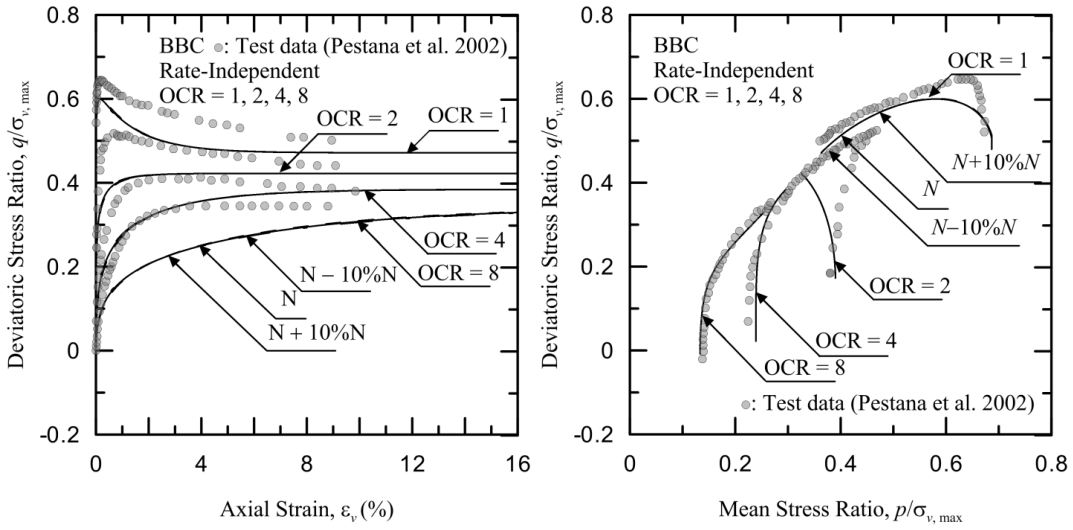

(Figure AI.1.27) Sensitivity of N at 10% variation for Boston Blue Clay, test data taken from Pestana et al. (2002)

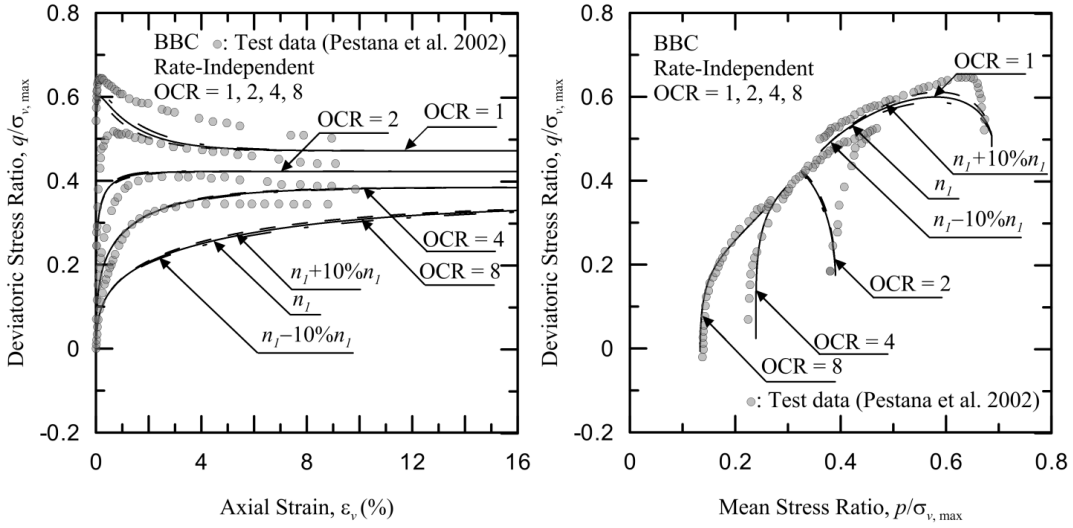

(Figure AI.1.28) Sensitivity of n_1 at 10% variation for Boston Blue Clay, test data taken from Pestana et al. (2002)

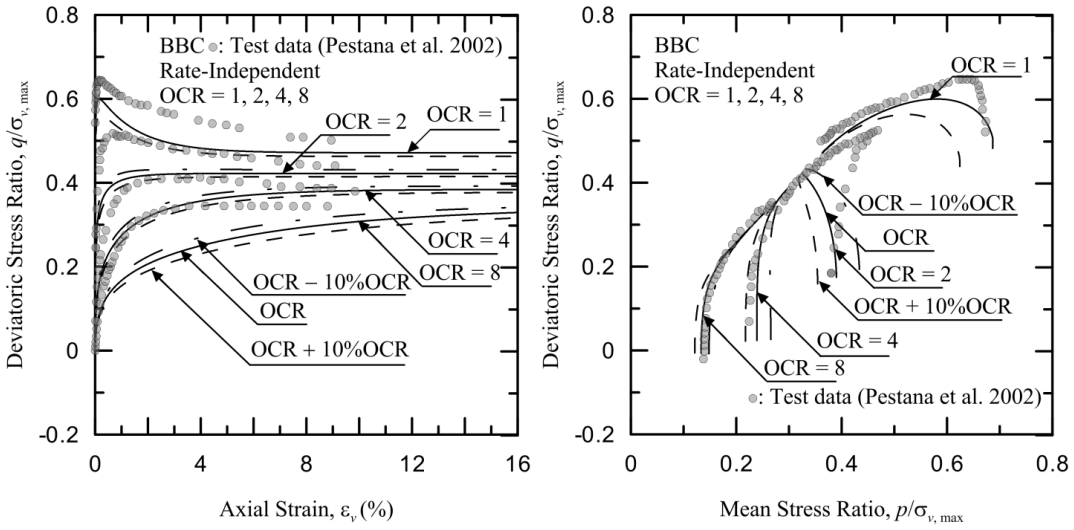

(Figure AI.1.29) Sensitivity of OCR at 10% variation for Boston Blue Clay, test data taken from Pestana et al. (2002)

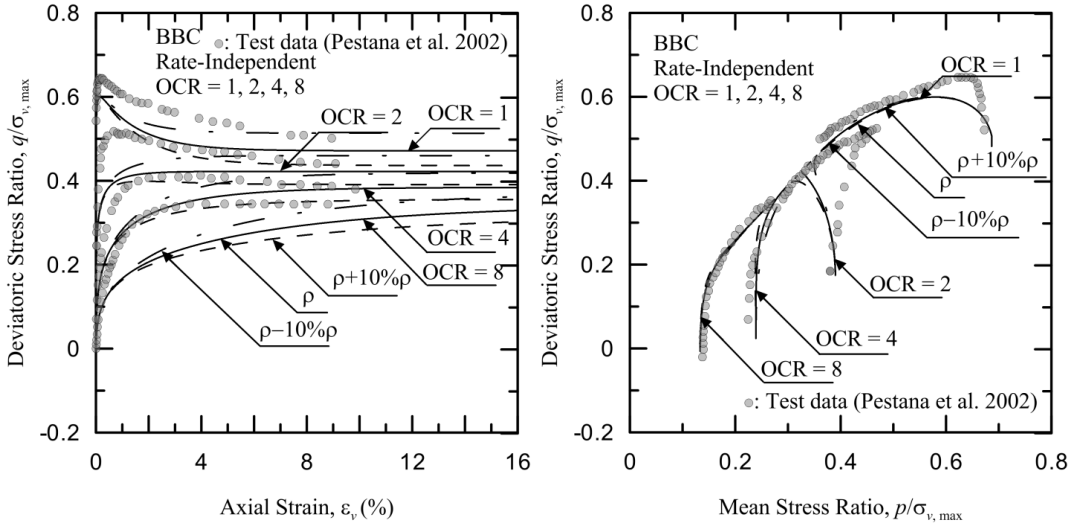

(Figure AI.1.30) Sensitivity of ρ at 10% variation for Boston Blue Clay, test data taken from Pestana et al. (2002)

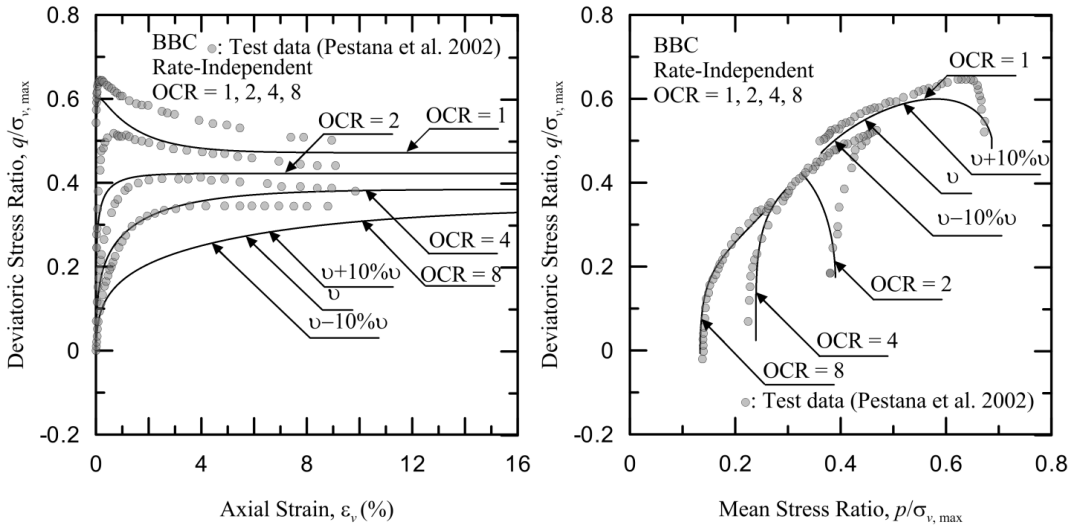

(Figure AI.1.31) Sensitivity of υ at 10% variation for Boston Blue Clay, test data taken from Pestana et al. (2002)

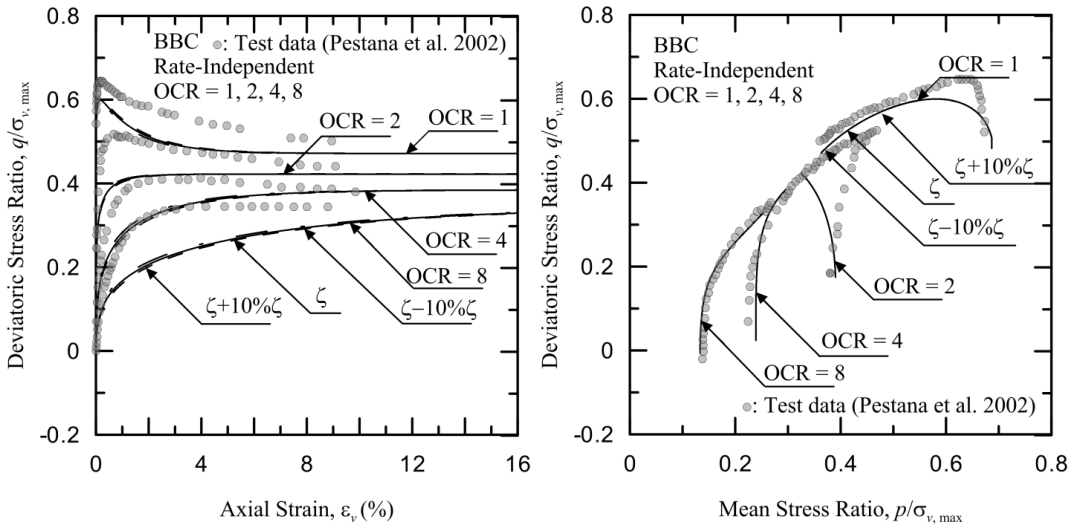

(Figure AI.1.32) Sensitivity of ζ at 10% variation for Boston Blue Clay, test data taken from Pestana et al. (2002)

Rate-independent sensitivity analysis for Boston Blue Clay at 20% variation:

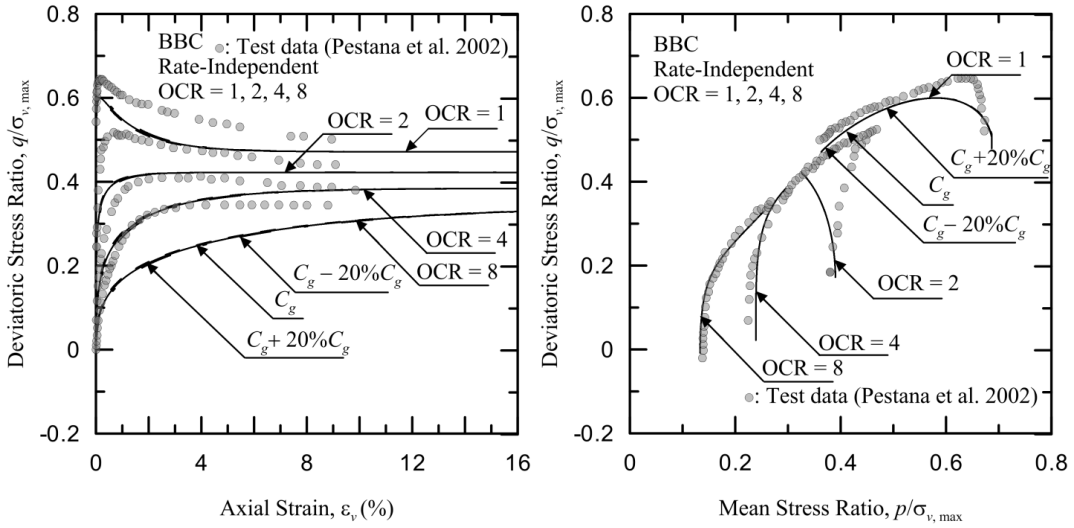

(Figure AI.1.33) Sensitivity of C_g at 20% variation for Boston Blue Clay, test data taken from Pestana et al. (2002)

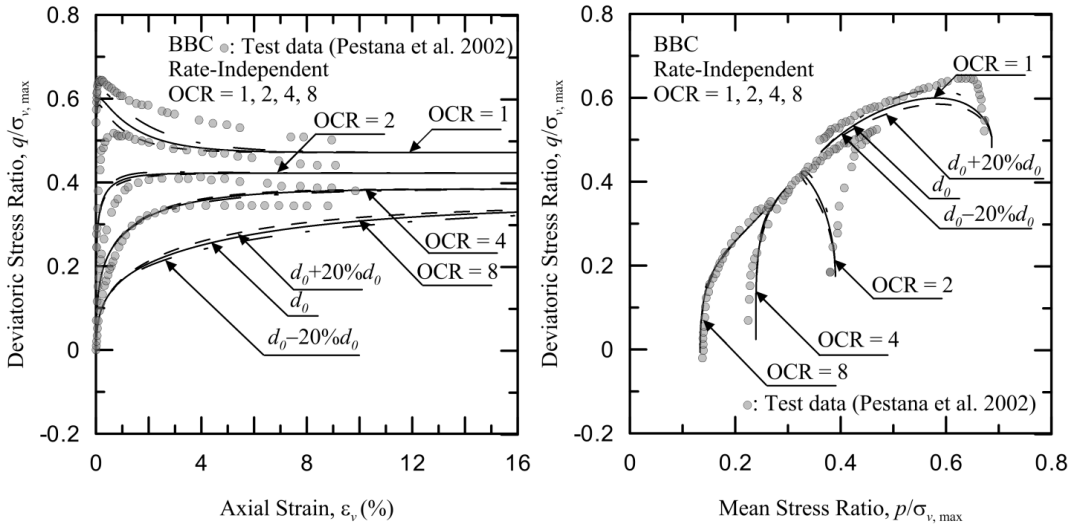

(Figure AI.1.34) Sensitivity of d_0 at 20% variation for Boston Blue Clay, test data taken from Pestana et al. (2002)

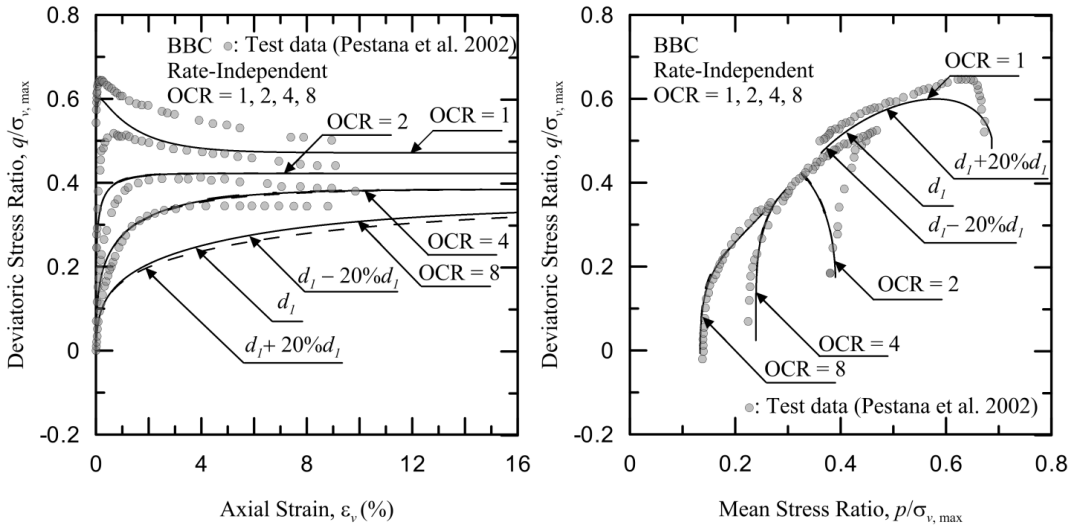

(Figure AI.1.35) Sensitivity of d_1 at 20% variation for Boston Blue Clay, test data taken from Pestana et al. (2002)

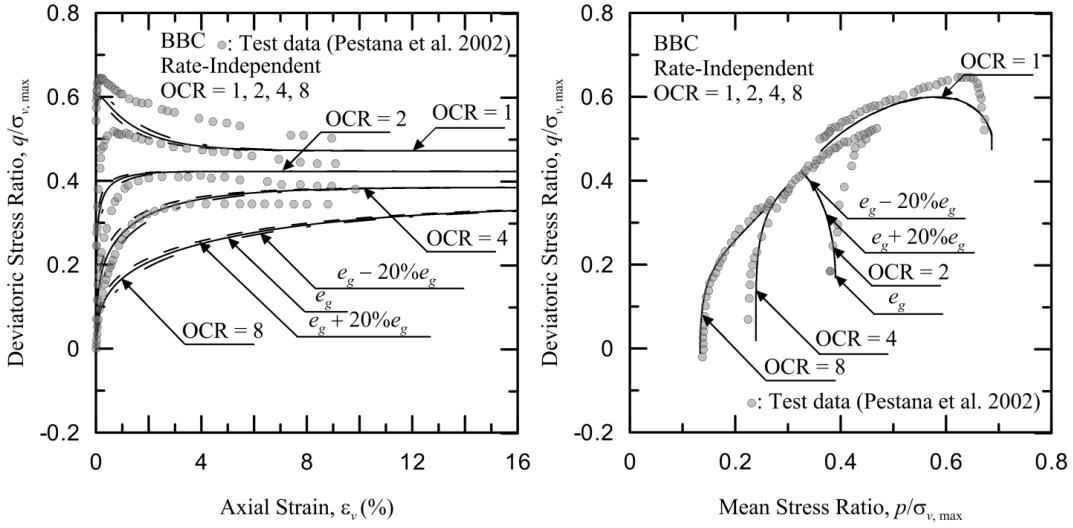

(Figure AI.1.36) Sensitivity of e_g at 20% variation for Boston Blue Clay, test data taken from Pestana et al. (2002)

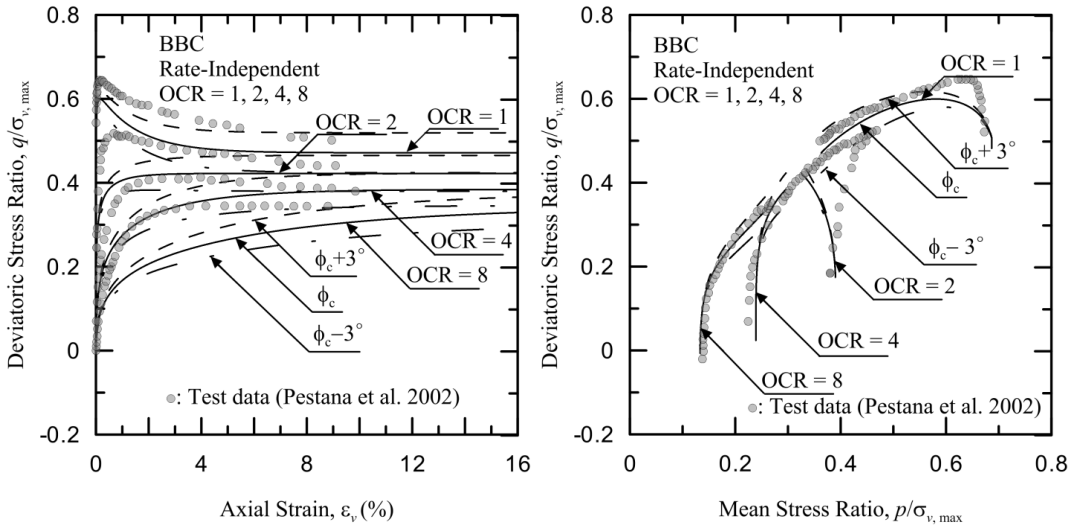

(Figure AI.1.37) Sensitivity of ϕ_c at 3° variation for Boston Blue Clay, test data taken from Pestana et al. (2002)

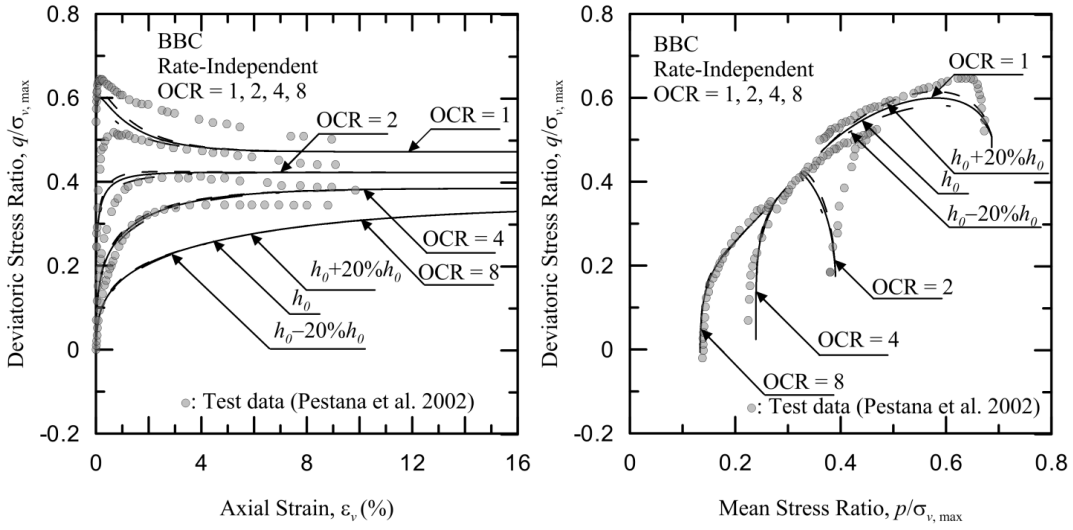

(Figure AI.1.38) Sensitivity of h_0 at 20% variation for Boston Blue Clay, test data taken from Pestana et al. (2002)

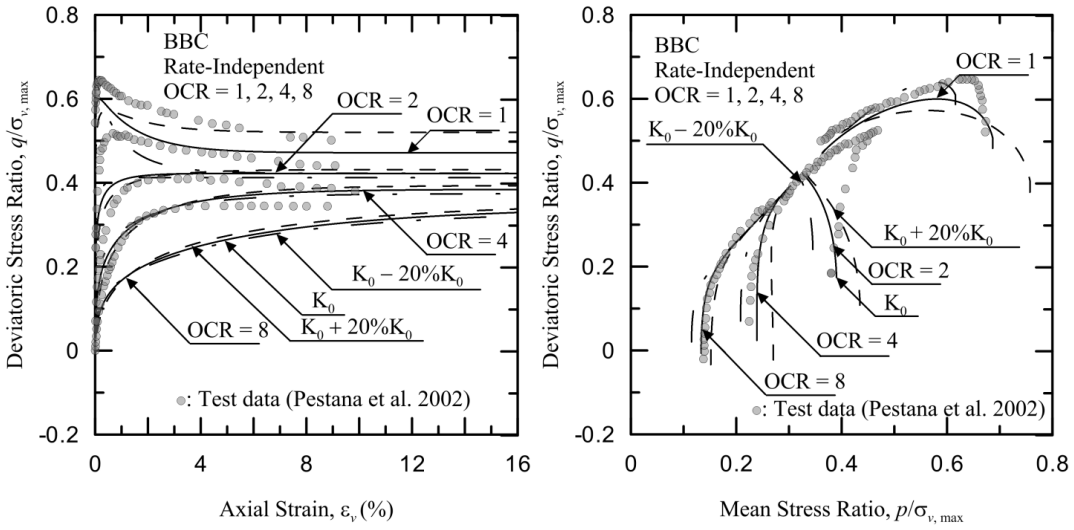

(Figure AI.1.39) Sensitivity of K_0 at 20% variation for Boston Blue Clay, test data taken from Pestana et al. (2002)

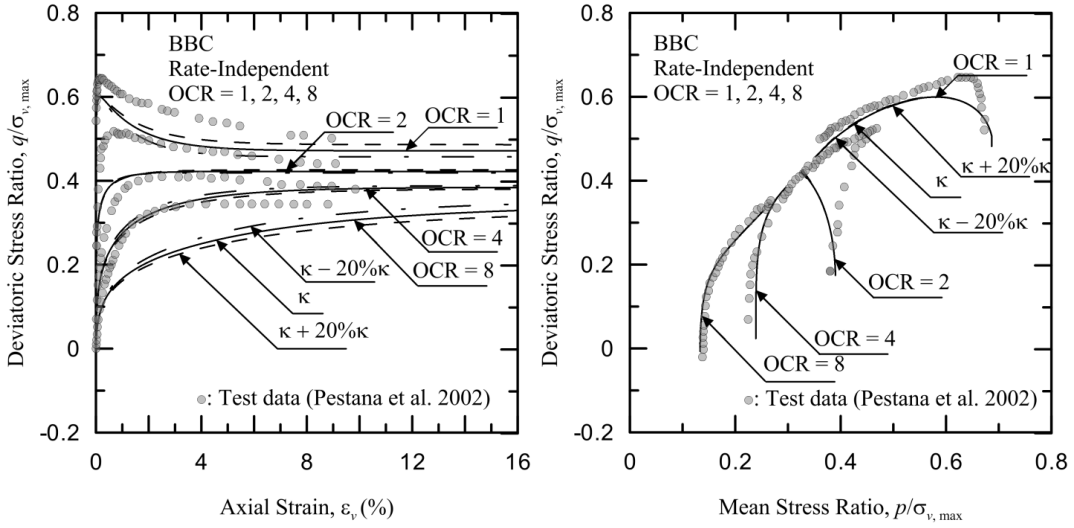

(Figure AI.1.40) Sensitivity of κ at 20% variation for Boston Blue Clay, test data taken from Pestana et al. (2002)

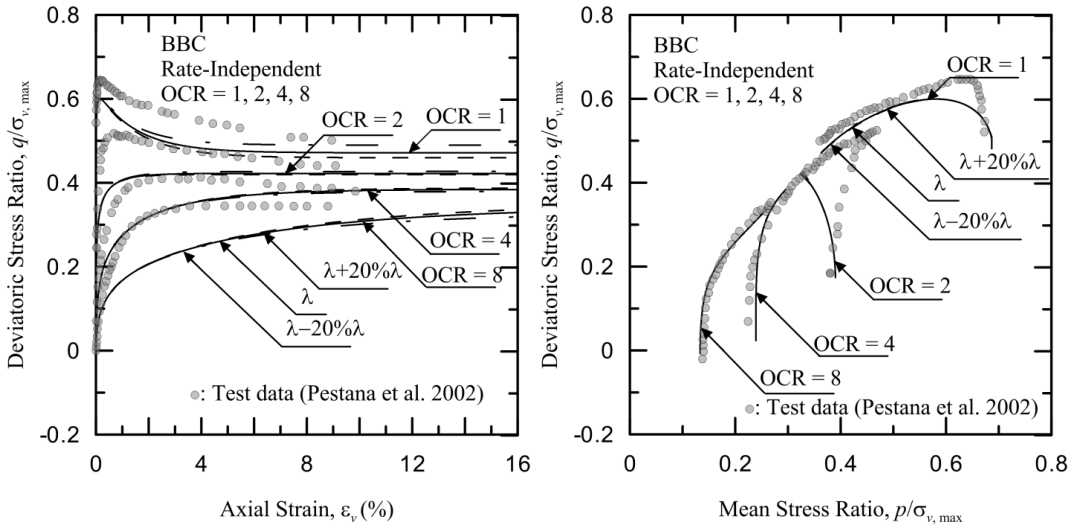

(Figure AI.1.41) Sensitivity of λ at 20% variation for Boston Blue Clay, test data taken from Pestana et al. (2002)

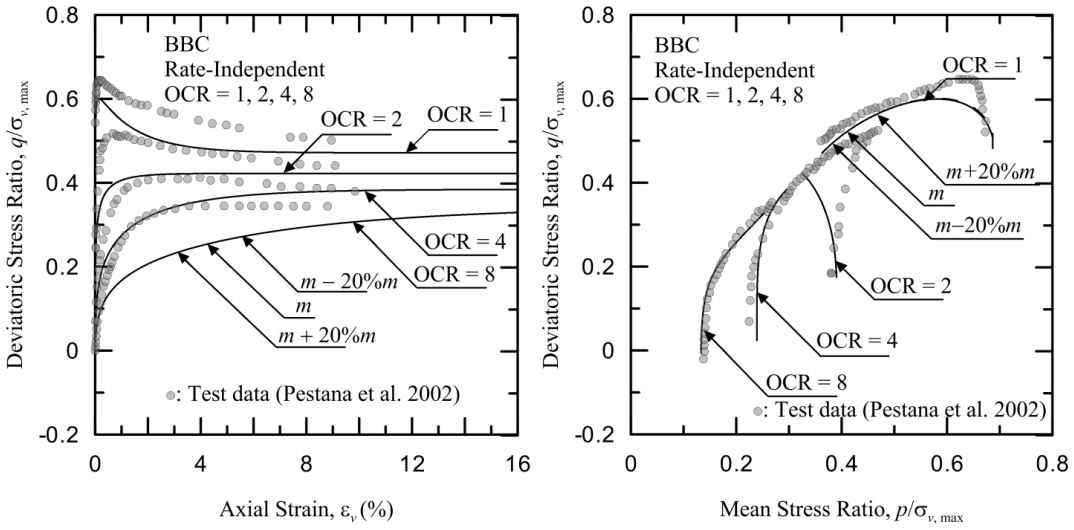

(Figure AI.1.42) Sensitivity of *m* at 20% variation for Boston Blue Clay, test data taken from Pestana et al. (2002)

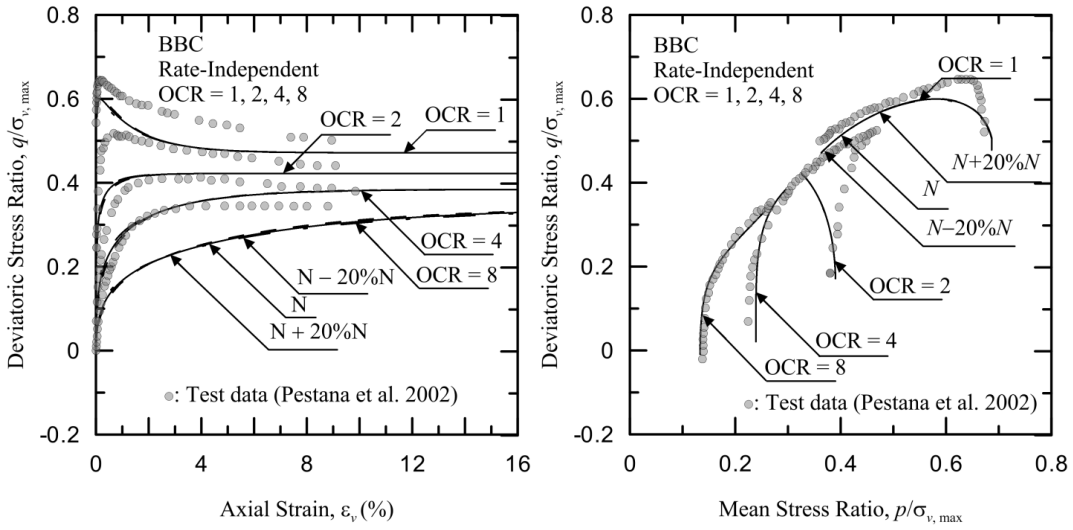

(Figure AI.1.43) Sensitivity of N at 20% variation for Boston Blue Clay, test data taken from Pestana et al. (2002)

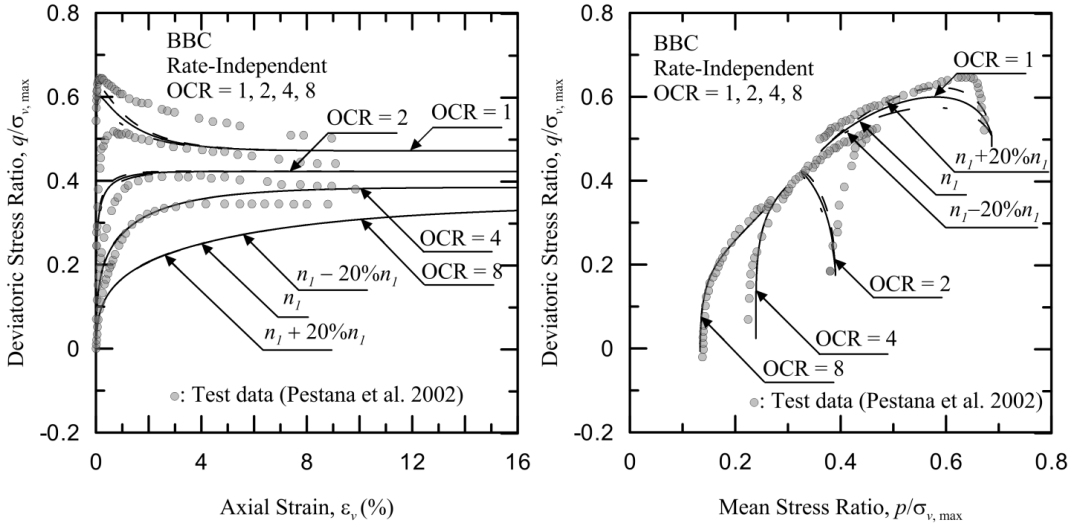

(Figure AI.1.44) Sensitivity of n_1 at 20% variation for Boston Blue Clay, test data taken from Pestana et al. (2002)

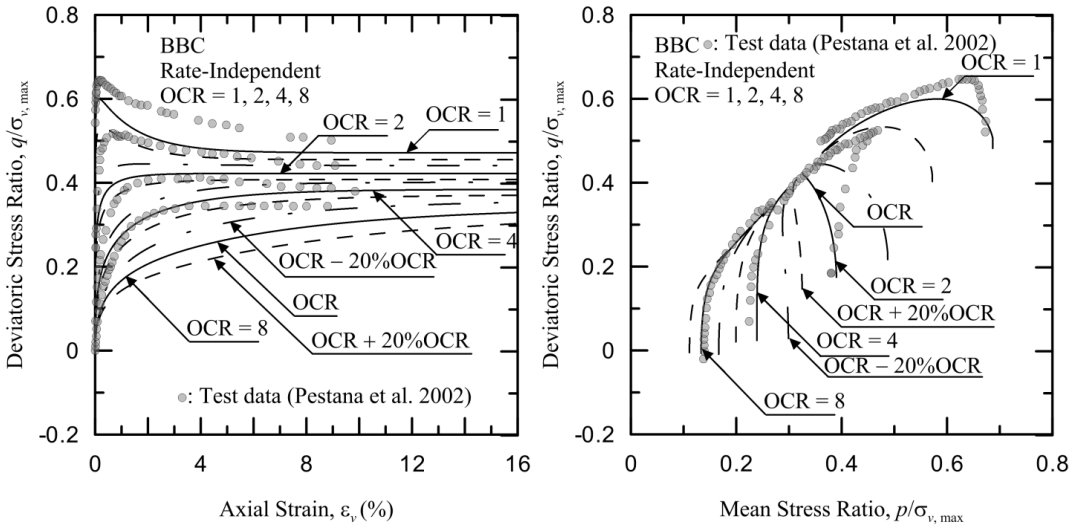

(Figure AI.1.45) Sensitivity of OCR at 20% variation for Boston Blue Clay, test data taken from Pestana et al. (2002)

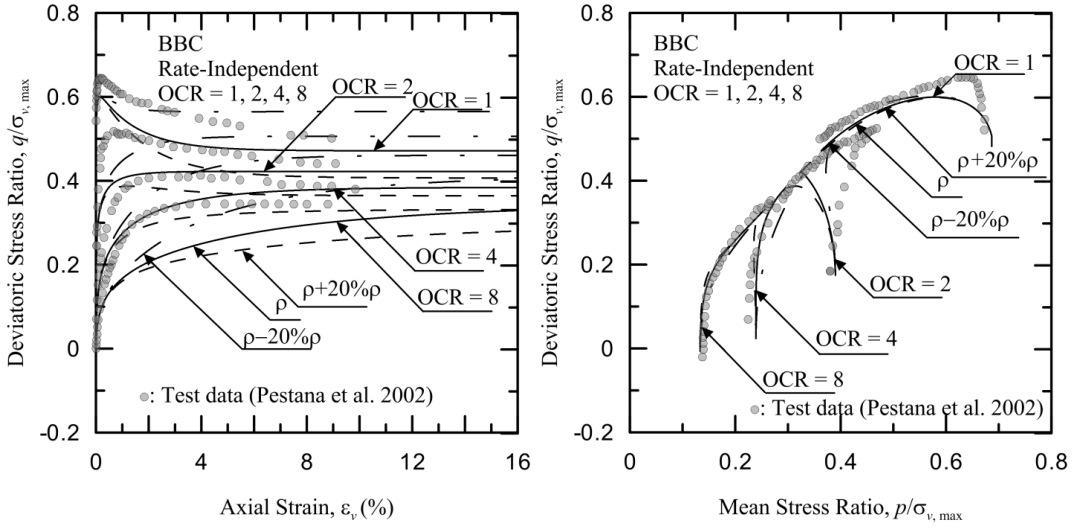

(Figure AI.1.46) Sensitivity of ρ at 20% variation for Boston Blue Clay, test data taken from Pestana et al. (2002)

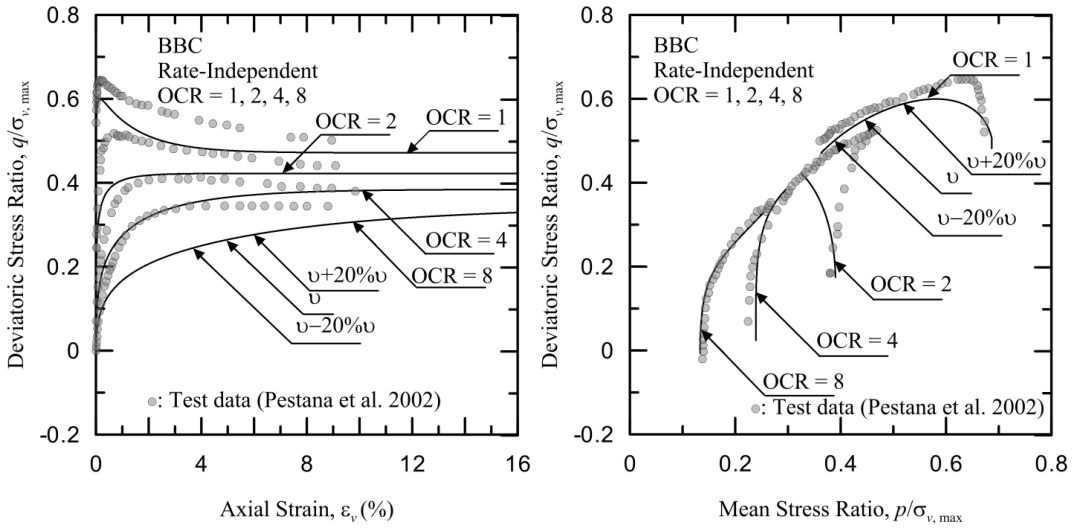

(Figure AI.1.47) Sensitivity of υ at 20% variation for Boston Blue Clay, test data taken from Pestana et al. (2002)

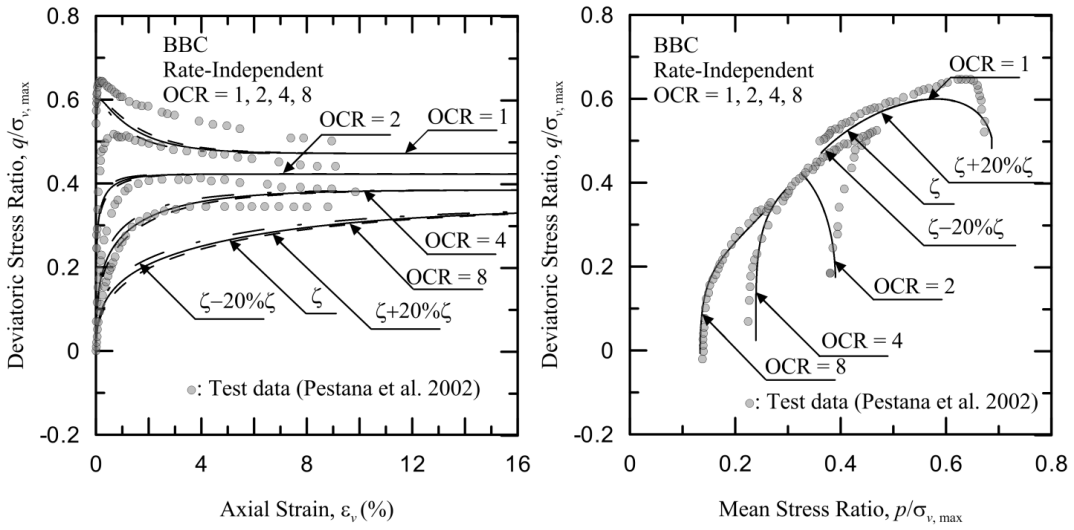

(Figure AI.1.48) Sensitivity of ζ at 20% variation for Boston Blue Clay, test data taken from Pestana et al. (2002)

Rate-dependent sensitivity analysis for Boston Blue Clay:

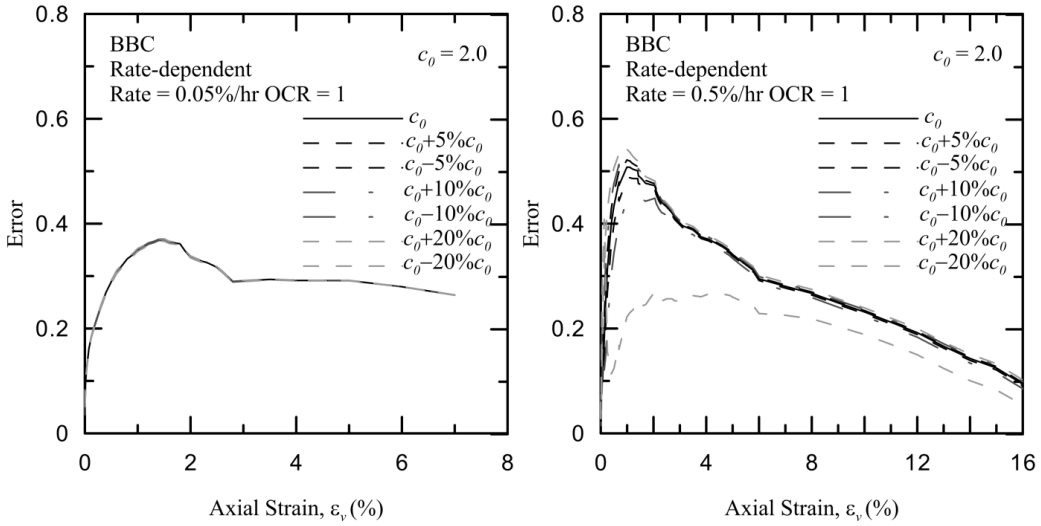

(Figure AI.1.49) Sensitivity error of c_0 at 5%, 10%, and 20% variation for Boston Blue Clay at OCR = 1

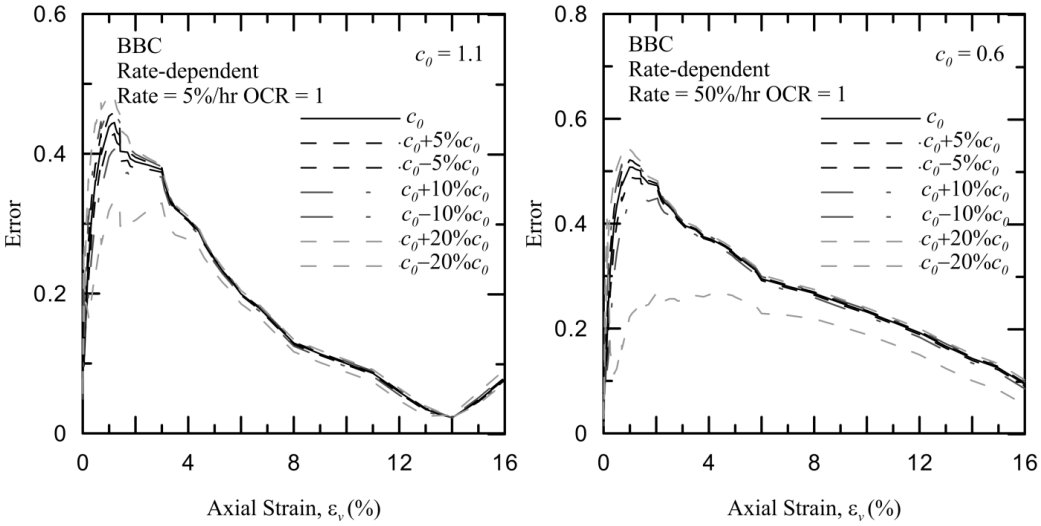

(Figure AI.1.50) Sensitivity error of c_0 at 5%, 10%, and 20% variation for Boston Blue Clay at OCR = 1

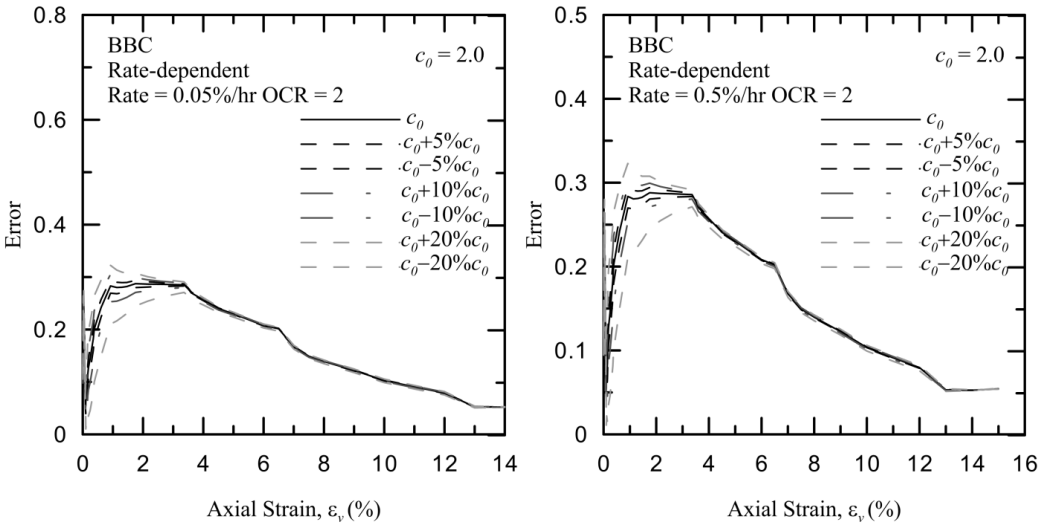

(Figure AI.1.51) Sensitivity error of c_0 at 5%, 10%, and 20% variation for Boston Blue Clay at OCR = 2

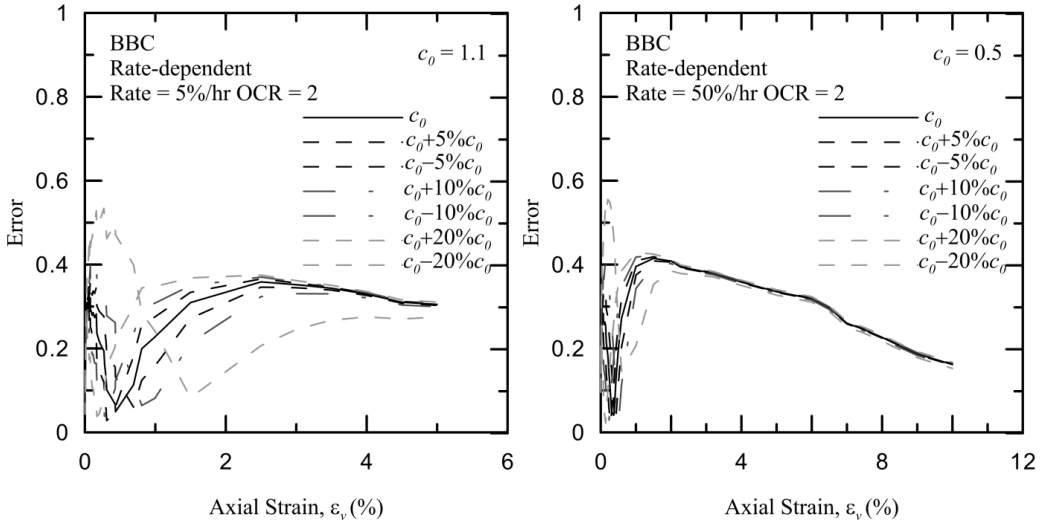

(Figure AI.1.52) Sensitivity error of c_0 at 5%, 10%, and 20% variation for Boston Blue Clay at OCR = 2

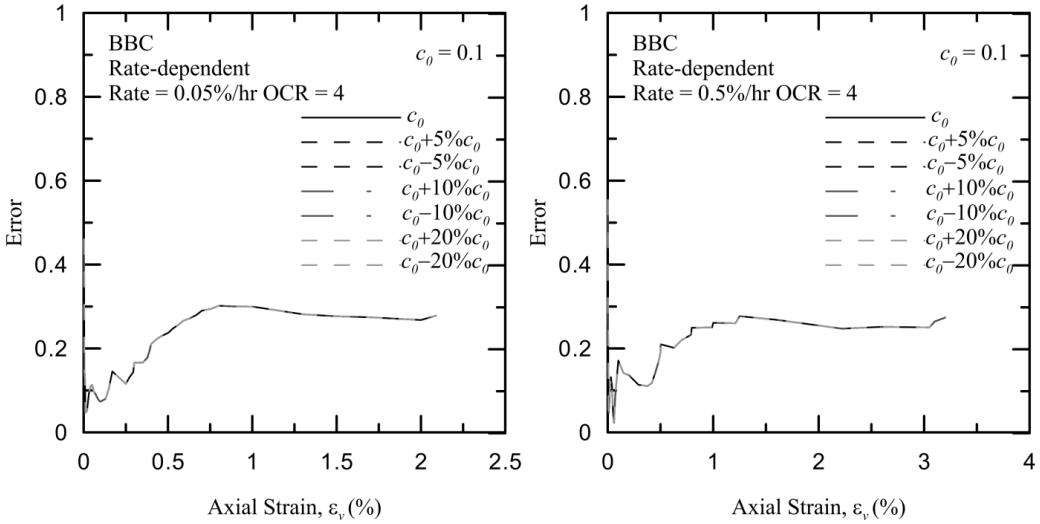

(Figure AI.1.53) Sensitivity error of c_0 at 5%, 10%, and 20% variation for Boston Blue Clay at OCR = 4

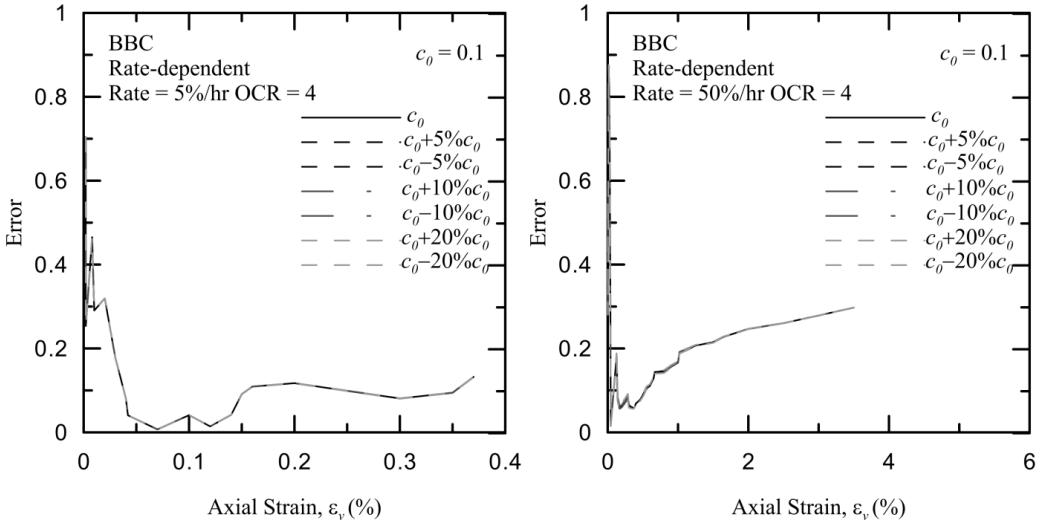

(Figure AI.1.54) Sensitivity error of c_0 at 5%, 10%, and 20% variation for Boston Blue Clay at OCR = 4

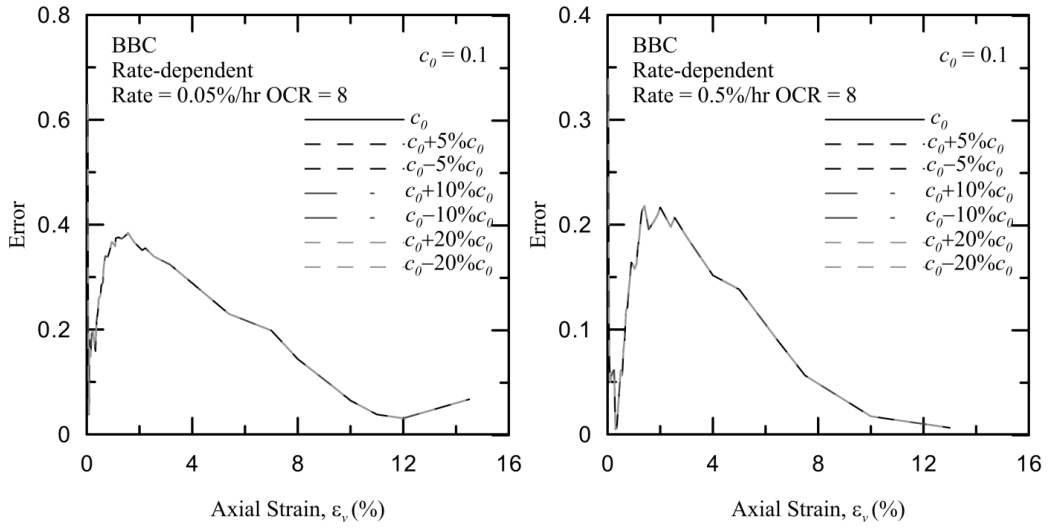

(Figure AI.1.55) Sensitivity error of c_0 at 5%, 10%, and 20% variation for Boston Blue Clay at OCR = 8

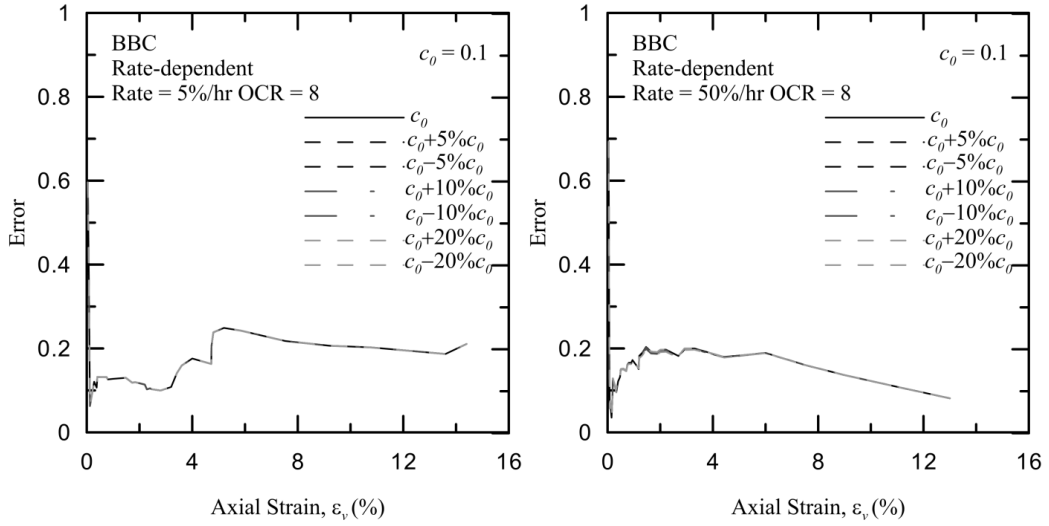

(Figure AI.1.56) Sensitivity error of c_0 at 5%, 10%, and 20% variation for Boston Blue Clay at OCR = 8

Rate-independent sensitivity analysis for Kaolin Clay at 5% variation:

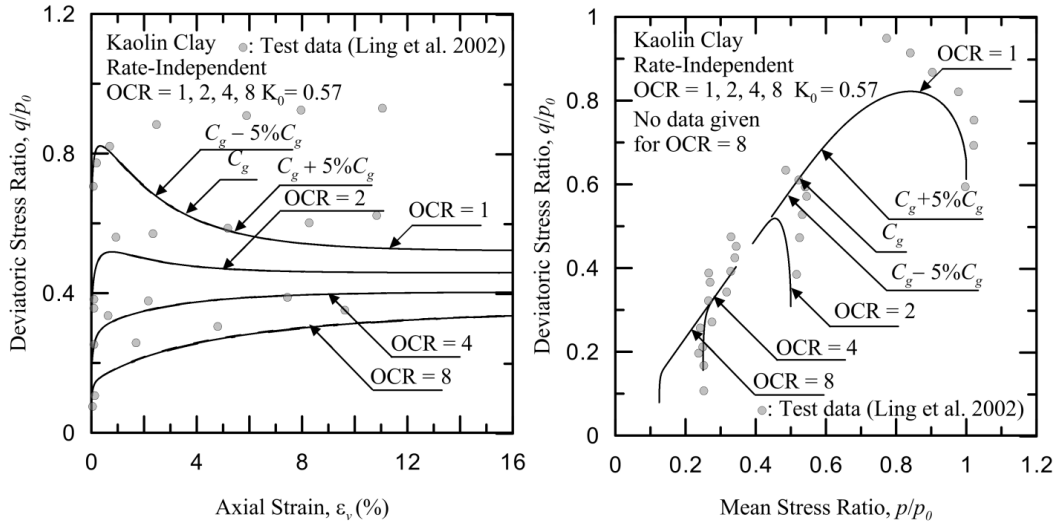

(Figure AI.1.57) Sensitivity of C_g at 5% variation for Kaolin Clay, test data taken from Ling et al. (2002)

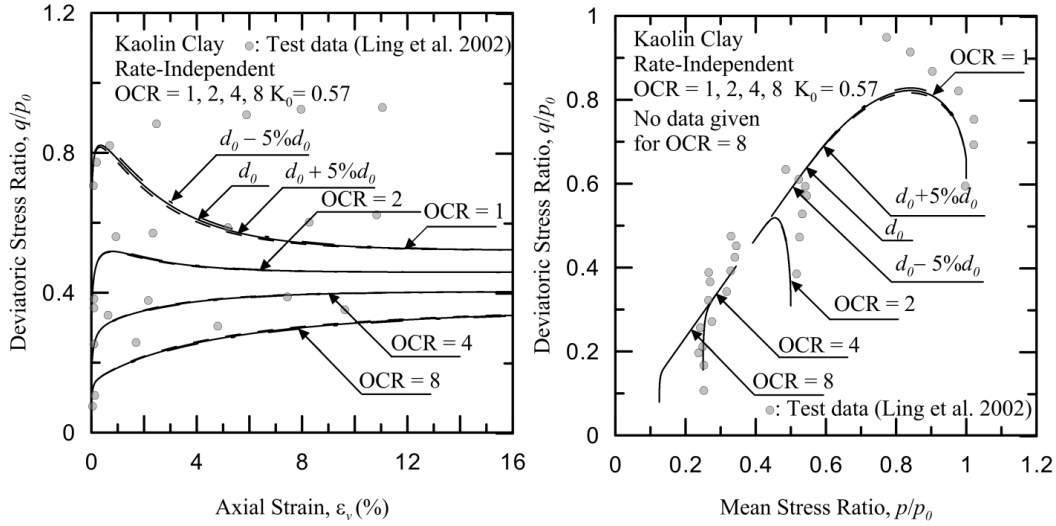

(Figure AI.1.58) Sensitivity of d_0 at 5% variation for Kaolin Clay, test data taken from Ling et al. (2002)

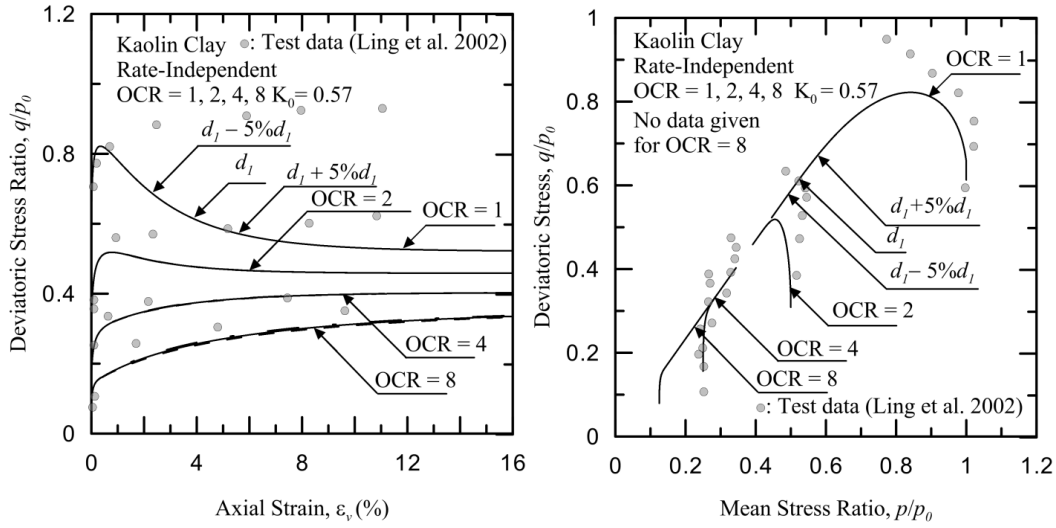

(Figure AI.1.59) Sensitivity of d_1 at 5% variation for Kaolin Clay, test data taken from Ling et al. (2002)

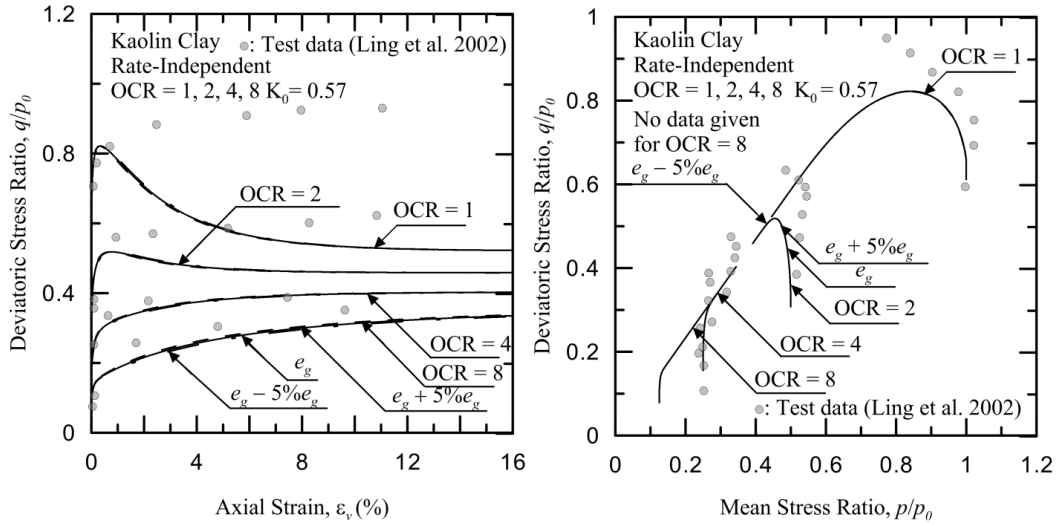

(Figure AI.1.60) Sensitivity of e_g at 5% variation for Kaolin Clay, test data taken from Ling et al. (2002)

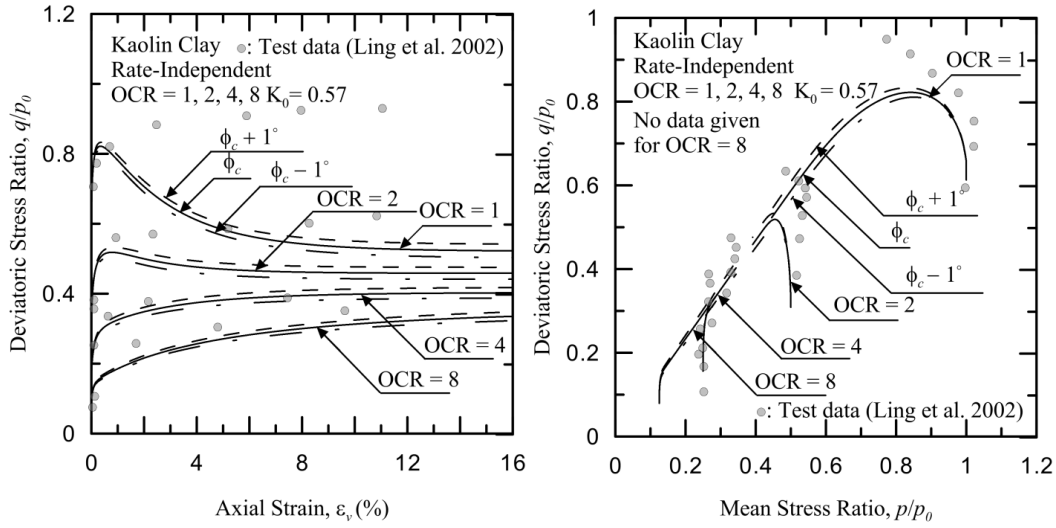

(Figure AI.1.61) Sensitivity of ϕ_c at 1° variation for Kaolin Clay, test data taken from Ling et al. (2002)

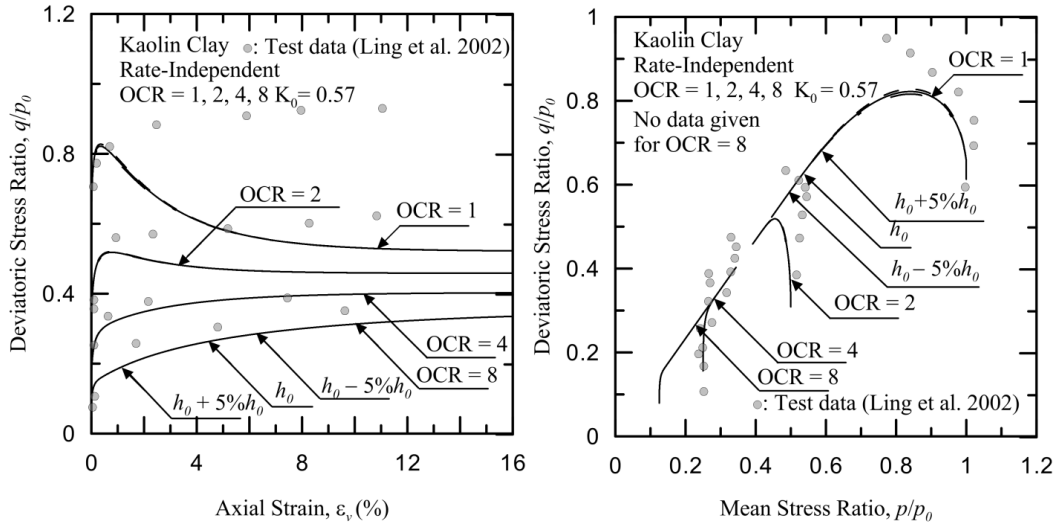

(Figure AI.1.62) Sensitivity of h_0 at 5% variation for Kaolin Clay, test data taken from Ling et al. (2002)

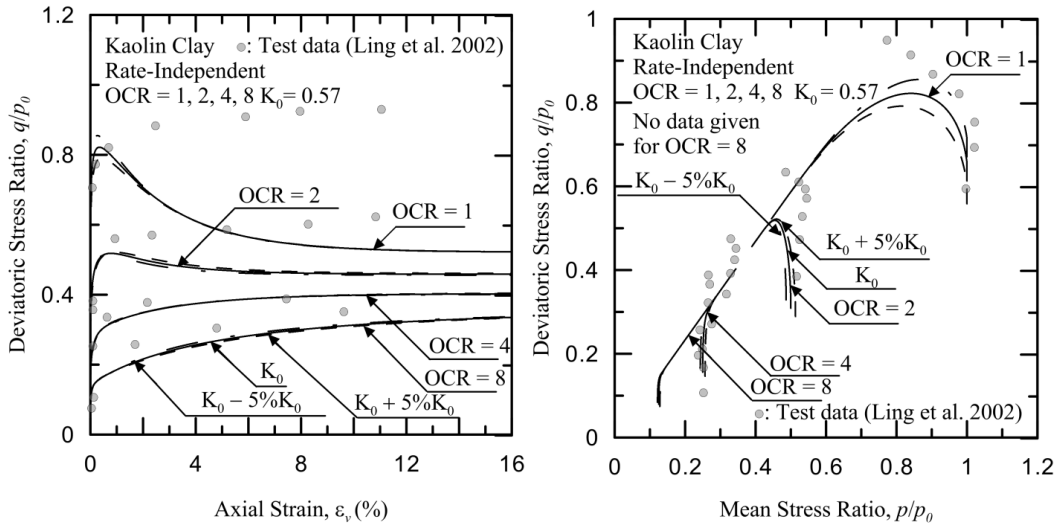

(Figure AI.1.63) Sensitivity of K_0 at 5% variation for Kaolin Clay, test data taken from Ling et al. (2002)

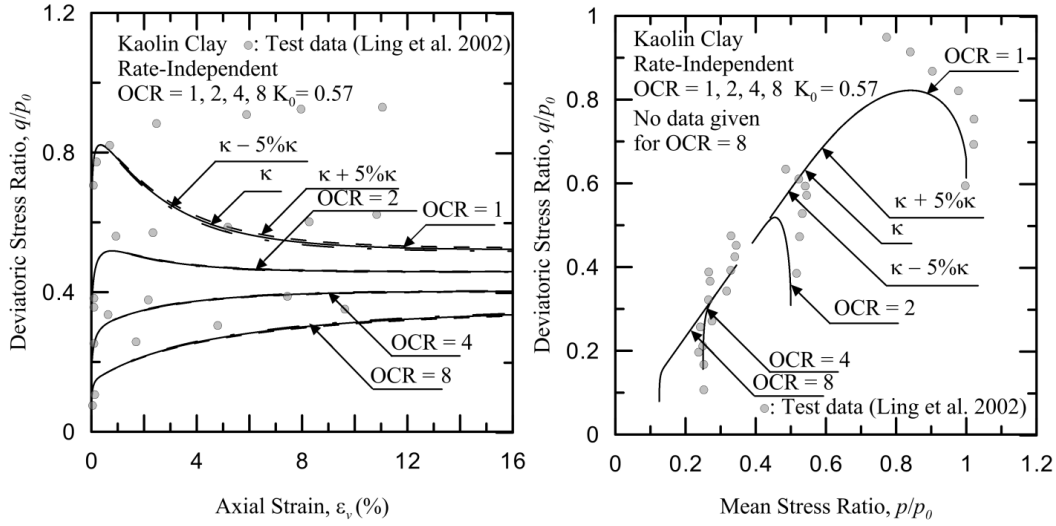

(Figure AI.1.64) Sensitivity of κ at 5% variation for Kaolin Clay, test data taken from Ling et al. (2002)

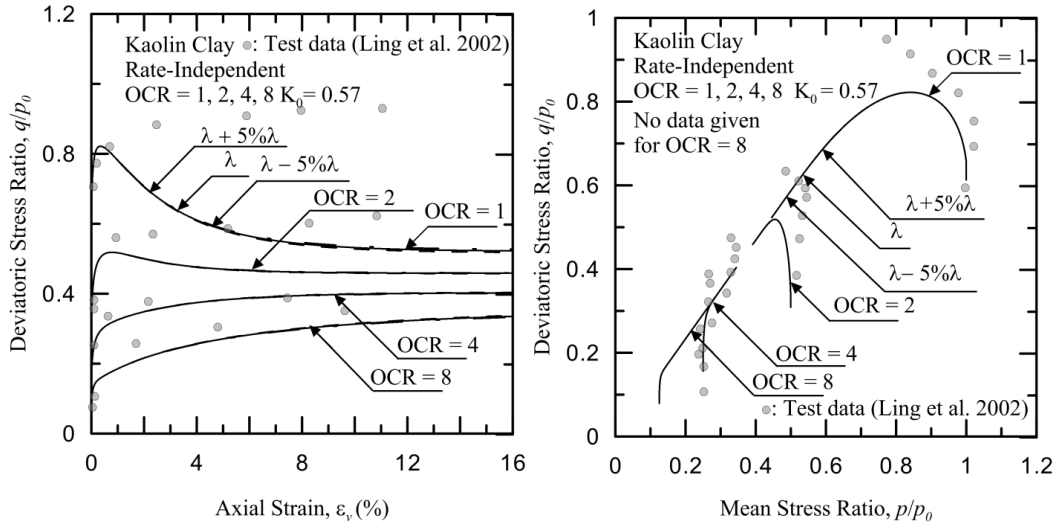

(Figure AI.1.65) Sensitivity of λ at 5% variation for Kaolin Clay, test data taken from Ling et al. (2002)

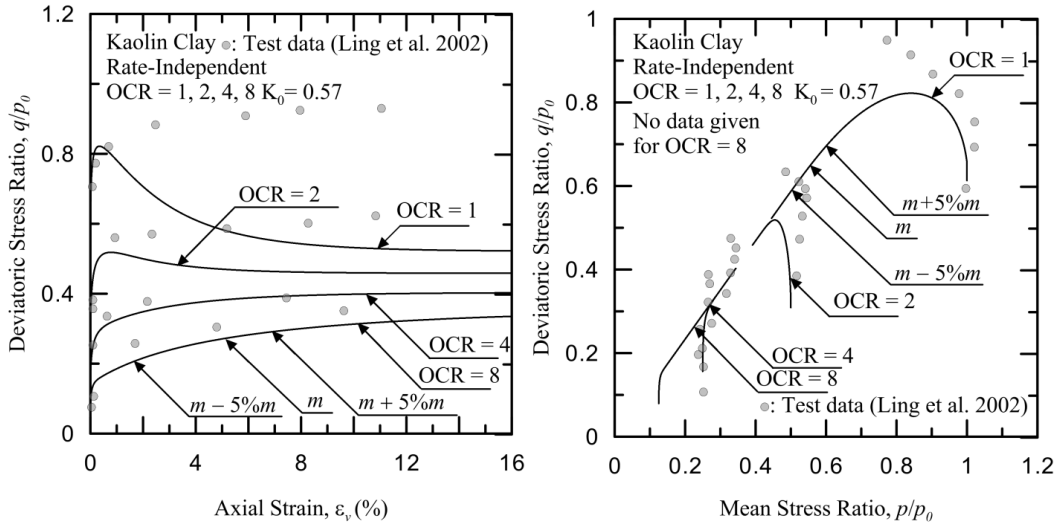

(Figure AI.1.66) Sensitivity of *m* at 5% variation for Kaolin Clay, test data taken from Ling et al. (2002)

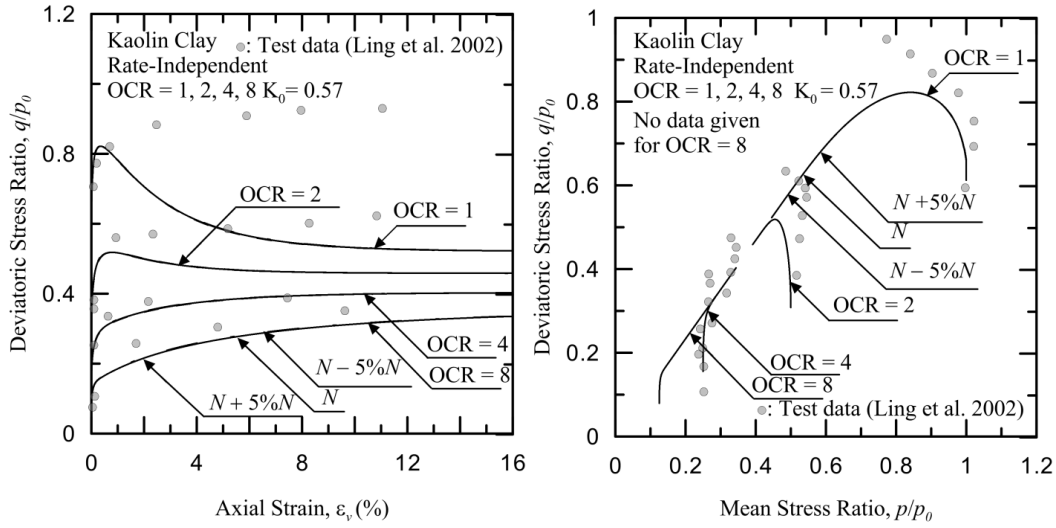

(Figure AI.1.67) Sensitivity of N at 5% variation for Kaolin Clay, test data taken from Ling et al. (2002)

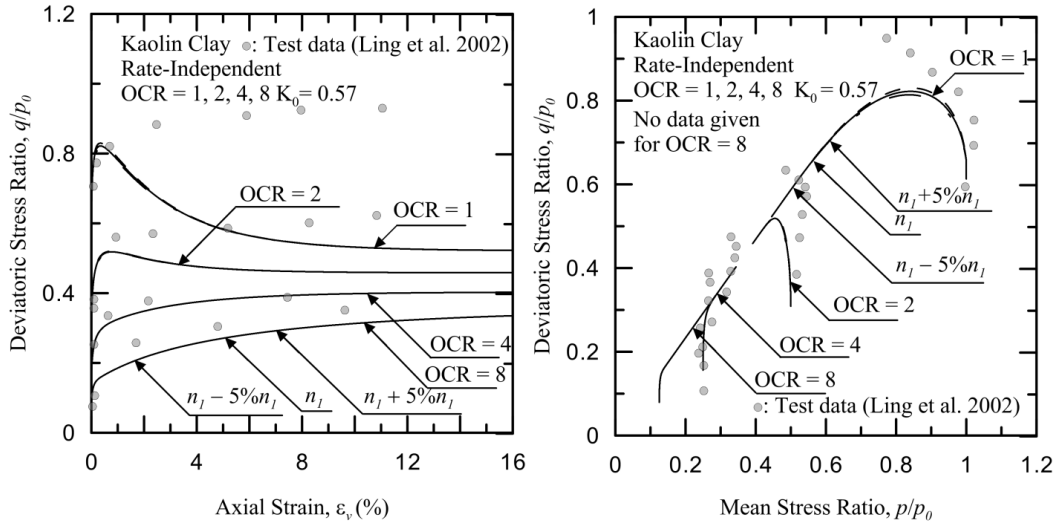

(Figure AI.1.68) Sensitivity of n_1 at 5% variation for Kaolin Clay, test data taken from Ling et al. (2002)

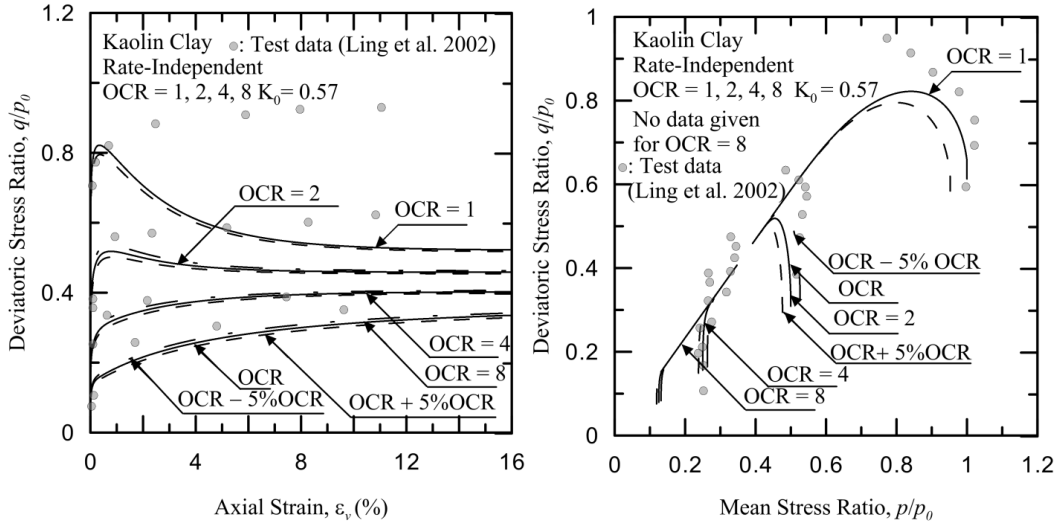

(Figure AI.1.69) Sensitivity of OCR at 5% variation for Kaolin Clay, test data taken from Ling et al. (2002)

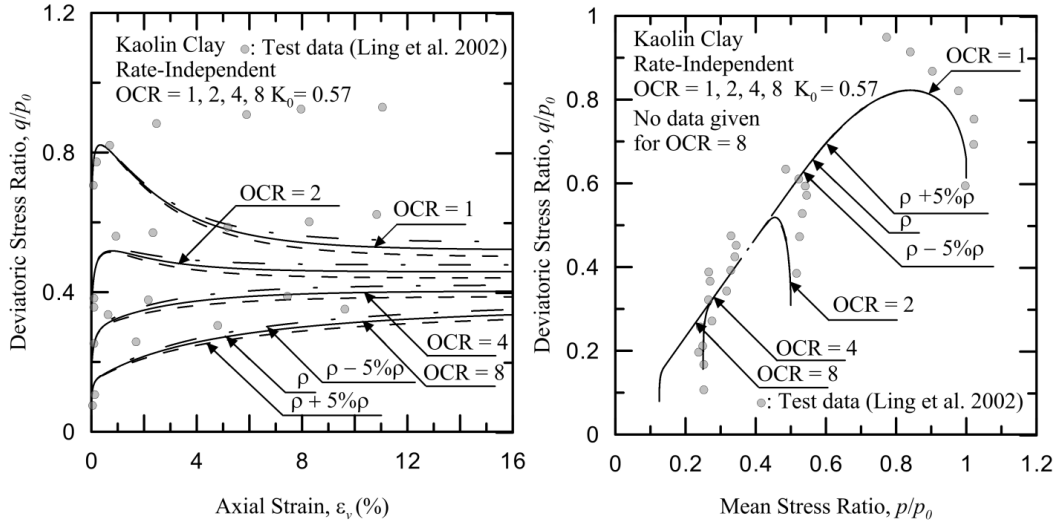

(Figure AI.1.70) Sensitivity of ρ at 5% variation for Kaolin Clay, test data taken from Ling et al. (2002)

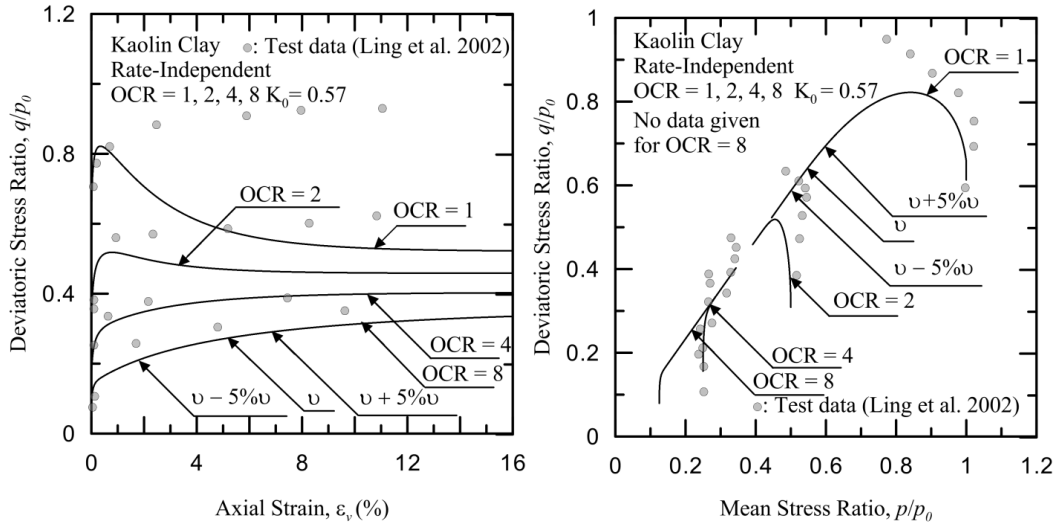

(Figure AI.1.71) Sensitivity of υ at 5% variation for Kaolin Clay, test data taken from Ling et al. (2002)

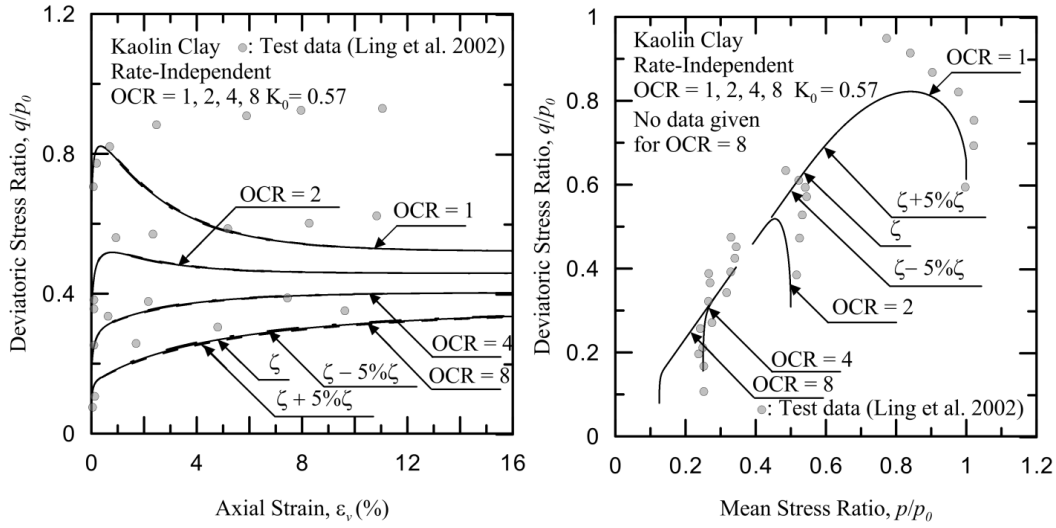

(Figure AI.1.72) Sensitivity of ζ at 5% variation for Kaolin Clay, test data taken from Ling et al. (2002)

Rate-independent sensitivity analysis for Kaolin Clay at 10% variation:

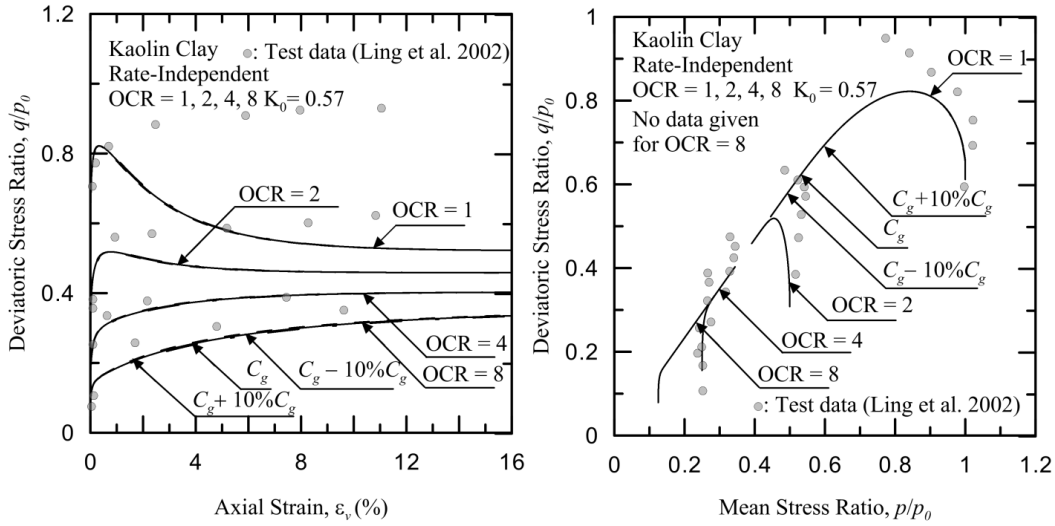

(Figure AI.1.73) Sensitivity of C_g at 10% variation for Kaolin Clay, test data taken from Ling et al. (2002)

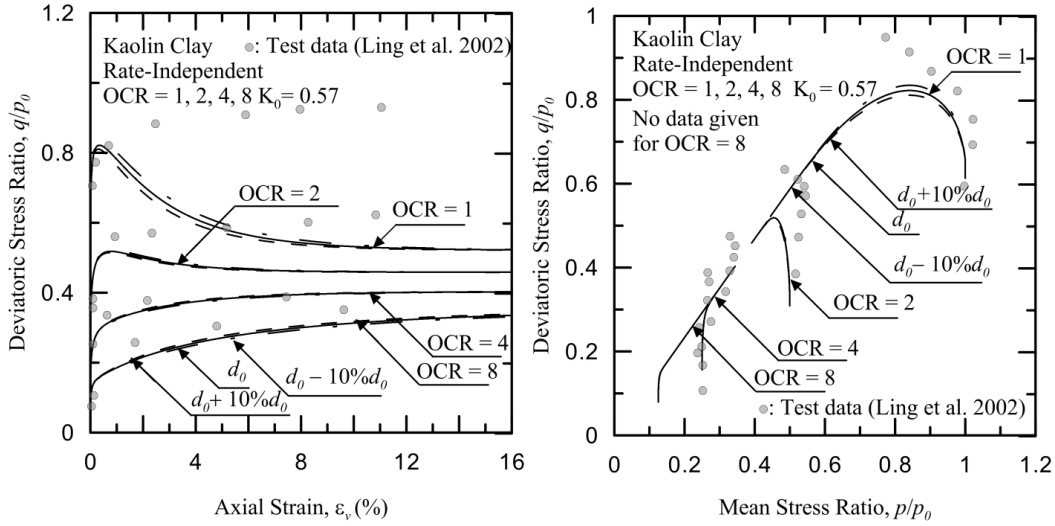

(Figure AI.1.74) Sensitivity of d_0 at 10% variation for Kaolin Clay, test data taken from Ling et al. (2002)

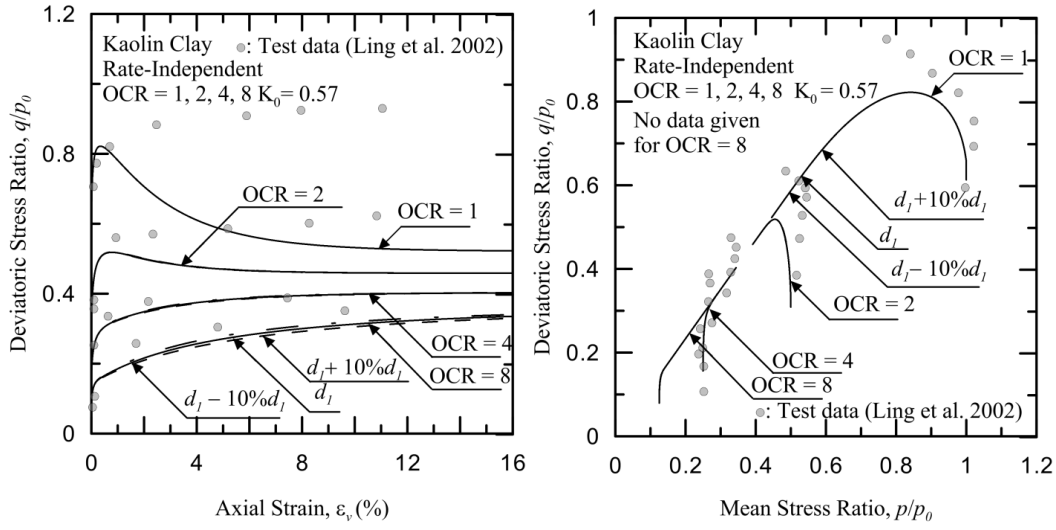

(Figure AI.1.75) Sensitivity of d_1 at 10% variation for Kaolin Clay, test data taken from Ling et al. (2002)

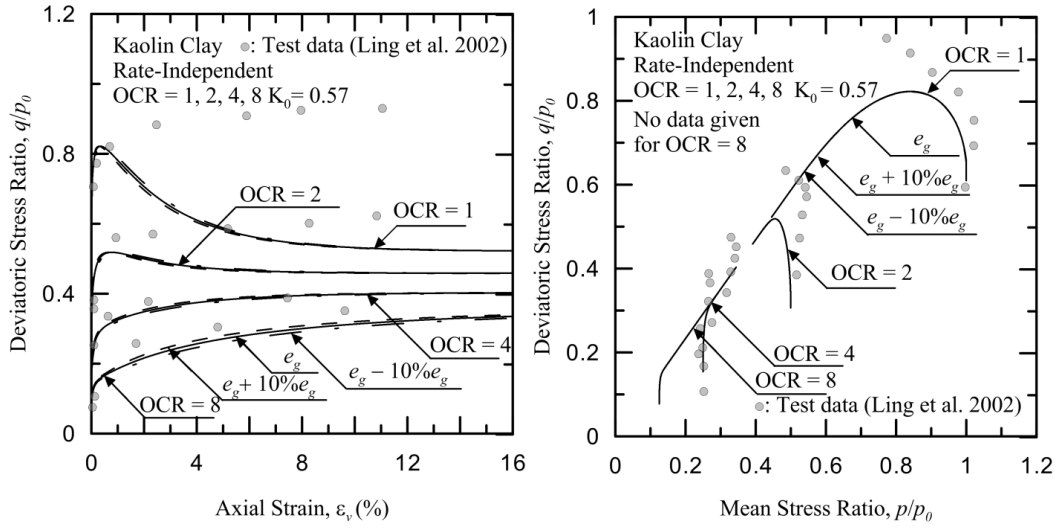

(Figure AI.1.76) Sensitivity of e_g at 10% variation for Kaolin Clay, test data taken from Ling et al. (2002)

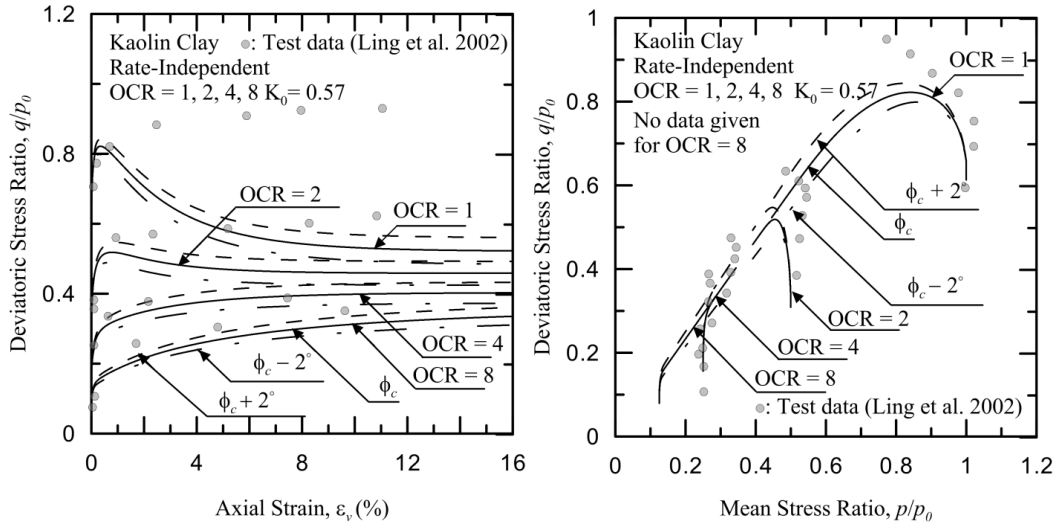

(Figure AI.1.77) Sensitivity of ϕ_c at 2° variation for Kaolin Clay, test data taken from Ling et al. (2002)

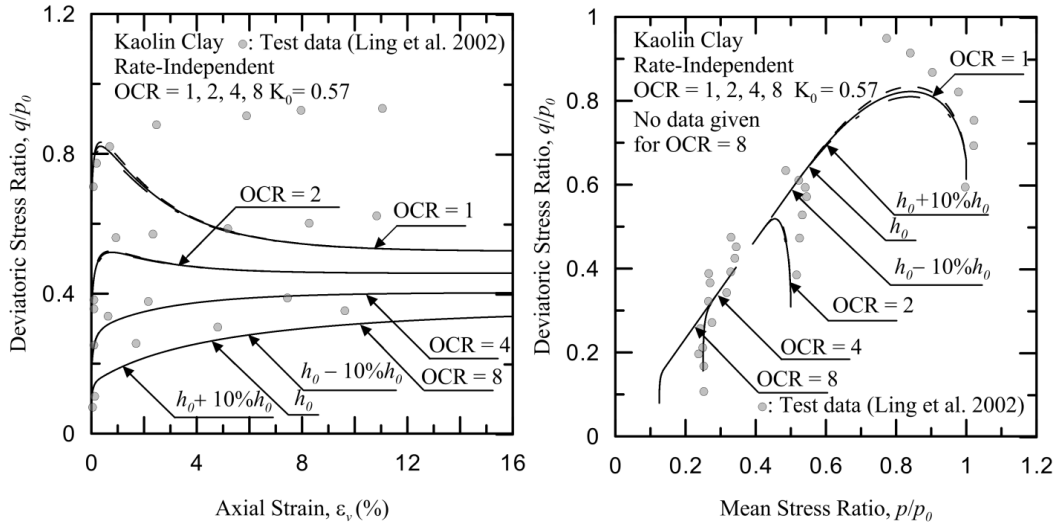

(Figure AI.1.78) Sensitivity of h_0 at 10% variation for Kaolin Clay, test data taken from Ling et al. (2002)

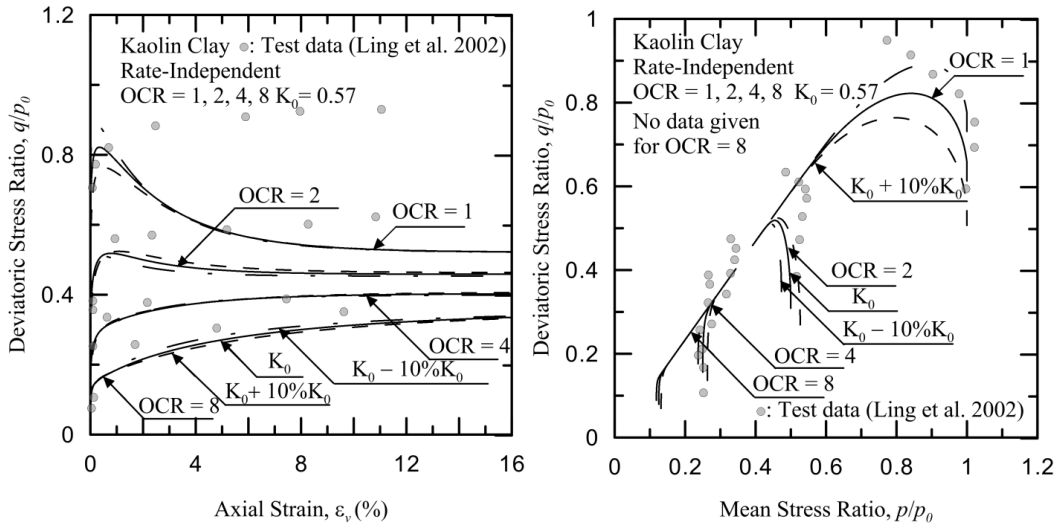

(Figure AI.1.79) Sensitivity of K_0 at 10% variation for Kaolin Clay, test data taken from Ling et al. (2002)

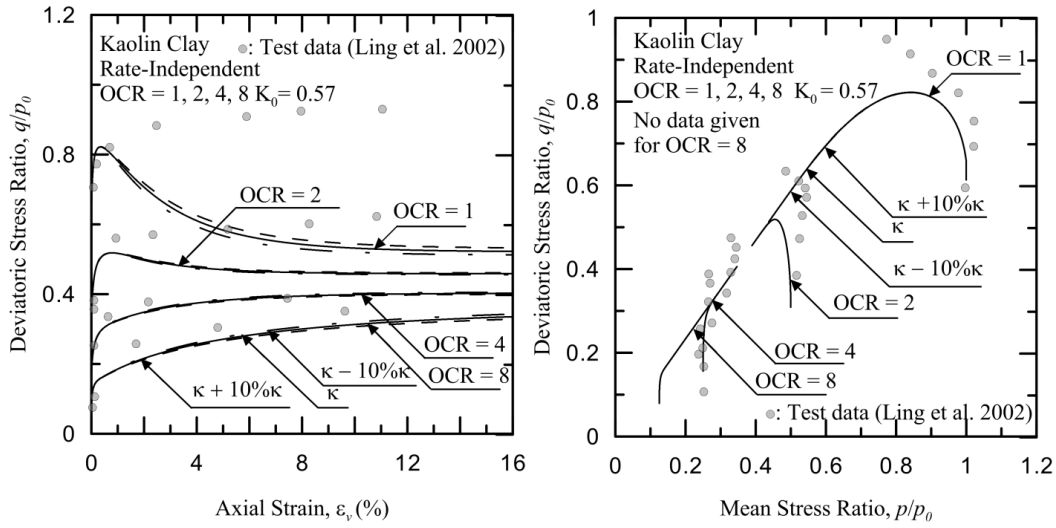

(Figure AI.1.80) Sensitivity of κ at 10% variation for Kaolin Clay, test data taken from Ling et al. (2002)

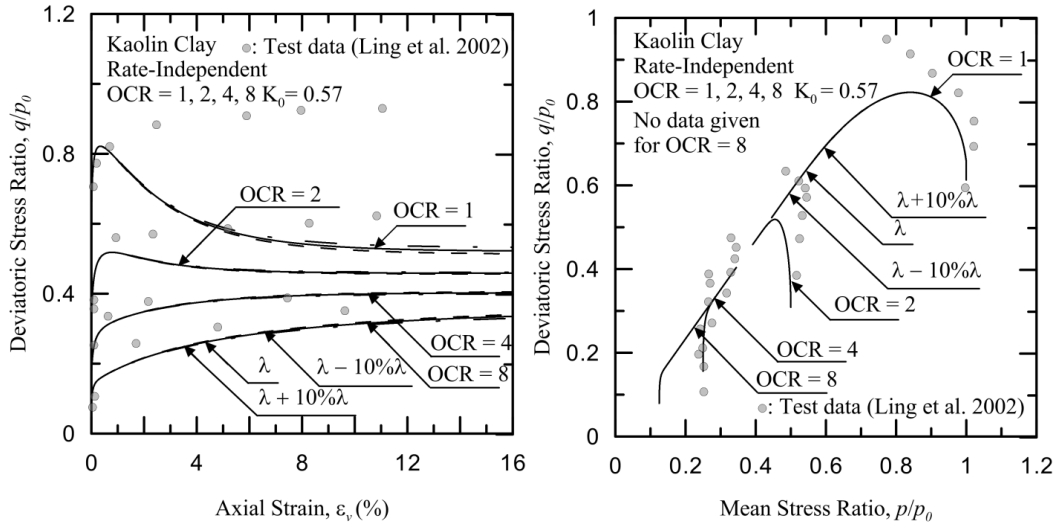

(Figure AI.1.81) Sensitivity of λ at 10% variation for Kaolin Clay, test data taken from Ling et al. (2002)

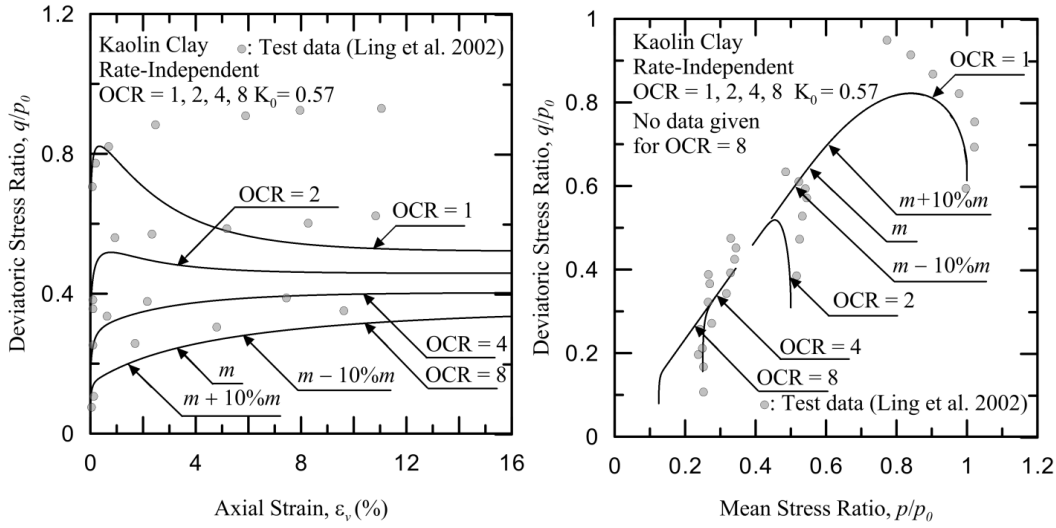

(Figure AI.1.82) Sensitivity of *m* at 10% variation for Kaolin Clay, test data taken from Ling et al. (2002)

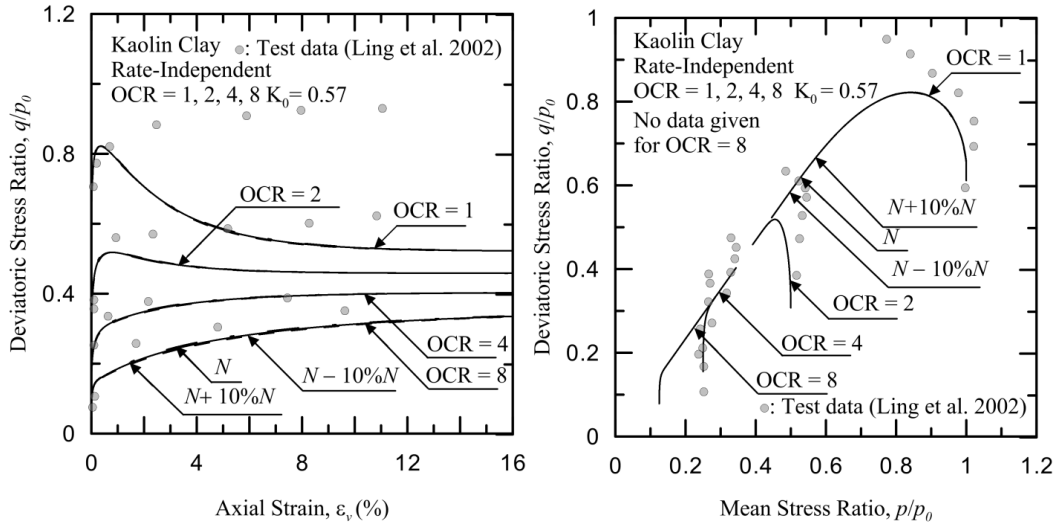

(Figure AI.1.83) Sensitivity of N at 10% variation for Kaolin Clay, test data taken from Ling et al. (2002)

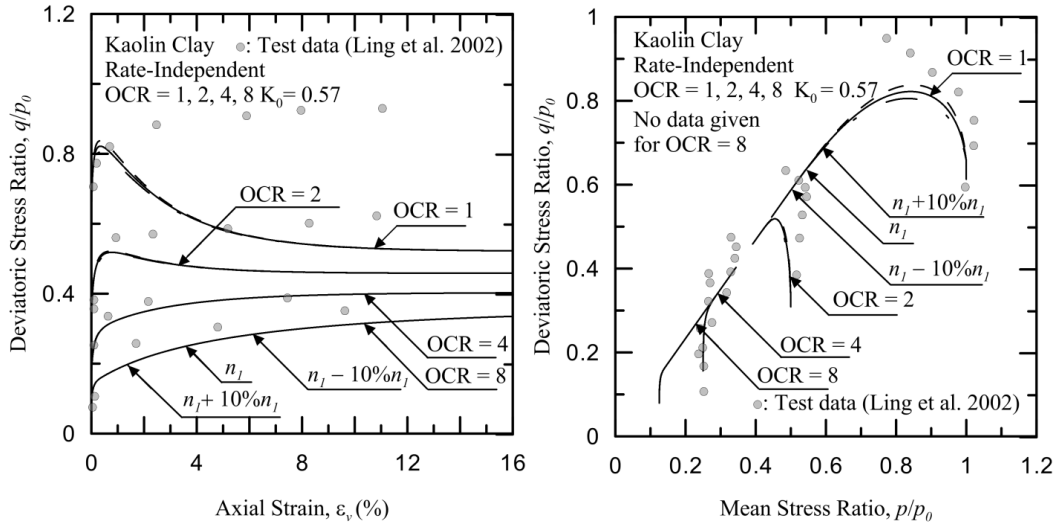

(Figure AI.1.84) Sensitivity of n_1 at 10% variation for Kaolin Clay, test data taken from Ling et al. (2002)

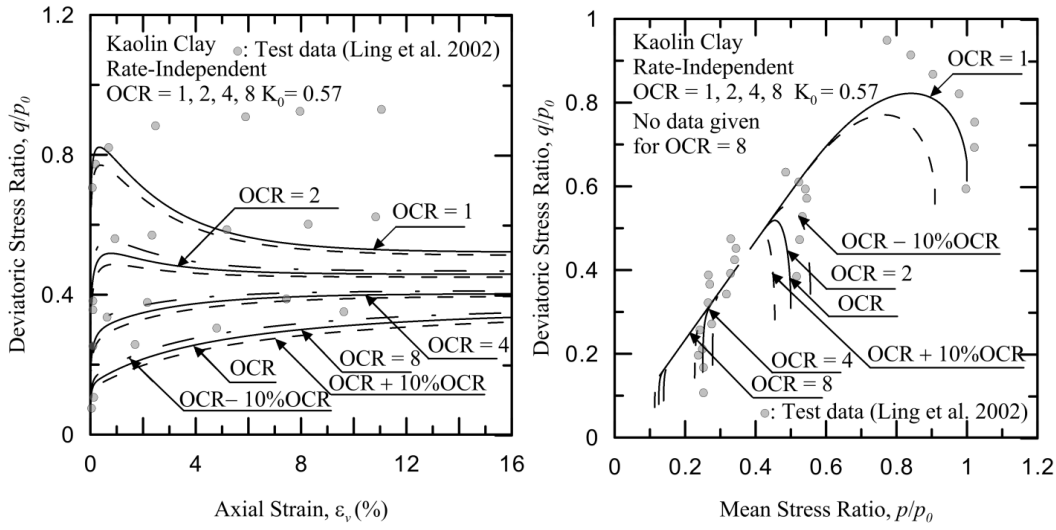

(Figure AI.1.85) Sensitivity of OCR at 10% variation for Kaolin Clay, test data taken from Ling et al. (2002)

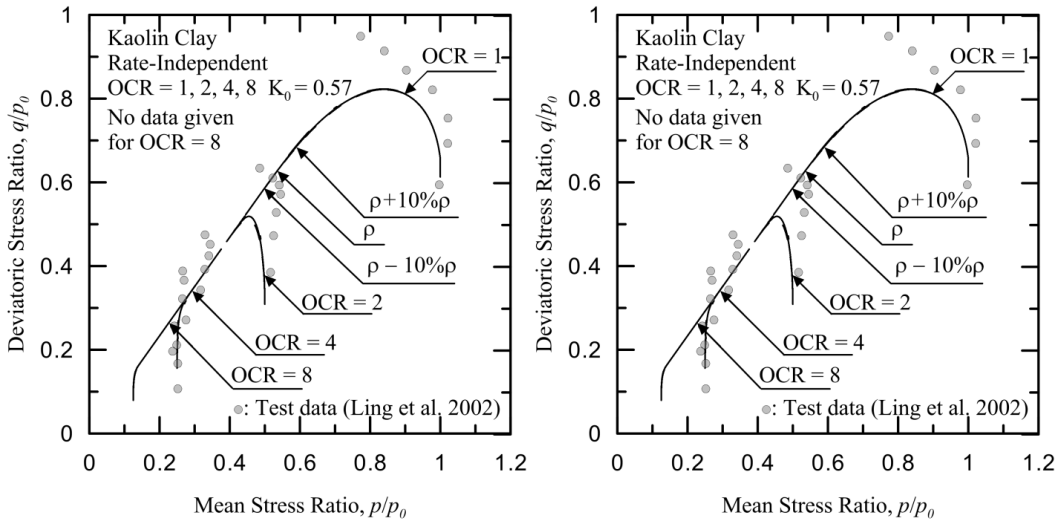

(Figure AI.1.86) Sensitivity of ρ at 10% variation for Kaolin Clay, test data taken from Ling et al. (2002)

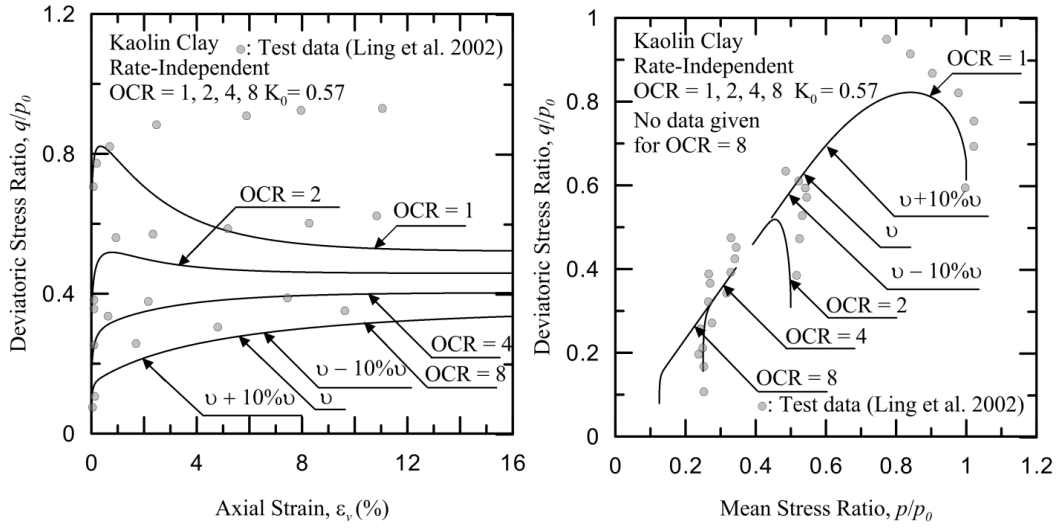

(Figure AI.1.87) Sensitivity of υ at 10% variation for Kaolin Clay, test data taken from Ling et al. (2002)

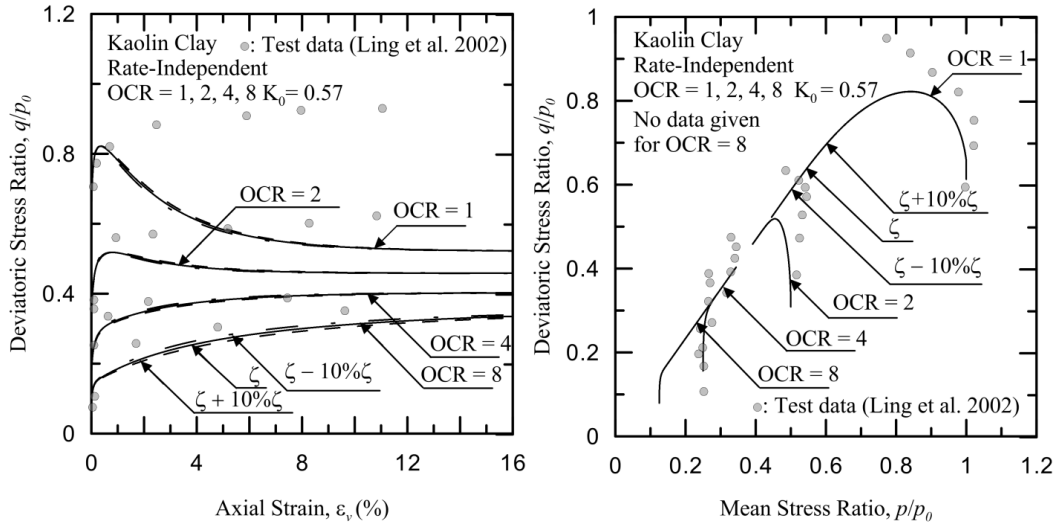

(Figure AI.1.88) Sensitivity of ζ at 10% variation for Kaolin Clay, test data taken from Ling et al. (2002)

Rate-independent sensitivity analysis for Kaolin Clay at 20% variation:

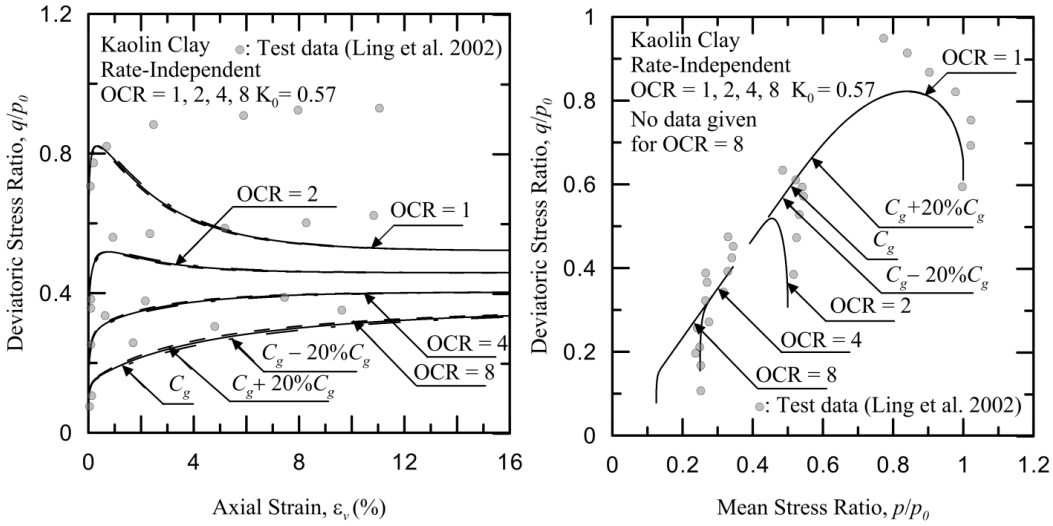

(Figure AI.1.89) Sensitivity of C_g at 20% variation for Kaolin Clay, test data taken from Ling et al. (2002)

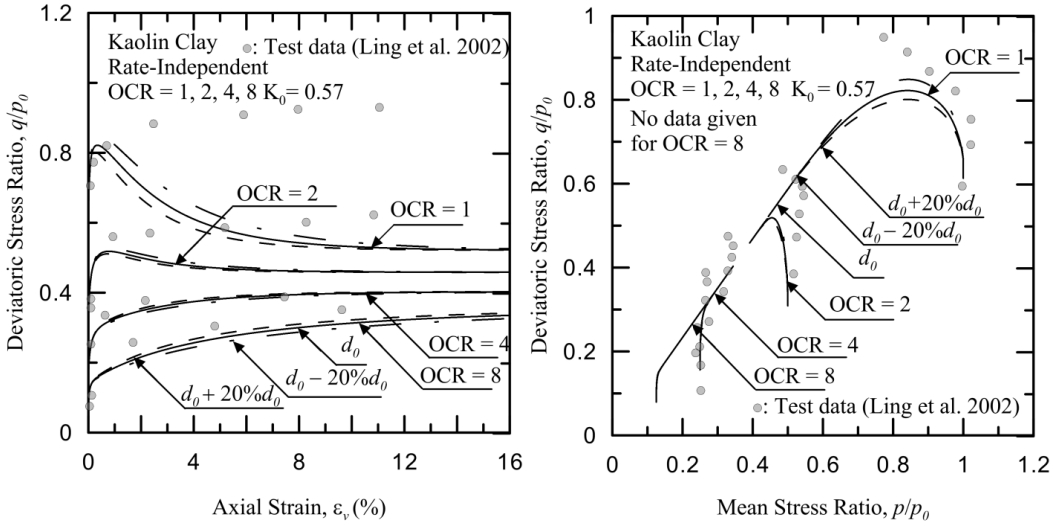

(Figure AI.1.90) Sensitivity of d_0 at 20% variation for Kaolin Clay, test data taken from Ling et al. (2002)

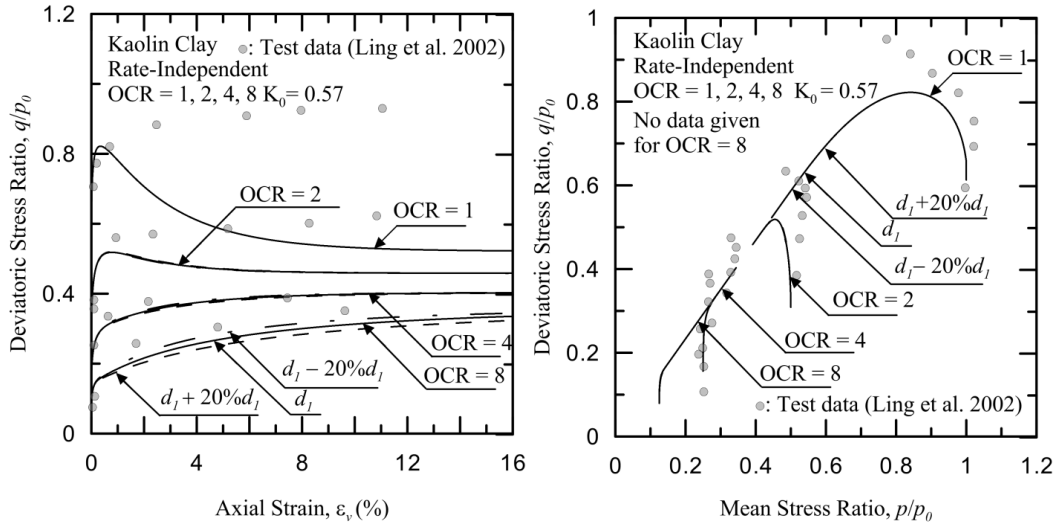

(Figure AI.1.91) Sensitivity of d_1 at 20% variation for Kaolin Clay, test data taken from Ling et al. (2002)

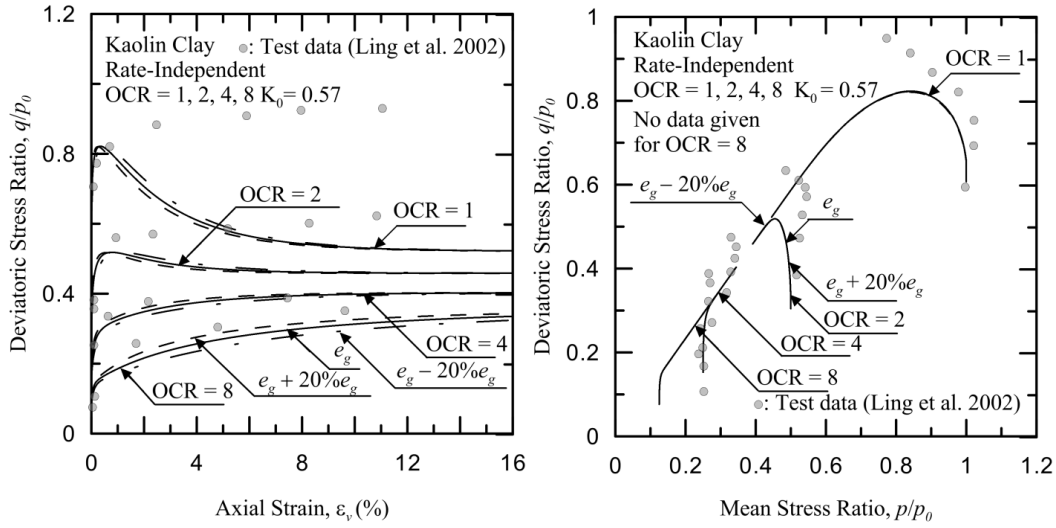

(Figure AI.1.92) Sensitivity of e_g at 20% variation for Kaolin Clay, test data taken from Ling et al. (2002)

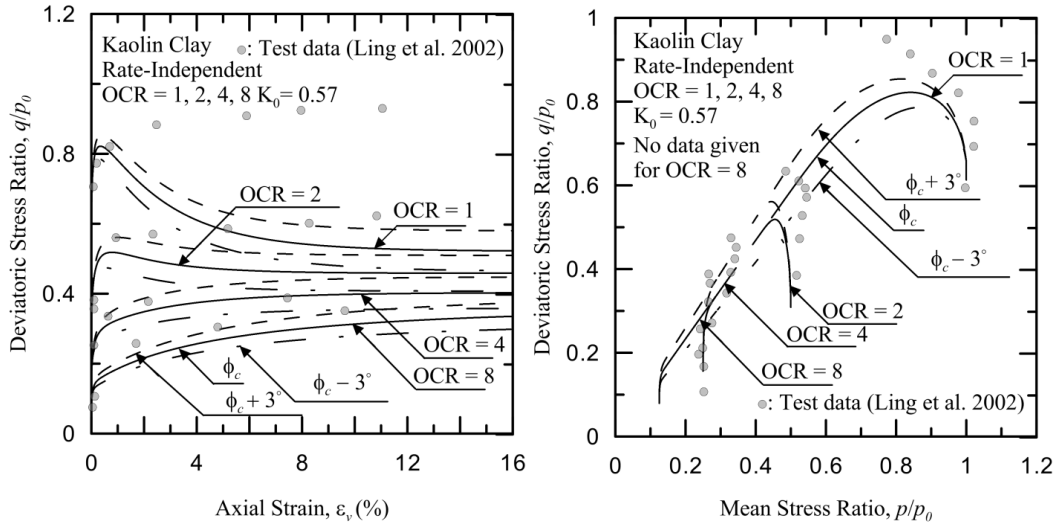

(Figure AI.1.93) Sensitivity of ϕ_c at 3° variation for Kaolin Clay, test data taken from Ling et al. (2002)

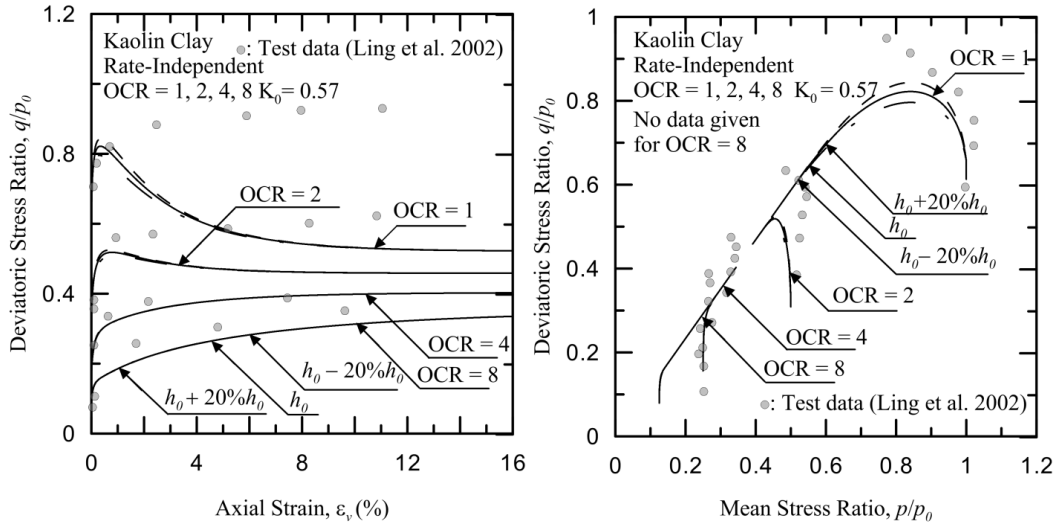

(Figure AI.1.94) Sensitivity of h_0 at 20% variation for Kaolin Clay, test data taken from Ling et al. (2002)

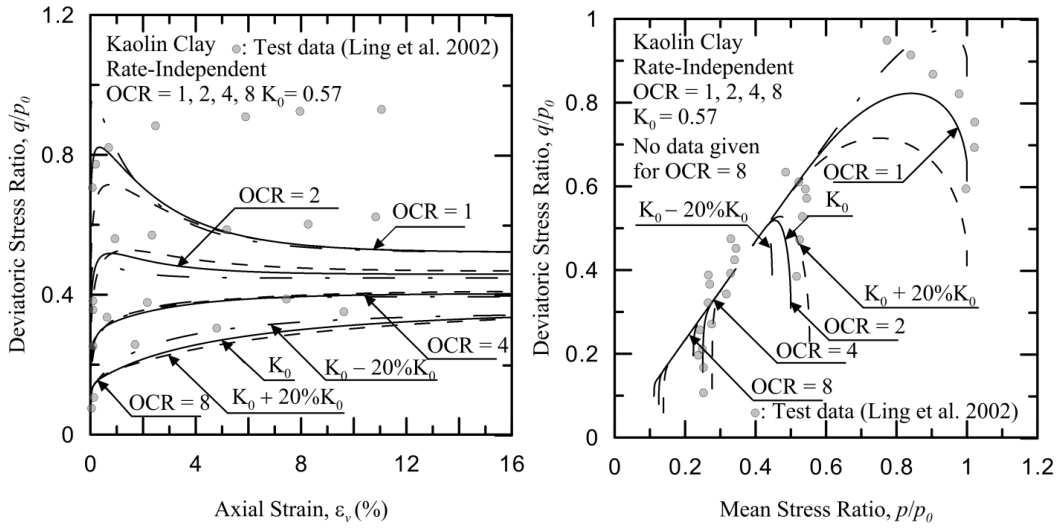

(Figure AI.1.95) Sensitivity of K_0 at 20% variation for Kaolin Clay, test data taken from Ling et al. (2002)

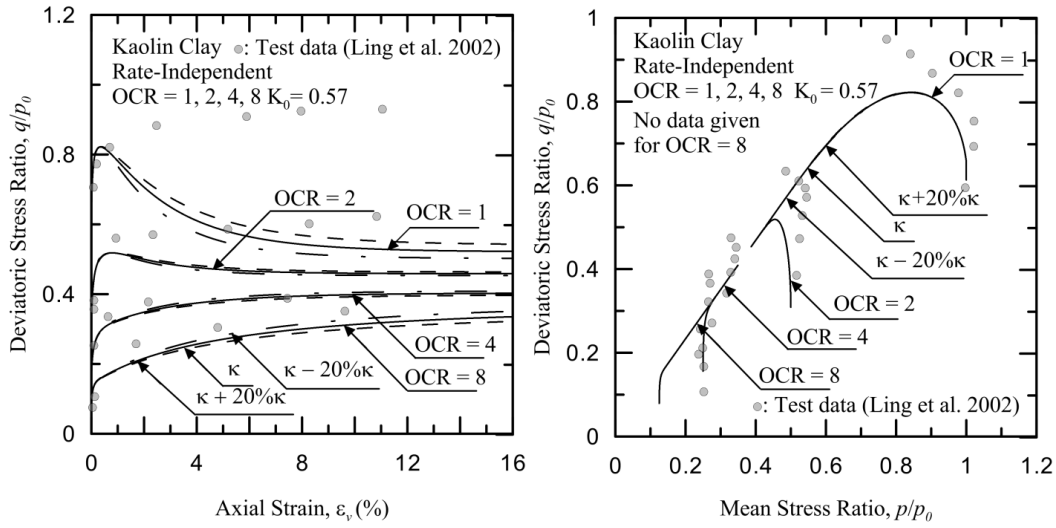

(Figure AI.1.96) Sensitivity of κ at 20% variation for Kaolin Clay, test data taken from Ling et al. (2002)

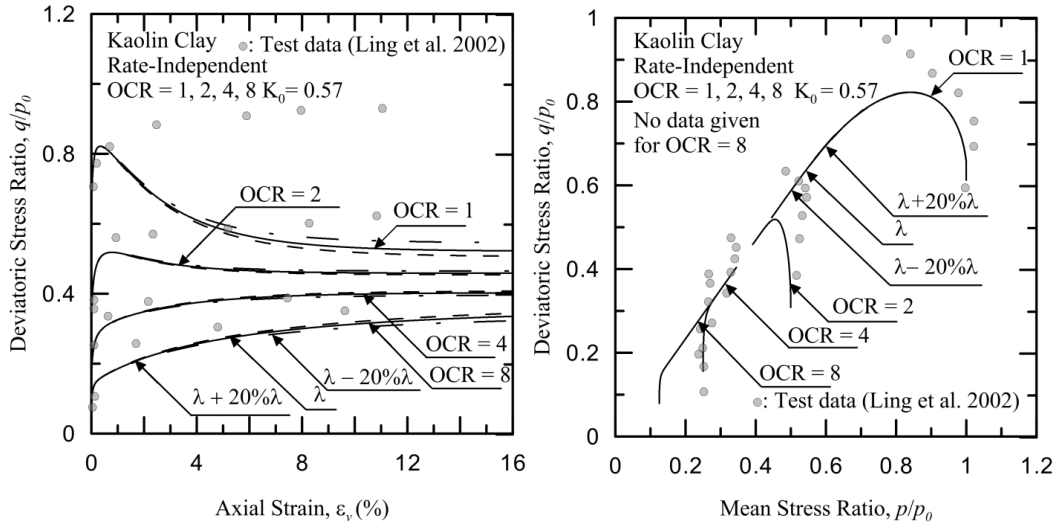

(Figure AI.1.97) Sensitivity of λ at 20% variation for Kaolin Clay, test data taken from Ling et al. (2002)

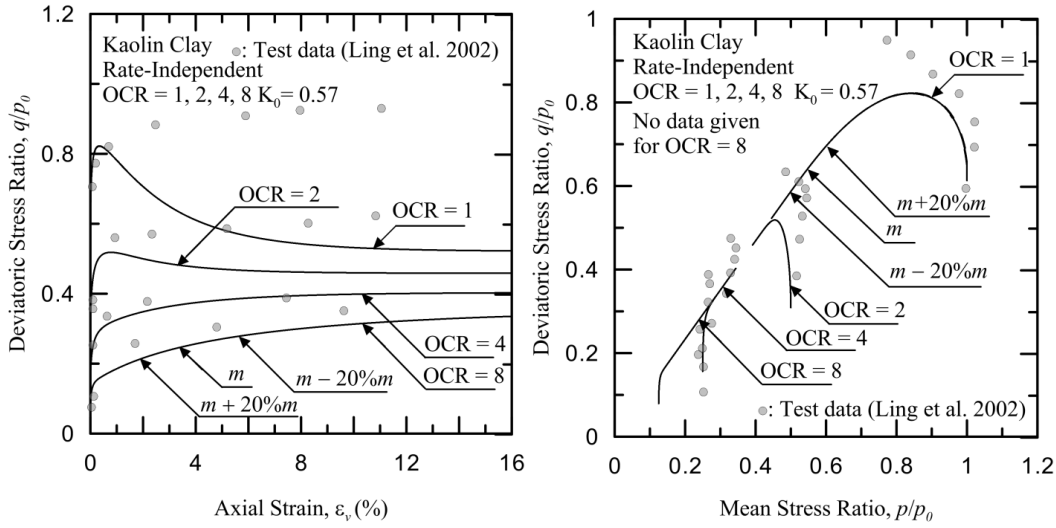

(Figure AI.1.98) Sensitivity of *m* at 20% variation for Kaolin Clay, test data taken from Ling et al. (2002)

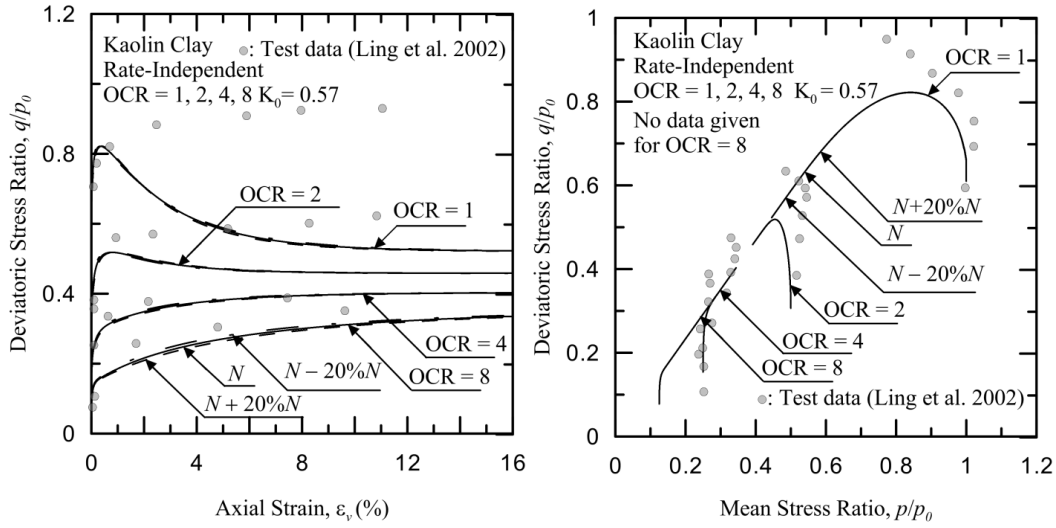

(Figure AI.1.99) Sensitivity of N at 20% variation for Kaolin Clay, test data taken from Ling et al. (2002)

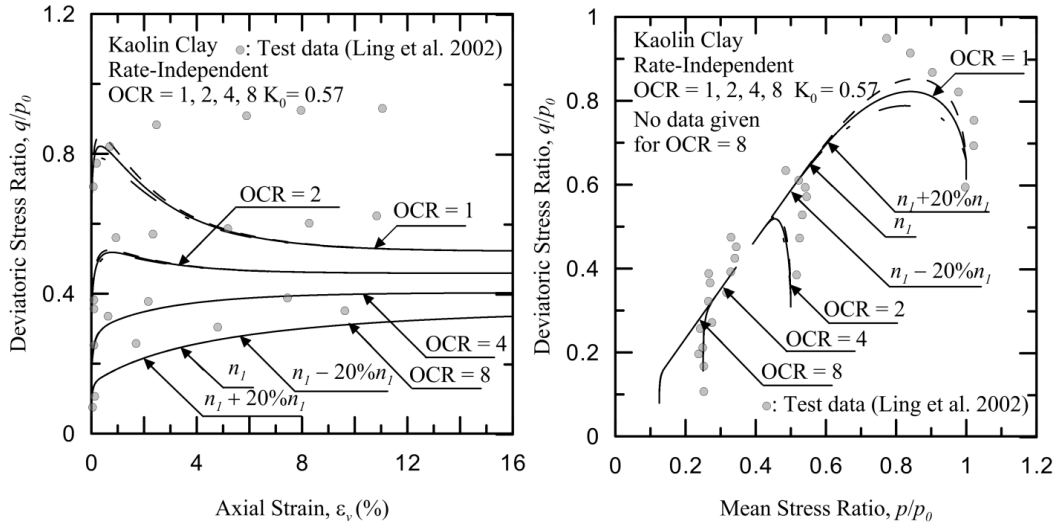

(Figure AI.1.100) Sensitivity of n_1 at 20% variation for Kaolin Clay, test data taken from Ling et al. (2002)

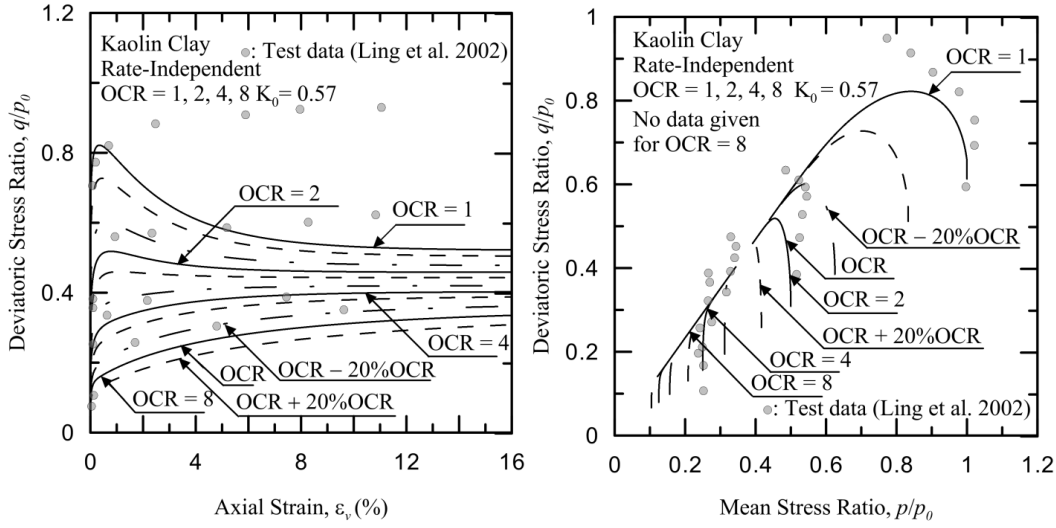

(Figure AI.1.101) Sensitivity of OCR at 20% variation for Kaolin Clay, test data taken from Ling et al. (2002)

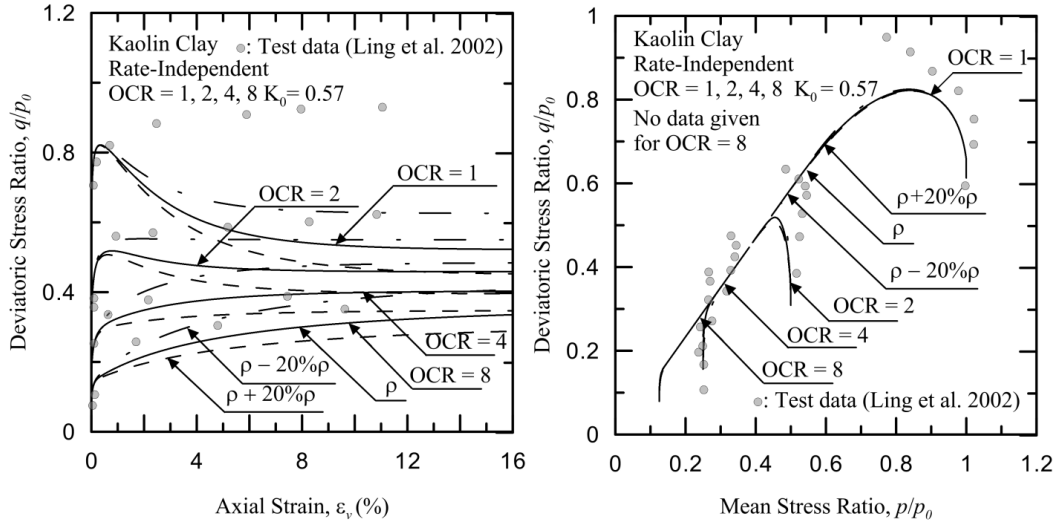

(Figure AI.1.102) Sensitivity of ρ at 20% variation for Kaolin Clay, test data taken from Ling et al. (2002)

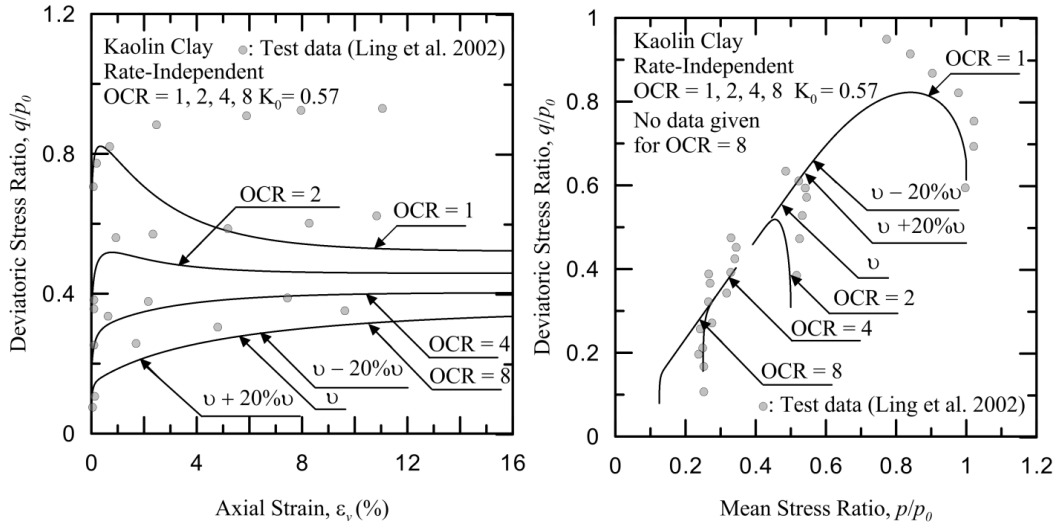

(Figure AI.1.103) Sensitivity of υ at 20% variation for Kaolin Clay, test data taken from Ling et al. (2002)

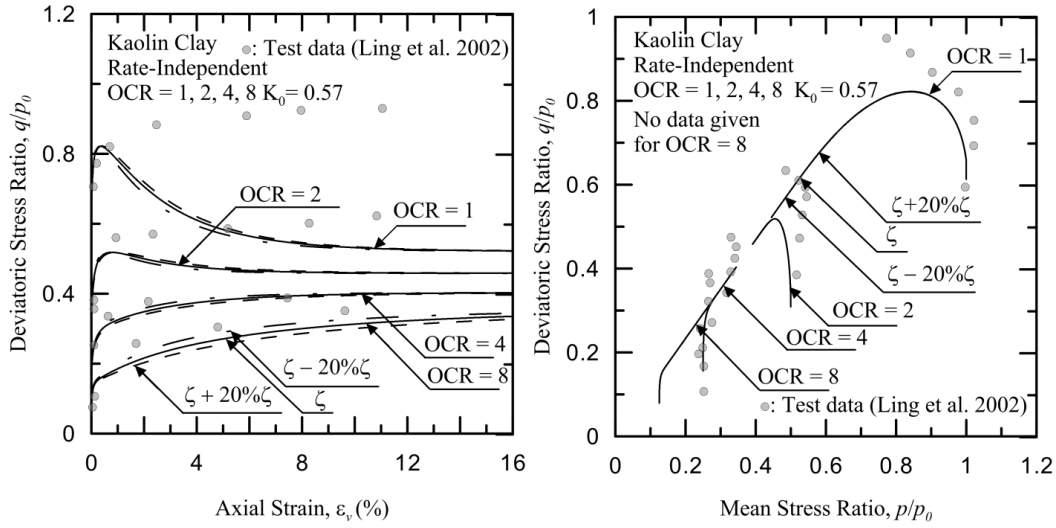

(Figure AI.1.104) Sensitivity of ζ at 20% variation for Kaolin Clay, test data taken from Ling et al. (2002)

Rate-independent sensitivity analysis for London Clay at 5% variation:

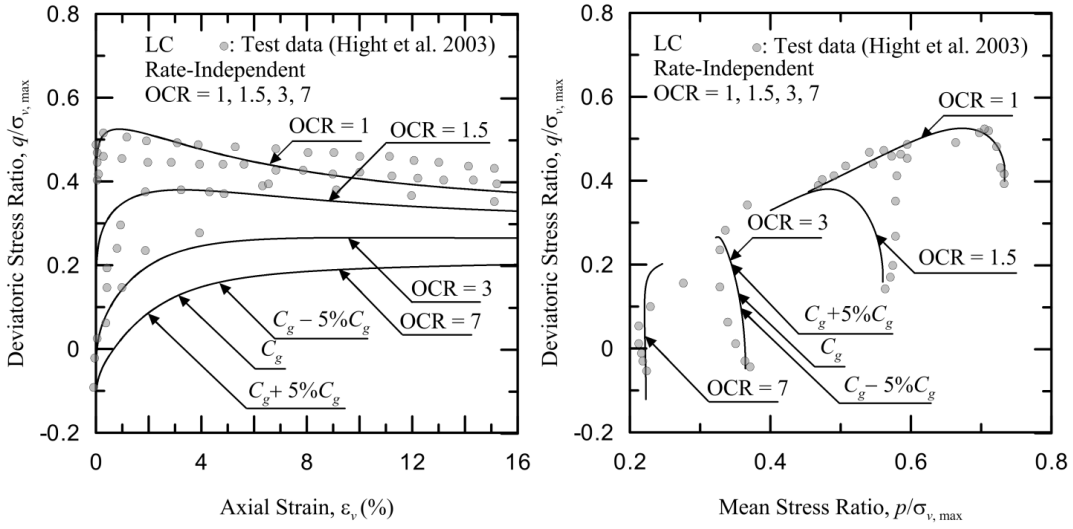

(Figure AI.1.105) Sensitivity of C_g at 5% variation for London Clay, test data taken from Hight et al. (2003)

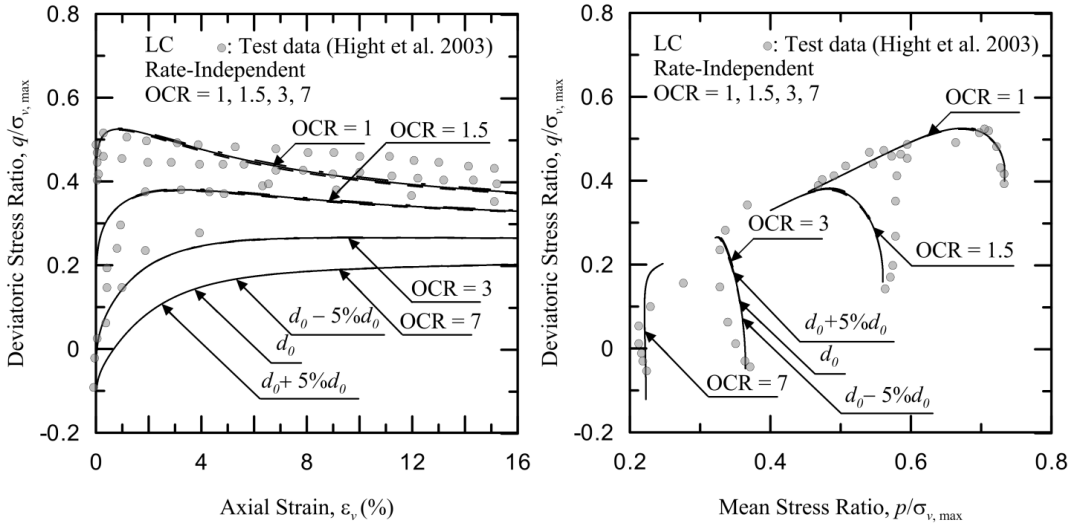

(Figure AI.1.106) Sensitivity of d_0 at 5% variation for London Clay, test data taken from Hight et al. (2003)

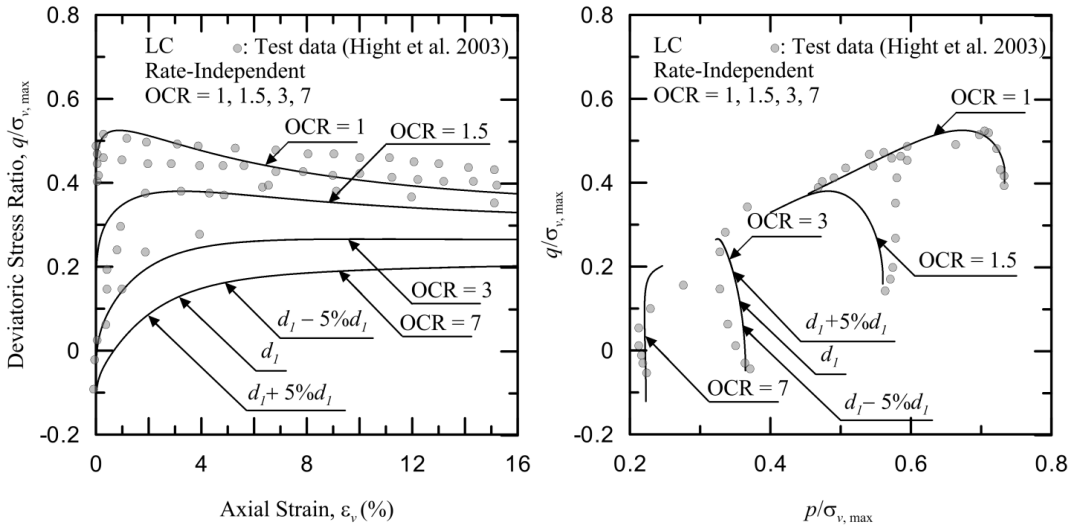

(Figure AI.1.107) Sensitivity of d_1 at 5% variation for London Clay, test data taken from Hight et al. (2003)

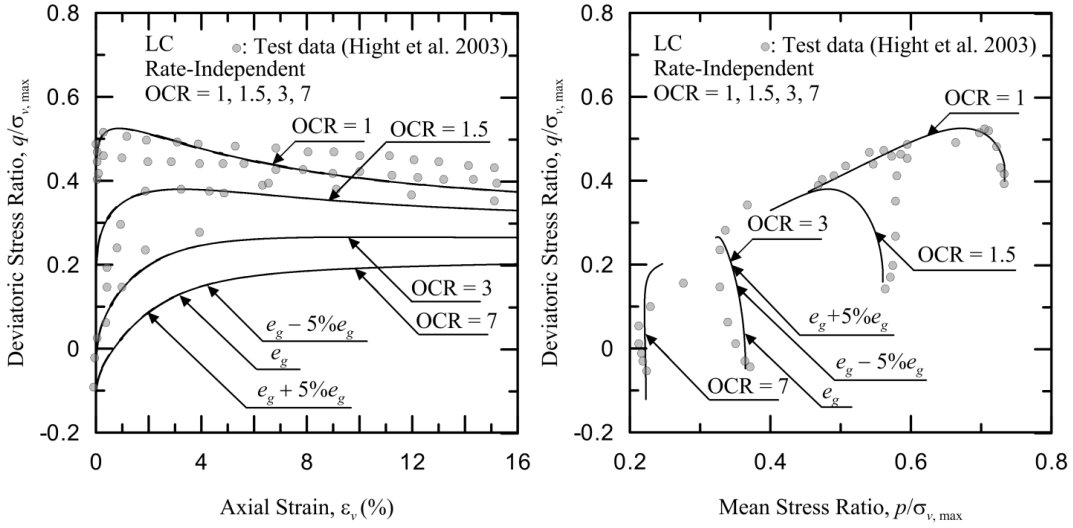

(Figure AI.1.108) Sensitivity of e_g at 5% variation for London Clay, test data taken from Hight et al. (2003)

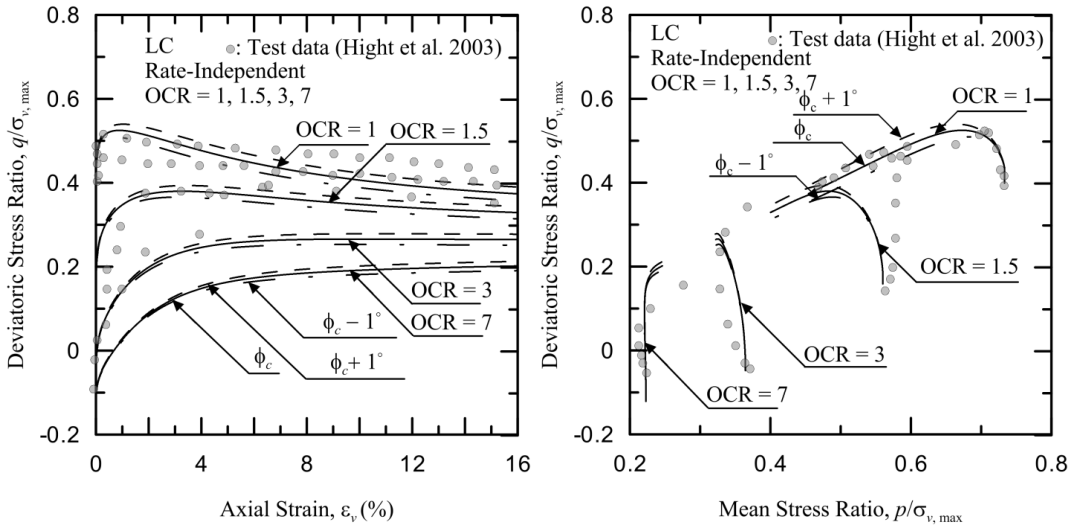

(Figure AI.1.109 Sensitivity of ϕ_c at 1° variation for London Clay, test data taken from Hight et al. (2003)

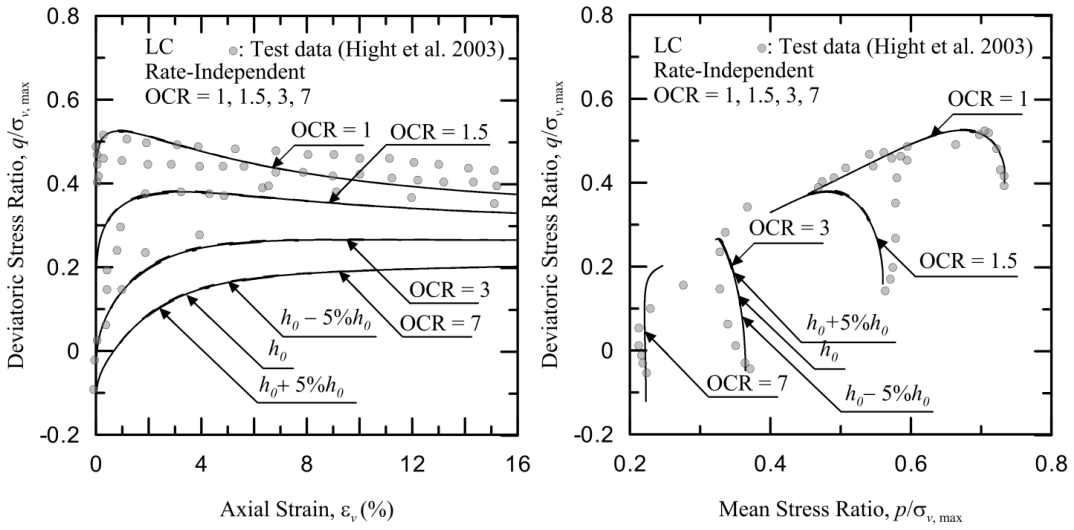

(Figure AI.1.110) Sensitivity of h_0 at 5% variation for London Clay, test data taken from Hight et al. (2003)

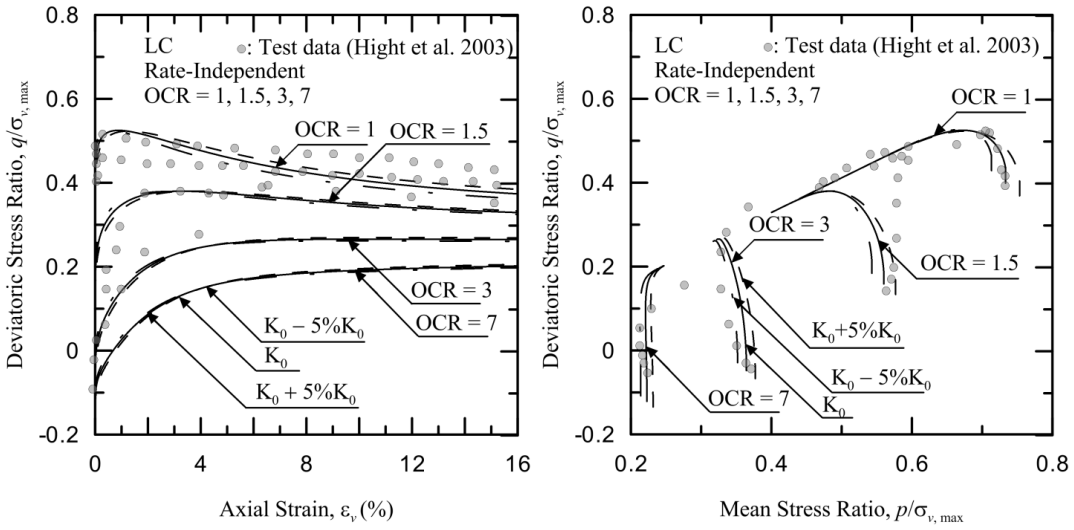

(Figure AI.1.111) Sensitivity of K_0 at 5% variation for London Clay, test data taken from Hight et al. (2003)

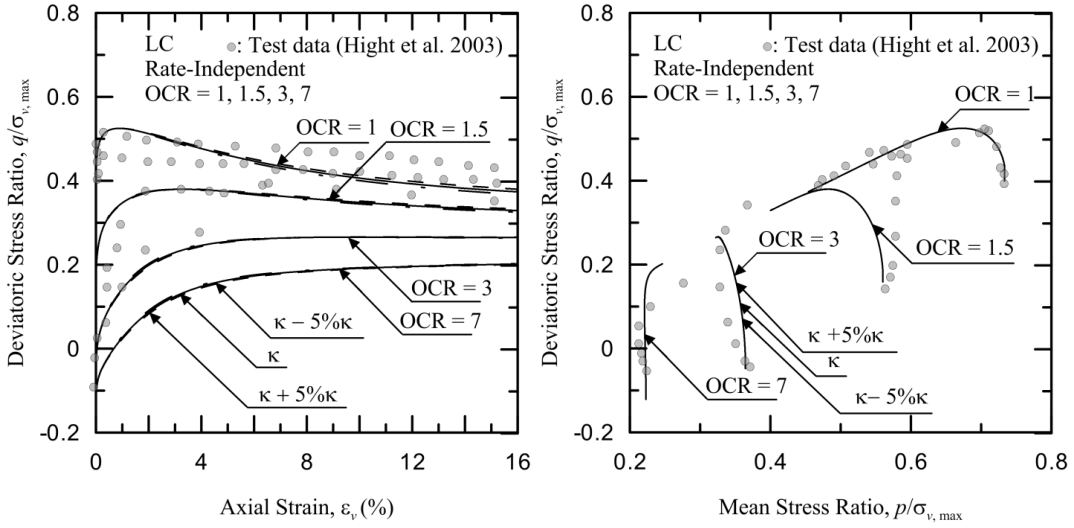

(Figure AI.1.112) Sensitivity of κ at 5% variation for London Clay, test data taken from Hight et al. (2003), stress-strain plot

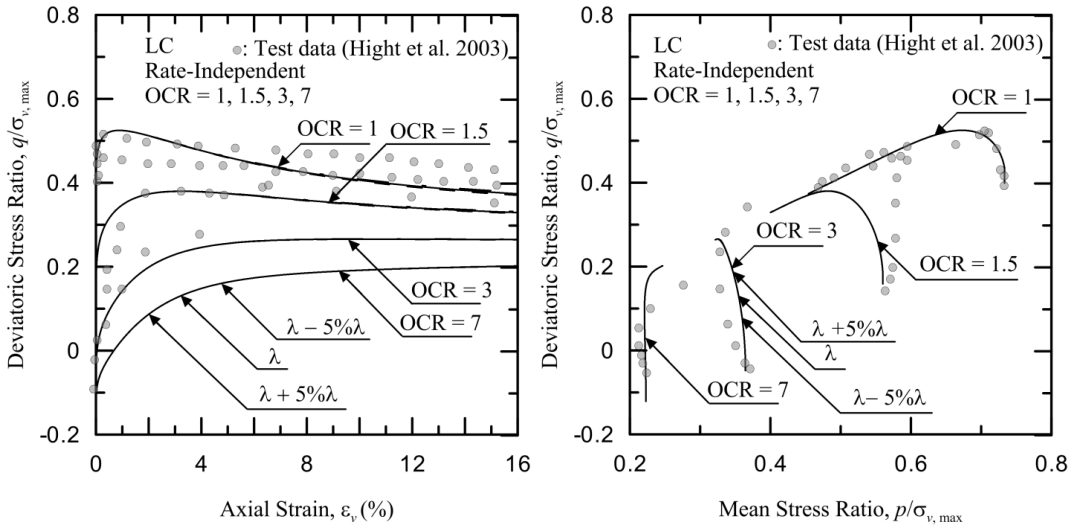

(Figure AI.1.113) Sensitivity of λ at 5% variation for London Clay, test data taken from Hight et al. (2003)

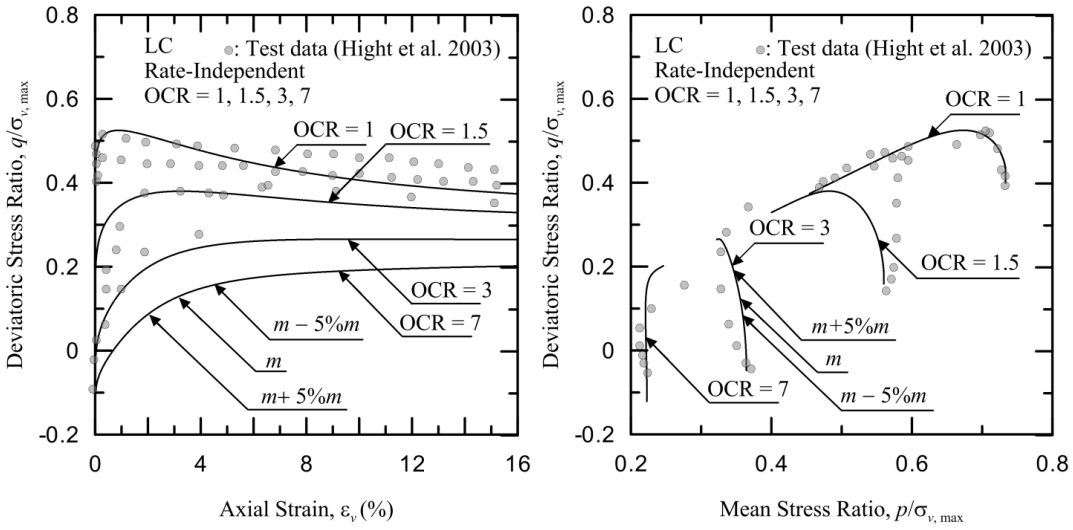

(Figure AI.1.114) Sensitivity of *m* at 5% variation for London Clay, test data taken from Hight et al. (2003)

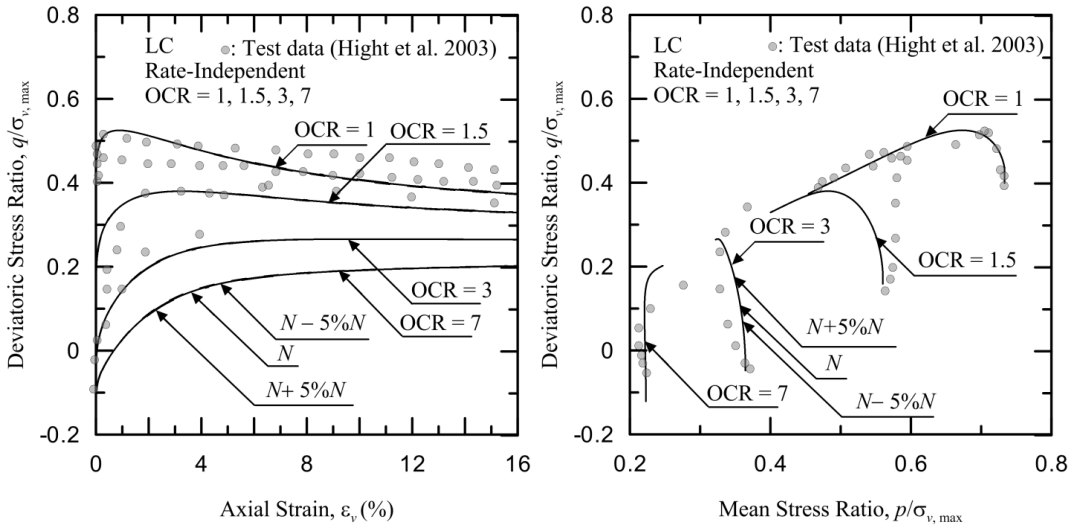

(Figure AI.1.115) Sensitivity of N at 5% variation for London Clay, test data taken from Hight et al. (2003)

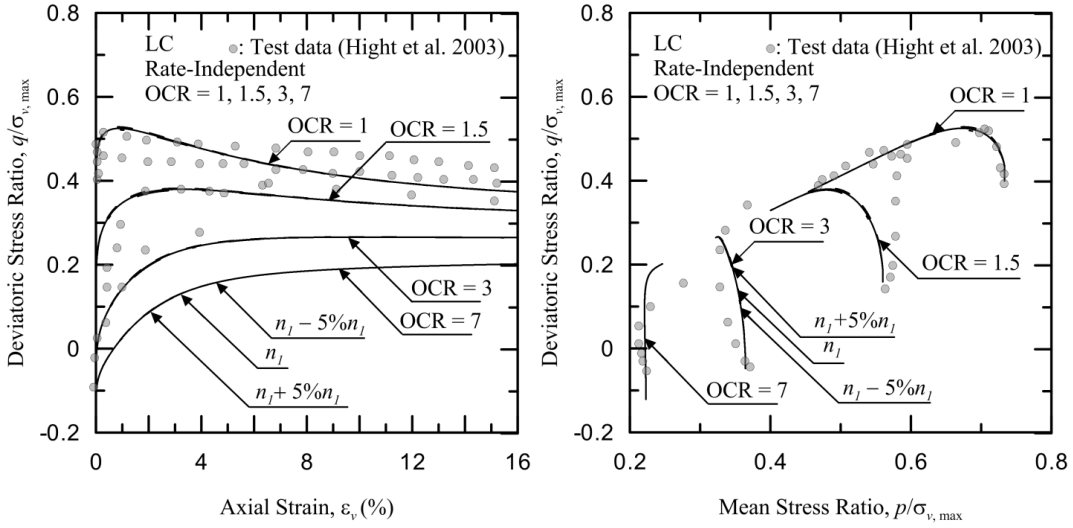

(Figure AI.1.116) Sensitivity of n_1 at 5% variation for London Clay, test data taken from Hight et al. (2003)

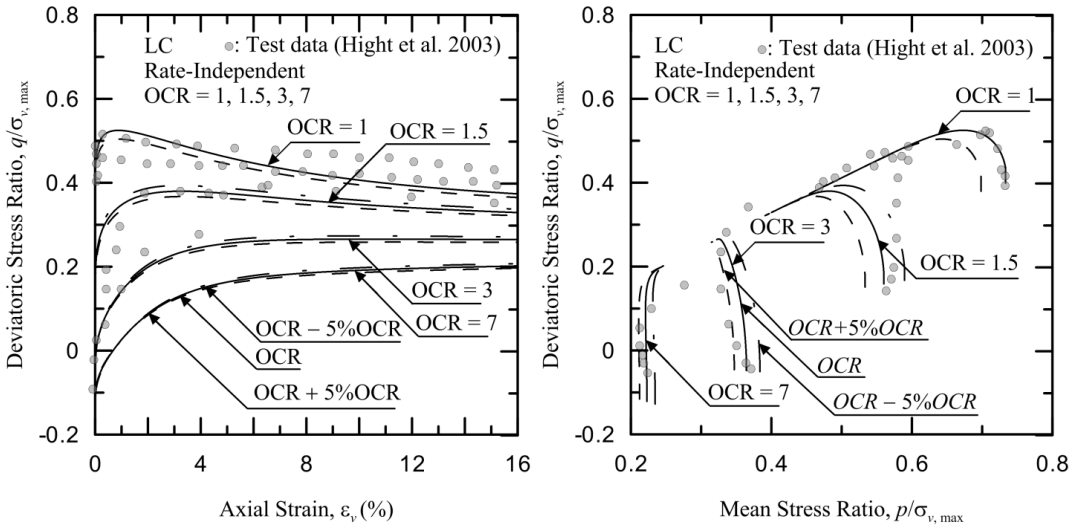

(Figure AI.1.117) Sensitivity of OCR at 5% variation for London Clay, test data taken from Hight et al. (2003)

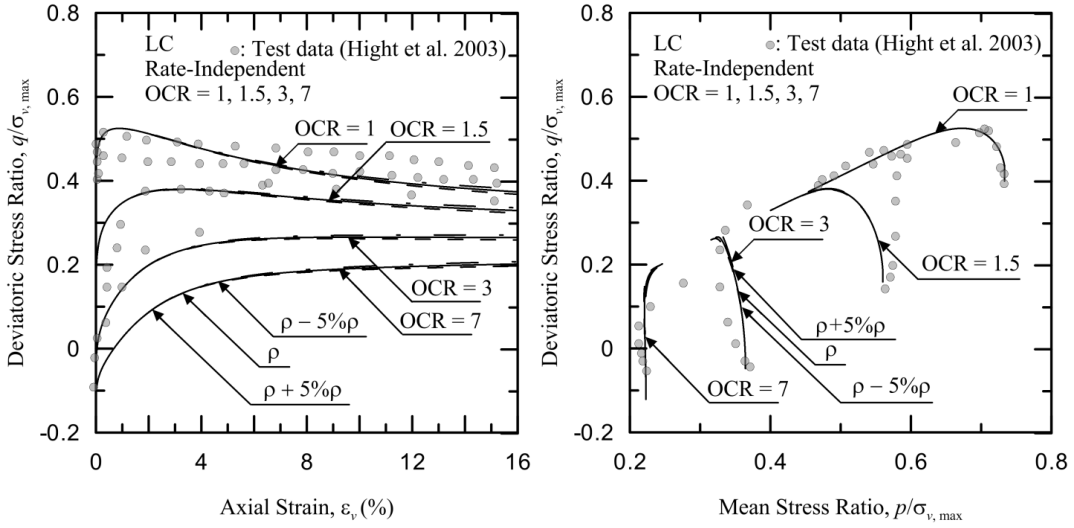

(Figure AI.1.118) Sensitivity of ρ at 5% variation for London Clay, test data taken from Hight et al. (2003)

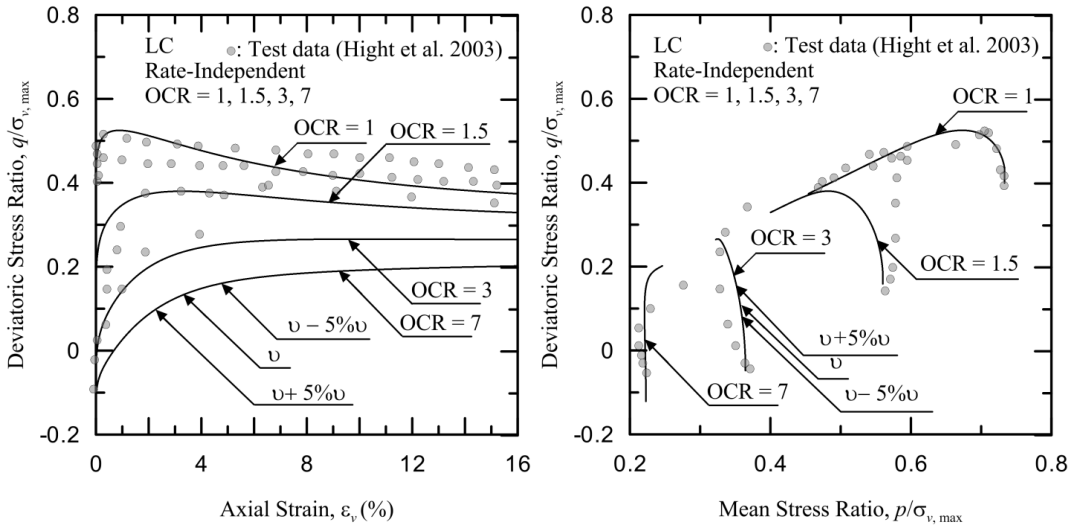

(Figure AI.1.119) Sensitivity of υ at 5% variation for London Clay, test data taken from Hight et al. (2003)

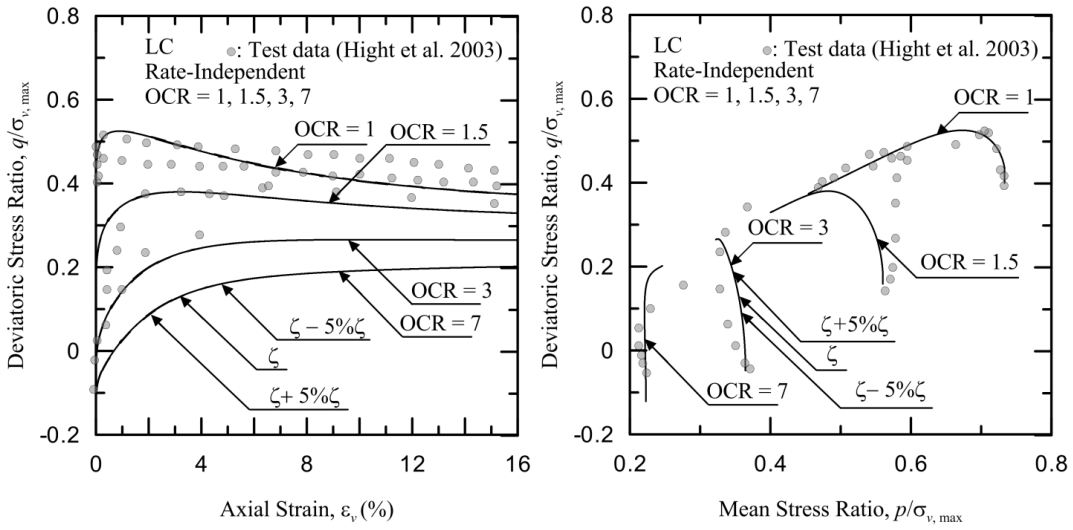

(Figure AI.1.120) Sensitivity of ζ at 5% variation for London Clay, test data taken from Hight et al. (2003)

Rate-independent sensitivity analysis for London Clay at 10% variation:

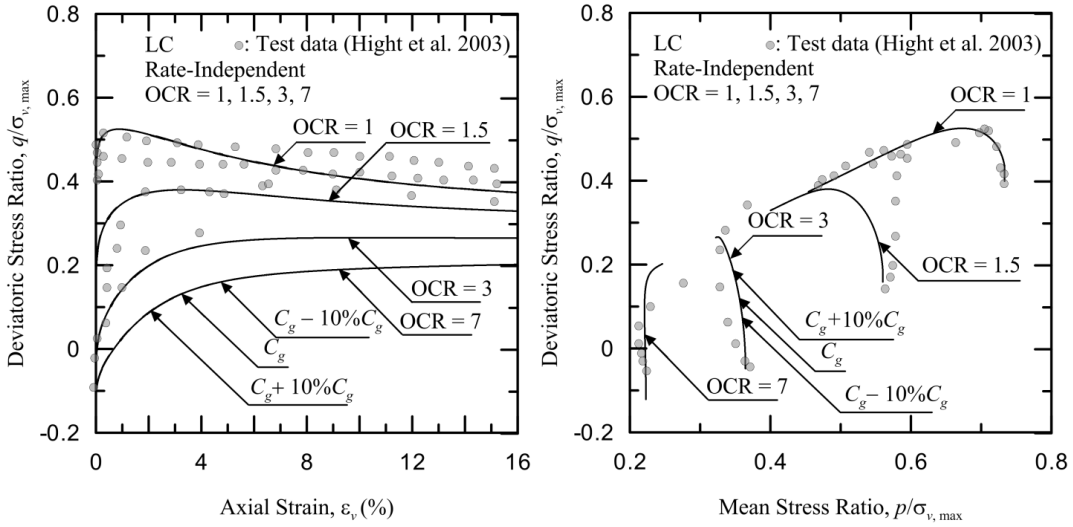

(Figure AI.1.121) Sensitivity of C_g at 10% variation for London Clay, test data taken from Hight et al. (2003)

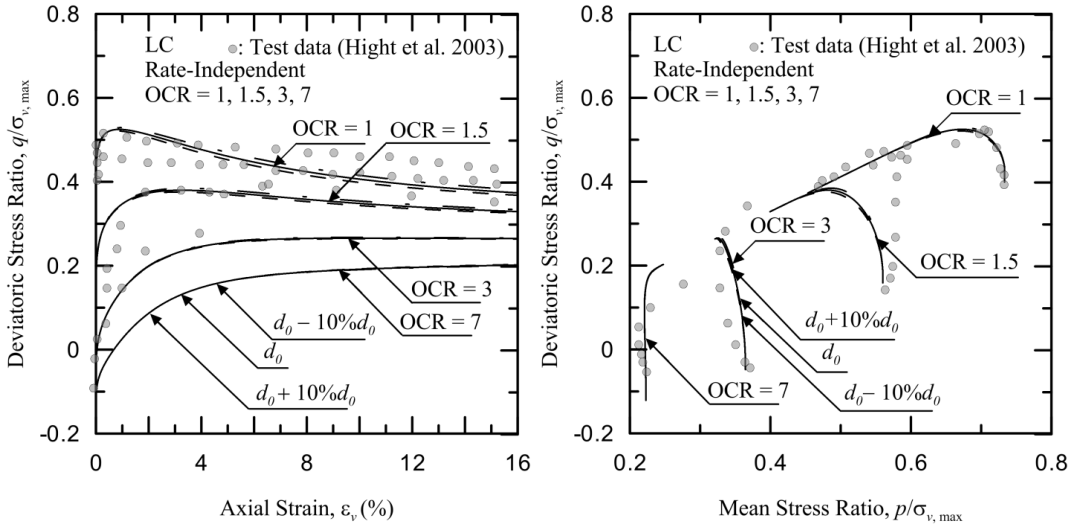

(Figure AI.1.122) Sensitivity of d_0 at 10% variation for London Clay, test data taken from Hight et al. (2003)

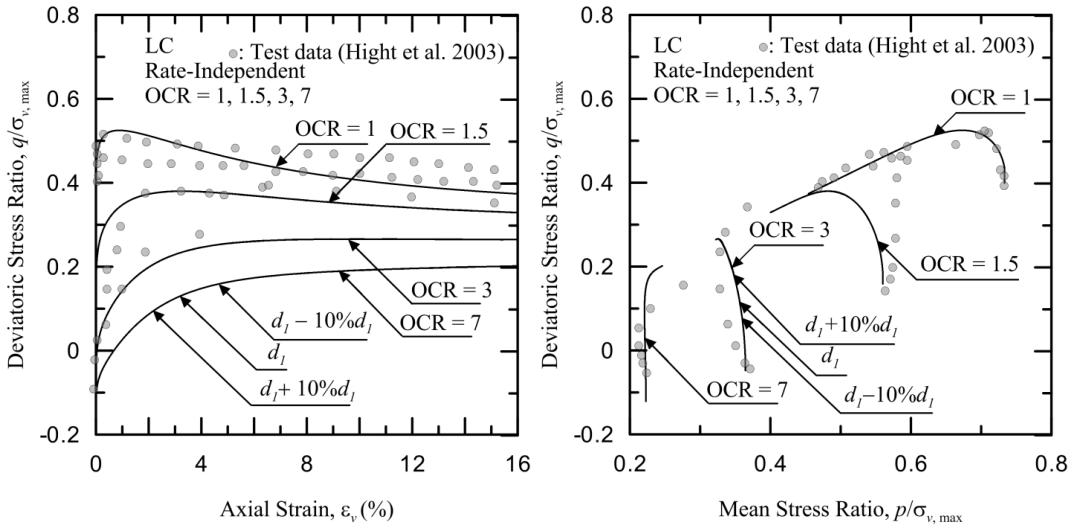

(Figure AI.1.123) Sensitivity of d_l at 10% variation for London Clay, test data taken from Hight et al. (2003)

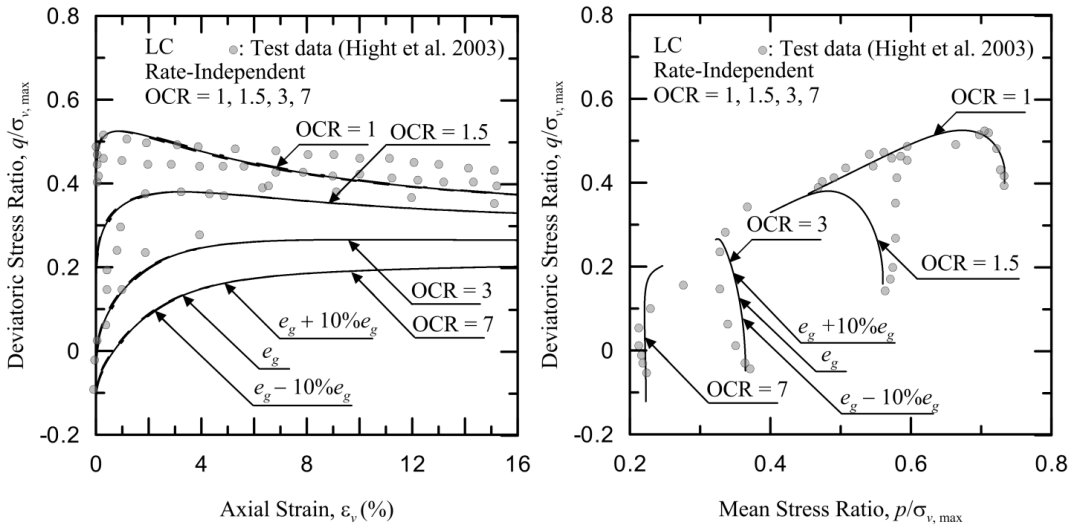

(Figure AI.1.124) Sensitivity of e_g at 10% variation for London Clay, test data taken from Hight et al. (2003)

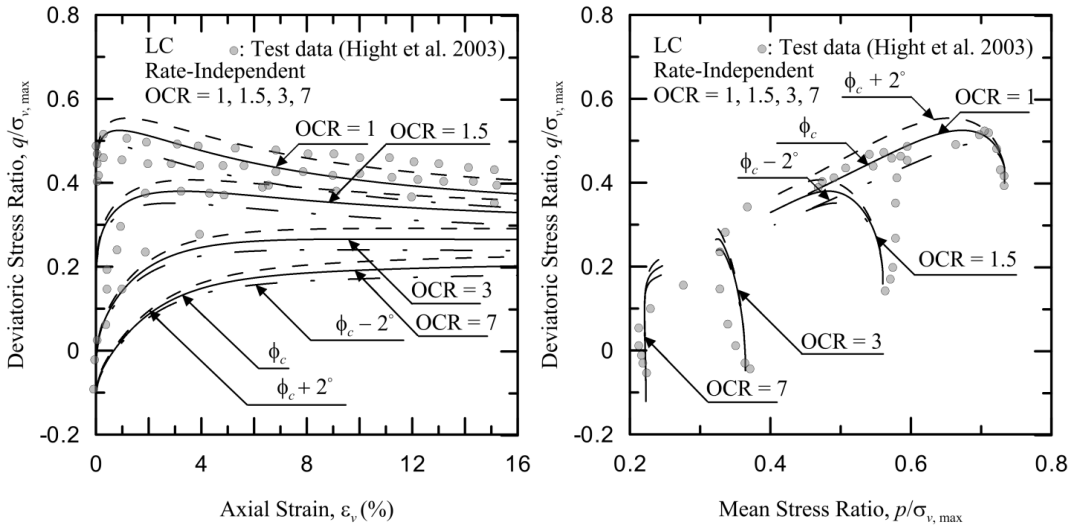

(Figure AI.1.125) Sensitivity of ϕ_c at 2° variation for London Clay, test data taken from Hight et al. (2003)

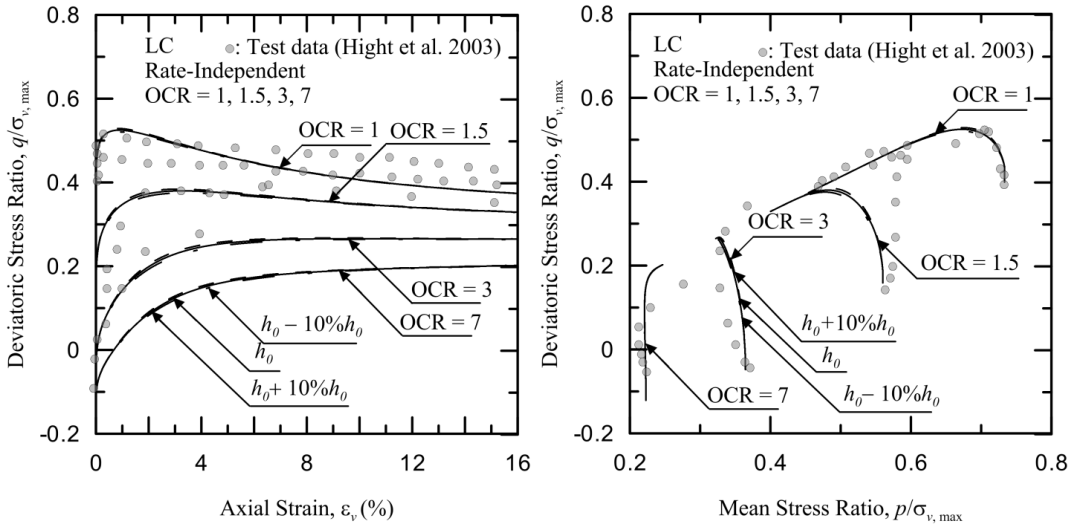

(Figure AI.1.126) Sensitivity of h_0 at 10% variation for London Clay, test data taken from Hight et al. (2003)

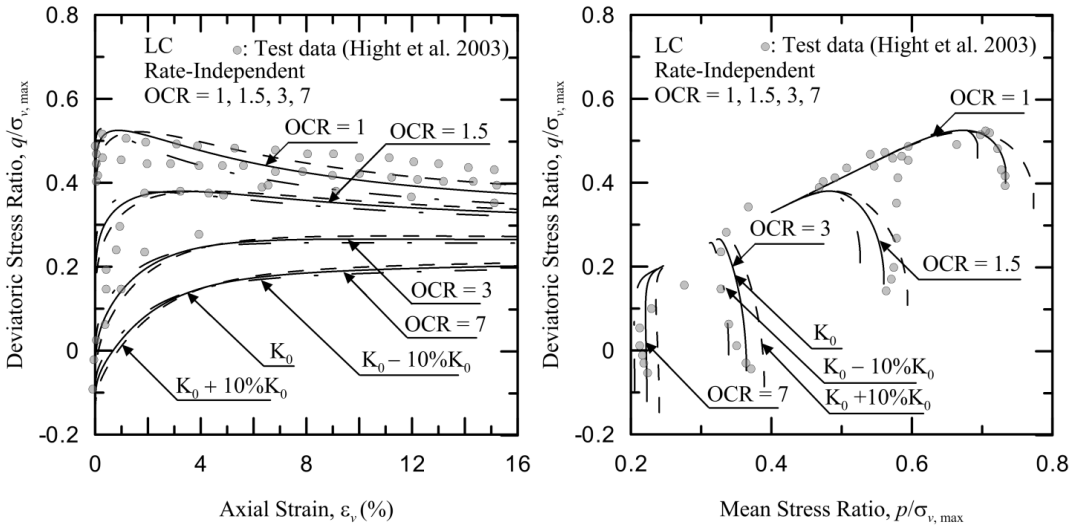

(Figure AI.1.127) Sensitivity of K_0 at 10% variation for London Clay, test data taken from Hight et al. (2003)

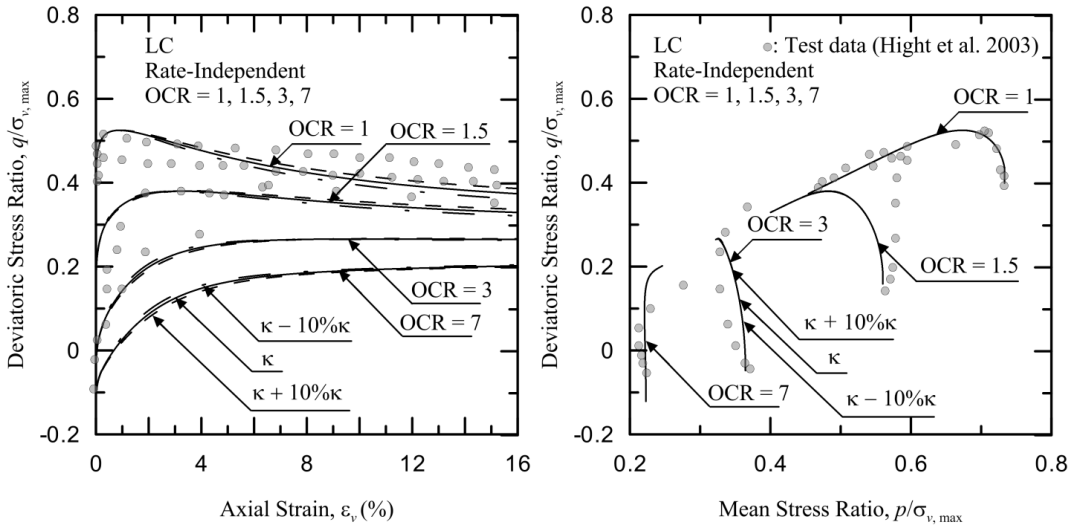

(Figure AI.1.128) Sensitivity of κ at 10% variation for London Clay, test data taken from Hight et al. (2003)

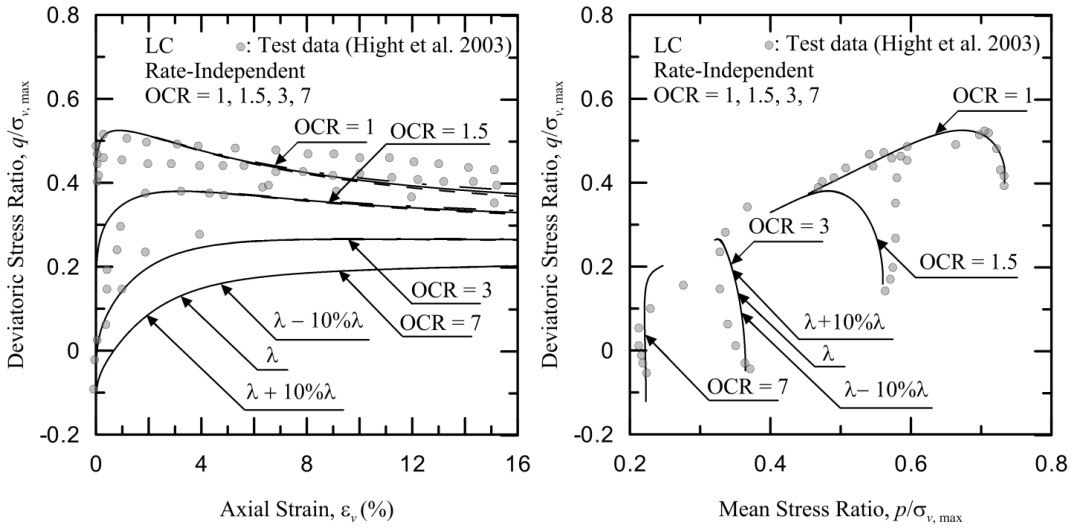

(Figure AI.1.129) Sensitivity of λ at 10% variation for London Clay, test data taken from Hight et al. (2003)

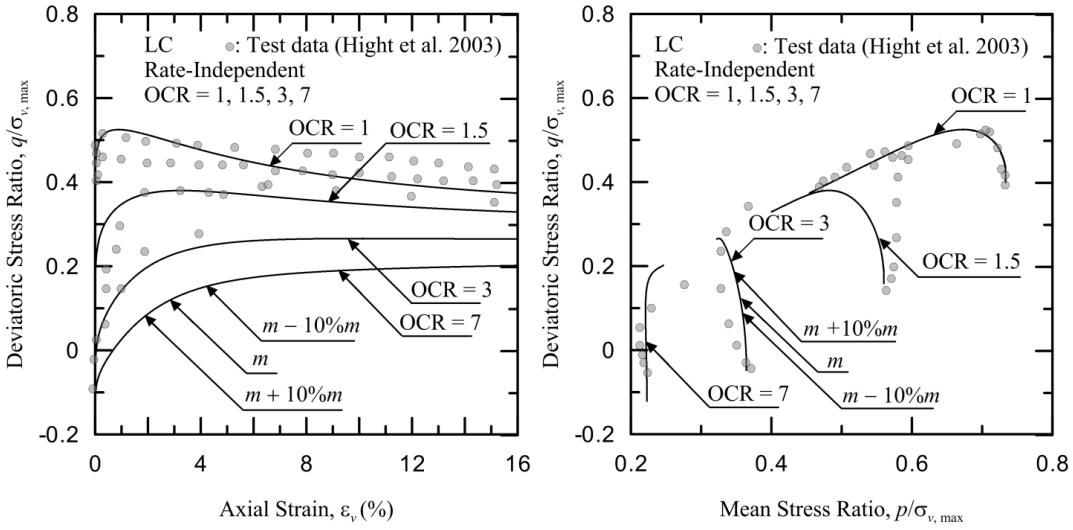

(Figure AI.1.130) Sensitivity of *m* at 10% variation for London Clay, test data taken from Hight et al. (2003)

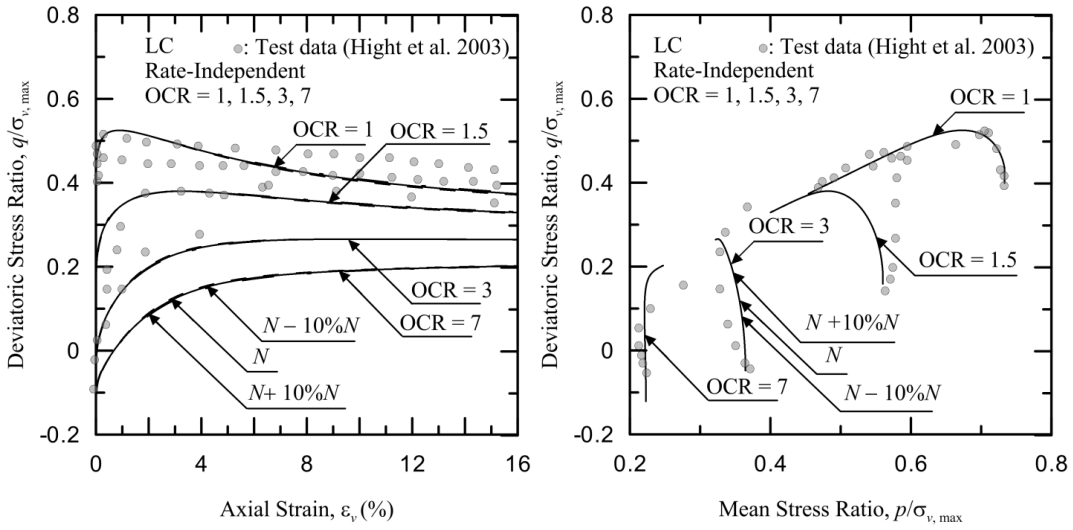

(Figure AI.1.131) Sensitivity of N at 10% variation for London Clay, test data taken from Hight et al. (2003)

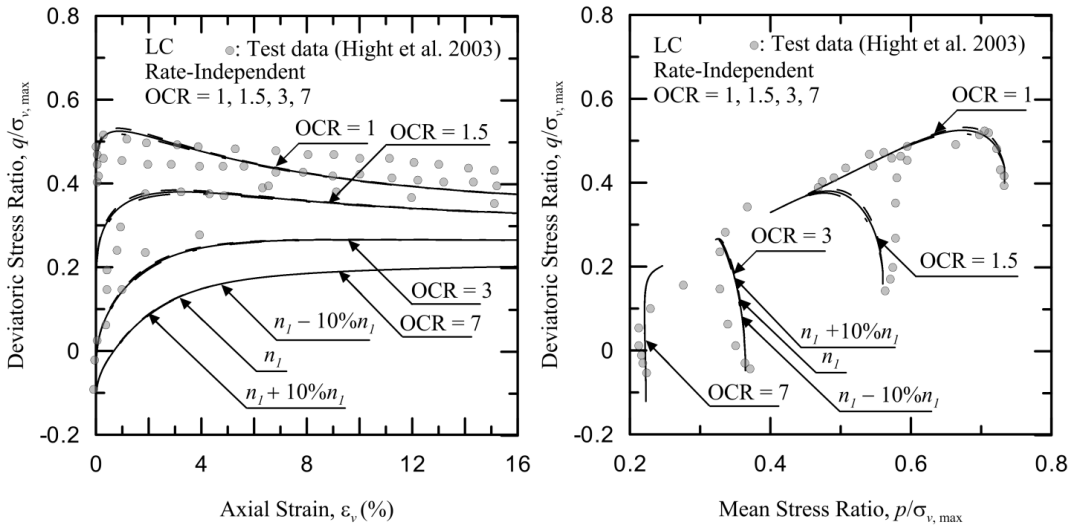

(Figure AI.1.132) Sensitivity of n_1 at 10% variation for London Clay, test data taken from Hight et al. (2003)

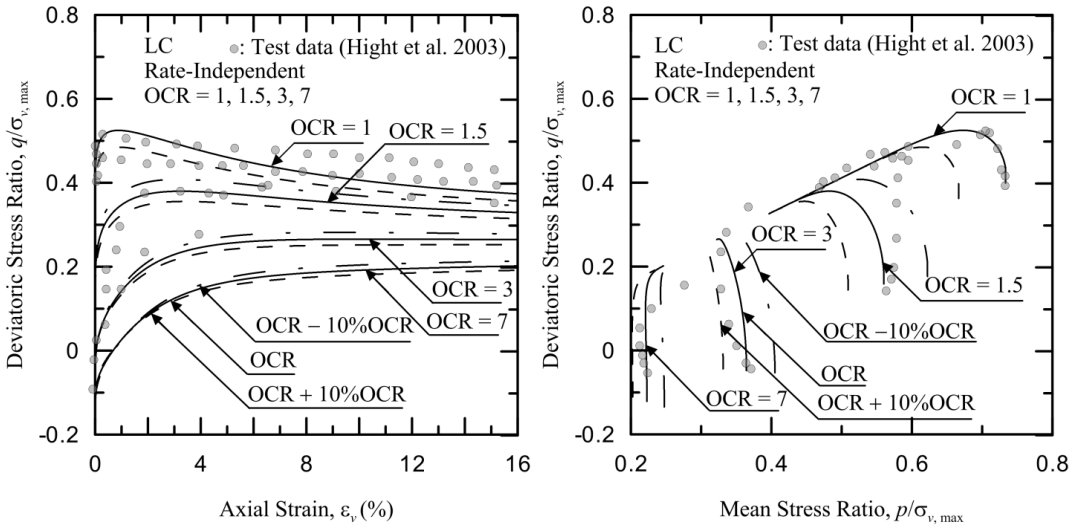

(Figure AI.1.133) Sensitivity of OCR at 10% variation for London Clay, test data taken from Hight et al. (2003)

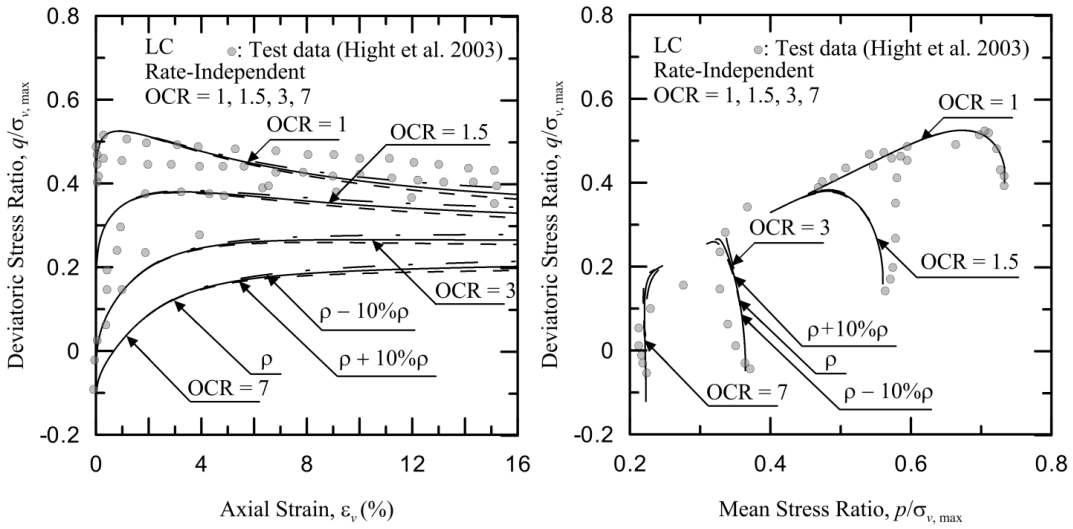

(Figure AI.1.134) Sensitivity of ρ at 10% variation for London Clay, test data taken from Hight et al. (2003)

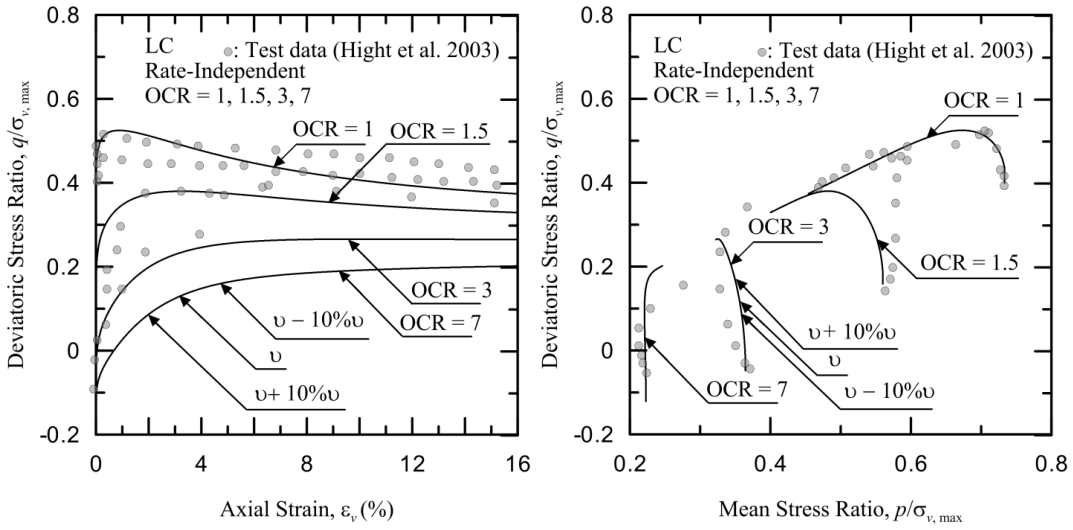

(Figure AI.1.135) Sensitivity of υ at 10% variation for London Clay, test data taken from Hight et al. (2003)

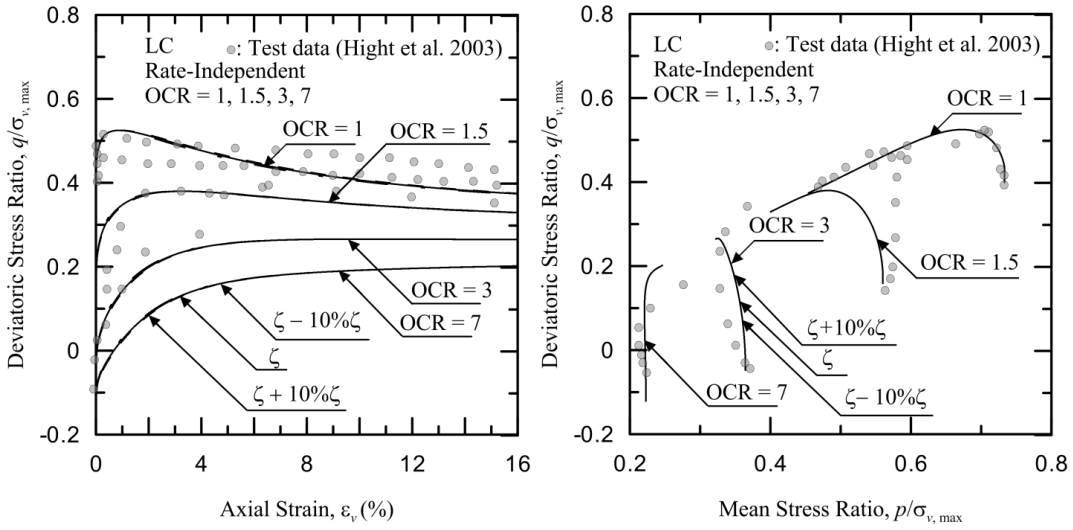

(Figure AI.1.136) Sensitivity of ζ at 10% variation for London Clay, test data taken from Hight et al. (2003)

Rate-independent sensitivity analysis for London Clay at 20% variation:

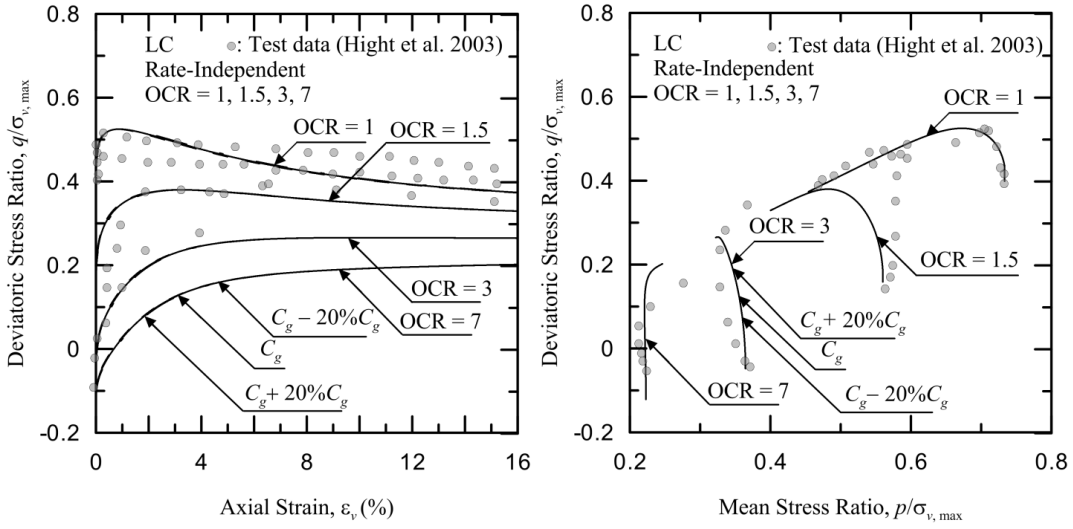

(Figure AI.1.137) Sensitivity of C_g at 20% variation for London Clay, test data taken from Hight et al. (2003)

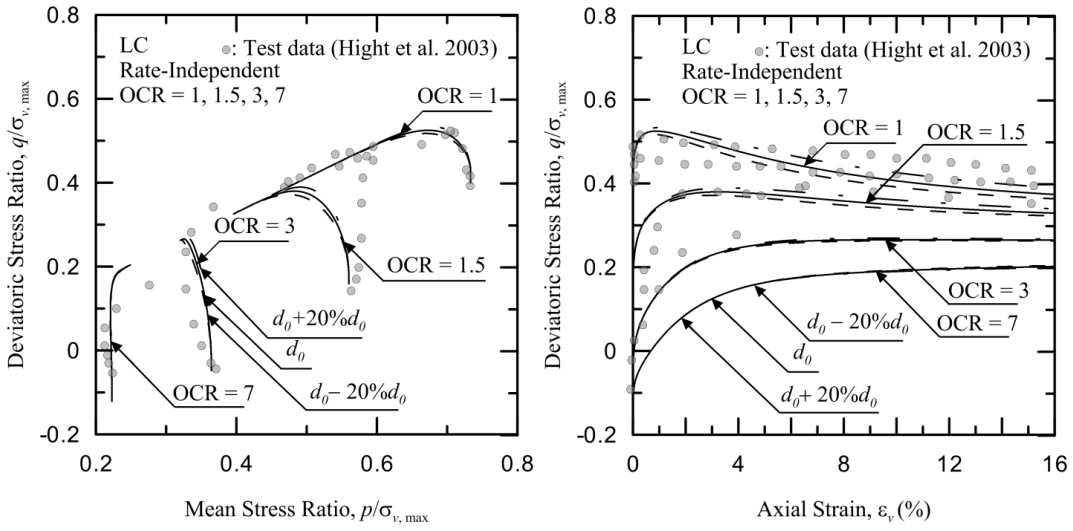

(Figure AI.1.138) Sensitivity of d_0 at 20% variation for London Clay, test data taken from Hight et al. (2003)

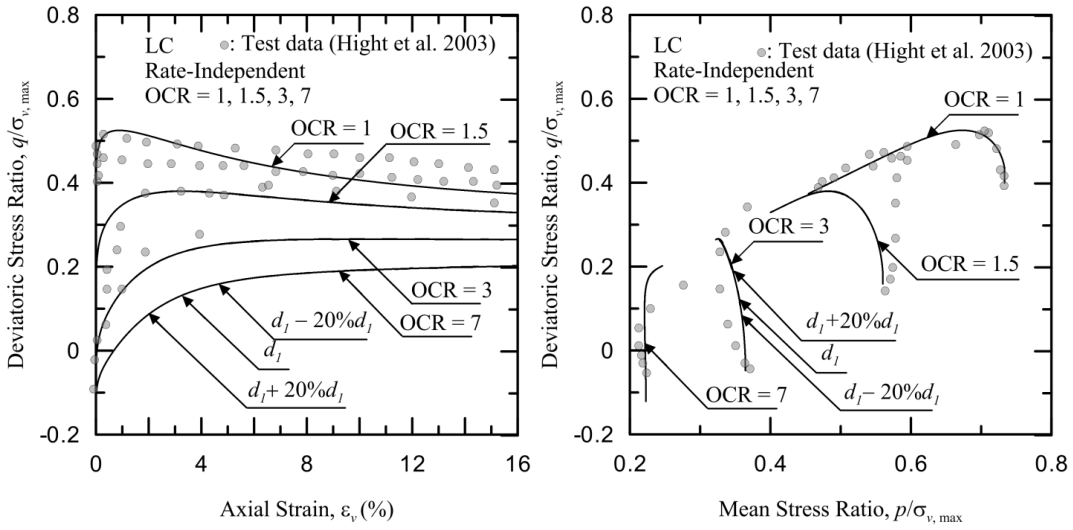

(Figure AI.1.139) Sensitivity of d_1 at 20% variation for London Clay, test data taken from Hight et al. (2003)

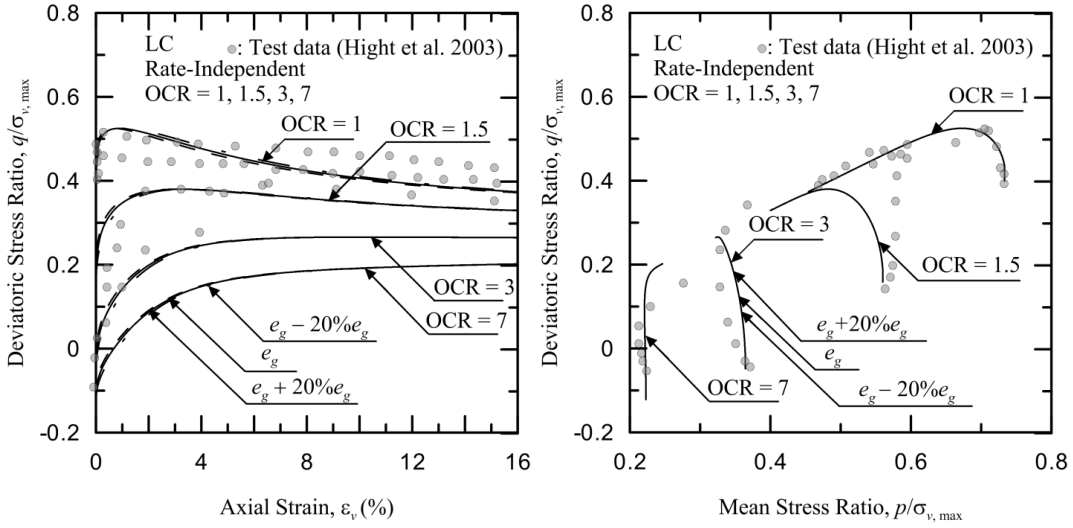

(Figure AI.1.140) Sensitivity of e_g at 20% variation for London Clay, test data taken from Hight et al. (2003)

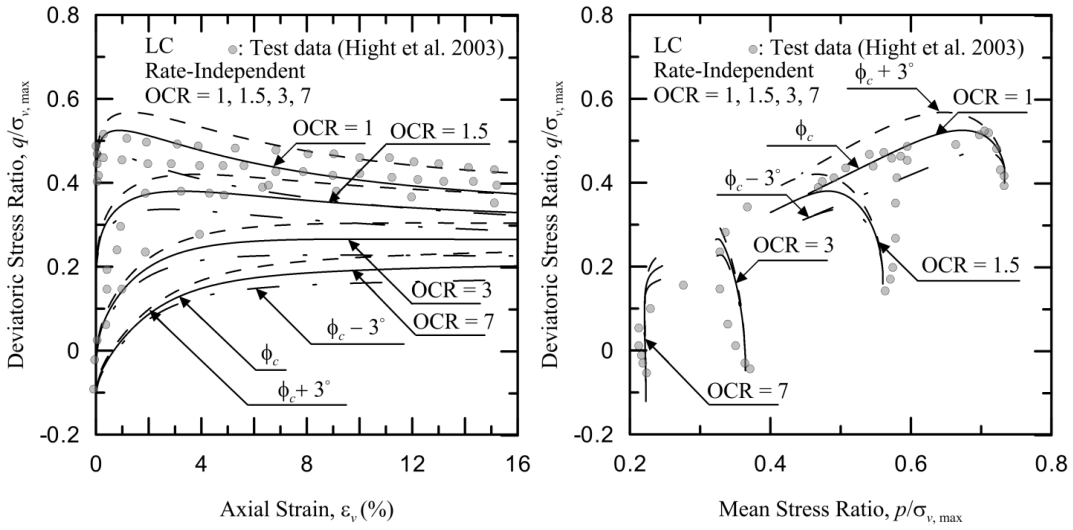

(Figure AI.1.141) Sensitivity of ϕ_c at 3° variation for London Clay, test data taken from Hight et al. (2003)

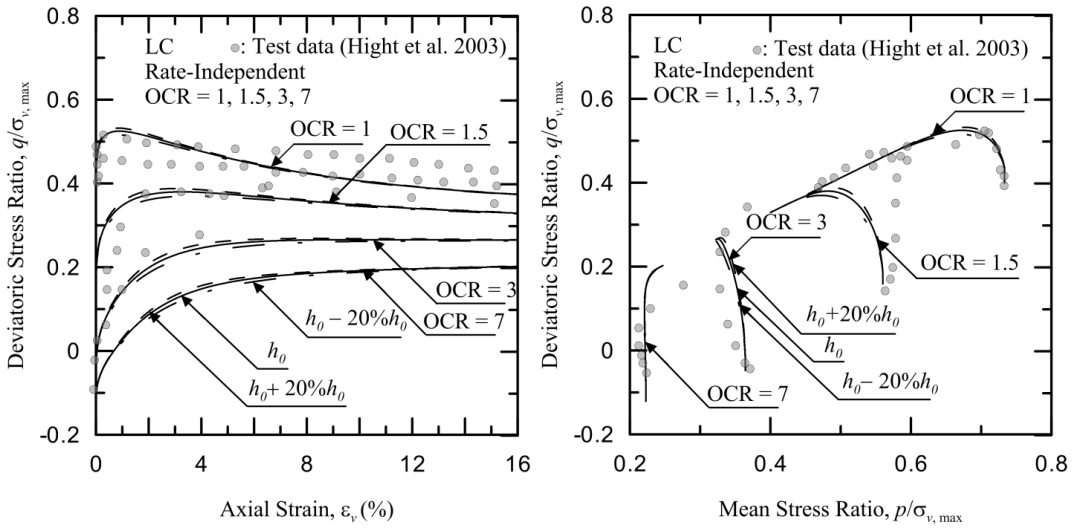

(Figure AI.1.142) Sensitivity of h_0 at 20% variation for London Clay, test data taken from Hight et al. (2003)

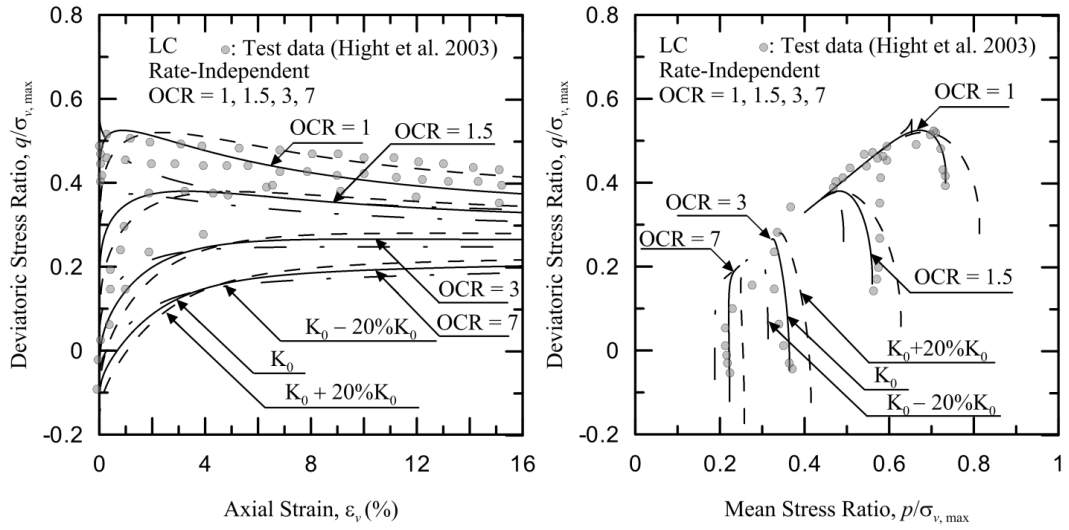

(Figure AI.1.143) Sensitivity of K_0 at 20% variation for London Clay, test data taken from Hight et al. (2003)

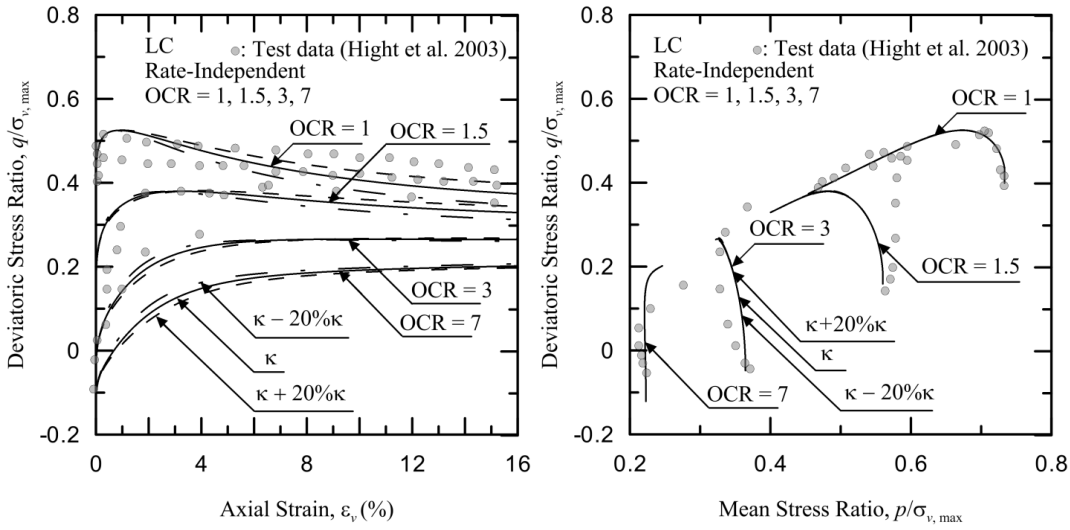

(Figure AI.1.144) Sensitivity of κ at 20% variation for London Clay, test data taken from Hight et al. (2003)

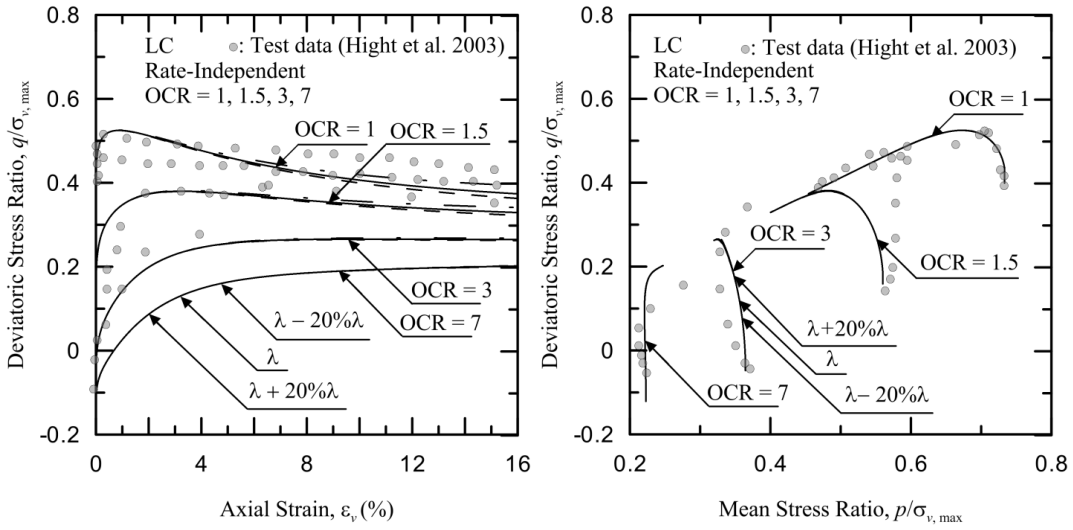

(Figure AI.1.145) Sensitivity of λ at 20% variation for London Clay, test data taken from Hight et al. (2003)

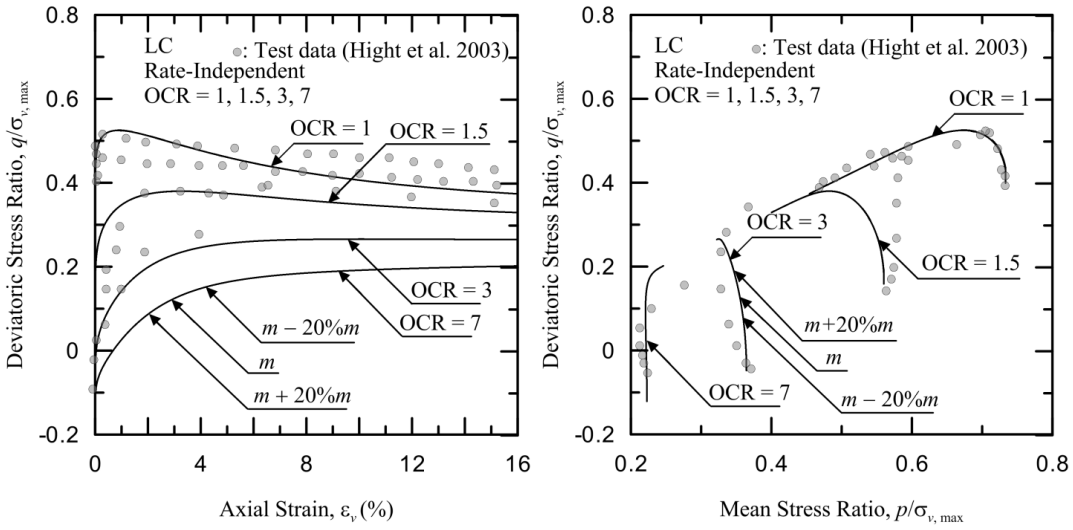

(Figure AI.1.146) Sensitivity of *m* at 20% variation for London Clay, test data taken from Hight et al. (2003)

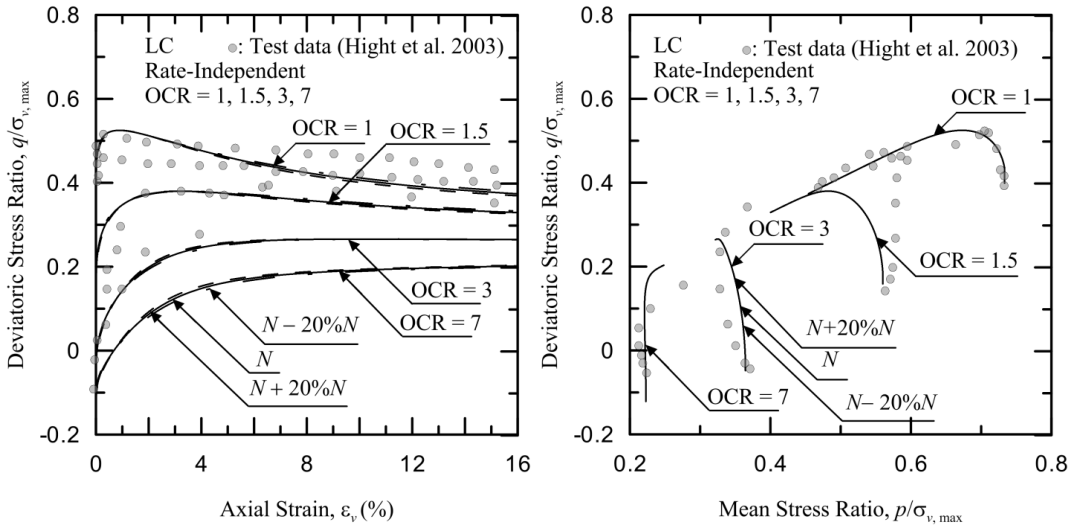

(Figure AI.1.147) Sensitivity of N at 20% variation for London Clay, test data taken from Hight et al. (2003)

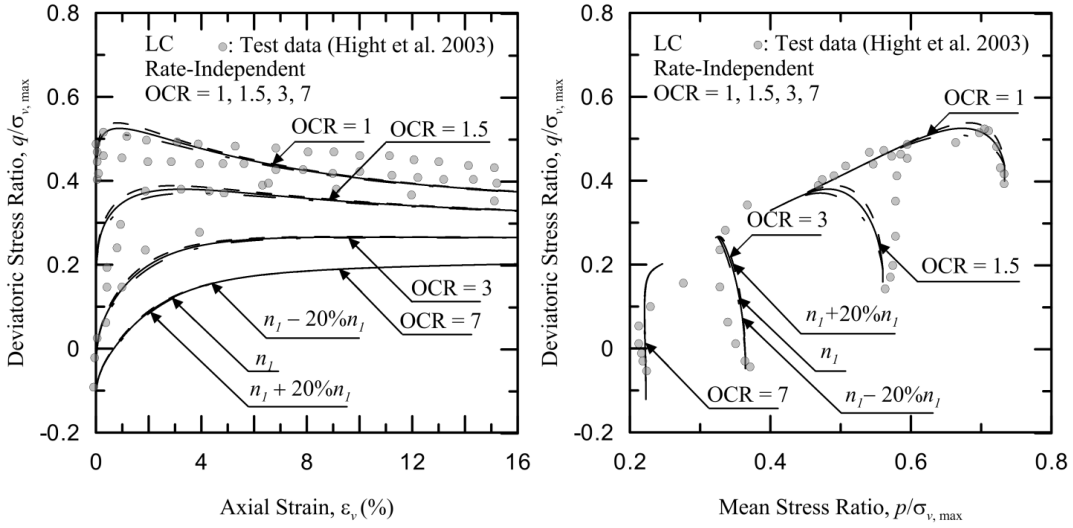

(Figure AI.1.148) Sensitivity of n_1 at 20% variation for London Clay, test data taken from Hight et al. (2003)

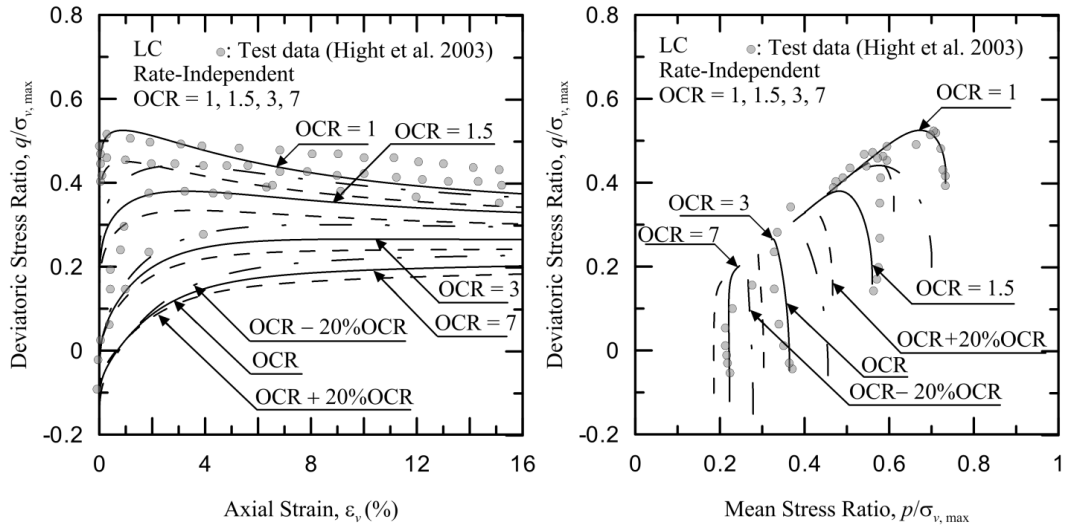

(Figure AI.1.149) Sensitivity of OCR at 20% variation for London Clay, test data taken from Hight et al. (2003)

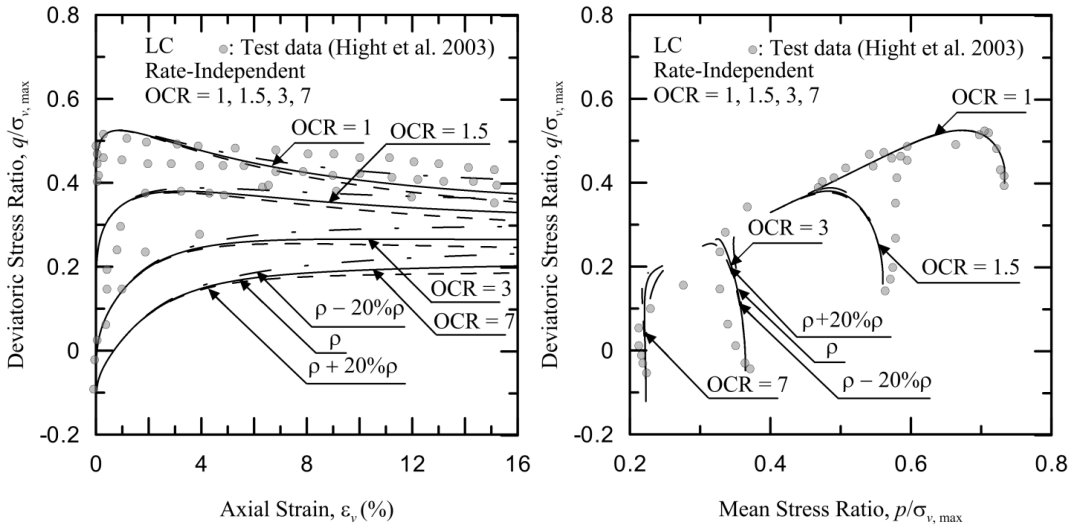

(Figure AI.1.150) Sensitivity of ρ at 20% variation for London Clay, test data taken from Hight et al. (2003)

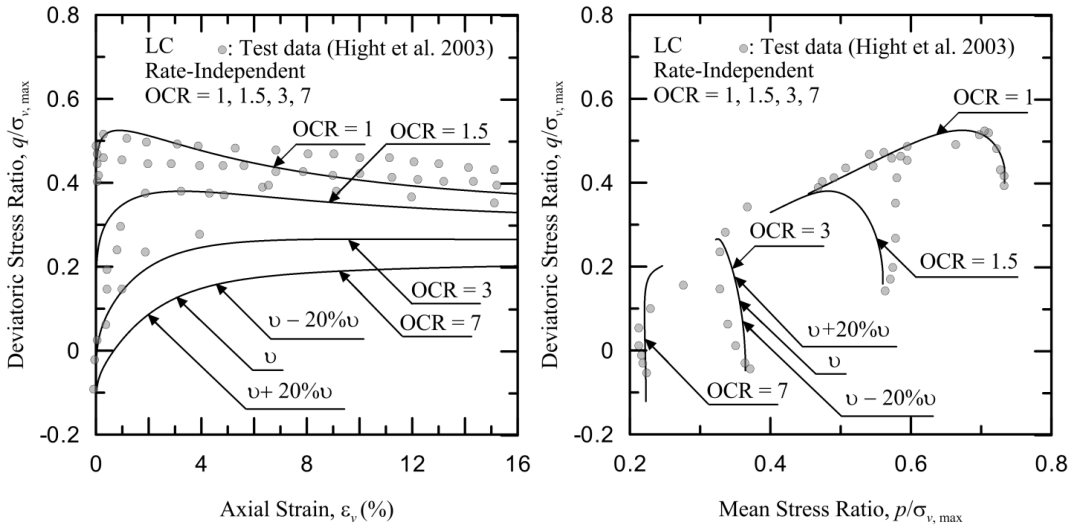

(Figure AI.1.151) Sensitivity of υ at 20% variation for London Clay, test data taken from Hight et al. (2003)

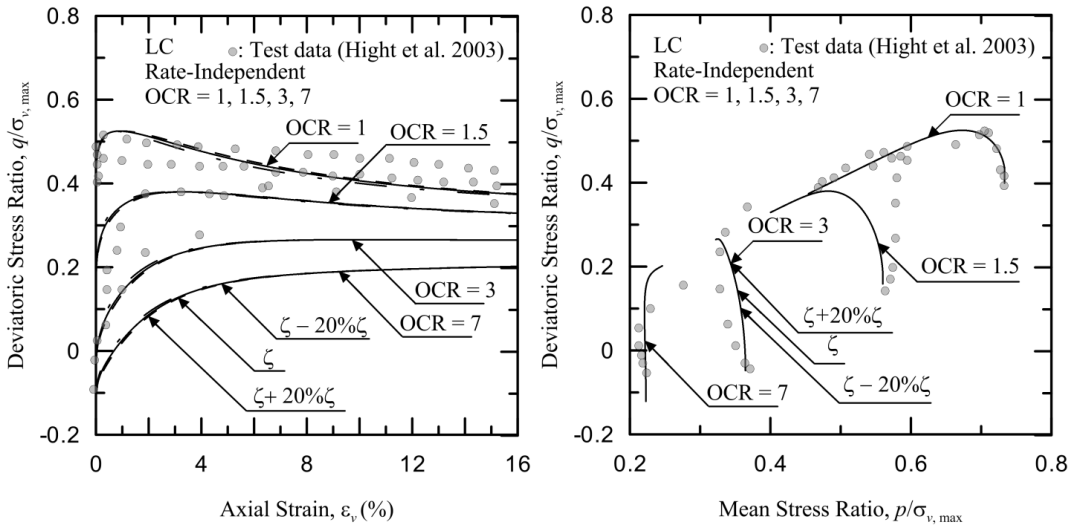

(Figure AI.1.152) Sensitivity of ζ at 20% variation for London Clay, test data taken from Hight et al. (2003)

Appendix II

AII.1 The Cutting Plane Algortithm

Of the return mapping methods two are commonly implemented, the closest point projection method (CPPM), and the cutting plane algorithm. The disadvantage with using the CPPM method or other Newton-Raphson methods is that they require the evaluation of the second derivative of their plastic potential function, often times in constitutive models evaluating this derivative is extremely difficult. Additionally, Newton-Raphson methods evaluate the derivatives of the plastic potential function within stress space outside of the yield surface, and in some instances this can cause divergence leading to instabilities in the constitutive model.

The cutting plane algorithm first begins with an intial stress state, $\sigma_{initial}$ the algorithm then creates an elastic stress prediction, if the algorithm predicts a new stress state in the viscoplastic domain (f>0), the behavior is plastic or in the case of time-dependent plasticty, viscoplastic. Since being outside the yeild surface violates the consistency condition, once outside the yeild surface a return path is iteratively plastically or viscoplastically relaxed to return to the yeild surface where f=0, or the final stress state σ_{final}. If the initial predicted stress state does not enter the plastic (for rate-independent) or viscoplastic domain (for rate-dependent) by touching or crossing the yeild surface then the behavior is elastic.

The consistency condition (Prager 1949) requeres that loading from a plastic state will result in another plastic deformation state. In plasticity this requires that the stress state remain on the yeild surface. In the proposed model, the stresss state is allowed to leave the yeild surface, but to satisfy the consistency condition it must return at the end of the correction loop (σ_{final}).

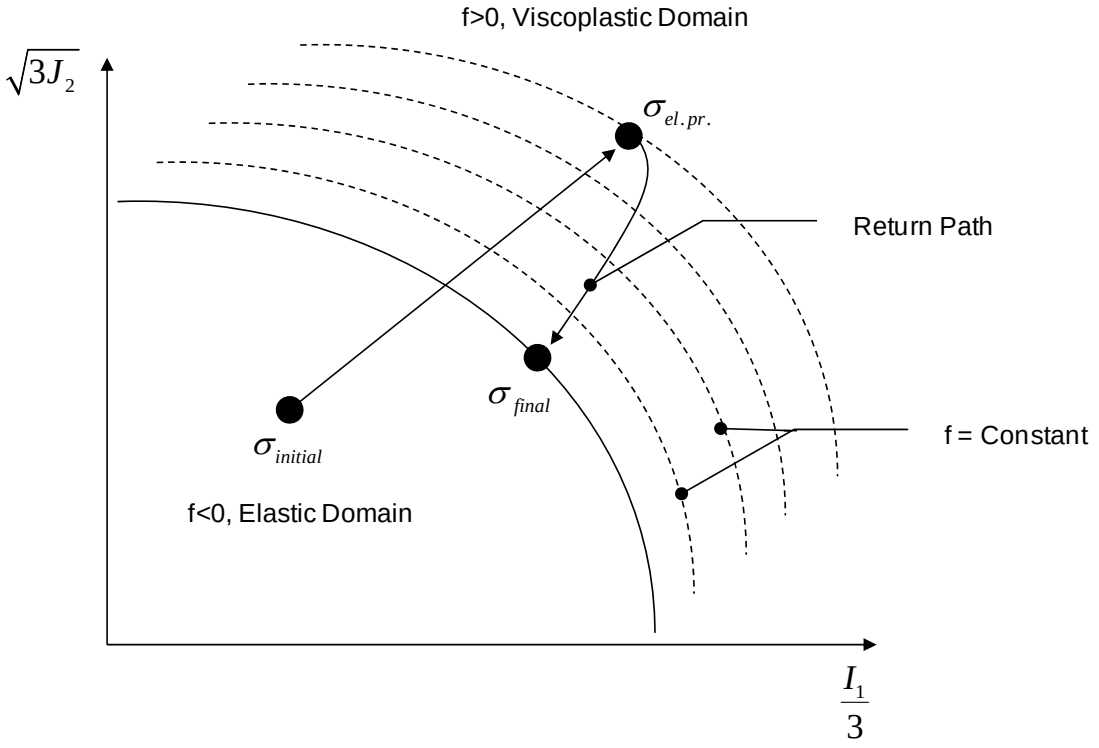

(Figure AII.1.1) Illustration of implicit stress-point algorithms
(After Ortiz and Simo, 1986)

In the proposed model the elastic and plastic components are evaluated independently, and then summed using the operator split technique. The operator split technique is described in Simo and Ortiz (1985). By utilizing this technique the loading step is fully elastic employing the elastic constitutive matrix, when the stress state is located on or outside the yield surface the stress is plastic or viscoplastic.

A review of stress-point algorithms can be found by Crisfield (1991), Abbo (1997), and Potts and Zdravkovic (1999). The cutting plane method was shown to be more computationally efficient than the CPPM, requiring fewer calculations (Manzari and Prachathananukit 2001). Figure AII.1.2 describes the numerical algorithm.

Numerical Algorithm for Rate Dependent Model

DATA INPUT : σ_n , $\dot{\varepsilon}$, $\Delta\varepsilon$

Trial Stresses : $\sigma_{n+1}^{trial} = \sigma_n + C\Delta\varepsilon$

If $f(\sigma_{n+1}) < 0$, elastic $\sigma_n = \sigma_{n+1}^{trial}$ RETURN

If $f(\sigma_{n+1}) \geq 0$, viscoplastic

Do While $f(\sigma_{n+1}) \geq 0$

a) Define initial iteration values $\dot{\lambda}$, $\Delta\sigma_n$

b) Update iteration values $\sigma_{n+1} = \sigma_n + \Delta\sigma_n$, $f(\sigma_{n+1})$ RETURN

OUTPUT : σ_{n+1} ,ε_{n+1}

(Figure AII.1.2) Numerical Algorithm for Rate-Dependent Model

AII.2 Rate-Dependent Model Proposed by Chakraborty (2009)

Chakraborty (2009) proposes a strain-rate-dependent modification to her rate-independent model. The equations are presented in table AII.2.1.

Description	Constitutive Equations	Parameter	References/Notes
Strain-Rate Dependence	$d_c = \sqrt{C_o\left[\xi_o^2 + \left(\bar{d}\right)^2\right]}$ $\bar{d} = \frac{\left\langle M_c - \sqrt{\frac{3}{2}}\sqrt{r:r}\right\rangle}{M_c}$ $p'_{ci} = \exp\left(\frac{\Gamma + (\lambda-\kappa)\ln(\rho) - e_{NC}}{(\lambda-\kappa)}\right)\frac{p'^{\frac{\lambda}{\lambda-\kappa}}_a}{p'^{\frac{\lambda}{\lambda-\kappa}}_c}$ $G_o = C_g \frac{(2.97-e_0)^2}{1+e_o} p'^{0.5} 100^{0.5} OCR^{0.2}\left(1 + b_{rate}\ln\left(1+\dot{\varepsilon}\right)\right)$	$a_{rate}, b_{rate}, c_{rate}, C_o$	Normalized distance of current stress state from Critical State Line Image Preconsolidation Pressure Strain rate dependent equation of G Chakraborty 2009

(Table AII.2.1) Rate-dependent equations from Chakraborty (2009)

AII.3 Cap Related Dilatancy Variable

The following presents a derivation the cap related dilatancy variable after Chakraborty (2009).

The mean stress rate and deviatoric stress rate can be expressed in terms of both the total volumetric strain-rate and the plastic strain-rate, in the case of the mean stress rate, for the deviatoric stress rate it can be expressed in terms of the total deviatoric strain-rate and the plastic deviatoric strain-rate. Where K is the bulk modulus of the soil and G is the shear modulus of the soil.

$$\dot{p} = K\left(\dot{\varepsilon}_v - \dot{\varepsilon}_v^p\right) \tag{AII.3.1}$$

$$\dot{q} = 3G\left(\dot{\varepsilon}_q - \varepsilon_q^p\right) \tag{AII.3.2}$$

Defining the ratio of deviatoric stress rate to mean stress rate as B

$$\frac{\dot{q}}{\dot{p}} = B \tag{AII.3.3}$$

where B can also be expressed as

$$B = \frac{1 - K_{o,NC}}{\frac{1}{3}\left(1 + 2K_{o,NC}\right)} \tag{AII.3.4}$$

and the plastic volumetric strain-rate can be expressed as

$$\dot{\varepsilon}_v^p = \frac{\dot{p}'_c}{p'_c}\frac{\lambda - \kappa}{1 + e} \tag{AII.3.5}$$

or

$$\dot{\varepsilon}_v^p = \frac{\lambda - \kappa}{1 + e}\exp\left(-\zeta\frac{p'_c - p'}{p'}\right)\frac{\langle \dot{p}' \rangle}{p'} \tag{AII.3.6}$$

thus the mean stress rate can be expressed as

$$\dot{p} = \frac{K\dot{\varepsilon}_v}{1+\frac{\lambda-\kappa}{1+e}\exp\left[-\zeta\frac{p'_c-p'}{p'}\right]\frac{K}{p'}} \tag{AII.3.7}$$

and the deviatoric stress rate can be expressed as

$$\dot{q} = \frac{BK\dot{\varepsilon}_v}{1+\frac{\lambda-\kappa}{1+e}\exp\left[-\zeta\frac{p'_c-p'}{p'}\right]\frac{K}{p'}} \tag{AII.3.8}$$

thus the plastic deviatoric strain-rate can be expressed as

$$\dot{\varepsilon}_q^p = \dot{\varepsilon}_v\left[\frac{2}{3}-\frac{\frac{BK}{3G}}{1+\frac{\lambda-\kappa}{1+e}\exp\left[-\zeta\frac{p'_c-p'}{p'}\right]\frac{K}{p'}}\right] \tag{AII.3.9}$$

thus

$$\frac{\dot{\varepsilon}_q^p}{\dot{\varepsilon}_v^p} = \frac{\left[\frac{2}{3}+\frac{2}{3}\frac{\lambda-\kappa}{1+e}\exp\left[-\zeta\frac{p'_c-p'}{p'}\right]\frac{K}{p'}-\frac{BK}{3G}\right]}{\frac{K}{p'}\frac{\lambda-\kappa}{1+e}\exp\left[-\zeta\frac{p'_c-p'}{p'}\right]} = \frac{1}{D^*} \tag{AII.3.10}$$

We note that for Isotropic consolidation, the term B=0.

Description	Constitutive Equations	Parameter	References/Notes
Stress-Strain Relations	$\dot{\sigma}'_{ij} = 2G\left(\dot{\varepsilon}_{ij} - \dot{\varepsilon}^{p}_{ij}\right) + \left(K - \frac{2}{3}G\right)\left(\dot{\varepsilon}_{kk} - \dot{\varepsilon}^{p}_{kk}\right)$		
Small-Strain Moduli	$G_o = C_g \frac{\left(2.97 - e_o\right)^2}{1 + e_o} p'^{0.5} 100^{0.5} OCR^{0.2}$ $K_i = G_o \frac{2\left(1+v\right)}{3\left(1-2v\right)}$	C_g, v	Small strain shear and bulk modulus, modified after Hardin and Richart (1963)
Elastic Moduli with Degradation	$G_{\min} = \frac{3\left(1-2v\right)}{2\left(1+v\right)} K_{\min}$ $K_{\min} = \frac{p'\left(1+e\right)}{\kappa}$ $G = G_{\min} + \left(G_o - G_{\min}\right)\exp\left[-\zeta\left(\frac{\left\|p' - p'_{ini}\right\|}{p_c} + \frac{\sqrt{3/2}\sqrt{\left(r_{ij} - \alpha_{ij,ini}\right)\left(r_{ij} - \alpha_{ij,ini}\right)}}{M_{cc}}\right)\right]$	v, ζ, κ	Large-strain shear and bulk modulus and the degradation equation of G

(Table AIII.1.1a) Rate-independent model constitutive equations

Description	Constitutive Equations	Parameter	References/Notes
Yield (Loading) Surface	$f = \sqrt{\left(s_{ij} - \alpha_{ij} p'\right)\left(s_{ij} - \alpha_{ij} p'\right)} - \sqrt{\frac{2}{3}} m p' = 0$	m	Manzari and Dafalias 1997, Loukidis and Salgado 2009
Bounding Dilatancy Critical State Surfaces	$M_d = g(\theta)\left(2M_{cc} + \frac{M_{cc} k_d \xi OCR}{1 - \exp\left(k_d \xi OCR\right)}\right)$ $M_c = g(\theta) M_{cc}$ $k_d = \frac{M_{cc}}{N - \Gamma}$	N	Modified after Dafalias and Manzari 2004, Loukidis and Salgado 2009
NC Line	$e_c = N - \lambda \ln\left(\frac{p'_c}{p'_a}\right)$	λ, N	
Shape of Dilatancy and Critical State surface in the π Plane	$g(\theta) = \frac{2^{n_s} c_1}{\left[1 + c_1^{1/n_s} - \left(1 - c_1^{1/n_s}\right)\cos(3\theta)\right]^{n_s}}$ $c_1 = \frac{M_{cc}}{3 + M_{cc}}$	n_s	Loukidis and Salgado 2009

(Table AIII.1.1b) Rate-independent model constitutive equations

Description	Constitutive Equations	Parameter	References/Notes
Plastic Modulus	$K_p = h_o \dfrac{G\ OCR}{\left[\sqrt{\frac{3}{2}}\sqrt{\left(r_{ij}-\alpha_{ij,ini}\right)\left(r_{ij}-\alpha_{ij,ini}\right)}\right]} \sqrt{\frac{2}{3}}\left(\sqrt{\frac{2}{3}}\left(M_b - m\right) - \alpha_{ij} n_{ij}\right)$	h_o	Modified after Li and Dafalias 2000, Loukidis and Salgado 2009
Non-Associated Flow Rule	$\dot{\varepsilon}_{ij}^{p} = \dot{\varepsilon}_{ij,shear}^{p} + \dot{\varepsilon}_{ij,cap}^{p}$ $\dot{\varepsilon}_{ij,shear}^{p} = \dot{\lambda}_{shear}\left(R'_{ij} + \frac{1}{3} D \delta_{ij}\right)$ $R'_{ij} = \dfrac{R'^{*}_{ij}}{\sqrt{R'^{*}_{ij} R'^{*}_{ij}}}$ $R'^{*}_{ij} = \left[1 + \frac{3}{2}\left(\frac{1-c_2}{c_2}\right) g_2(\theta)\cos(3\theta)\right] n_{ij} - \left[3\sqrt{\frac{3}{2}}\left(\frac{1-c_2}{c_2}\right) g_2(\theta)\right]\left(n_{ik} n_{kj} - \frac{1}{3}\delta_{ij}\right)$ $\dot{\varepsilon}_{ij,cap}^{p} = \dot{\lambda}_{cap}\left(\dfrac{\frac{1}{K} + \frac{1}{p'}\frac{\lambda-\kappa}{1+e} - \frac{B}{2G}}{\left[\frac{1}{p'}\frac{\lambda-\kappa}{1+e}\right]\left(\frac{B}{\sqrt{r_{ij} r_{ij}}}\right)} R'_{ij} + \frac{1}{3}\delta_{ij}\right)$ $B = \dfrac{1 - K_{o,NC}}{\frac{1}{3}\left(1 + 2K_{o,NC}\right)}$	c_2	Obtained from Dafalias and Manzari 2004, Loukidis and Salgado 2009 To incorporate clay behavior

(Table AIII.1.1c) Rate-independent model constitutive equations

Description	Constitutive Equations	Parameter	References/Notes
Dilatancy Equation	$D = \frac{D_o}{M_{cc} OCR}\left(\sqrt{\frac{2}{3}}\left(M_d - m\right) - \alpha_{ij} n_{ij}\right)$ $D_o = d_0 e^{\left(d_1 (1 - OCR)\right)}$	d_o, d_1	Dafalias and Manzari 2004, Loukidis and Salgado 2009 Modified to simulate OCR effects
Shape of Plastic Potential in π Plane	$g_2(\theta) = \frac{2c_2}{\left[\left(1 + c_2\right) - \left(1 + c_2\right)\cos\left(3\theta\right)\right]}$	c_2	Loukidis and Salgado 2009
Kinematic Hardening of Yield Surface	$\dot{\alpha}_{ij} = \dot{\lambda}_{shear} \frac{K_p}{p'} \frac{\left(\sqrt{\frac{2}{3}}\left(M_b - m\right) n_{ij} - \alpha_{ij}\right)}{\left(\sqrt{\frac{2}{3}}\left(M_b - m\right) - \alpha_{ij} n_{ij}\right)}$		Manzari and Dafalias 1997

(Table AIII.1.1d) Rate-independent model constitutive equations

Description	Constitutive Equations	Parameter	References/Notes
Stress-Strain Relations	$\dot{\sigma}'_{ij} = 2G\left(\dot{\varepsilon}_{ij} - \dot{\varepsilon}^{p}_{ij}\right) + \left(K - \frac{2}{3}G\right)\left(\dot{\varepsilon}_{kk} - \dot{\varepsilon}^{p}_{kk}\right)$		
Small-Strain Moduli	$G_o = C_g \frac{\left(2.97 - e_o\right)^2}{1 + e_o} p'^{0.5} 100^{0.5} OCR^{0.2} \left(1 + \log\left(1 + 5\left(\dot{\varepsilon}\right)^{0.09}\right)\right)$ $K_i = G_o \frac{2\left(1+v\right)}{3\left(1-2v\right)}$	C_g, v	Small strain shear and bulk modulus, modified after Hardin and Richart (1963)
Elastic Moduli with Degradation	$G_{\min} = \frac{3\left(1-2v\right)}{2\left(1+v\right)} K_{\min}$ $K_{\min} = \frac{p'\left(1+e\right)}{\kappa}$ $G = G_{\min} + \left(G_o - G_{\min}\right)\exp\left[-\zeta\left(\frac{\left\|p' - p'_{ini}\right\|}{p_c} + \frac{\sqrt{3/2}\sqrt{\left(r_{ij} - \alpha_{ij,ini}\right)\left(r_{ij} - \alpha_{ij,ini}\right)}}{M_{cc}}\right)\right]$	v, ζ, κ	Large-strain shear and bulk modulus and the degradation equation of G

(Table AIV.1.1a) Rate-dependent model constitutive equations

Description	Constitutive Equations	Parameter	References/Notes
Yield (Loading) Surface	$f=\sqrt{\left(s_{ij}-\alpha_{ij}p'\right)\left(s_{ij}-\alpha_{ij}p'\right)}-\sqrt{\frac{2}{3}}mp'=0$	m	Manzari and Dafalias 1997, Loukidis and Salgado 2009
Bounding Dilatancy Critical State Surfaces	$M_d=g(\theta)\left(2M_{cc}+\frac{M_{cc}k_d\xi OCR}{1-\exp(k_d\xi OCR)}\right)$ $M_c=g(\theta)M_{cc}$ $k_d=\frac{M_{cc}}{N-\Gamma}$	N	Modified after Dafalias and Manzari 2004, Loukidis and Salgado 2009
NC Line	$e_c=N-\lambda\ln\left(\frac{p'_c}{p'_a}\right)$	λ, N	
Shape of Dilatancy and Critical State surface in the π Plane	$g(\theta)=\frac{2^{n_s}c_1}{\left[1+c_1^{1/n_s}-\left(1-c_1^{1/n_s}\right)\cos(3\theta)\right]^{n_s}}$ $c_1=\frac{M_{cc}}{3+M_{cc}}$	n_s	Loukidis and Salgado 2009

(Table AIV.1.1b) Rate-dependent model constitutive equations

Description	Constitutive Equations	Parameter	References/Notes
Plastic Modulus	$K_p = h_o \dfrac{G\ OCR}{\left[\sqrt{\frac{3}{2}}\sqrt{\left(r_{ij}-\alpha_{ij,ini}\right)\left(r_{ij}-\alpha_{ij,ini}\right)}\right]} \sqrt{\frac{2}{3}}\left(\sqrt{\frac{2}{3}}\left(M_b - m\right) - \alpha_{ij} n_{ij}\right)$	h_o	Modified after Li and Dafalias 2000, Loukidis and Salgado 2009
Non-Associated Flow Rule	$\dot{\varepsilon}_{ij}^{p} = \dot{\varepsilon}_{ij,shear}^{p} + \dot{\varepsilon}_{ij,cap}^{p}$ $\dot{\varepsilon}_{ij,shear}^{p} = \dot{\lambda}_{shear}\left(R'_{ij} + \frac{1}{3} D \delta_{ij}\right)$ $R'_{ij} = \dfrac{R'^{*}_{ij}}{\sqrt{R'^{*}_{ij} R'^{*}_{ij}}}$ $R'^{*}_{ij} = \left[1 + \frac{3}{2}\left(\frac{1-c_2}{c_2}\right) g_2(\theta)\cos(3\theta)\right] n_{ij} - \left[3\sqrt{\frac{3}{2}}\left(\frac{1-c_2}{c_2}\right) g_2(\theta)\right]\left(n_{ik} n_{kj} - \frac{1}{3}\delta_{ij}\right)$ $\dot{\varepsilon}_{ij,cap}^{p} = \dot{\lambda}_{cap}\left(\dfrac{\frac{1}{K} + \frac{1}{p'}\frac{\lambda-\kappa}{1+e} - \frac{B}{2G}}{\left[\frac{1}{p'}\frac{\lambda-\kappa}{1+e}\right]\left(\frac{B}{\sqrt{r_{ij} r_{ij}}}\right)} R'_{ij} + \frac{1}{3}\delta_{ij}\right)$ $B = \dfrac{1 - K_{o,NC}}{\frac{1}{3}\left(1 + 2K_{o,NC}\right)}$	c_2	Obtained from Dafalias and Manzari 2004, Loukidis and Salgado 2009 To incorporate clay behavior

(Table AIV.1.1c) Rate-dependent model constitutive equations

Description	Constitutive Equations	Parameter	References/Notes
Dilatancy Equation	$D = \frac{D_o}{M_{cc} OCR}\left(\sqrt{\frac{2}{3}}\left(M_d - m\right) - \alpha_{ij} n_{ij}\right)$		Dafalias and Manzari 2004, Loukidis and Salgado 2009
Shape of Plastic Potential in π Plane	$g_2(\theta) = \frac{2c_2}{\left[\left(1+c_2\right) - \left(1+c_2\right)\cos\left(3\theta\right)\right]}$	c_2	Loukidis and Salgado 2009
Kinematic Hardening of Yield Surface	$\dot{\alpha}_{ij} = \dot{\lambda}_{shear} \frac{K_p}{p'} \frac{\left(\sqrt{\frac{2}{3}}\left(M_b - m\right) n_{ij} - \alpha_{ij}\right)}{\left(\sqrt{\frac{2}{3}}\left(M_b - m\right) - \alpha_{ij} n_{ij}\right)}$		Manzari and Dafalias 1997

(Table AIV.1.1d) Rate-dependent model constitutive equations

Description	Constitutive Equations	Parameter	References/Notes
Strain-Rate Dependence	$\Gamma_0 = \Gamma\left(1 + c_0\left(\log\left(\frac{c_0}{10}\dot{\varepsilon} + 1\right)\right)\log\left(d_c + 1\right)\right)$	$\dot{\varepsilon}$, c_0, d_0, d_1	
	$d_c = \sqrt{c_0\xi_0^2 + c_0\left(\frac{M_{cc} - \eta}{M_{cc}}\right)^2}$		Rate-dependent State parameter
	$\xi_0 = e - \Gamma + \lambda\log\left(\frac{p}{100}\right)$		
	$\xi = e - \Gamma_0 + \lambda\log\left(\frac{p}{100}\right)$		Rate-dependent Dilatancy parameter
	$D_0 = d_0\left(\left(1 + \left(\log\left(\dot{\varepsilon} + 1\right)\right)\right)e^{\left(d_1(1 - OCR)\right)}\right)$		
	$P_c = P_1\left(1.3\left(\dot{\varepsilon}\right)^{0.05}\right)$		Rate-dependent Cap term

(Table AIV.1.1e) Rate-dependent model constitutive equations

LIST OF REFERENCES

1. Abbo, A. J. (1997). "Finite Element Algorithms for Elastoplasticity and Consolidation." *Ph.D. Dissertation*, University of Newcastle, Australia.

2. Abdel-Hady, M., and Herrin., M. (1966). "Characteristics of Soil-Asphalt as a Rate Process." *Journal of the Highway Division, Proceedings of ASCE*, 92(HW1), 49–69.

3. Adachi, T., and Oka, F. (1982a). "Constitutive Equations for Normally Consolidated Clay Based on Elasto-viscoplasticity." *Soils and Foundations*, 22(4), 57-70.

4. Adachi, T., and Oka, F. (1982b). ''Constitutive Equations for Normally Consolidated Clays and Assigned Works for Clay.'' *Results of the International Workshop on Constitutive Relations for Soils* (Grenoble, G. Gudehus et al., eds.), 123–140.

5. Adachi, T., and Okano, M. (1974). "A Constitutive Equation for Normally Consolidated Clay." *Soils and Foundations*, 14, 55–73.

6. Adachi, T., Oka, F., and Mimura, M. (1987). ''Mathematical Structure of an Overstress Slasto-viscoplastic Model for Clay.'' *Soils and Foundations*, 27(3), 31–42.

7. Adachi, T., Oka, F., and Mimura, M. (1996). ''State of the art: Modeling Aspects Associated with Time Dependent Behavior of Soils.'' *Measuring and Modeling Time Dependent Soil Behavior, ASCE, Geotechnical Special*

Publication No. 61 (T. C. Sheahan and V. N. Kaliakin, eds.), New York, 61–95.

8. Adachi, T., Oka, F., and Poorooshasb, H. B. (1990). ‘‘A Constitutive Model for Frozen Sand.’’ *Transactions of the ASME*, 112, 208–212.

9. Adachi, T., Oka, F., and Zhang, F. (1997). ‘‘An Elasto-viscoplastic Constitutive Model With Strain Softening.’’, *Numerical Models in Geomechanics* (S. Pietruszczak and G. Pande, eds.), Balkema, Rotterdam, The Netherlands, 81–86.

10. Akai, K., Adachi, T., Ando, N. (1975). “Existence of a Unique Stress Strain-Time Relation of Clays.” *Soils and Foundations*, 15(1), 1-16.

11. Alberro, J. and Santoyo, E. (1973). "Long Term Behavior of Mexico City Clay", *Proceedings, 8th ICSMFE*, Moscow, 1, 1-9.

12. Al-Tabbaa, A, Stegemann, J.A. (2005). “Stabilization/Solidification Treatment and Remediation: Advances in s/s for Waste and Contaminated Land.” *Proceedings of the International Conference on Stabilization/Solidification Treatment and Remediation*, University of Cambridge, United Kingdom, 12-13.

13. Atkinson, J .H. and Richardson, D. (1987). "The Effect of Local Drainage in Shear Zones on the Undrained Strength of Overconsolidated Clay." *Géotechnique*, 37(3), 393-403.

14. Bardet, J. P. (1986). “Bounding Surface Plasticity Model for Sands.” *Journal of Engineering Mechanics*, 112 (11), 1198-1217.

15. Been, K. and Jefferies, M. G. (1985). "A State Parameter for Sands." *Géotechnique*, 35(2), 99-112.

16. Berre, T. and Bjerrum, L. (1973). "Shear Strength of Normally Consolidated Clays." *Proceedings of 8th International Conference on Soil Mechanics and Foundation Engineering,* 1, 39–49.

17. Biscontin, G., (2001). "Modeling the Dynamic Behavior of Lightly Overconsolidated Soil Deposits on Submerged Slopes." *PhD thesis,* University of California, Berkeley, USA.

18. Biscontin, G. and Pestana, J. M. (2001). "Influence of Peripheral Velocity on Vane Shear Strength of an Artificial Clay." *ASTM Geotechnical Journal*, 24(4), 423-429.

19. Bjerrum, L. (1967). "Engineering Geology of Norwegian Normally Consolidated Marine Clays as Related to Settlements of Buildings." *Géotechnique*, 17(2), 81-118.

20. Bjerrum, L., Simons, N. and Torblaa, I. (1958). "The Effect of Time on the Shear Strength of Soft Marine Clay." *Proceedings of Brussels Conference on Earth Pressure Problems*, 1, 148–158.

21. Borja, R. I. (1992). ''Generalized Creep and Relaxation Model for Clays.'' *Journal of Geotechnical Engineering*, *ASCE,* 118(11), 1765–1786.

22. Borja, R. I. and Kavazanjian, E. (1985). ''A Constitutive Model for the Stress–Strain–Time Behaviour ''Wet'' Clays.'' *Géotechnique*, 35 (3), 283–298.

23. Borja, R. I., Kavazanjian, E., Jr., Hsieh, H. S. (1990). ‘‘Double-Yield Surface Cam-Clay Plasticity Model: II. Implementation and Verification.’’ *Journal of Geotechnical Engineering*, *ASCE,* 116 (9), 1402–1421.

24. Bouchard, R., (1982). “Effet de la Vitesse Sur le Comportement Oedomètrique de l’argil de Batiscan.” *M.Sc. Thesis*, Universitè Laval, Quebec, P.Q.

25. Boukpeti, N., Mróz, Z., Drescher, A. (2002). “A Model for Static Liquefaction in Triaxial Compression and Extension.” *Canadian Geotechnical Journal*, 39(6), 1243–1253.

26. Boukpeti, N., Mróz, Z., Drescher, A. (2004) “Modeling Rate Effects in Undrained Loading of Sands.” *Canadian Geotechnical Journal*, 41(2), 342–350.

27. Casagrande, A. and Shannon, W. L. (1948). “Strength of Soils Under Dynamic Loads.” *Proceedings of the American Society of Civil Engineers*, 74(4), 591–608.

28. Chakraborty, T. (2009). “Development of a Clay Constitutive Model and its Application to Pile Boundary Value Problems.” *PhD Thesis,* Purdue University, West Lafayette, USA.

29. Christensen R.W. and Wu T.H. (1964). “Analysis of Clay Deformation as a Rate Process.” *Journal of Soil Mechanics and Foundation Division, ASCE*, 90(6), 125-157.

30. Crawford, C. B. (1959). “The Influence of Rate of Strain on Effective Stresses in Sensitive Clay.” *ASTM Special Technical Publication*, no. 254, 36–68.

31. Crisfield, M. A. (1991). “Non-Linear Finite Element Analysis of Solids and Structures.” Vol. 1, *John Wiley & Sons*, New York.

32. Cristescu, N. (1991). ‘‘Nonassociated Elastic Viscoplastic Constitutive Equations for Sand.’’ *International Journal of Plasticity*, 6, 41–64.

33. Dafalias, Y. F. (1982). ‘‘Bounding Surface Elastoplasticity-Viscoplasticity for Particulate Cohesive Media.’’ *International Union of Theoretical and Applied Mechanics Conference on Deformation and Failure of Granular Materials* (P. A. Vermeer and H. J. Luger, eds.), 97–107.

34. Dafalias, Y. F. and Manzari, M. T. (2004). “Simple Plasticity Sand Model Accounting for Fabric Change Effects.” *Journal of Engineering Mechanics*, *ASCE*, 130(6), 622- 634.

35. Dafalias, Y. F., Manzari, M. T. and Papadimitriou, A. G. (2006). “SANICLAY: Simple Anisotropic Clay Plasticity Model.” *International Journal of Numerical and Analytical Methods in Geomechanics*, 30, 1231–1257.

36. Dafalias, Y. F., Papadimitriou, A. G. and Li, X. S. (2004). “Sand Plasticity Model Accounting for Inherent Fabric Anisotropy.” *Journal of Engineering Mechanics*, *ASCE*, 130(11), 1319-1333.

37. Desai, C. S., and Zhang, D. (1987). ‘‘Viscoplastic Model for Geological Materials with Generalized Flow Rule.’’ *International Journal of Numerical and Analytical Methods in Geomechanics*, 11, 603–620.

38. Di Benedetto, H., Tatsuoka, F., Ishihara, M. (2002). "Time-Dependent Deformation Characteristics of Sand and Their Constitutive Modeling." *Soils and Foundations*, 42(2), 1-22.

39. di Prisco C. and Imposimato S. (2003). "Non Local Numerical Analyses of Strain Localization in Dense Sand." *Mathematical and Computer Modeling*, 37, 497-506.

40. di Prisco C., Imposimato S., Aifantis E. C., (2002). "A Visco-plastic Constitutive Model for Granular Soils Modified According to Non-local and Gradient Approaches." *International Journal of Numerical and Analytical Methods in Geomechanics,* 26, 121-138.

41. di Prisco, C., and Imposimato, S. (1996). ''Time Dependent Mechanical Behaviour of Loose Sands.'' *Mechanics of Cohesive-Frictional Materials*, 1(1), 45– 73.

42. di Prisco, C., Imposimato, S., and Vardoulakis, I. (2000). ''Mechanical Modeling of Drained Creep Triaxial Tests on Loose Sand.'' *Géotechnique*, 50(1), 73–82.

43. Díaz-Rodríguez, J. A., Martínez-Vasquez, J. J., Santamarina, J. C. (2009). "Strain-Rate Effects in Mexico City Soil." *Journal of Geotechnical and Geoenvironmental Engineering*, *ASCE*, 135(2), 300-305.

44. Fearon, R. E., Chandler, R. J. and Bommer, J. J. (2004). "An Investigation of the Mechanisms Which Control Soil Behavior at Fast Rates of Displacement."

Proceedings of Advances in Geotechnical Engineering: the Skempton Conference, Thomas Telford, London.

45. Feda, J. (1992). "Creep of Soils and Related Phenomena, developments in Geotechnical Engineering." *Elsevier Science*, North–Holland, Amsterdam, The Netherlands, 68.
46. Gasparre, A. (2005). "Advanced Laboratory Characterization of London Clay," *PhD Thesis*, Imperial College London.
47. Gasparre, A., Nishimura, S., Minh, N. A., Coop, M. R., Jardine, R. J. (2007a). "The Stiffness of Natural London Clay." *Géotechnique*, 57(1), 33-7.
48. Gasparre, A., Nishimura, S., Coop, M. R., and Jardine, R. J. (2007b). "The Influence of Structure on the Behaviour of London Clay." *Géotechnique*, 57(1), 19-31.
49. Hájek, V., Mašín, D., and Boháč, J. (2009). "Capability of Constitutive Models to Simulate Soils with Different OCR Using a Single Set of Parameters." *Computers and Geotechnics*, 36, 655-664.
50. Hardin, B. O. (1978). "The Nature of Stress-Strain Behavior of Soils", State-of – the-Art Report, Proceedings of the ASCE Specialty Conference on Earthquake Engineering and Soil Dynamics, Pasadena, 1978, 3-90.
51. Hardin, B. O. and Richart, F. E., Jr. (1963). "The Nature of Stress-Strain Behavior of Soils." *Journal of Soil Mechanics and Foundations Division*, *ASCE*, 89(1), 33-65.
52. Hicher, P.Y. (1988). "The Viscoplastic Behavior of Bentonite." in *Rheology*

53. Hight, D.W., Gens, A., De Campos, T.M.P. and Takahashi, M. (1983). "Factors Influencing the Interpretation of *In-situ* Strength Tests in Insensitive Low Plasticity Clays." *Behaviour of Off-Shore Structures, Proceedings of the International Conference*, 2, 438-450.

54. Hight, D.W., McMillan, F., Powell, J.J.M., Jardine, R.J., Allenou, C.P. (2003). "Some Characteristics of London Clay," Characterization of Engineering Properties of Natural Soils, Balkema, pp.851-908.

55. Hinchberger, S. D. and Rowe, K. R. (2005). "Evaluation of the Predictive Ability of Two Elastic-Viscoplastic Constitutive Models." *Canadian Geotechnical Journal,* 42, 1675–1694.

56. Hohenemser, K. and Prager, W. (1932). ''Uber die Ansatze der Mechanic Isotroper Kontinua.'' *Z. Angew. Math. Mech.,* 12, 216–226.

57. Hsieh, H. S., Kavazanjian, E., Borja, R. I. (1990). ''Double-Yield Surface Cam-Clay Plasticity Model. I: Theory.'' *Journal of Geotechnical Engineering*, *ASCE,* 116(9), 1381–1401.

58. Hueckel, T. and Nova, R. (1979). "Some Hysteresis Effects of the Behavior of Geologic Media." International Journal of Solids and Structures, 15(8), 625-642.

59. Jung, B. C. (2005). "Modeling of Strain Rate Effects on Clays in Simple Shear." *Masters Thesis*, Texas A&M University, Texas, USA.

60. Jung, B. C. and Biscontin, G. (2006). "Modeling of Strain Rate Effects on Clay in Simple Shear." GeoCongress.

61. Kaliakin, V. N. (1985). “Bounding Surface Elastoplasticity Viscoplasticitv for Clays.” *Doctorate Dissertation*, University of California.

62. Kaliakin, V. N. and Dafalias, Y. F. (1990a). “Theoretical Aspects of the Elastoplastic-Viscoplastic Bounding Surface Model for Cohesive Soils.” *Soils and Foundations*, 30(3), 11-24.

63. Kaliakin, V. N. and Dafalias, Y. F. (1990b). “Verification of the Elastoplastic-Viscoplastic Bounding Surface Model for Cohesive Soils.” *Soils and Foundations*, 30(3), 25-36.

64. Kaliakin, V. N. and Dafalias, Y. F. (1991). “Details Regarding the Elastoplastic-Viscoplastic Bounding Surface Model for Isotropic Cohesive Soils.” *Civil Engineering Report No. 91-1*, University of Delaware, Newark, Delaware.

65. Katona, M. G. (1984). ‘‘Evaluation of Viscoplastic Cap Model.’’ *J. Geotech. Eng.,* 110(8), 1106–1125.

66. Katti, D. R., Tang, J., Yazdani, S. (2003). “Undrained Response of Clays to Varying Strain Rate.” *Journal of Geotechnical and Geoenvironmental Engineering*, ASCE, 129(3), 278-282.

67. Kavazanjian, E., and Mitchell, J. K. (1977). ‘‘A General Stress–Strain–Time Formulation for Soils.’’ *Proceedings of 9th International Conference on Soil Mechanics and Foundation Engineering*, 113–120.

68. Kavazanjian, E., and Mitchell, J. K. (1980). “Time-Dependent Deformation Behavior of Clays.” *Journal of Geotechnical and Geoenvironmental Engineering*, ASCE, 106(6), 611-630.

69. Kulhawy, F. H. and Mayne, P. W. (1990). “Manual on Estimating Soil Properties for Foundation Design." *Report. EL-6800, Electric Power Research Institute,* Palo Alto.

70. Kutter, B. L. and Sathialingam, N. (1992). “Elastic-Viscoplastic Modeling of the Rate-Dependent Behavior of Clays.” *Géotechnique*, 42 (3), 427–441.

71. Lacerda, W. A. and Houston, W. N. (1973). ‘‘Stress Relaxation in Soils.’’ *Proceedings of 8th International Conference on Soil Mechanics and Foundation Engineering*, 1/34, 221–227.

72. Ladd, C.C. and Varallyay, J. (1965). The influence of the stress system on the behavior of saturated clays during undrained shear. Research Report No R65-11, Department of Civil Engineering, MIT, Cambridge, MA.

73. Ladd, C.C., C.E. Williams, D.H., Connell, L., Edgers (1972). "Engineering Properties of Soft Foundation Clays at Two South Louisiana Levee Sites." *MIT Res. Rpt. No. R72-26*.

74. Leahy, D. (1980). “Contribution á l’étude du Comportement Oedométrique des Argiles.” *M.Sc. Thesis*, Université Laval, Quebec, P.Q.

75. Leblond, P. (1981). “Mesure et Caractéristiques de la Perméabilité des Argiles Champlain.” *M.Sc. Thesis*, Université Laval, Quebec, P.Q.

76. Lefebvre, G. and LeBoeuf, D. (1987). “Rate Effects and Cyclic Loading of Sensitive Clays.” *Journal of Geotechnical Engineering*, *ASCE,* 113(5), 476–489.

77. Leroueil, S., Tavenas, F., Trak, B., La Rochelle, P., Roy, M., (1978). "Construction pore pressures in clay foundations under embankments. Part I: the Saint-Alban test fills." *Canadian Geotechnical Journal*, 15(1), 54-65.

78. Leroueil, S., Tavenas, F., Samson, L., Morin, P. (1983). "Preconsolidation Pressure of Champlain Clays – Part II: Laboratory Determination." *Canadian Geotechnical Journal*, 20(4), 803-816.

79. Li, X. S. and Dafalias, Y. F. (2000). "Dilatancy of Cohesionless Soils." *Géotechnique*, 50(4), 449-460.

80. Liingaard, M., Augustensen, A., Lade, P. V. (2004). "Characterization of Models for Time-Dependent Behavior of Soils." *Int. J. Geomech. ASCE*, 4(3), 157-177.

81. Ling, H. I., Yue, D., Kaliakin, V., Themelis, N.J. (2002). "An Anisotropic Elasto-Plastic Bounding Surface Model for Cohesive Soils" *Journal of Engineering Mechanics*, *ASCE*, 128(7), 748-758.

82. Loukidis, D. (2006). "Advanced Constitutive Modeling of Sands and Applications to Foundation Engineering." *Doctoral Dissertation*, Purdue University, West Lafayette, USA.

83. Loukidis, D. and Salgado, R. (2009). "Modeling Sand Response Using Two-Surface Plasticity." *Computers and Geotechnics*, 36, 166–186.

84. Ludwick, P. (1922). ''Uber den Einfluss der Deformationsgeschwindigkeit bei bleibenden Deformationen mit besonderer Berucksichtigung der Nachwirkungserscheinungen.'' *Phys. Z.,* 10(12), 411–417.

85. Lupini, J. F. (1980). “The Residual Strength of Soils.” *Doctoral Dissertation*, University of London.

86. Lupini, J. F., Skinner, A. E., Vaughan, P. R. (1981). "The Drained Residual Strength of Cohesive Soils." *Géotechnique*, 31(2), 181-213.

87. Malvern, L. E. (1951). ‘‘The Propagation of Longitudinal Waves of Plastic Deformation in a Bar of Metal Exhibiting a Strain Rate Effect.’’ *J. Appl. Mech.,* 18, 203–208.

88. Manzari, M. T. (1994). “Finite Deformation Analysis and Constitutive Modeling of Non-cohesive Soils for Liquefaction Problems.” *Doctoral Dissertation*, University of California, Davis.

89. Manzari, M. T. and Dafalias, Y. F. (1997). “A Critical State Two-Surface Plasticity Model for Sands.” *Géotechnique*, 47(2), 255-272.

90. Marchand, G. (1982). “Quelques Considerations sur le Comportement Avant Rupture des Pentes Argileuses Naturelles.” *M.Sc. Thesis*, Université Laval, Quebec, P.Q.

91. Matešić, L. and Vucetic, M. (2003). “Strain-Rate Effect on Soil Secant Modulus at Small Cyclic Strains.” *Journal of Geotechnical and Geoenvironmental Engineering*, ASCE, 129(6), 536–549.

92. Manzari, M. T. and Prachathananukit, R. (2001). “On Integration of a Cyclic Soil Plasticity Model.” *International Journal for Numerical Methods in Engineering*, 25(6), 525-549.

93. Mesri, G. (1973). ‘‘Coefficient of Secondary Compression.’’ *Journal of Soil Mechanics and Foundation Division, ASCE*, 99(1), 123–137.

94. Mesri, G. and Godlewski, P. M. (1977). ‘‘Time and Stress-Compressibility Interrelationship.’’ *Journal of Geotechnical Engineering*, *ASCE,* 103(5), 417–430.

95. Mimura, M. and Sekiguchi, H. (1985). ‘‘A Review of Existing Viscoplastic Constitutive Models Regarding the Performance of Creep Rupture Prediction.’’ *Proc., 40th Japan Nat. Conf., JSCE*, 1097–1100 (in Japanese).

96. Morin, P., Leroueil, S., Samson, L. (1983). “Preconsolidation Pressure of Champlain Clays. Part I. In-Situ Determination.” *Canadian Geotechnical Journal*, 20(4), 782-802.

97. Mukabi J.N. and Tatsuoka F. (1999) “Influence of Reconsolidation Stress History and Strain Rate on the Behaviour of Kaolin Over a Wide Range of Strain.” 12th ARC: Geotechnics for Developing Africa, Durban, South Africa., 365-377.

98. Murayama, S. and T. Shibata (1964). "Flow and Stress Relaxation of Clays." *Intl. Union of Theoretical and Appl. Mech., Symposium on Rheology and Soil Mechanics*, Grenoble, 99-129.

99. Nishimura, S. (2005). “Laboratory study on anisotropy of natural London Clay.” *PhD Thesis*, Imperial College London.

100. Murayama, S. and Shibata, T. (1958). ‘‘On the Rheological Characteristic of Clay, Part I’’. *Bulletin no. 26,* Kyoto University, Japan.

101. Oka, F. (1985). ‘‘Elasto-Viscoplastic Constitutive Equations with Memory and Internal Variables.’’ *Comput. Mech.,* 1, 59–69.

102. Oka, F., Adachi, T., Mimura, M. (1988). ‘‘Elasto-Viscoplastic Constitutive Models for Clays.’’ *Proceedings of International Conference on Rheology and Soil Mechanics*, Elsevier, Science, New York, 12–28.

103. Oka, F., Adachi, T., Yashima, A. (1994). “Instability of an Elasto-Viscoplastic Constitutive Model for Clay and Strain Localization.” *Mechanics of Materials*, 18, 119–129.

104. Oka, F. and Adachi, T. (1985). ‘‘An Elasto-Plastic Constitutive Equation of Geologic Materials with Memory.’’ *Proceedings of 5th International Conference on Numerical Methods in Geomechanics*, 293–300.

105. Oka, F., Higo, Y., Kimoto, S. (2002). “Effect of Dilatancy on the Strain Localization of Water-Saturated Elasto-Viscoplastic Soil.” *International Journal of Solids and Structures,* 39, 3625–3647.

106. Oka, F., Kodaka, T., Kim, Y. (2004). “A Cyclic Viscoelastic-Viscoplastic Constitutive Model for Clay and Liquefaction Analysis of Multi-Layered Ground.” *International Journal for Numerical and Analytical Methods in Geomechanics*, 28(2), 131-179.

107. Olszak, W. and Perzyna, P. (1966a). ‘‘On Elastic-Viscoplastic Soils, Rheology and Soil Mechanics.’’ *International Union of Theoretical and Applied Mechanics Symposium, Grenoble*, Springer, Berlin.

108. Olszak, W. and Perzyna, P. (1966b). ‘‘The Constitutive Equations of the Flow Theory for a Nonstationary Yield Condition.’’ *Proceedings of 11th International Congress of Applied Mechanics*, Springer, Berlin, 545–553.

109. Olszak, W. and Perzyna, P. (1970). Stationary and Nonstationary Viscoplasticity, McGraw-Hill, New York, 53–75.

110. O'Reilly, M.P., S.F. Brown, R.F. Overy (1989). "Viscous Effects Observed in Tests on an Anisotropically Normally Consolidated Silty Clay." *Géotechnique*, 39(1), 153-158.

111. Ortiz, M. and Simo, J. C. (1986). "An Analysis of a New Class of Integration Algorithms for Elastoplastic Constitutive Relations." 23, 353-366.

112. Papadimitriou, A. G. and Bouckovalas, G. D. (2002). "Plasticity Model for Sand Under Small and Large Cyclic Strains: a Multiaxial Formulation." *Soil Dynamics and Earthquake Engineering*, 22 (3), 191-204.

113. Paquin, G. (1983). "Contribution á l'étude de la Déstructuration et Restructuration des Argiles Sensible." *M.Sc. Thesis*, Université Laval, Quebec, P.Q.

114. Perzyna, P. (1963). "The Constitutive Equations for Rate Sensitive Plastic Materials." *Quarterly of Applied Mathematics,* 20, 321-332.

115. Perzyna, P. (1966). "Fundamental Problems in Viscoplasticity." *Advances in Applied Mechanics*, 9, 244–377.

116. Potts, D. M. and Zdravkovic L. (1999). "Finite Element Analysis in Geotechnical Engineering: Theory," *Thomas Telford, Ltd.*

117. Prager, W. (1949), "Recent Developments in the Mathematical Theory of Plasticity", Journal of Applied Physics, 20(3), 235-241.

118. Prandtl, L. (1928). *Z. Angew. Math. Mech.* 8, 249-251.

119. Prashant, A. (2004). "Three-Dimensional Mechanical Behavior of Kaolin Clay with Controlled Microfabric Using True Triaxial Testing." *PhD. Dissertation*, University of Tennessee, Knoxville, USA.

120. Ramiah, B. K., Dayalu, N. K., Purushothamaraj, P. (1970). "Influence of Chemicals on Residual Strength of Silty Clay." *Soils and Foundations*, 10, 25-36.

121. Richardson, A. M., Jr., and Whitman, R. V. (1963). "Effect of Strain-Rate Upon Undrained Shear Resistance of a Saturated Remoulded Fat Clay." *Géotechnique*, 13(4), 310–324.

122. Samson, L., Leroueil, S., Morin, P., Le Bihan, J., P. (1981). "Pression de Préconsolidation des Argiles Sensibles." Report prepared for the Division of Building Research of the National Research Council of Canada, Ottawa, Ont., 5 vols., 850p.

123. Schofield, A.N. and Wroth, C.P. (1968). *Critical State Soil Mechanics*, McGraw-Hill, London.

124. Sekiguchi, H. (1985). ''Macrometric Approaches—Static—Intrinsically Time Dependent Constitutive Laws of Soils.'' *Rep., ISSMFE Subcommittee on Constitutive Laws of Soils and Proc. of Discussion Session 1A*, Int. Society of Soil Mechanics and Foundation Engineering, Subcommittee on Constitutive Laws of Soils, *11th ICFMFE*, San Francisco, 66–98.

125. Sheahan TC. (1991). "An Experimental Study of the Time-Dependent Undrained Shear Behavior of Resedimented Clay Using Automated Stress Path Equipment." *Doctoral Dissertation*, MIT, Cambridge, MA.

126. Sheahan, T.C., Ladd, C.C., Germaine, J.T. (1996). “Rate Dependent Undrained Shear Behaviour of Saturated Clay.” *Journal of Geotechnical and Geoenvironmental Engineering, ASCE*, 122 (2), 99–108.

127. Sheahan, T. C., Ladd, C. C., Germaine, J. T. (1994). "Time-Dependent Triaxial Relaxation Behavior of a Resedimented Clay." *Geotech. Test. J.*, 17(4), 444-452.

128. Sheahan, T.C. (2005). “A Soil Structure Index to Predict Rate Dependence of Stress-Strain Behavior.” Testing, Modeling and Simulation in Geomechanics, ASCE, Geotechnical Special Publication, no. 143, 81-97.

129. Simo, J. C. and Ortiz, M. (1985). “A Unified Approach to Finite Deformation Elastoplastic Analysis Based on the Use of Hyperelastic Constitutive Equations.” *Computer Methods in applied Mechanics and Engineering*, 49, 221-245.

130. Singh, A. and Mitchell, J. K. (1968). ‘‘General Stress–Strain–Time Function for Soils.’’ *J. Soil Mech. Found. Div.,* 94(1), 21–46.

131. Skempton, A.W. (1985). “Residual Strength of Clays in Landslides, Folded Strata and the Laboratory.” *Géotechnique*, 35 (1), 3-18.

132. Sokolovsky, V. V. (1948). ‘‘Propagation of Elastic-Viscoplastic Waves in Bar.’’ *Dokl. Akad. Nauk SSSR,* 60, 775–778 (in Russian).

133. Sorensen, K.K., Baudet, B. A., Simpson, B. (2007). “Influence of Structure on the Time-Dependent Behaviour of a Stiff Sedimentary Clay.” *Géotechnique*, 57(1), 113–124.

134. Tatsuoka, F. and Kohata, Y. (1995). "Stiffness of Hard Soils and Soft Rocks in Engineering Applications." *First Int. Conf. on Pre-failure Deformation Characteristics of Geomaterials*, Sapporo, 2, 947-1063.

135. Tatsuoka, F., Ishihara, M., Maruyama, N. (2000). "On the Structure of One-Dimensional Model for Time-Dependent Deformation Properties of Geomaterials." *Proc. of Japan Conf. on Geotech. Engrg.,* Gifu, 1, 305-306 (in Japanese).

136. Tatsuoka, F., Ishihara, M., Di Benedetto, H., Kuwano, R. (2002). "Time-Dependent Deformation Characteristics of Geomaterials and Their Simulation." *Soils and Foundations*, 42(2), 103-129.

137. Tatsuoka, F., Lo Presti, D., Kohata, Y. (1995). "Deformation Characteristics of Soils and Soft rocks Under Monotonic and Cyclic Loads and Their Relationships." *3rd Int. Conf. on Recent Advances in Geotechnical Earthquake Engineering and Soil Dynamics*, St. Louis.

138. Tavenas, F., Leroueil, S., La Rochelle, P., Roy, M. (1978). ''Creep Behavior of an Undisturbed Lightly Overconsolidated Clay.'' *Canadian Geotechnical Journal*, 15(3), 402–423.

139. Terzaghi, K., Peck, R. B., Mesri, G. (1996). Soil Mechanics in Engineering Practice. 3rd Ed., Wiley, New York.

140. Tika, T. M., Vaughan, P. R., Lemos, L. J. L. (1996). "Fast Shearing of Pre-Existing Shear Zones in Soils." *Géotechnique*, 46(2), 197-233.

141. Ting, J. M. (1983). "Tertiary Creep Model for Frozen Sands." *Journal of Geotechnical Engineering, ASCE,* 109(7), 932-945.

142. Tong, X. and Tuan, C. (2007). "Viscoplastic Cap Model for Soils Under High Strain Rate Loading." *Journal of Geotechnical and Geoenvironmental Engineering*, *ASCE*, 133(2), 206-214.

143. Vaid, Y. P. and Campanella, R. G. (1977). "Time-Dependent Behavior of Undisturbed Clay." *Journal of Geotechnical Engineering Division*, *ASCE*, 103(7), 693–709.

144. Whitman, R. V. (1960). "Some Considerations and Data Regarding the Shear Strength of Clays." *Proceedings of Research Conference on Shear Strength of Cohesive Soils*, University of Colorado, Boulder, Colorado, 581-614.

145. Yin, J. H. and Graham, J. (1989a). ''Viscous-Elastic-Plastic Modeling of One-Dimensional Time-Dependent Behaviour of Clays.'' *Canadian Geotechnical Journal*, 26, 199–209.

146. Yin, J. H. and Graham, J. (1989b). ''General Elastic Viscous Plastic Constitutive Relationships for 1D Straining in Clays.'' *Proceedings of 3rd International Symposium on Numerical Models in Geomechanics*, 108–117.

147. Yin, J. H. and Graham, J. (1994). ''Equivalent Times and One Dimensional Elastic Visco-Plastic Modelling of Time-Dependent Stress Strain Behaviour of Clays.'' *Canadian Geotechnical Journal*, 31, 45–52.

148. Yin, J. H. and Graham, J. (1996). ''Elastic Visco-Plastic Modeling of One-Dimensional Consolidation.'' *Géotechnique*, 46(3), 515–527.

149. Yin, J.-H., Graham, J., Clark, J. I., Gao, L. (1994). ‘‘Modeling Unanticipated Pore-Water Pressures in Soft Clays.’’ *Canadian Geotechnical Journal*, 31, 773–778.

150. Yue, D. (2001). “An Anisotropic and Time-Dependent Bounding Surface Model for Clays and its Application to a Containment System Constructed Over a Soft Foundation.” *Doctoral Dissertation*, Columbia University, New York.

151. Zhou, H. and Randolph, M.F. (2007). “Computational Techniques and Shear Band Development for Cylindrical and Spherical Penetrometers in Strain-Softening Clay.” International Journal of Geomechanics, 7(4), 287–295.

152. Zhou, C., Yin, J., Zhu, J., Cheng, C. (2005). “Elastic Anisotropic Viscoplastic Modeling of the Strain-Rate-Dependent Stress-Strain Behavior of K_0 – Consolidated Natural Marine Clays in Triaxial Shear Tests.” *International Journal of Geomechanics*, ASCE, 5(3), 218-232.

153. Zienkiewicz, O. C. and Cormeau, I. C. (1974). “Viscoplasticity, Plasticity and Creep in Elastic Solids: A Unified Numerical Solution Approach.” *International Journal of Numerical Methods in Engineering*, 8, 821–845.

154. Zienkiewicz, O.C., Humpheson, C., Lewis. R.W. (1975). “Associated and Non-Associated Viscoplasticity and Plasticity in Soil Mechanics.” *Géotechnique*, 25, 671–689.